Anal. Methods Environ. Chem. J. 6 (1) (2023) 5-16

AMECJ

Research Article, Issue 1
Analytical Methods in Environmental Chemistry Journal
Journal home page: www.amecj.com/ir

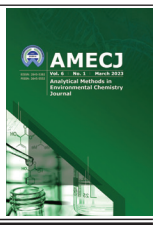

Adsorption behavior of Crystal Violet dye in aqueous solution using Co^{+2} hectorite composite as adsorbent surface

Ahmed Jaber Ibrahim[a,*]
[a] *Scientific Research Center, Al-Ayen University, ThiQar 64011, Iraq*

ARTICLE INFO:
Received 15 Nov 2022
Revised form 1 Feb 2023
Accepted 25 Feb 2023
Available online 30 Mar 2023

Keywords:
Adsorption,
UV-Vis spectrophotometer,
Crystal violet,
Isotherm,
Thermodynamics,
Kinetics

ABSTRACT
This study focused on the adsorption behavior of the cationic Crystal Violet (CV) dye from aqueous solutions using a Co^{+2}–hectorite composite as an adsorbent surface. The initial and equilibrium CV dye concentrations were determined using a UV-Vis spectrophotometer. The results were discussed and presented for the impacts of pH, primary CV dye concentration, composite dosage, and temperature. The optimum conditions were found for eliminating Crystal Violet dye from the aqueous solution at a pH 4, ideal temperature 293 K, and 0.5 g L^{-1} of composite dose. The pseudo-second-order kinetic, intraparticle diffusion analyzed the tests' data and film diffusion models. Each model's defining features have been identified, and these models were in good agreement and in charge of regulating the adsorption reaction. The adsorption operation was also thermodynamically examined to determine thermodynamic variables such as Gibbs free energy (ΔG^o), entropy (ΔS^o), activation energy (Ea), and enthalpy (ΔH^o). The negative value of Gibbs free energy (ΔG^o) and enthalpy (ΔH^o) indicated that the adsorption process was a spontaneous and exothermic reaction. While the activation energy (Ea) data which fell within the normal range for physisorption, was discovered to be 22.434 kJ mol^{-1}. This result proved that physical adsorption occurs between the CV dye and the adsorbent surface (Co^{+2}–hectorite composite).

1. Introduction

Although synthetic dyes are widely utilized in the textile sector, 20 to 40 % of these pigments still end up in effluents [1-3]. The majority of pigments contain hazardous and cancer-causing substances. They also pose a significant hazard to the health of people and the environment since they are resistive and so stable in a recovering ecosystem [4]. Therefore, before the dye-containing wastewater is released into the environment, the dyes must be removed to safeguard persons and ecosystems from pollution. The elimination of contaminants in plastics, pulp, dyestuffs, paper effluents, and textiles has been documented using several physical, chemical, and biological decolorization processes. However, these sectors had only welcomed a small number of them [5–18]. Adsorption is the best option for producing the most significant outcomes among the several dye removal procedures since it may be used to eliminate specific groups of chemical contaminants from aqueous solutions. Adsorption is preferable to compete for systems for utilizing recycled water regarding low cost, formability and styling simplicity, ease of use, and sensitivity to harmful contaminants. According to several studies

*Corresponding Author: Ahmed Jaber Ibrahim
Email: ahmed.jibrahim@alayen.edu.iq
https://doi.org/10.24200/amecj.v6.i01.219

[19,20], activated charcoal and polymer resins are the best adsorbents for eliminating pigments from suitably saturated sewage. The adsorption capability of some reactive dyes by activated carbon is known to be relatively poor. The sewage treatment process utilizing clay-basic [21], AC-ZnO nanostructure [22], cotton [23], Ultraviolet-activated sodium perborate [24], halloysite nanotubes [25], electrospun nanofiber mat [26], chitosan [27], and natural zeolite-basic [18] has thus been the subject of Previous studies. Because of their large surface area and molecular sieve composition, Clay-based materials are efficient organic cation pollutant adsorbents [3]. The generality widely utilized layered silicate is hectorite. Tetrahedral substituted and octahedral substituted are the two structural kinds. Hectorite is an excellent adsorbent for eliminating dye from comparatively saturated wastewater. This is attributed to the fact that hectorite has a unique structure with internal channels that permits the passage of solutes and bonded organic and inorganic ions into the structure of hectorite.

This article suggested using a Co^{+2}-hectorite composite as an Adsorbent surface to absorb crystal violet (CV) dye from aqueous solutions. The results were discussed and presented for the impacts of pH, primary CV dye concentration, composite dosage, and temperature. The data from the tests were analyzed by the pseudo-second-order kinetic, intra-particle diffusion, and film diffusion models. Each model's defining features have been identified. The adsorption operation was also thermodynamically examined to determine thermodynamic variables such as Gibbs free energy (ΔG^o), entropy (ΔS^o), activation energy (Ea), and enthalpy (ΔH^o).

2. Materials and Methods

2.1. Instruments

Thermostatic Controlled shaker (SHKE4000, Thermo Fisher Scientific; USA), UV-Vis spectrophotometer (UV-3600i Plus, Shimadzu, Japan), pH meter (model 744 Metrohm; Germany), Ultrasonic cleaner (WUC-A 1,2- Witeg Labortechnik GmbH; Germany), Mechanical stirrer (Eurostar 60 digital, IKA; China) and vacuum drying oven (Model VD 56-BINDER GmbH; Germany) were used.

2.2. Chemicals

All chemicals with high purity were purchased from the original Company. The chemicals such as, Crystal Violet (CV) dye ($C_{25}H_{30}ClN_3$, Mwt 407.986 dalton, CAS N.: 548-62-9, Tokyo Chemical Industry Co., Japan; Fig. 1), hectorite ($Na_{0.3}(Mg, Li)_3Si_4O_{10}(OH)_2$, Mwt 360.58 dalton, CAS N.: 12173-47-6, Spectrum Chemical Co., USA), hydrochloric acid 37% (HCL, CAS N.: 7647-01-0, Sigma-Aldrich Chemie GmbH Co., USA), and Cobalt chloride ($CoCl_2$, CAS N.: 7646-79-9, American Elements Co., USA) were prepared for this research.

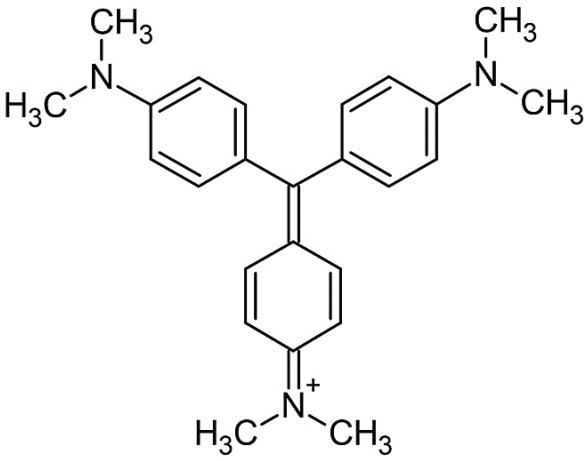

Fig. 1. The structural formula of Crystal Violet dye

2.3. Preparation of Co^{+2}-hectorite composite

The ion-exchanged technique was used to prepare the sorbent in a single step. Two grams of hectorite were mixed with 0.2 liters of distilled water and swirled for 2 hours. Using hydrochloric acid (1M, HCl) solution, the colloidal dispersion's pH was reduced to 6. Cobalt chloride ($CoCl_2$) solution was added in the calculated amount while stirring for 8 hours. The final dispersion was cleaned by distilled water. At 80°C, the product was dried after centrifugation.

2.4. Adsorbate

Crystal Violet (CV) dye was used as the model guest to examine the adsorption capability. Using a UV-Vis spectrophotometer with a range of 200 - 800 nm, the

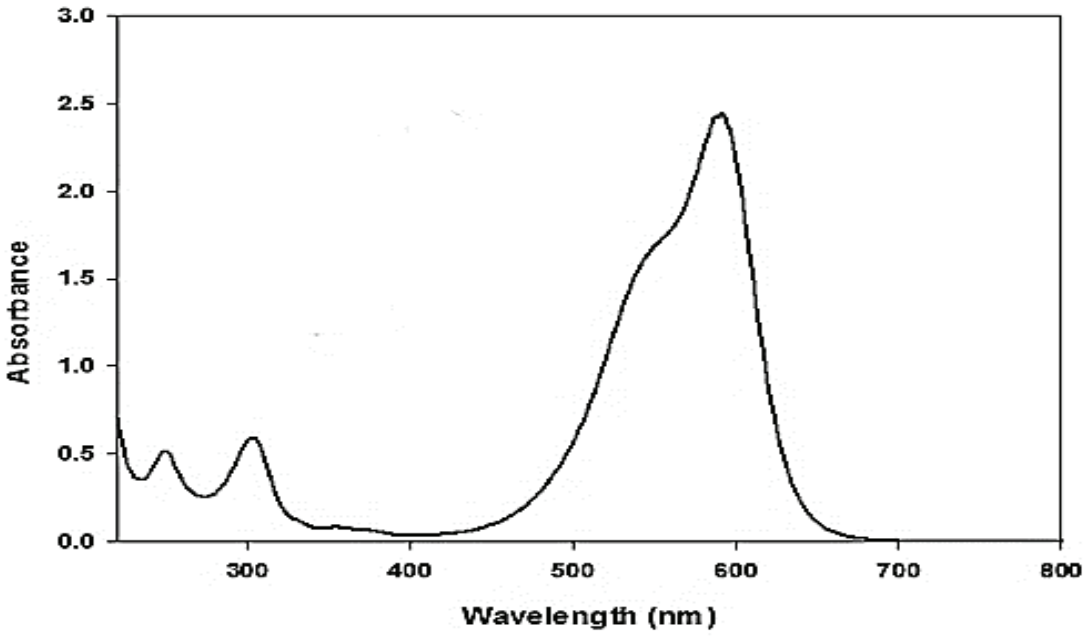

Fig. 2. The UV-Vis spectrum of Crystal violet dye

maximum wavelength of 585 nm was determined, which corresponds to the highest absorption of the dye solution, as shown in Figure 2. To create the stock solution, distilled water was used to dissolve a carefully weighed quantity of CV dye. The solutions for adsorption testing were made at the necessary concentrations by applying serial dilutions to the stock solution. First, a calibration curve for CV dye was drawn. In kinetic and thermodynamic studies, this curve was used to translate data on concentration from absorbance measurements.

2.5. Adsorption process

At various temperatures, adsorption studies were conducted in a controlled thermostatic shaker. Up until the point of equilibrium, the shaking persisted. The initial and equilibrium CV dye concentrations were determined using a UV-Vis spectrophotometer. The adsorption capability of the adsorbent was determined using these data. It was possible to determine the quantity of CV adsorbed (qe) at equilibrium. The mass balance is shown in Equation 1.

$$qe=v(C_0- C_e)/W \qquad \text{(Eq.1)}$$

Where v is the volume of dye solution used (L), is the primary dye concentration in the liquid phase (g L^{-1}), is the liquid phase dye concentration at equilibrium (g L^{-1}), and W is the mass of sorbent utilized (g). By adding 0.03 g sorbent at various temperatures to 0.060 L of crystal violet solution (0.150 g L^{-1}), kinetic investigations were conducted. The liquid phase crystal violet concentration was monitored at predetermined intervals.

3. Results and Discussion

3.1. The influence of solution pH

The influence of solution pH for the elimination of CV dye by Co^{+2}-hectorite complex was studied in the range of 2–12 under the conditions: 0.150 g L^{-1} CV dye concentration, 0.5 g L^{-1} Composite dosages, 293 temperature, and 1 hour Contact time). The implies of the repeated experimental outcomes are plotted in Figure 3. The experimental results showed that the degree of adsorption of CV dye on the Co^{+2}-hectorite composite reached 95% when the pH of the solution was 4. Therefore, the optimal pH was considered to be 4, which achieves the maximum adsorption of CV dye. On this basis, the remainder of the subsequent tests were carried out at this optimum pH value. Other investigators

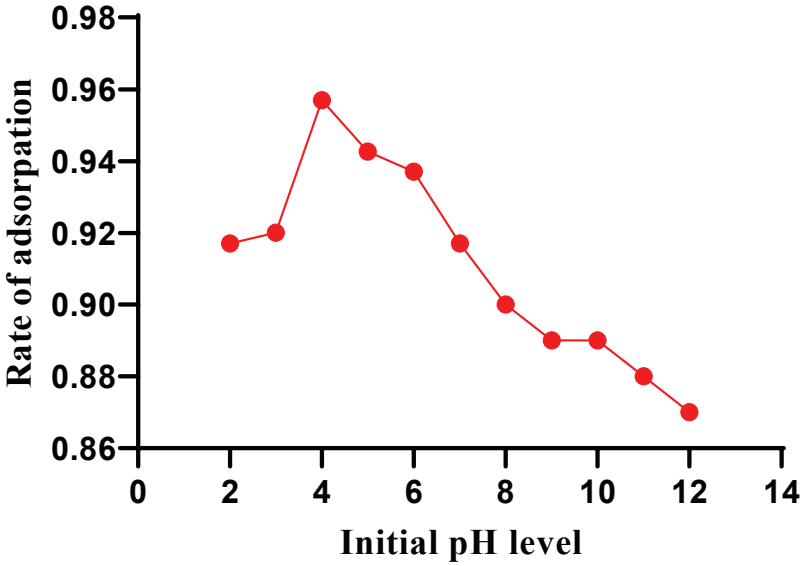

Fig. 3. Influence of pH of CV dye adsorption on Co^{+2}-hectorite composite

have shown a tendency similar to the adsorption process of the Congo red azo dye as a function of pH [28].

3.2. Effect of sorbent composite dose

Between 0.5 and 1.5 g L^{-1} of Co^{+2}-hectorite composite, the dose was tested under the conditions: (primary CV dye concentration 0.5 g L^{-1}, 0.6 g L^{-1}, 0.7 g L^{-1} , ph=4, 293 K temperature and 8 hour Contact time) to see how it affected CV dye adsorption. Figure 4 of the findings indicates a decrease in with an increase in Co^{+2}-hectorite dosage. Because a greater adsorbent dose decreases the adsorption sites' unsaturation, there is relatively less adsorption at larger adsorbent doses. CV dye can quickly arrive at the adsorption locations, and the qe rises when the amount of adsorbent is modest. Because less of the adsorbent's adsorptive capacity is being utilized with an increase in adsorbent amount, the correlating increase in adsorption reaction per unit cluster is decreased.

Higher adsorbent dosages caused particle aggregation, reducing the overall surface area and the multitude of active adsorption locations. The highest CV dye adsorption in this research was accomplished at a Co^{+2}-hectorite dose of 0.5g remaining trials were carried out at this concentration.

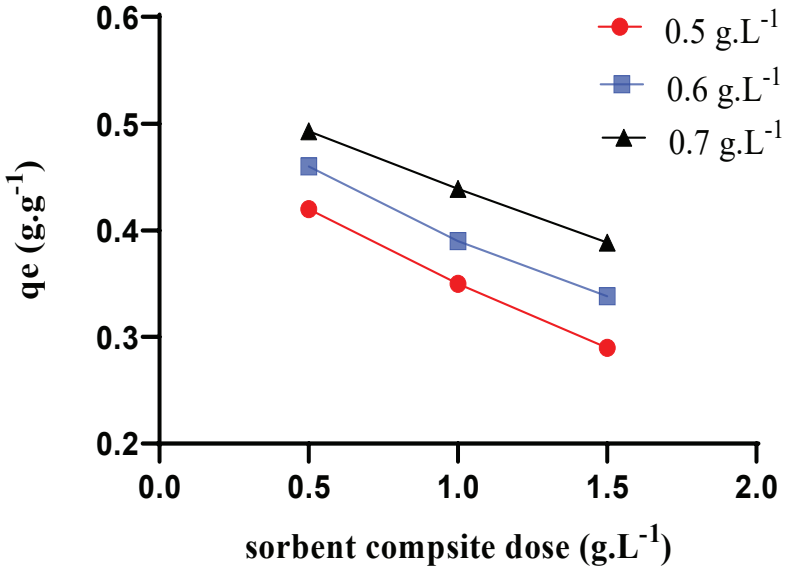

Fig. 4. Effect of sorbent composite dose on CV dye adsorption

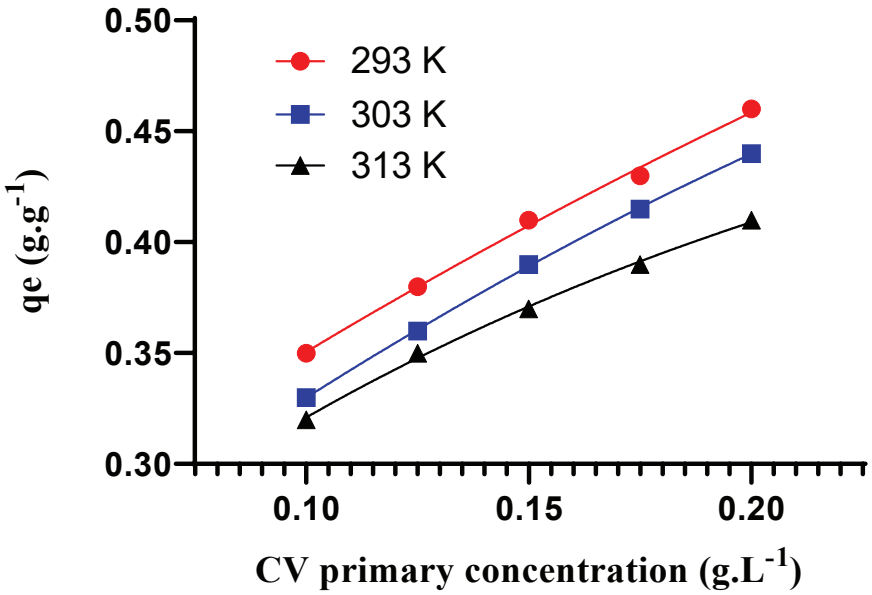

Fig. 5. Influence of primary dye concentration and temperature on the adsorption process

3.3. Effect of primary crystal violet (CV) dye concentration and temperature

It is unclear how varied CV dye concentrations affect how well Co^{+2}-hectorite composite removes CV because the effluent from various industries may include varying amounts of dye. This study examined the adsorption of concentrations of 0.100, 0.125, 0.150, 0.175, and 0.200 g L^{-1} CV dye for the Co^{+2}–hectorite composite. The duplicate data's means are shown in Figure 5, which shows that the concentration of CV dye has a significant influence on the adsorption capability of the Co^{+2}-hectorite composite. Based on the data shown in Figure 5, the qe of Co^{+2}-hectorite rose at various temperatures when the primary CV dye concentration was raised**.** This is explained by the reality that free adsorption locations are accessible at the start of the test and by the fact that there was a more effective mass transfer rate during the first contact period when the CV dye concentration was at its highest.

The impact of temperature on the CV dye adsorption equilibrium on the Co^{+2}-hectorite surface is also depicted in Figure 5. For a primary concentration of 0.100-0.200 g L^{-1}, it can be seen that the qe declined as the temperature rose, indicating an exothermic process. Though the impact of temperature on the adsorption equilibrium was negligible at the low starting concentration of CV dye (0.100 g L^{-1}), it was still present.

3.4. The investigation of intra-particle diffusion and film diffusion

To determine whether external film diffusion or intraparticle diffusion affected the removal rate, the Weber-Morris kinetic model was used s as Equation 2[29].

$$qt = K_{id} t^{0.5} + C \qquad \text{(Eq.2)}$$

where represents the removal capacity (mg g^{-1}) at time(t), K_{id} represents the intra-particle diffusion rate constant (mg per g $min^{0.5}$), and C represents a constant whose value is proportionate to the limit layer (mg g^{-1}).

When the adsorption system corresponds with the intra-particle diffusion mechanism, a plot of qt versus $t^{0.5}$ should have a straight line with a slope of K_{id} and an intercept of C, according to Equation 2. Figure 6 shows a plot of the means of the replicated experimental outcomes. There are two distinct zones in Figure 6. The first straight and the second linear sections are attributed to macro- and micro-

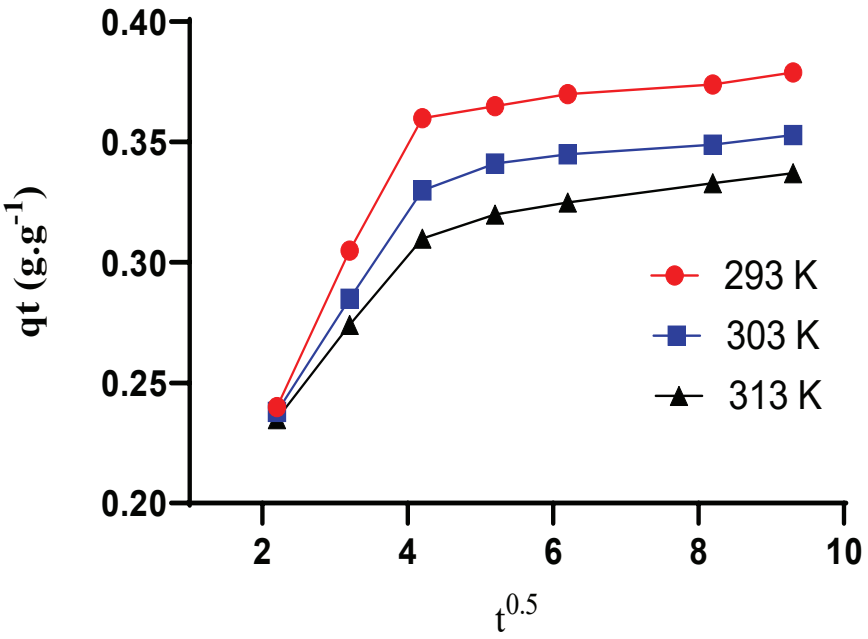

Fig. 6. Scatter plot of qt versus $t^{0.5}$ for adsorption of CV dye on Co^{+2}-hectorite composite at studied temperatures

pore diffusion, respectively. The immediate use of the adsorbing locations on the adsorbent superficial is blamed in the first section. The second section's phenomenon is linked to an extremely slow CV diffusion into the least accessible adsorption sites—the micro-pores—from the surface film. Additionally, this promotes the sluggish quiet rate of adsorbate movement from the liquid stage to the surface of the adsorbent. The mass transfer rate variance between the adsorption reaction's first and end phases explains why the straight line deviates from the original line. The straight line's continued departure from the point of origin suggests that pore diffusion is not the lone rate-limiting process [30].

To support the above findings, the intra-particle diffusion coefficients (Dp) were estimated by Equation 3.

$$Dp = \frac{(0.03\, r0^2)}{t\ 0.5} \qquad \text{(Eq.3)}$$

where r_0 (m) represents the mean radius of the adsorbent particles and $t^{0.5}$ (min) the time needed to fulfill half of the adsorption.

The rate-limiting phase will be intra-particle diffusion, referring to Sushanta et al. [31], if the predicted intra-particle diffusion coefficient (DP) level is in the scope 10^{-15}-10^{-18} m^2 per S. According to Table 1, which was used in this investigation, the computed *DP* level varied from $1.65x10^{-14}$ to $2.47x10^{-14}$ m^2 s^{-1} at various temperatures, implying that intra-particle diffusion reaction is not the primary process limiting CV dye adsorption onto Co^{+2}-hectorite surface.

Table 1. The adsorption process's film diffusion coefficient (DF) and intra-particle diffusion coefficients (DP) at the temperatures studied

Temperature (k)		DP (m^2 S^{-1})	DF (m^2 S^{-1})	r_0(m)
293	77.44	1.65 x 10^{-14}	3.44 x 10^{-13}	6.54 x 10^{-4}
303	63.36	2.02 x 10^{-14}	4.21 x 10^{-13}	
313	51.87	2.47 x 10^{-14}	5.63 x 10^{-13}	

Equation 4 has been used to compute the film diffusion coefficients (DF), to examine the adsorption kinetics reactions.

$$DF = \frac{(0.23\ r\ 0\delta Cs)}{(Clt_{0.5})} \qquad \text{(Eq.4)}$$

Where CS is the concentration of adsorbate in the solid phases, Cl is the concentration of adsorbate in the liquid phase, and r^0 and $t^{0.5}$ share the identical meaning as earlier, and d is the film thickness (10^{-5}m) [31]. The computed film diffusion coefficient (DF) value will fall between 10^{-10} and 10^{-12} m^2 per second if the film diffusion reaction is the rate-limiting step's controlling factor. The predicted levels of DF were discovered to be in the arrange of 10^{-13} m^2s^{-1} (Table 1), indicating that the film diffusion reaction was not the lone phase in the adsorption process that was rate-limiting. Intra-particle and film diffusions in this study served to regulate the kinetic process. The kinetic reaction was governed by film diffusion since the CV concentration was high at the beginning of the adsorption process. CV molecules started to diffuse inside Co^{+2}-hectorite when they were adsorbed on the surface of the composite, and the adsorption reaction was what controlled this.

3.5. Thermodynamics study

The pseudo-second-order [32] model has been investigated about kinetic modeling to determine the adsorption mechanism (Equation 5).

$$\frac{t}{qt} = \frac{1}{k2q^2e} + \frac{1}{qe}\ t \qquad \text{(Eq.5)}$$

Where qe is the equilibrium adsorption capability ($g.g^{-1}$), k_2 is the pseudo-second-order adsorption rate constant (g min g^{-1}), and qt is the amount of CV adsorbed at time t (g g^{-1}). To determine rate parameters, the straight line plots of t/qt vs. t for the pseudo-second-order models have also been investigated (Fig. 7). Table 2 contains the correlation coefficients r^2, k, and qe at numerous temperatures. The Arrhenius equation (Eq. 6) can express the pseudo-second-order rate constants as a temperature performance.

$$\boldsymbol{ln\ k = ln\ A - Ea/RT} \qquad \text{(Eq.6)}$$

Where k is the rate constant, A is the frequency coefficient, Ea is the activation energy, R is the gas constant, and T is the temperature in Kelvin.
Figure 8 shows a visualization of the means of the replicated experimental outcomes.

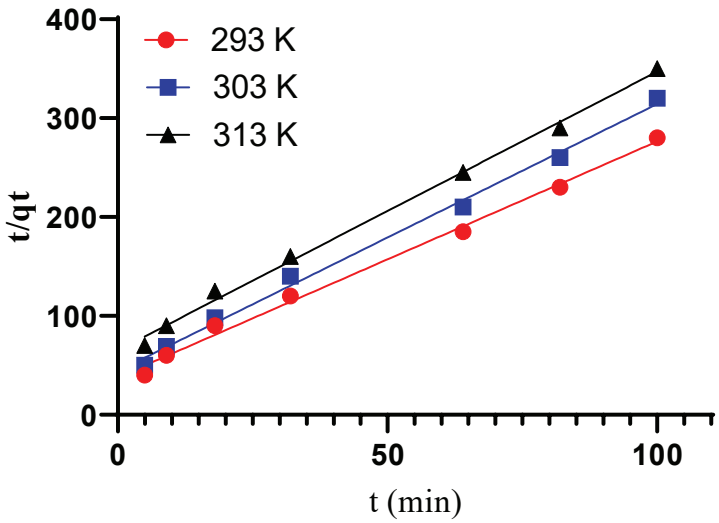

Fig. 7. The pseudo-second-order kinetics model for the adsorption of CV dye onto Co^{+2}-hectorite composite at studied temperatures

Table 2. The Arrhenius activation energy (Ea) and pseudo-second-order kinetics parameter values for the adsorption process at temperatures studied

Temperature (k)	(kJ mol^{-1})	r^2	qe (g g^{-1})	k^2
293		0.9996	0.335	2.087
303	22.434	0.9954	0.317	2.794
313		0.9965	0.302	3.587

The Ea is calculated using Equation 6 (Table 2). The size of the activation energy gives a clue as to the primary kind of adsorption, either chemical or physical. Physisorption processes typically have activation energies between 5 and 40 kJ mol^{-1}, whereas greater activation energies (between 40 and 800 kJ.mol^{-1}) point to chemisorption. The dispersive interaction between the crystal violet and the Co^{+2}-hectorite surface implies it. The Gibbs free energy (ΔG^o), enthalpy change (ΔH^o), and entropy change (ΔS^o), which are thermodynamic characteristics, have been calculated to assess the viability and exothermic characteristic of the adsorption reaction. Equation 7 relates the process's change in Gibbs free energy to the equilibrium constant (k).

$$\Delta Go = -RTlnK \qquad \text{(Eq. 7)}$$

The below formula shows how the standard free energy change at constant temperature is also correlated with enthalpy and entropy changes (Eq. 8).

$$LnK = -\frac{\Delta Ho}{RT} + \frac{\Delta So}{R} \qquad \text{(Eq. 8)}$$

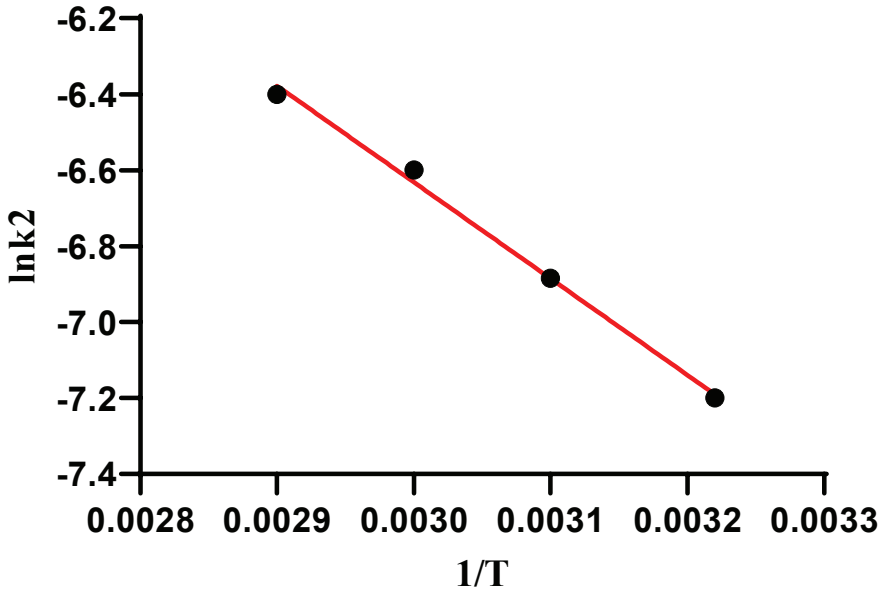

Fig. 8. Arrhenius Scatter plots for the adsorption of CV dye onto Co^{+2}-hectorite at studied temperatures

The slope and intercept of Scatter plots of lnK vs 1/T are utilized to evaluate the levels of ΔG^o and ΔS^o (Fig. 9). Table 3 contains the obtained values. Indicating the viability and spontaneity of the CV adsorption reaction on the Co^{+2}-hectorite surface, the Gibbs free energy (ΔG^o) levels were observed to be decreasingly negative with temperature. It is discovered that the enthalpy change (ΔH^o) values are negative, indicating the exothermic character of the adsorption process. The fact that the (ΔH^o) value is less than 40 kJ.mol^{-1} shows that the crystal violet adsorption by the composite of Co^{+2}-hectorite is physisorption. The results from the current study are comparable to those from Xia's study [28] on the adsorption reaction of congo red azo dye from aqueous solution by ODA-hectorite and CTAB-hectorite as adsorbent surfaces.

4. Conclusion

The results of this investigation demonstrate the efficiency of Co^{+2}-hectorite composite as an adsorbent surface for eliminating Crystal Violet (CV) dye from aqueous solutions. The elimination of CV worked best at a pH of 4. The ideal temperature and composite dose were 293°K and 0.5 g L^{-1}, respectively. The experimental results and the pseudo-second-order kinetic model were in good agreement, as indicated by the straight lines in t/qt vs t plots. Intra-particle and film diffusions were in charge of regulating the adsorption reaction. The exothermic and spontaneous response of CV adsorption on Co^{+2}-hectorite composite is revealed by evaluating the thermodynamic parameters. The activation energy for adsorption, which fell within the normal range for physisorption, was discovered

Table 3. Thermodynamic variables for the adsorption process

Temperature (*k*)	Distribution coefficient (k)	ΔG^o (kJ mol^{-1})	ΔH^o (kJ mol^{-1})	ΔS^o (kJ mol^{-1})
293	4.654	-3.745		
303	3.324	-2.926	-31.546	-94.883
313	2.067	-1.768		

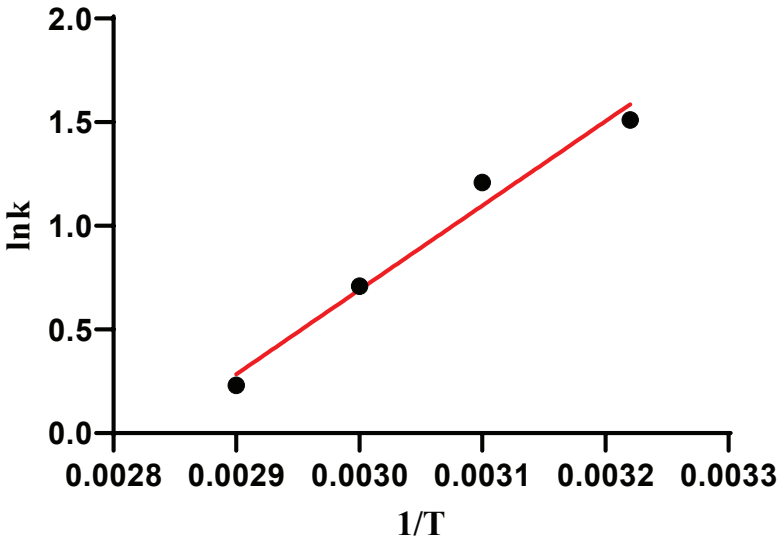

Fig. 9. Scatter plot of lnK vs. 1/T for CV dye adsorption onto Co^{+2}-hectorite composite.

to be 22.434 kJ mol^{-1}. The outcomes would benefit the design of wastewater treatment facilities that remove the dye.

5. Acknowledgements

The structural formula of the Physical Chemistry Lab., Chemistry Department, College of Education for Pure Science (Ibn-al Haitham), University of Baghdad, supports this research.

6. References

[1] F. Kooli, S. Rakass, Y. Liu, M. Abboudi, H.O. Hassani, S.M. Ibrahim, F. Wadaani, R. Al-Faze, Eosin removal by Cetyl trimethylammonium-Cloisites: influence of the surfactant solution type and regeneration properties, Mol., 24 (2019) 3015. https://doi.org/10.3390/molecules24163015.

[2] F.M. Valadi, A. Ekramipooya, M.R. Gholami, Selective separation of Congo Red from a mixture of anionic and cationic dyes using magnetic-MOF: Experimental and DFT study, J. Mol. Liq., 318 (2020) 114051. https://doi.org/10.1016/j.molliq.2020.114051.

[3] P. S. Kumar, G. J. Joshiba, C. C. Femina, P. Varshini, S. Priyadharshini, M. A. Karthick, R. Jothirani, A critical review on recent developments in the low-cost adsorption of dyes from wastewater, Desalin. Water Treat., 172 (2019) 395-416. https://doi.org/10.5004/dwt.2019.24613.

[4] S. Benkhaya, S. M'rabet, A. El Harfi, Classifications, properties, recent synthesis and applications of azo dyes, Heliyon, 6 (2020) e03271. https://doi.org/10.1016/j.heliyon.2020.e03271.

[5] G. Crini, E. Lichtfouse, Advantages and disadvantages of techniques used for wastewater treatment, Environ. Chem. Lett., 17 (2019) 145-155. https://doi.org/10.1007/s10311-018-0785-9.

[6] S. Samsami, M. Mohamadizaniani, M.H. Sarrafzadeh, E.R. Rene, M. Firoozbahr, Recent advances in the treatment of dye-containing wastewater from textile industries: Overview and perspectives, Proc. Safe. Environ. Prot., 143 (2020) 138-163. https://doi.org/10.1016/j.psep.2020.05.034.

[7] E. Routoula, S.V. Patwardhan, Degradation of anthraquinone dyes from effluents: a review focusing on enzymatic dye degradation with industrial potential, Environ. Sci. Technol., 54 (2020) 647-664. https://doi.org/10.1021/acs.est.9b03737.

[8] A. Tkaczyk, K. Mitrowska, A. Posyniak, Synthetic organic dyes as contaminants of the aquatic environment and their implications for ecosystems: A review, Sci. Total Environ., 717 (2020) 137222. https://doi.org/10.1016/j.scitotenv.2020.137222.

[9] L. Largitte, R. Pasquier, A review of the kinetics adsorption models and their application to the adsorption of lead by an activated carbon, Chem. Eng. Res. Desi., 109 (2016) 495-504. https://doi.org/10.1016/j.cherd.2016.02.006.

[10] C. Santhosh, V. Velmurugan, G. Jacob, S.K. Jeong, A.N. Grace, A. Bhatnagar, Role of nanomaterials in water treatment applications: a review, Chem. Eng. J., 306 (2016) 1116-1137. https://doi.org/10.1016/j.cej.2016.08.053.

[11] M. Berradi, R. Hsissou, M. Khudhair, M. Assouag, O. Cherkaoui, A. El Bachiri, A. El Harfi, Textile finishing dyes and their impact on aquatic environs, Heliyon, 5 (2019) e02711. https://doi.org/10.1016/j.heliyon.2019.e02711.

[12] M.T. Yagub, T.K. Sen, S. Afroze, H.M. Ang, Dye and its removal from aqueous solution by adsorption: a review, Adv. Coll. Inter. Sci., 209 (2014) 172-184. https://doi.org/10.1016/j.cis.2014.04.002.

[13] T.A. Saleh, Protocols for synthesis of nanomaterials, polymers, and green materials as adsorbents for water treatment technologies, Environ. Tech. Innov., 24

(2021) 101821. https://doi.org/10.1016/j.eti.2021.101821.

[14] X. Liu, H. Pang, X. Liu, Q. Li, N. Zhang, L. Mao, M. Qiu, B. Hu, H. Yang, X. Wang, Orderly porous covalent organic frameworks-based materials: superior adsorbents for pollutants removal from aqueous solutions, Innovation, 2 (2021) 100076. https://doi.org/10.1016/j.xinn.2021.100076.

[15] I.C. Ossai, A. Ahmed, A. Hassan, F.S. Hamid, Remediation of soil and water contaminated with petroleum hydrocarbon: A review, Environ. Tech. Innov., 17 (2020) 100526. https://doi.org/10.1016/j.eti.2019.100526.

[16] J. Liu, G. Zhang, Recent advances in synthesis and applications of clay-based photocatalysts: a review, Phys. Chem. Chem. Phys., 16 (2014) 8178-8192. https://doi.org/10.1039/C3CP54146K.

[17] Z. Wang, Z. Wang, S. Lin, H. Jin, S. Gao, Y. Zhu, J. Jin, Nanoparticle-templated nanofiltration membranes for ultrahigh performance desalination, Nat. comm., 9 (2018) 1-9. https://doi.org/10.1038/s41467-018-04467-3.

[18] D. Yue, Y. Jing, J. Ma, C. Xia, X. Yin, Y. Jia, Removal of neutral red from aqueous solution by using modified hectorite, Desalination, 267 (2011) 9-15. https://doi.org/10.1016/j.desal.2010.08.038

[19] N.U.M. Nizam, M.M. Hanafiah, E. Mahmoudi, A.A. Halim, A.W. Mohammad, The removal of anionic and cationic dyes from an aqueous solution using biomass-based activated carbon, Sci. Rep., 11 (2021) 1-17. https://doi.org/10.1038/s41598-021-88084-z

[20] C.F. Mok, Y.C. Ching, F. Muhamad, N.A. Abu Osman, N.D.Hai, C.R. Che Hassan, Adsorption of dyes using poly (vinyl alcohol)(PVA) and PVA-based polymer composite adsorbents: a review, J. Poly. Environ., 28 (2020) 775-793. https://doi.org/10.1007/s10924-020-01656-4

[21] I. Chaari, E. Fakhfakh, M. Medhioub, F. Jamoussi, Comparative study on adsorption of cationic and anionic dyes by smectite rich natural clays, J. Mol. Struct., 1179 (2019) 672-677. https://doi.org/10.1016/j.molstruc.2018.11.039

[22] A.J. Ibrahim, ZnO nanostructure synthesis for the photocatalytic degradation of azo dye methyl orange from aqueous solutions utilizing activated carbon, Anal. Meth. Environ. Chem. J., 5 (2022) 5-19. https://doi.org/10.24200/amecj.v5.i04.200

[23] A.N.M.A. Haque, R. Remadevi, O.J. Rojas, X. Wang, M. Naebe, Kinetics and equilibrium adsorption of methylene blue onto cotton gin trash bioadsorbents, Cellulose, 27 (2020) 6485-6504. https://doi.org/10.1007/s10570-020-03238-y

[24] A.J. Ibrahim, Ultraviolet-activated sodium perborate process (UV/SPB) for removing humic acid from water, Anal. Meth. Environ. Chem. J., 5 (2022) 5-18. https://doi.org/10.24200/amecj.v5.i03.191

[25] Y.M. Vargas-Rodríguez, A. Obaya, J.E. García-Petronilo, G.I. Vargas-Rodríguez, A. Gómez-Cortés, G. Tavizón, J.A. Chávez-Carvayar, Adsorption studies of aqueous solutions of methyl green for halloysite nanotubes: Kinetics, isotherms, and thermodynamic parameters, Amer. J. Nanom., 9 (2021) 1-11. http://pubs.sciepub.com/ajn/9/1/1

[26] J.A. Naser, T.A. Himdan, A.J. Ibraheim, Adsorption kinetic of malachite green dye from aqueous solutions by electrospun nanofiber Mat, Orient. J. Chem., 33 (2017) 3121-3129. http://dx.doi.org/10.13005/ojc/330654

[27] A.B. Fradj, A. Boubakri, A. Hafiane, S.B. Hamouda, Removal of azoic dyes from aqueous solutions by chitosan enhanced ultrafiltration, Res. Chem., 2 (2020) 100017. https://doi.org/10.1016/j.rechem.2019.100017

[28] C. Xia, Y. Jing, Y. Jia, D. Yue, J. Ma, X. Yin, Adsorption properties of congo red from aqueous solution on modified hectorite: Kinetic and thermodynamic studies, Desalination, 265 (2011) 81-87. https://doi.org/10.1016/j.desal.2010.07.035

[29] B. Obradović, Guidelines for general adsorption kinetics modeling, Hemi. Ind., 74 (2020) 65-70. https://doi.org/10.2298/HEMIND200201006O

[30] Y. Kuang, X. Zhang, S. Zhou, Adsorption of methylene blue in water onto activated carbon by surfactant modification, Water, 12 (2020) 587. https://doi.org/10.3390/w12020587

[31] S. Debnath, U.C. Ghosh, Kinetics, isotherm and thermodynamics for Cr(III) and Cr(VI) adsorption from aqueous solutions by crystalline hydrous titanium oxide, J. Chem. Therm., 40 (2008) 67-77. https://doi.org/10.1016/j.jct.2007.05.014

[32] A.S. Özcan, B. Erdem, A. Özcan, Adsorption of Acid Blue 193 from aqueous solutions onto Na–bentonite and DTMA–bentonite, J. Coll. Inter. Sci., 280 (2004) 44-54. https://doi.org/10.1016/j.jcis.2004.07.035

Anal. Methods Environ. Chem. J. 6 (1) (2023) 17-28

AMECJ

Research Article, Issue 1
Analytical Methods in Environmental Chemistry Journal
Journal home page: www.amecj.com/ir

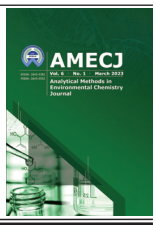

Preparation of recycled polystyrene derivatives to remove heavy metal ions from contaminated water

Hadi Salman Al-Lami[a,*], Hussein Ali Al-Mosawi[a], and Nadhum Abdulnabi Awad[a]
[a]*Department of Chemistry, College of Science, University of Basrah, Basrah, Iraq*

ARTICLE INFO:
Received 7 Dec 2022
Revised form 17 Feb 2023
Accepted 4 Mar 2023
Available online 30 Mar 2023

Keywords:
Sulfonated polystyrene,
Chitosan,
Grafting,
Acrylamide,
Heavy metals,
Flame atomic absorption spectrometer

ABSTRACT
In recent years, numerous researchers have concentrated on the process of turning waste into usable materials. Polystyrene and its modifications have received great attention over the past few decades due to their outstanding ion exchange behavior toward various toxic heavy metals in aqueous solutions. Therefore, this study is concerned with the preparation of three different cationic polymeric resins for the removal of Pb^{2+}, Cd^{2+}, and Fe^{3+} heavy metal ions from their contaminated water samples based on the sulfonated single-used polystyrene teacup waste (SPS), which was used to prepare sulfonated polystyrene-g-acrylamide monomer (SPS-g-Acryl) and sulfonated polystyrene-g-chitosan (SPS-g-Chit) using commercial chitosan (DD=85%) originally extracted from shrimp cortex. The concentrations of the selected heavy metal ions were measured before and after each experiment with a flame atomic absorption spectrometer (F-AAS). The analytical studies started by exploring the influence of pH (2, 4, 6, and 8) on removing the heavy metal ions Pb^{2+}, Cd^{2+}, and Fe^{3+} from their aqueous solutions. The obtained results revealed that as the pH of the analyzed ion solution is increased, the removal efficiency for ions increases. All three resins (SPS, SPS-g-Acryl, and SPS-g-Chit) had different removal efficiencies for the investigated ions, with SPS-g-Chit resin being the best in both batching and column loading methods, and they could be compared in the following order: SPS-g-Chit > SPS-g-Acryl > SPS, and it could be reused after regeneration.

1. Introduction

Water is one of the most crucial natural resources for the survival of all living forms, food security, economic development, and welfare. De-pollution is a gift from Mother Nature to the globe that cannot be replicated for many purposes and costs a lot to ship [1]. The world's freshwater habitats represent about 5% of the Earth's land area but contain 2.84 billion km3 of freshwater. Only one percent of the earth's water is in rivers and streams. Despite the small amounts, the presence of large volumes of flowing water is critical. The exponential development of the population and increased industrialization have led to an enormous rise in freshwater consumption in recent decades. Heavy metal pollution of the water environment threatens human health in most countries. It has increased recently along with economic development and population growth, primarily from mining, electroplating, and the production and shipment of batteries. They damage the body, including the skin, lungs, head, liver, and kidneys, and cause tumors, birth defects, and other conditions. Consequently, the quality of drinking

*Corresponding Author: Hadi Salman Al-Lami
Email: hadi.abbas@uobasrah.edu.iq
https://doi.org/10.24200/amecj.v6.i01.223

water is declining, and there is a need for better water management and a method for preventing water contamination and providing pure water [2]. This explains why, for the government and experts, water contamination has become a study subject [3]. Both the water and its geographic and seasonal supply, as well as their surface and groundwater content, are very important for climate, economic growth, and development. Because of increased population growth, urbanization, expansion of agriculture, and more, these factors influence water quality. Polluted water affects the lives of today's people and those of future generations, as its effects continue to be long-lasting. If water is contaminated in a city, all livelihoods and citizens are confronted with drinking poisoned water because they have no alternative. The damage to the human body (skin, lungs, head, liver, and kidneys) causes tumors, birth defects, and other conditions. We concluded that the quality of drinking water is declining because of increasing population, agricultural practices, and industrialization, and there is a need for better water management and a method for preventing water contamination and providing pure water [2].

Due to the issues above, a substantial focus has recently been placed on developing more effective, less expensive, and long-lasting wastewater treatment systems that do not add to environmental stress or pose a health risk to humans. In recent years, extensive testing has been done to develop alternative and cost-effective water and wastewater technologies. Coagulation, membrane processes, adsorption, dialysis, flotation, osmosis, and photocatalytic degradation are some methods used to remove hazardous substances from water. However, as seen in Figure 1, various sources of pollutants are in the water [4].

Many methods have been studied to treat heavy metals from wastewater; these can be chemical, physical, or biological. The most promising technologies to overcome these constraints are adsorption and ion exchange [5,6]. Given the various industrial applications of large quantities of ion exchange resins consumed after being used for specified periods, depending on the operating conditions, they should be replaced by new ones [7,8]. This prompted us to look for a less expensive alternative method of providing it. In

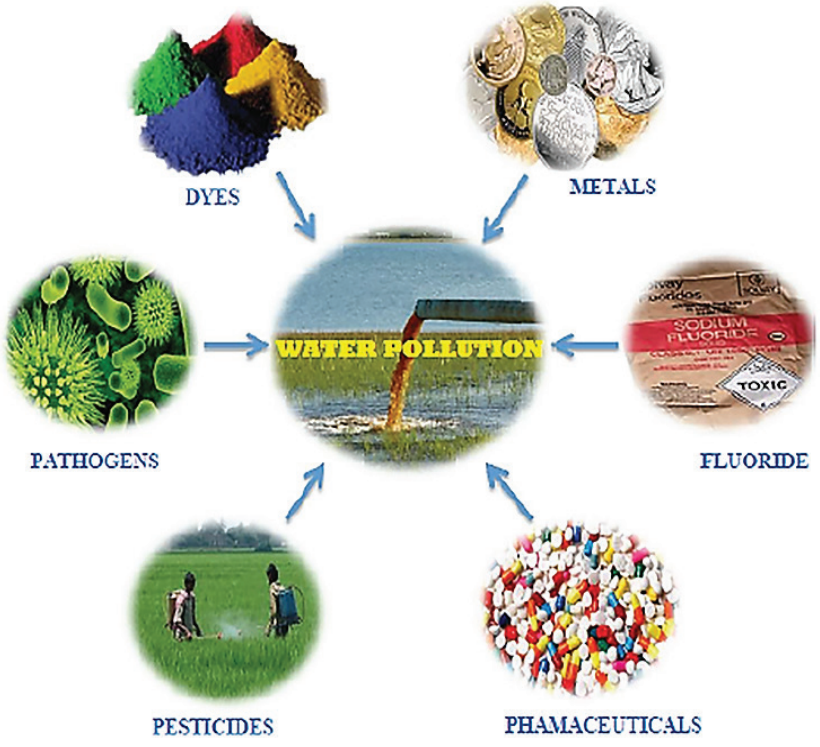

Fig. 1. Some sources of pollutants in water [4]

previous work, sulfonation and grafting acrylamide monomer and chitosan polymerization synthesized two ion exchange resins from recycled polystyrene single-used teacup waste [9]. They were used as ion exchangers to determine the total hardness of tap water. Both prepared resins were characterized by FTIR, which confirmed the properness of the sulfonation and grafting processes on sulfonated polystyrene, respectively. The grafting process causes an increase in the efficiency of the sulfonated polystyrene resin in removing the hardness of tap water. Polystyrene sulfonating reduces the volume of solid waste and contributes to environmental cleanliness.

The results of our investigation into the technical viability are presented in this research using sulfonated polystyrene-g-acrylamide (SPS-Acryl). Sulfonated polystyrene-g-chitosan (SPS-Chit) derived from polystyrene single-use teacups after sulfonation (SPS) for heavy metal removal in batch experiments and continuous fixed bed column experiments for checking their feasibility if applied in practice are presented in this research. In addition to reducing environmental degradation, recycling this material as an ion exchange material also limits the exploitation of natural resources.

2. Experimental

2.1. Materials and instrument

Sulfuric acid (96%) was used as a sulfonating agent; Chitosan (80 mesh, DD = 85) and acrylamide monomer were used as grafting materials; nitric acid and ammonium hydroxide solution were purchased from Sigma-Aldrich. Cadmium (II) nitrate, iron (III) chloride, and lead (II) nitrate were purchased from Global Chemical Company (L.L.C; GCC) and used as sources for heavy metal ions in pollutant samples. The concentrations of the Pb^{2+}, Cd^{2+}, and Fe^{3+} heavy metal ions were measured with a flame atomic absorption spectrometer (F-AAS, Varian AA240 FS, USA). The IKA magnetic stirrer was purchased from Sigma Aldrich (IKA®C-MAG MS; SKU: Z671835, Germany). Digital pH meter purchased from Thermo Fisher Scientific (USA).

2.2. Sulfonated polystyrene preparation (SPS)

The single-use polystyrene teacups were collected and washed several times with tap and distilled water before drying at room temperature. As mentioned in the literature, sulfonated polystyrene and SPS-g-acrylamide monomers were prepared [9,10]. In a 250 mL round bottom flask, 20 g of chopped waste teacups made of polystyrene were added. 50 mL of 96% sulfuric acid was added, and the mixture was continuously stirred at room temperature. The mixture was then refluxed for approximately 4 hours at 60–65°C. Sulfonated polystyrene was obtained through separation and filtration after adding cold, distilled water stopped the reaction. Following a pH-neutralizing wash with distilled water, it was dried at 60°C.

2.3. Synthesis of SPS-g-acrylamide resin (SPS-g-Acryl)

SPS-g-acrylamide was prepared by grafting acrylamide monomers onto the prepared SPS. This was done by weighing 5.0 g of SPS resin and placing it in a 100 mL 2-neck round bottom flask filled with 50 mL distilled water and equipped with a magnetic stirrer. After that, 5 g of acrylamide monomer was gradually added. The mixture was stirred at 40 °C for 3 hours to complete the grafting process. The resin was then dried at 60 °C after being rinsed with distilled water to remove any non-grafted monomer [10,11]. Scheme 1 shows the grafting reaction of the acrylamide monomer on the sulfonated polystyrene.

2.4. Synthesis of SPS-g-chitosan resin (SPS-g-Chit)

In a 100 mL round bottom flask, 5.0 g of chitosan was dissolved in 75 mL of 2% acetic acid, and the solution was gradually added to 5 g of SPS. The mixture was then heated for 3 hours at 60–65 °C. The SPS-g-Chit was filtered and rinsed three times with deionized water and acetone after allowing the liquid to cool to room temperature. The white product was dried using a vacuum desiccator [12,13]. The grafting reaction of the chitosan on the sulfonated polystyrene is depicted in Scheme 2.

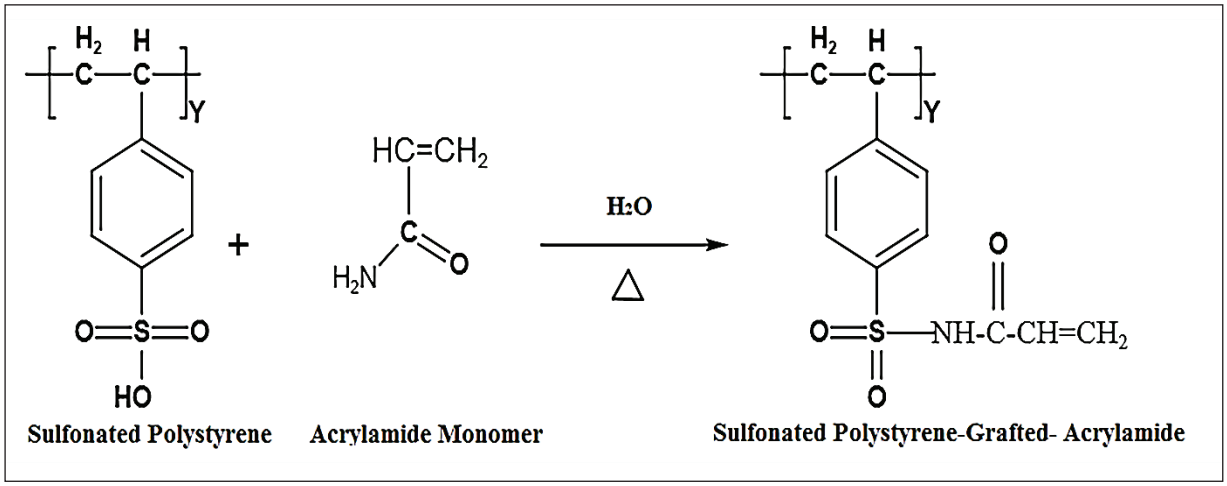

Scheme 1. The chemical equation of grafting acrylamide onto SPS resin

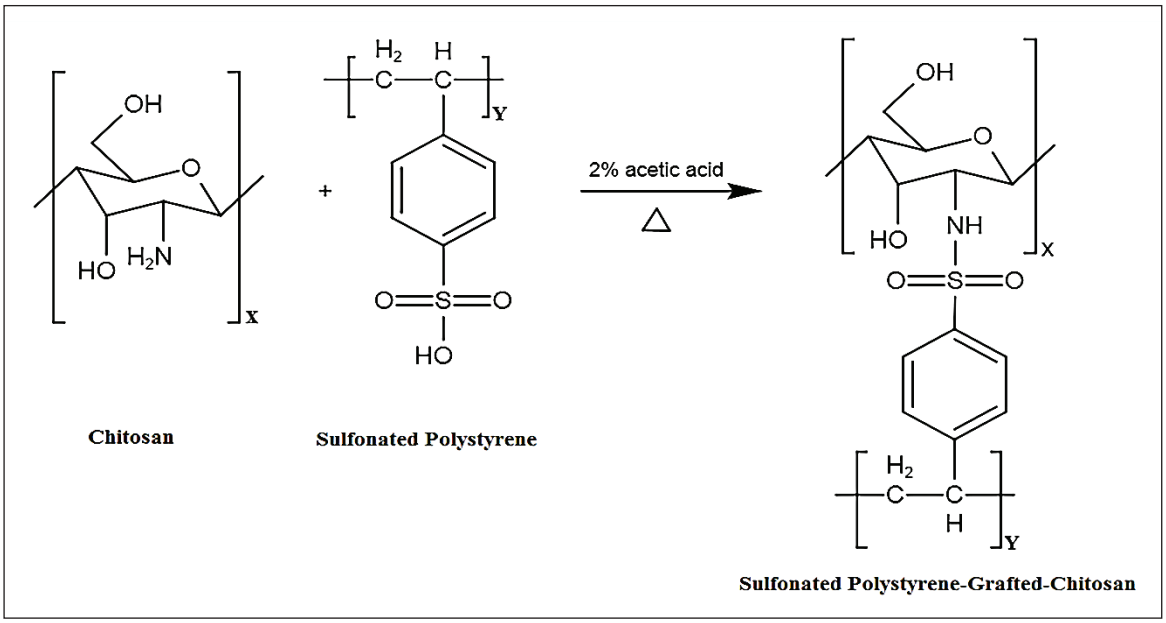

Scheme 2. The grafting reaction of SPS resin with Chitosan

2.5. Preparation of heavy metal ion standard solutions

standard solutions containing different concentrations of the element ions (Pb^{2+}, $Cd^{2+,}$ and Fe^{3+}) were made by diluting 1000 mg L^{-1} stokes solutions of their salts to 50 mg L^{-1} with double-distilled water. The salts of these elements used were $FeCl_3.6H_2O$, $Cd(NO_3)_2.4H_2O$, and $Pb(NO_3)_2$ [14]. All the concentrations of heavy metal ion solutions were measured before and after each experiment with a Flame atomic absorption spectrometer (Sens, Japan).

2.6. Heavy metal ions removal in batch method

Batch-mode ion exchange experiments were performed in beakers under constant time and temperature conditions [15,16]. The effect of SPS, SPS-g-Acryl, and SPS-g-Chit resins was studied in different pH ranges (2–8) to investigate the changeability and bonding of heavy metal ions (Pb^{2+}, Cd^{2+}, and Fe^{3+}) to the resins.

2.7. Study the effect of the pH on the resins by batch method

One gram of each resin (SPS, SPS-g-Acryl, and SPS-g-Chit) was treated with 25 ml of prepared aqueous solutions of Pb^{2+}, Cd^{2+}, and Fe^{3+} in pH ranges of 2, 4, 6, and 8 [17,18]. Each bottle containing resins was left at room temperature for an hour of shaking (175 rpm min^{-1}). After being filtered, the filtrate was collected in 50 mL of a plastic bottle.

2.8. Heavy metal ions removal by column method

This experiment was carried out to investigate the practicability of using SPS, SPS-g-Acryl, and SPS-g-Chit resins for heavy metal removal in a continuous flow column [19,20]. The water solution containing a mixture of the three heavy metal ions (Pb^{2+}, Cd^{2+}, and Fe^{3+}) was continuously passed through a vertical glass column with a height of 20 cm and a diameter of 1 cm. The operational parameters were set at a flow rate of 1 mL min^{-1}, an inlet heavy metal concentration of 50 mg L^{-1}, and 10 g of each prepared resin, as shown in Scheme 3. All tests were run continuously until the heavy metal removal efficiency decreased significantly. Finally, the concentrations of the Pb^{2+}, Cd^{2+}, and Fe^{3+} ions were determined with a flame atomic absorption spectrometer (F-AAS)

2.9. Regeneration of the loaded resins

For regeneration experiments, the best-loaded resin with metal ion removal obtained at pH 8 from a column method was chosen. One gram of the loaded resin was treated for a half-hour in a column system with a flow rate of 1 mL per minute with 30 mL of 0.1 N HNO_3 before being washed directly with 30 mL of deionized water and collected in plastic bottle samples [21].

2.10. Examination of single and mixture heavy metal ions by column method

A column with a 15 cm length and a 2.5-mm inner diameter was chosen for the analytical studies. It was then loaded with 1.0 g of SPS, SPS-g-Acryl, and SPS-g-Chit resins, and 25 mL of metal ion solutions (Pb^{2+}, Cd^{2+}, and Fe^{3+}) at a flow rate of 1 mL min^{-1} with a 50 mg L^{-1} concentration at pH 8. A mixture of the three ions (Pb^{2+}, Cd^{2+}, and Fe^{3+}) was prepared in 25 ml with a 16.6 mg L^{-1}, and the pH was adjusted to 8. The column was charged with 1 g of each resin. The mixture of ion solutions was allowed to flow through the loaded column at a rate of 1 mL min^{-1}. The descending solution was collected in portions for each component over an approximately 30-minute interval. The concentrations of the heavy metals were measured with F-AAS.

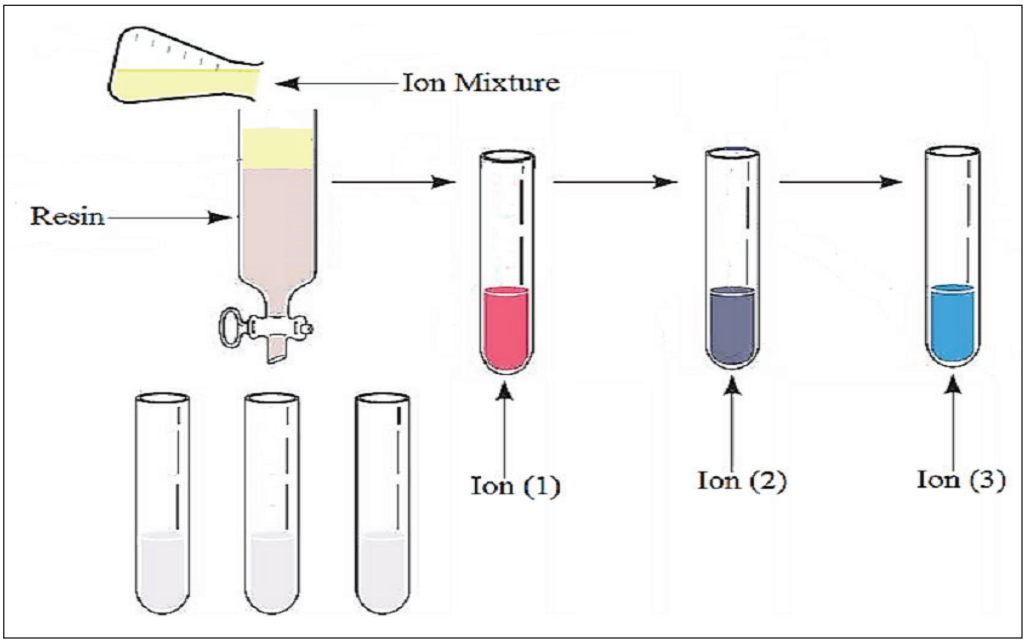

Scheme 3. The Schematic diagram for heavy metal ions removal by column method

3. Results and Discussion

The sulfonation reaction by sulfuric acid provides sulfonic groups $SO3H^+$ attached to the polystyrene backbone chains, giving ion exchange capacity to the polystyrene, which will be a center for the grafted acrylic monomer and chitosan polymer material to make up copolymers attached to the sulfonated polystyrene [10-12]. One advantage of this approach is the ability to precisely modify characteristics by adjusting the grafting or sulfonating conditions. The activation of the backbone polymer, the grafting of a monomer onto the produced polymer and the subsequent functionalization of the grafted polymer are all steps in the graft copolymerization technique of ion-exchange synthesis, yielding a product with high chemical selectivity [22,23]. Because heavy metals are typically produced by known sources, removing them rather than releasing them into the environment is preferable. The ion exchange capacity of the made resins is determined by the nature of the active groups, whose selectivity varies depending on the heavy metal ions and pH, the temperature and concentration employed, the nature of those ions, and the number of active groups. All of these are important in defining pH-dependent changeability. The pH was controlled by dilute solutions of 0.01 N nitric acid and 0.01 N ammonia solution [10]. The effect of the pH on the changeability of the three heavy metal ions (Pb^{2+}, Cd^{2+}, and Fe^{3+}) with the active groups of the prepared resins; SPS, SPS-g-Acryl, and SPS-g-Chit, was investigated by changing the pH from 2 to 8 with an initial concentration of ion solutions of 50 mg L^{-1}. Since metal cations attached to -SO_3H in functional groups were released and H+ ions were added after the ion exchange reaction, the pH after equilibrium was slightly reduced. Therefore, the metal precipitation did not take place [24,25].

3.1. Efficiency for heavy metal removal in the batch method

3.1.1.Sulfonated polystyrene resin (SPS)

The efficiency of the SPS resin was determined by measuring the concentration of the unabsorbed heavy metal ions present in the filtrate solutions of the metal ions separately. The results obtained are shown in Table 1 and Figure 2. It was found that Pb^{2+} has a low efficiency (7%) at pH 6 (46.34 mg L^{-1}) and high efficiency (33%) at pH 8 (16.73 mg L^{-1}). While cadmium ion has a low efficiency (٪٧٣) at pH ١٣,٥١) ٤ mg L^{-1}) and high efficiency (77%) at pH 8 (11.7 mg L^{-1}), and Fe^{3+} has the highest efficiencies slightly above (٪٩٨) at all pH values. This positively reflected the ability of the three prepared resins to work as ion exchange resins for heavy metal removal with high efficiency even with a low initial concentration. Using sulfonated polystyrene resin to separate Zn^{2+}, Cu^{2+}, and Cd^{2+} heavy metal ions from their solutions, Tran and his coworkers came to the same conclusion [6].

Table 1. The efficiency of SPS resin in a batch method towards different heavy metal ions at different pH (Unit: mg L^{-1})

pH	Pb	%Efficiency Pb	Fe	%Efficiency Fe	Cd	%Efficiency Cd
2	50.00	0.00	0.41	99.18	12.77	74.46
4	40.76	18.48	0.64	98.72	13.51	73.00
6	46.34	7.32	0.72	98.56	13.11	73.80
8	16.73	66.54	0.70	98.60	11.70	77.00

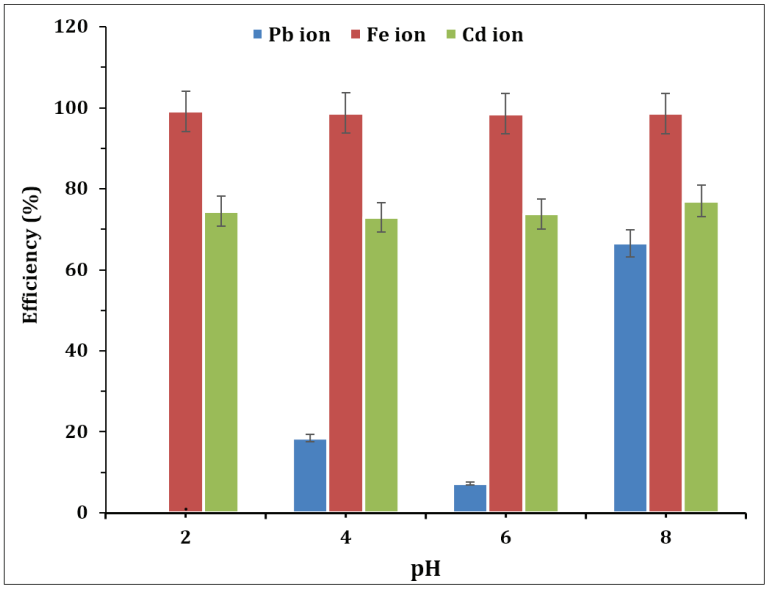

Fig. 2. The efficiency of SPS resin towards various metal ions at different pH in a batch method.

Table 2. Efficacy of SPS-g-Acryl in a batch method resin towards different metal ions at different pH (Unit: mg L^{-1})

pH	Pb	Efficiency Pb%	Fe	Efficiency Fe%	Cd	Efficiency Cd%
2	47.03	5.94	45.96	8.10	17.18	65.64
4	40.23	19.54	34.25	31.50	14.87	70.30
6	45.80	8.40	2.60	95.00	14.16	71.70
8	12.53	75.00	0.52	99.00	9.47	81.70

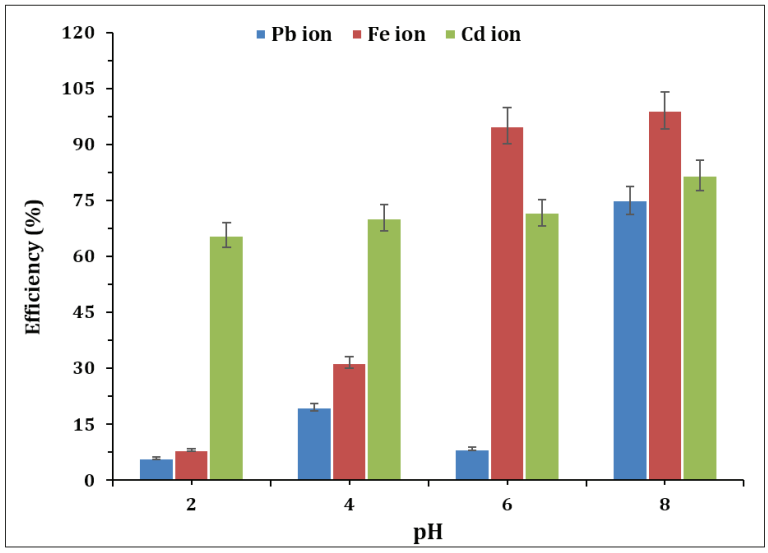

Fig. 3. The efficiency of SPS-g-Acryl resin towards various metal ions at different pH using the batch method

3.1.2.Sulfonate polystyrene-g-acrylamide (SPS-g-Acryl)

It is widely understood that most polymers used in water and wastewater treatment are acrylamide-based. The basic acrylamide monomer may be combined to provide polymers of varying iconicity. Though related, these exhibit somewhat different properties based on their monomer characteristics and how the copolymerization reaction takes place. SPS-g-acrylamide for water treatment due to its high cationic charge content. This polymer is primarily nonionic at pH <4, but deprotonation to the cationic form (SPS-g-Acryl) occurs at increasing pH (8) [26]. The effect of different pH values, which are 2, 4, 6, and 8, respectively, was studied for removing three heavy metal ions by SPS-g-Acryl resin, and the results are shown in Table 2 and Figure 3. It is noted that the Pb^{2+} ion had a low efficiency (5.94%) at pH 2 (47.03 mg L^{-1}) and high efficiency (75%) at pH 8 (12.53 mg L^{-1}). On the other hand, for Cd^{2+}, efficiency is low (65.64%) at pH 2 (17.18 mg L^{-1}) and high (81.70%) at pH 8 (9.47 mg L^{-1}). While for Fe^{3+}, lower efficiency (8.1%) was obtained at pH 2 (45.96 mg L^{-1}) and high efficiency (99%) at pH 8 (0.52 mg L^{-1}).

3.1.3.Sulfonated polystyrene-grafted-chitosan (SPS-g-Chit)

Sulfonated polystyrene is a polymerized styrene monomer by the sulfonation process. This process produces a grafted polymer with improved properties of this material and increases the crosslinking process, which leads to the expansion of the polymeric network [27.28]. When chitosan is grafted onto this network, it will lead to better properties due to the high functionality of the chitosan polymer, in addition to relying on the active groups whose work was previously mentioned and how their efficiency increases with increasing pH [29,30]. The effect of different pH values (2, 4, 6, and 8) was also investigated, and the results are shown in Table 3 and Figure 4. Pb^{2+} ions had a low efficiency (45.38%) at pH 2 (27.31 mg L^{-1}) and a high efficiency (85%) at pH 8 (7.5 mg L^{-1}). Whereas, Cd^{2+} and Fe^{3+} ions presented the highest efficiencies at all pH values, slightly higher than 99% (Table 3).

3.2. Treatment of single heavy metal ions by column method

Chromatography is a physical method of analysis and separation that uses a stationary phase with a large surface area and a mobile phase that flows through and generally contains the sample. The ion exchange column belongs to the (solid-liquid) chromatography category. When a mixture of two or more ions runs through the column in quantities that are minor compared to the column's total exchange capacity. It was completely absorbed by the resin and then separated from its constituents using an appropriate effluent to elute out the weakly bound ionic resin first, then the second ion, and so on. Elution is the process of separating these ions

Table 3. The efficiency of SPS-g-Chit in a batch method resin towards different metal ions at different pH (Unit: mg L^{-1})

pH	Pb	%Efficiency Pb	Fe	%Efficiency Fe	Cd	%Efficiency Cd
2	27.31	45.38	0.02	99.96	2.53	95.00
4	15.96	68.08	0.003	99.99	0.37	99.26
6	15.38	69.24	0.01	99.98	0.35	99.30
8	7.50	85.00	0.01	99.98	0.35	99.30

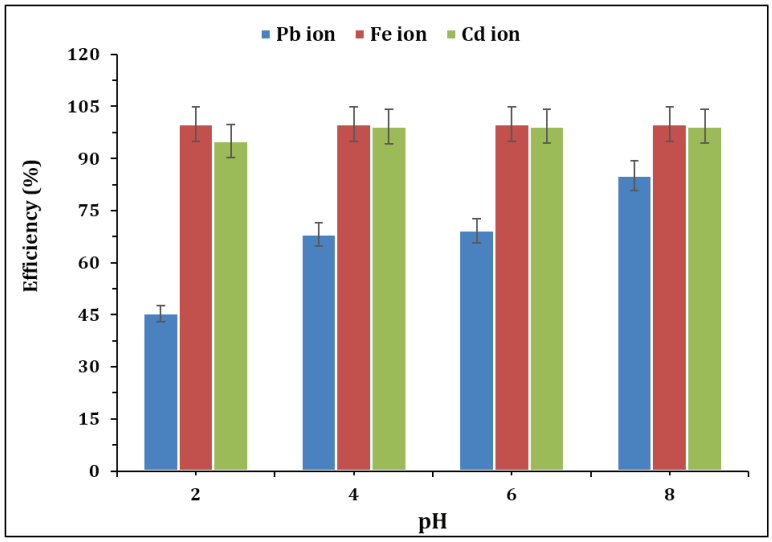

Fig. 4. The efficiency of SPS-g-Chit resin in a batch method towards various metal ions at different pH

until they are separated quantitatively. The Flame atomic absorption spectrometer method is. The optimum pH of 8 is favorable due to the partial hydrolysis of metal ions. As previously stated, the best efficiency result in pH obtained from the batch method revealed that the SPS-g-Chit resin was the most effective at ion exchange toward the three metal ions studied. Therefore, it was used for the removal of single metal ions by the column method. The pH 8 for the SPS-g-Chit resin is an exchange efficiency of 98.51% for Pb^{2+} and 99.76% for Cd^{2+}, whereas the exchange effectiveness of Fe^{3+} is reduced to 78.36%.

3.3. Treatment of heavy metal ions mixture

Table 4 shows that the efficiency of the SPS-Chit resin showed a high exchange efficiency for Pb^{3+} and Cd^{2+}. The grafting process of SPS with chitosan added another active group to increase the ion exchange efficiency of the SPS. The chitosan is characterized by its great affinity with metal ions due to its high content of amine groups in a rational manner, where the exchange mechanism depends on each of the protons of these amine groups or metal ions, as well as cross-linking, which tends to enlarge the polymeric network, resulting in better efficiency [31]. This was also confirmed in our previous studies; adsorption capacities were higher when the active group concentration increased [8,10,11]. The resin presented no exchange effectiveness for Fe^{3+}. This may be due to the ferric ions' ionic size differing from the ionic volume of lead and cadmium; these ions will compete for the exchange.

Table 4. The efficiency of SPS-g-Chit resin in a column method towards different metal ions at other times (Unit: mg L^{-1})

Time (min)	Pb	%Efficiency Pb	Fe	%Efficiency Fe	Cd	%Efficiency Cd
30	0.417	98.00	16.6	0	0.733	95.00
60	0	100	16.6	0	0.05	99.60
90	0	100	16.6	0	0.037	99.70
120	0	100	16.6	0	0.022	99.80
150	0	100	16.6	0	0.01	99.90

Table 5. Regeneration of the SPS-g-Chit resin

Metal Ion	Conc. (mg L^{-1})	Regeneration Efficiency(%)
Pb	0.14	99.72
Cd	0.10	99.81
Fe	7.85	84.31

3.4. Regeneration of Loaded Resins

The SPS-g-Chit resin was selected for the ion exchange regeneration resin experiment because it has the greatest changeability toward the three metal ions used in this study (Pb^{2+}, Cd^{2+}, and Fe^{3+}). Table 5 shows the outcomes that were attained. It demonstrates that after around an hour of treatment, the lead and cadmium ions showed the maximum percentage of regenerating efficiency, confirming their robust specifications regarding loading capacity and the ability to use the SPS-g-Chit resin as an ion exchanger in industrial processes.

4. Conclusion

Recycling single-use teacups and shrimp cortex chitosan as ion exchange materials limits the extraction of natural resources and reduces environmental pollution. Ion exchange resins can be produced and used with less expense using alternative materials; one such material is polystyrene waste that has been sulfonated, and its grafted acrylamide monomer and chitosan polymer derivatives have the potential to have a higher ion exchange capacity. H+s competing with metal ions at lower pH levels were discovered to be responsible for better results in treating metal ions at higher pH levels of 8. In terms of their active groups, chemical structures, and stereotypical structures, the produced resins varied in performance depending on the metal ion and resin type used. In conclusion, as the raw material used to create ion exchange resin is made from waste materials, sulfonated polystyrene and using chitosan originally extracted from shrimp cortex are thought to be technically and environmentally possible to remove heavy metals at a reasonable cost.

5. Acknowledgements

The authors thank the Department of Chemistry, College of Science, University of Basrah, Basrah, Iraq for supporting this work.

6. References

[1] G.W. Wetzel, Limnology, Lake and river ecosystems, Limnology, 37 (2001) 490-525. https://doi.org/10.1016/C2009-0-02112-6

[2] C. Cude, Oregon water quality index: A tool for evaluating water quality management effectiveness, J. Am. Water Res. Assoc., 37 (2001)125-137. http://dx.doi.org/10.1111/j.1752-1688.2001.tb05480.x

[3] C. Ramakrishnaiah, C. Sadashivaiah, G. Ranganna, Assessment of water quality index for the groundwater in Tumkur Taluk, Karnataka state, India, E-J. Chem., 6(2) (2009) 523-530. https://doi.org/10.1155/2009/757424

[4 G. Krantzberg, A. Tanik, J.S. Antunes do Carmo, A. Indarto, A. Ekdal, Advances in water quality control, J. Water Resour. Prot., 2 (2010) 995-996. https://doi.org/10.4236/jwarp.2010.212119

[5] T.A. Kurniawan, G.Y.S. Chan, W.-H. Lo, S. Babel, Comparisons of low-cost adsorbents for treating wastewaters laden with heavy metals, Sci. Total Environ., 366 (2006) 409–426. https://doi.org/10.1016/j.scitotenv.2005.10.001

[6] A.T.K. Tran, T.T. Pham, Q.H. Nguyen, N.T.T. Hoang, D.T. Bui, M.T. Nguyen, M.K. Nguyen, B.V. der Bruggen, From waste disposal to valuable material: Sulfonating polystyrene waste for heavy metal removal, J. Environ. Chem. Eng., 8 (5) (2020) 1-15. https://doi.org/10.1016/j.jece.2020.104302

[7] R. Geyer, J.R. Jambeck, K.L. Law, Production, use, and fate of all plastics ever

made, Sci. Adv., 3 (2017) e1700782. https://doi.org/10.1126/sciadv.1700782

[8] H. S. Al-Lami, M. A. Al-Marzok, Regenerating of consuming ion-exchange resin by graft polymerization for steam boiler wastewater treatment, Desalin. Water Treat., 222 (2021) 127-136. https://doi.org/10.5004/dwt.2021.27115

[9] R. S. Purbowatiningrum, N. B. A. Prasetya, T. D. Kusworo, H. Susanto, Sulfonated polystyrene and its characterization as a material of electrolyte polymer, IOP Conf. Series: J. Phys. Conf. Ser., 1025 (2018) 1-7. https://doi.org/10.1088/1742-6596/1025/1/012133

[10] H.A. Al-Mosawi, H.S. Al-Lami, N.A. Awad, Synthesis and characterization of some recycled polystyrene and chitosan based copolymers for water hardness removal, Bas. J. Sci., 39 (3) (2021) 496-514. https://doi.org/10.29072/basjs.2021311

[11] M. T. Sultan, H.S. Al-Lami, A.H. Al-Dujiali, Synthesis and characterization of alumina-grafted acrylic acid monomer and polymer and its adsorption of phenol and p-chlorophenol, Desalin. Water Treat., 150 (2019) 192-203. https://doi.org/10.5004/dwt.2019.23593

[12] E.S. Al-Allaq, H.S. Al-Lami, A.H. Al-Mowali, Synthesis and adsorption study of some chitosan acidic derivatives as dispersants for ceramic alumina powders, Egypt. J. Chem., 63(7) (2020) 2717-2736. https://doi.org/10.4236/jwarp.2010.212119_

[13] A.G. Ibrahim, A.Z. Sayed, H.A. El-Wahab, M. M. Sayah, Synthesis of poly(acrylamide-graft-chitosan) hydrogel: optimization of the grafting parameters and swelling studies, Am. J. Polym. Sci. Tec., 5 (2019) 55-62. https://doi.org/10.11648/j.ajpst.20190502.13

[14] P.A. Turhanen, J.J. Vepsäläinen, S. Peräniemi, Advanced material and approach for metal ions removal from aqueous solutions, Sci. Rep., 5 (2015) 1-8. https://doi.org/10.1038/srep08992

[15] L. Zhang, Y. Zeng, Z. Cheng, Removal of heavy metal ions using chitosan and modified chitosan: A review, J. Mol. Liq., 214 (2016) 175–191. http://dx.doi.org/10.1016/j.molliq.2015.12.013

[16] I. Bekri-Abbes, S. Bayoudh, M. Baklouti, E. Papon, D. Leclercq, Converting waste polystyrene into adsorbent: optimization of reaction parameters and properties, Prog. Rubber Plast. Recycle. Technol., 22 (2006) 179–193. https://doi.org/10.1177/147776060602200303

[17] A.K. Mishra, A.K. Sharma, Synthesis of γ-cyclodextrin/chitosan composites for the efficient removal of Cd(II) from aqueous solution, Int. J. Biol. Macromol., 49 (2011) 504–512. https://doi.org/10.1016/j.ijbiomac.2011.06.002

[18] Y. Wen, J. Ma, J. Chen, C. Shen, H. Li, W. Liu, Carbonaceous sulfur-containing chitosan–Fe(III): A novel adsorbent for efficient removal of copper (II) from water, Chem. Eng. J., 259 (2015) 372–380. https://doi.org/10.1016/j.cej.2014.08.011

[19] O. Hamdaoui, Dynamic sorption of methylene blue by cedar sawdust and crushed brick in fixed bed columns, J. Hazard. Mater., 138 (2006) 293–303. https://doi.org/10.1016/j.jhazmat.2006.04.061

[20] D. Núñez, J.A. Serrano, A. Mancisidor, E. Elgueta, K. Varaprasad, P. Oyarzún, R. Cáceres, W. Ide, B.L. Rivas, Heavy metal removal from aqueous systems using hydroxyapatite nanocrystals derived from clam shells, RSC Adv., 9 (2019) 22883–22890. https://doi.org/10.1039/C9RA04198B

[21] F. Dardel, T.V. Arden, Ion Exchangers in Ullmann's encyclopedia of industrial chemistry, Wiley-VCH, Weinheim, 2008. https://doi.org/10.1002/14356007.a14_393.pub2

[22] M.M. Nasef, H. Saidi, Preparation of crosslinked cation exchange membranes by radiation grafting of styrene/divinylbenzene mixtures onto PFA films, J. Membr. Sci., 216 (2003) 27-38. https://doi.org/10.1016/S0376-

7388(03)00027-9

[23] E.Y. Safronova, D.V. Golubenko, N.V. Shevlyakova, M.G. D'yakova, V.A. Tverskoi, L. Dammak, D. Grande, A.B. Yaroslavtsev, New cation-exchange membranes based on cross-linked sulfonated polystyrene and polyethylene for power generation systems, J. Membr. Sci., 515 (2016) 196-203. https://doi.org/10.1016/j.memsci.2016.05.006

[24] T. Liu, L.W. Zhong, L. Lin, Y. Xi, Enhanced chitosan\FeO nanoparticles beads for hexavalent chromium removal from wastewater, Chem. Eng. J., 189 (2012)169-202. https://doi.org/10.1016/j.cej.2012.02.056

[25] A. Tzereme, E. Christodoulou, G.Z. Kyzas, M. Kostoglou, D.N. Bikiaris, D.A. Lambropoulou, Chitosan grafted adsorbents for diclofenac pharmaceutical compound removal from single-component aqueous solutions and mixtures, Polymers, 11(3) (2019) 497-520. https://doi.org/10.3390/polym11030497

[26] D.A.Mortimer,Syntheticpolyelectrolytes—A review, Polym. Int., 25 (1991) 29-41. https://doi.org/10.1002/pi.4990250107

[27] C.P. Jiménez-Gómez, J.A. Cecilia, Chitosan: A natural biopolymer with a wide and varied range of applications, Molecules, 25(17) (2020) 3981. https://doi.org/10.3390/molecules25173981

[28] A.S.K. Kumar, U. Chinta, R. Vidya, N. Rajesh, Microwave assisted preparation of n-butyl acrylate grafted chitosan and its application for Cr (VI) adsorption, Int. J. Bio. Macro., 66 (2014)135-143. https://doi.org/10.1016/j.ijbiomac.2014.02.007

[29] S.P. Kuang, Z. Wang, L. Liu, Z. Wu, Preparation of triethylenetetramine grafted magnetic chitosan for adsorption of Pb (II) ion from aqueous solutions, J. Hazard. Mater., 260 (2013) 210-219. https://doi.org/10.1016/j.jhazmat.2013.05.019

[30] R.S. Dongre, Chitosan-derived synthetic ion exchangers: characteristics and applications, new trends in ion exchange studies, London, Intech Open, 2018. https://doi.org/10.5772/intechopen.78964

[31] F.M. Alminderej, A.M. Younisa, A.E. Albadri, W.A. El-Sayed, Y. El-Ghoul, R. Ali, A.M.A. Mohamed, S.M. Saleh, The superior adsorption capacity of phenol from aqueous solution using modified date palm nanomaterials: A performance and kinetic study, Arab. J. Chem., 15 (2022) 104120. https://doi.org/10.1016/j.arabjc.2022.104120

Anal. Methods Environ. Chem. J. 6 (1) (2023) 29-57

AMECJ

Research Article, Issue 1
Analytical Methods in Environmental Chemistry Journal
Journal home page: www.amecj.com/ir

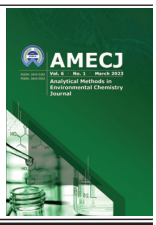

A review of colorimetric and fluorometric detection of arsenic: arsenate and arsenite

Madhawa Pradeepa Nawarathne [a], Ruvini Lakmali Weerensinghe [b], and Chathuranga Dharmarathne [c,*]

[a] *Postgraduate Institute of Science, University of Peradeniya, Sri Lanka*
[b] *Faculty of Graduate Studies, University of Sri Jayewardenepura, Sri Lanka*
[c] *Department of Biological Sciences, Macquarie University, Sydney, NSW, Australia*

ARTICLE INFO:

Received 6 Dec 2022
Revised form 24 Jan 2023
Accepted 27 Feb 2023
Available online 28 Mar 2023

Keywords:
Arsenate,
Arsenite,
Colorimetric,
Fluorometric,
Nanoparticles

ABSTRACT

Arsenic is a highly toxic metalloid that forms different chemical states in nature, including arsenate and arsenite, as common inorganic forms. Exposure to arsenic may cause adverse effects on human health and the environment. Therefore, the detection of arsenic is critical. Exploring new approaches with low detection ranges and high sensitivity is crucial. This review paper consists of optical methods, including colorimetric and fluorometric methods, which detect arsenite and arsenate (μg L^{-1}). Initially proposed colorimetric approaches such as the Gutzeit and molybdenum blue method can easily to use. However, the production of toxic substances limits their applications. Later, structurally modified molecules, nanoparticle-based assays, and their modifications are used for arsenic detection. Fluorometric methods also have noticeable attention to arsenic detection. Fluorescent approaches reported in this paper are based on semiconductor nanomaterials, other nanomaterials, and their modifications, etc. In addition, arsenate's catalytic and inhibitory activity on enzyme activity can be used to detect arsenic through colorimetric and fluorometric methods. This review highlighted the advantages, disadvantages, comparisons, and uses of colorimetric and fluorometric methods in detecting arsenite and arsenate.

1. Introduction

Arsenic is the 20th most abundant and widely distributed element in the earth's crust. It is categorized as a metal and as a metalloid [1]. Arsenic occurs in several chemical oxidation states in nature, such as As (V), As (III), As (0), and As (-III) [2]. Also, it can exist in both organic and inorganic forms. Inorganic arsenic exists as arsenate [As (V)] and arsenite [As (III)], while organic forms are monomethyl arsenic acid (MMA), dimethyl arsenic acid (DMA), dithiol arsenate (DTA), etc. [3]. Even the trace concentration of arsenic shows higher toxicity than most other heavy metals. Both inorganic forms of arsenate and arsenite are hazardous and toxic. Among them, arsenite is considered the most toxic form [4]. Contaminated groundwater, wastewater, and drinking water are the main sources of arsenic that enter the environment through industrial operations, agricultural activities, etc. [4-6]. Exposure to arsenic in the long term can cause adverse effects on human health, such as skin cancers, skin lesions, neurotoxicity, cardiovascular disease, diabetes, etc. [5]. Therefore, the detection and removal of arsenic are critical to human health. The World Health Organization (WHO) and US Environmental Protection Agency (USEPA) have stipulated some guidelines with a 0.01 mg L^{-1} 10 μg

*Corresponding Author: Chathuranga Dharmarathne
Email: chathurangadharma@gmail.com
https://doi.org/10.24200/amecj.v6.i01.224

L^{-1} permissible limit of arsenic for drinking water [6]. Therefore, a series of techniques are developed to monitor the arsenic concentration. Numerous laboratory techniques, including Atomic Absorption Spectroscopy (AAS) [7], Atomic Fluorescence Spectroscopy (AFS) [8], Inductively Coupled Plasma Atomic Emission Spectroscopy (ICP-AES) [9], Inductively Coupled Plasma Mass Spectroscopy (ICP-MS) [9,10], Graphite Furnace Atomic Absorption (GFAA), Hydride Generation Atomic Adsorption (HGAA) and Neutron Activation analysis [11] are some of the methods which currently being used. They provide accurate detection of arsenic even at trace concentrations. High expensive instrumentation, the requirement for sophisticated laboratory setup, significant maintenance and operation expertise, and producing highly toxic chemicals during the process are the drawbacks of these methods. Also, the inability to be used in the field is one of the significant practical limitations [12]. Therefore, various chromatographic methods, electrochemical methods [13, 14], and optical methods are developed to overcome these limitations [15]. Among them, optical methods are essential due to their high sensitivity, selectivity, simplicity in operation, fast response, cost-effectiveness, and offer field monitoring. Therefore, optical methods are considered as promising techniques for arsenic detection [14,16,17,18]. This review presents current optical methods including colorimetric and fluorometric methods for detecting arsenate and arsenite.

2. Experimental

The different technologies based on colorimetric and fluorometric methods were used to detect and analyse arsenic (arsenite and arsenate) in various matrixes.

2.1. Colorimetric detection of arsenite and arsenate

2.1.1.Advancement of colorimetric methods and detection based on structurally modified molecules.

Colorimetric methods are based on the Gutzeit reaction, which detects arsenic quantitatively. This method relies on the reaction of arsenic gas with hydrogen ions to form a yellow stain on mercuric chloride paper in the presence of reducing agents. However, certain limitations are followed when analyzing the groundwater samples, and it generates highly toxic arsine gas and byproducts of mercuric compounds. Therefore, protective equipment is required for the analysis procedure [19,20]. In addition, traditional methods such as molybdenum blue [21-25], ethyl violet, and gallocyanin can be used for sensing arsenic, yet, the interferences intervened with the results, and low sensitivity hinders its applicant the resulting [26]. Therefore, scientists have continuously tried to remove the generation of toxic chemicals and interferences in the detection. Some arsenic detection methods are involved with structurally modified molecules. For example, norbornene-based rhodamine monomers (Nor-Rh) and their polymer form (PNor-Rh) are used for very selective detection of arsenite colorimetrically and fluorometrically in the presence of potassium iodate and hydrochloric acid. They used an open form of rhodamine which is pink and highly luminescent. When arsenite was present in the sample, the reaction led to the oxidation of As (III) to As (V) by iodate reduction reaction to iodine. As a result, the solution changed its pink color to brown colorimetrically and observed green color fluorometrically. With the increase in arsenite concentration, the intensity of the brown color increased. As a result, they developed a simple and easy practical device based on a polymer-coated paper strip for field analysis. Also, they synthesized a thiol-based norbornene monomer (Nor-Th) and its polymer form (PNor-Th) for arsenite removal from water [27]. Aptamers are single-strand RNA or DNA oligonucleotides that can bind with target ions or molecules. Recently aptamers are used as a recognition element for developing arsenic detection methods [28-33]. For example, Zhou and colleagues [33] proposed a method for colorimetric detection of arsenite based on regulating hemin peroxidase catalytic activity using arsenic binding aptamers. They used

an arsenic-binding DNA aptamer called Ars-3. Hemin acts as a catalyst that can catalyze many oxidation reactions. But the catalytic activity of hemin is very slow in the aqueous medium. Catalytic activity can be improved by hemin binding onto the surface of nanosheets or covered with guanine-rich oligonucleotide by forming an active form of the G-quadruplex structure. Arsenic binding aptamers can inhibit hemin catalytic activity temporarily. In the presence of arsenite, As (III) binds to Ars-3 and forms an aptamer-As (III) complex. Therefore, an oxidation reaction occurs in TMB molecules to generate yellow diamine products. While the absence of arsenite, Ars-3 aptamers complex with pyrrole rings of hemin. As a result, the catalytic activity of hemin is decreased and generates blue products of cation radicals. Therefore, this method is susceptible and selective for arsenite. Figure 1 shows the schematic description of the As (III) detection by arsenic binding aptamers.

Traditional methods are easy to perform and inexpensive, yet restrained by the generation of toxic products. In addition, the difficulty increases due to complex redox reactions and complex separations. Therefore, other anions and cations can interfere with the analysis. The same assay can be used for both colorimetric and fluorometric detections. Also, redox reactions are specific to the analyte. Therefore, the involvement of other ions can be negligible. These assays/polymer-coated paper strips can be used for field analysis [33,34].

2.1.2. Usage of metal nanoparticles

Researchers enhanced the involvement of novel methods with non-toxic product generation. Recently, they have used metal nanoparticles and their modifications to detect heavy metals, including arsenic, to obtain a visual color change in the analysis [35]. It is based on the excellent optical properties of nanoparticles, such as high sensitivity, selectivity, and high extinction coefficient in visible regions. Gold nanoparticles [36-40] and silver nanoparticles [41-49] are mainly used for analysis procedures. Color change occurs due to the aggregation of nanoparticles with the target analyte and size-dependent Surface Plasmon resonance (SPR) properties of nanoparticles [48,49].

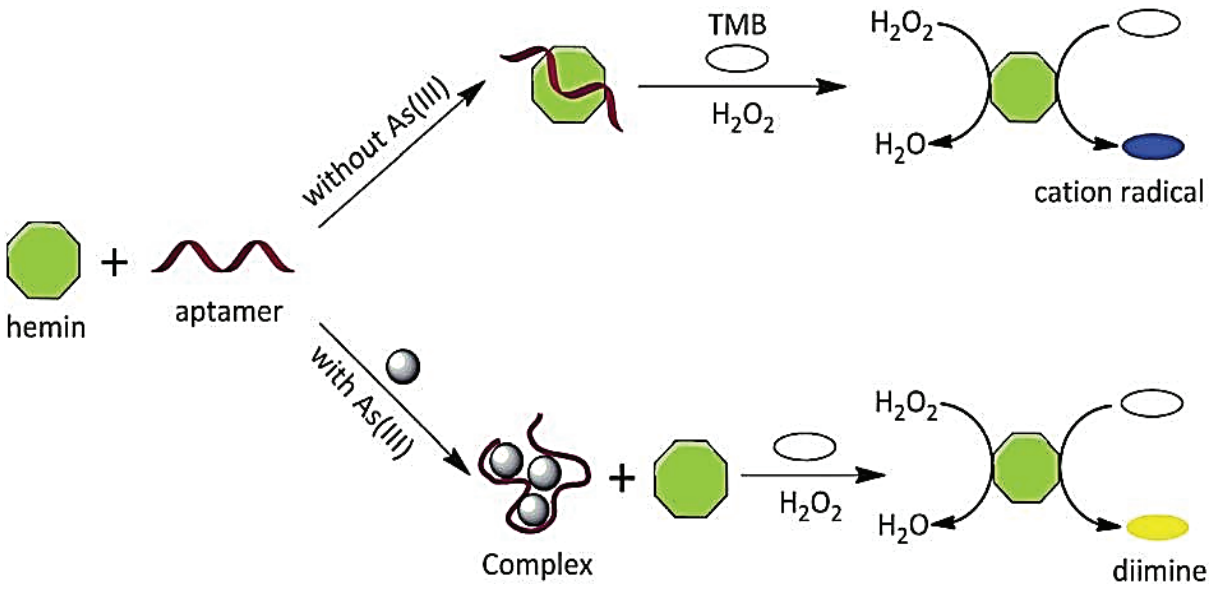

Fig. 1. Schematic description of the colorimetric detection of As (III) based on the inhibition of hemin peroxidase activity by arsenic-binding aptamers [33]

2.1.2.1. Detection based on the modified silver nanoparticles.

Recently, nanotechnology has been commonly used in optical detection due to the uniqueness of its chemical, biological, and physical properties. Different types of nanoparticles show different functions by providing different optical, fluorescent, and magnetic properties. And their modifications enhance their detection ability [50]. Thiol-based ligands are commonly used because they have an excellent capacity to bind with arsenic [51,52]. As an example, a multiligands assay was synthesized for the detection of arsenite based on silver nanoparticles (AgNPs) which were modified by multiligands containing glutathione (GSH), dithiothreitol (DTT) and asparagine (Asn). Thiol-based ligands bind to the surface of AgNPs, which can vastly enhance the selectivity toward the arsenite. Aggregation occurs due to the formation of As-O and As-S linkages between GSH/DTT/Asn-AgNPs and As (III). Color change occurs from yellow to light pink and purple with increased arsenite concentration. Figure 2 shows the GSH/DTT/Asn-AgNPs complex formation and aggregation with arsenite. This method is promising for the colorimetric detection of arsenite with high sensitivity, low cost, and facility for rapid onsite detection [52].

In addition, arsenic adsorbents such as iron (III) oxide are widely used for detection procedures. Siangproh and his group [53,54] developed silver nanoplates (AgNPls) to detect arsenite and arsenate. Although, the matrix effect interferes with the detection. Therefore, they synthesized and applied ferrihydrite-coated silica gel (SiO_2-Fh) modified by the Eric Arifin method to adsorb arsenic (arsenate and arsenite). SiO_2-Fh has a high affinity to selectively adsorb arsenic and avoid the matrix effect. When arsenic adsorbs onto the SiO_2-Fh, the dark blue color of AgNPls was changed to purple, pink, orange, and yellow respective to the concentrations of arsenic present in the sample. Both arsenate and arsenite show similar behavior on the color changes of AgNPls. Therefore, this method is suitable for the determination of total inorganic arsenic.

2.1.2.2. Detection based on the modified gold nanoparticles

Gold nanoparticles (AuNPs) have numerous applications in the optical detection of heavy metals, including arsenate, arsenite, and aromatic compounds [54,55]. Most of the AuNPs based assays rely on modifications with specific binding ligands. Priyadarshani *et al.* [55] synthesized gold nanorod (GNR) based sensor GNR-PEG-DMSA. It is highly sensitive, specific, and cost-effective for rapidly detecting arsenite and arsenate. GNR-PEG-DMSA sensor is synthesized through conjugation of GNR with poly (ethylene glycol) methyl ether thiol (mPEG-SH) followed by the addition of meso-2,3-dimercaptosuccinic acid. CTAB is

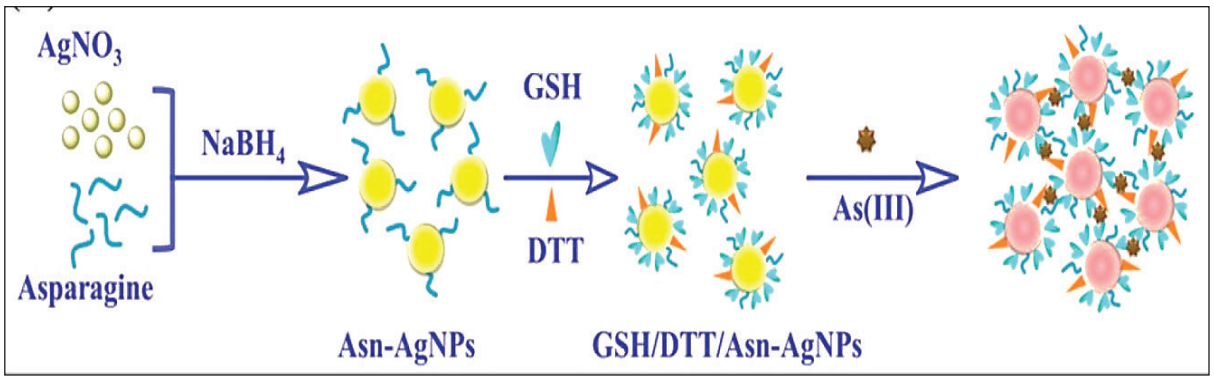

Fig. 2. Illustration of synthesis of GSH/DTT/Asn-AgNPs used as a colorimetric probe for As (III) detection [52]

used as a surfactant which is capped with GNR, and the stability of the sensor is maintained by PEG. DMSA is a ligand that covalently binds to GNR and has a high affinity to arsenic. Also, the arsenite and arsenate bind with free –SH groups of DMSA, which are present on the surface of GNR. Aggregation initiates with the formation of As-thiolate complexes between nanorods. The Colour of the solution changes from dark bluish-purple to almost colorless. This sensor has a regenerating ability using strong chelating agents like EDTA. Also, it can be used to quantitatively determine the total arsenic in a sample using a small amount of sensor materials. Figure 3 shows the synthesis of the GNR-PEG-DMSA sensor and its interactions with As (III) and As (V).

The same group proposed Europium functionalized single gold nanoparticle-based new sensor GNP-MMT@Eu for colorimetric detection of trace concentration of both As (III) and As (V). Nanosensor is synthesized by chemical conjugation of GNPs with 2-mercapto-4-methyl-5-thiazoleacetic acid (MMT) followed by fluorescent europium chloride [Eu (III)]. Aggregation occurs in the presence of arsenite or arsenate by binding to the surface of GNP-MMT@Eu. It occurs through coordinated Eu-OH groups consisting on the surface of GNP-MMT@Eu via electrostatic attraction and covalent-type interactions. Afterward, it forms the GNP-MMT@Eu-As (III)/As (V) complex. Arsenate shows rapid and more sensitive color changes for the nanosensor than the arsenite. The initial color of the sensor gradually changes from red to blue. Sensor-based paper strips can detect total arsenic content in field applications, and most importantly, the sensors can be regenerated. Here, Figure 4 shows the synthesis of gold nanosensors and its interaction with As (III) and As (V) [56]. Zhang and co-workers [57] proposed an arsenate detection method based on the inhibitory effect of arsenate on acid phosphatase (ACP) bioactivity using citrate-capped AuNPs as the optical reporter [57-59]. They used adenosine 5'-monophosphate (AMP) as the substrate and prevented AuNPs from aggregation. The activity of ACP hydrolyses the charged nucleotide into the uncharged nucleoside. The presence of ACP dephosphorylation of AMP to adenosine and resulting adenosine leads to the aggregation by nucleoside binds to AuNPs through metal-ligand interaction by replacing weakly bound citrate. As a result, the color change occurred from red to purple to blue. But in the presence of As (V), the color of the solution reversed from blue through purple to the initial red color due to the inhibitory

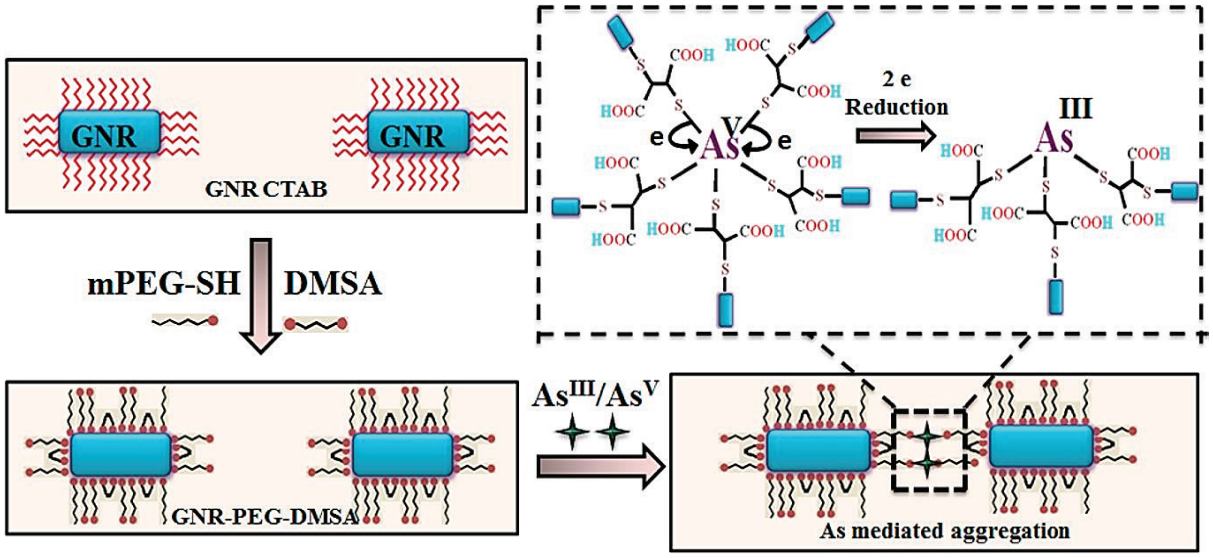

Fig. 3. Illustration of the fabrication of GNR-PEG-DMSA sensor and its interactions with As (III) and As (V) [55]

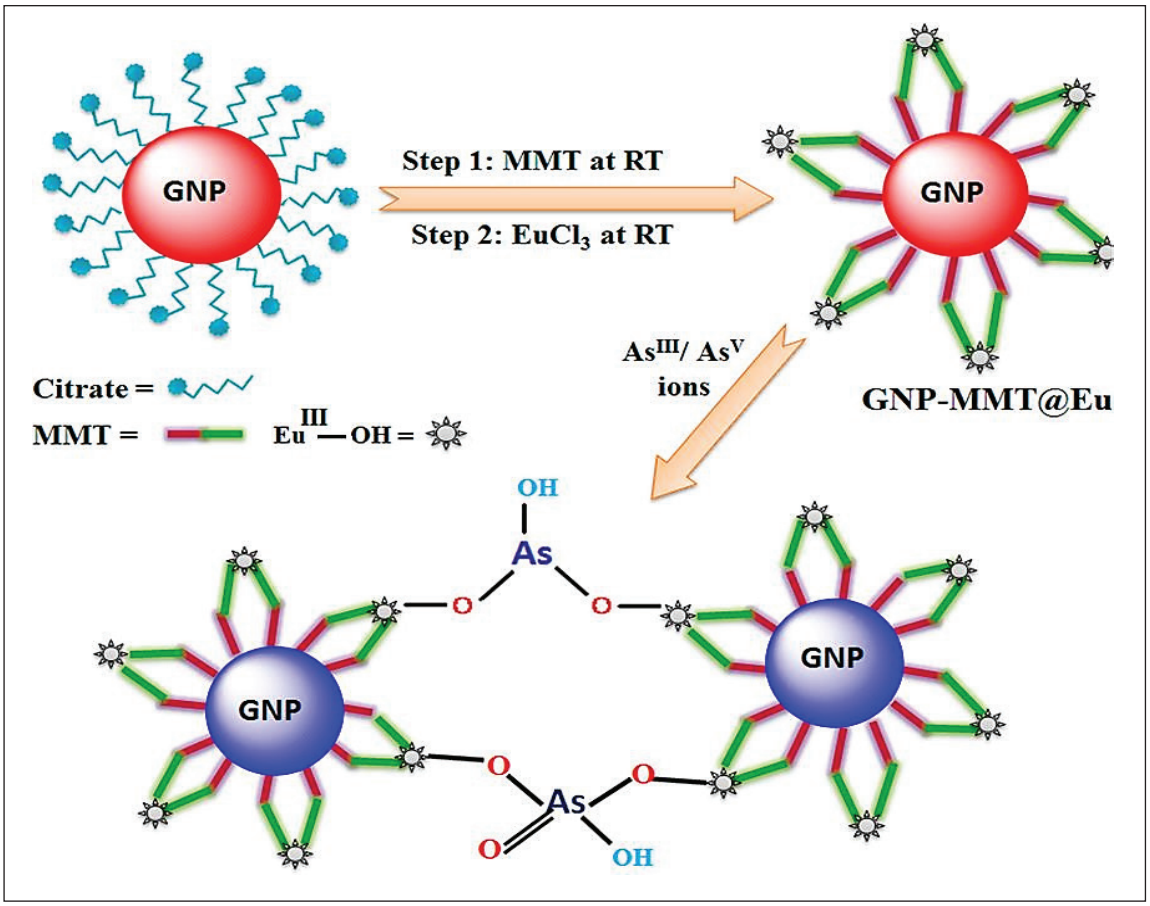

Fig. 4. Schematic of the synthesis of the gold nanosensor, GNP-MMT@Eu, and its aggregation with arsenate and arsenite [56]

effect of As (V) on ACP activity by competing with AMP in the enzymatic reaction. The color change occurred respectively with the As (V) concentration increment. This sensor has a remarkable sensitivity towards As (V). However, there are some limitations in this assay. Their visible detection limit is a bit higher than the standard limit of WHO, and certain concentrations of Cu^{2+}, F^-, and $H_2PO_4^-$ can interfere with arsenate detection. Figure 5 shows the catalytic activity of ACP on AMP with As (V) and without As (V) and color changes in AuNPs.

A simple paper-based microfluidic device was developed to rapidly detect arsenite in low concentrations with a low detection range. The microfluidic device is based on modified gold nanoparticles (Au-TA-TG), that can rapidly interact with arsenite to produce a visible dark bluish-black precipitate at the interfacial zone. Figure 6 depicts the schematic diagram of the microfluidic device, which is made up of "Y"-shaped Whatman filter paper and two arms that are immersed in modified gold nanoparticle solution and arsenic sample separately. Due to the capillary action of the "Y"-shaped device, fluids start flowing into the channel. When Au-TA-TG solution meets arsenite ions, a bluish-black precipitate can be observed quickly. Thioctic acid (TA) and thioguanine (TG) are used to modify gold nanoparticles that have a specific ability to bind and interact with arsenite. The color change occurs due to the aggregation of gold nanoparticles and arsenite. The portable, power-free microfluidic device is cost-effective and safe, which makes it suitable for environmental analysis [60].

Tetradecyl (tri hexyl) phosphonium chloride has a strong interaction with arsenite. This ionic liquid is modified with gold nanoparticles to produce highly

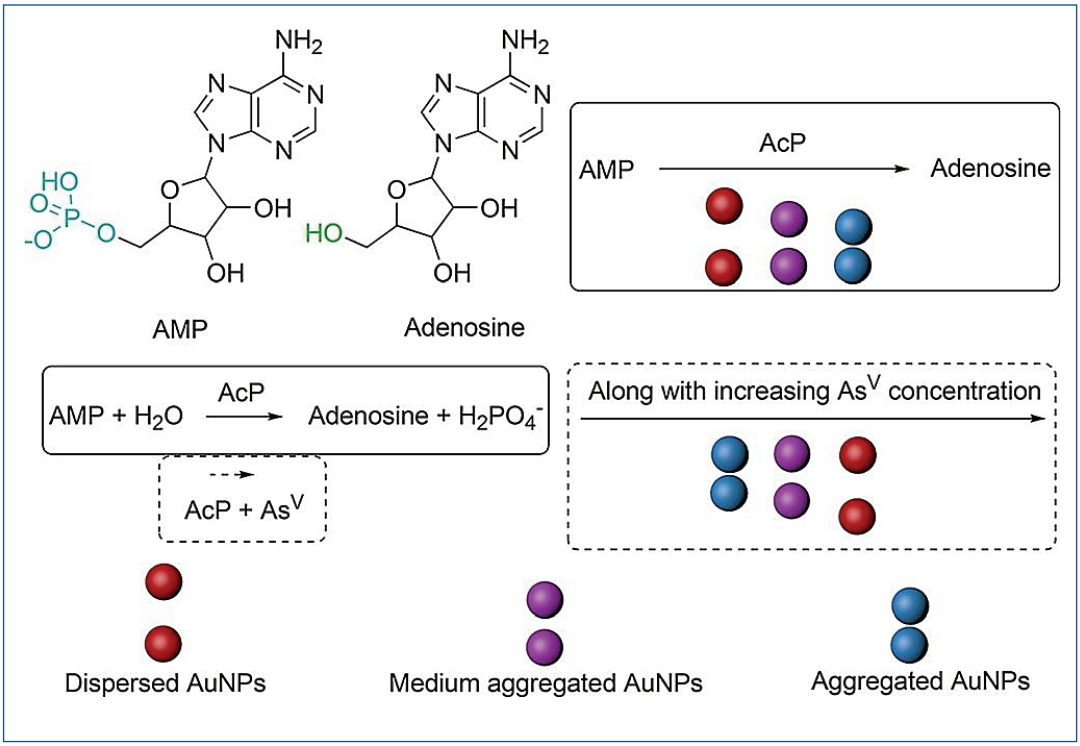

Fig. 5. Illustration of bioactivity of ACP on AMP with arsenate and without arsenate and color changes in AuNPs with an increment of arsenate concentration [57]

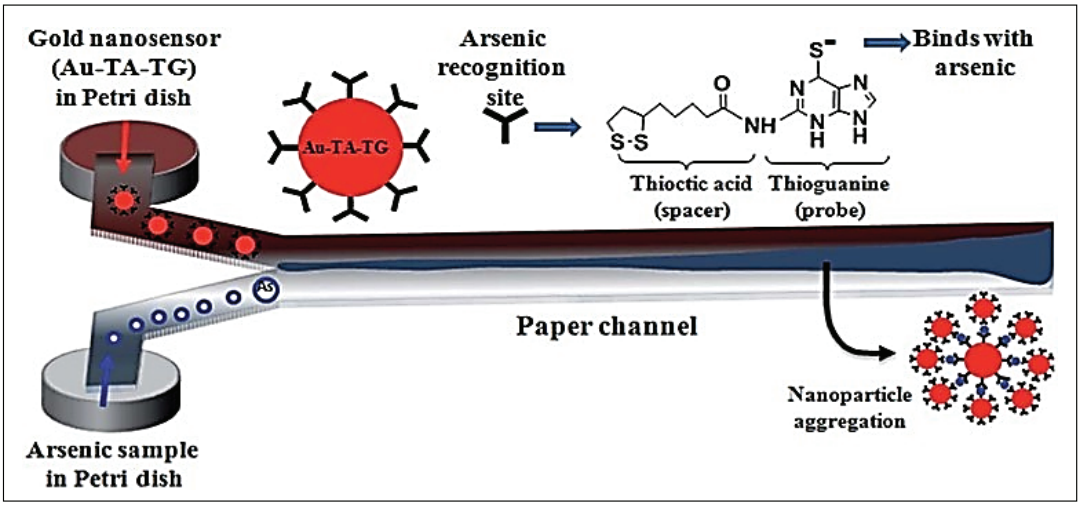

Fig. 6. Illustration of a paper-based microfluidic device for the detection of arsenite using modified gold nanoparticles (Au-TA-TG) [60]

sensitive visual observations for arsenite detection, with the probe color changing from red to blue in the presence of arsenite. The total amount of inorganic arsenic can be determined using this probe. The low cost and high tolerance to common ions make the probe suitable for field analysis. Figure 7 shows the behavior of the probe in the presence of arsenite and arsenate [61].

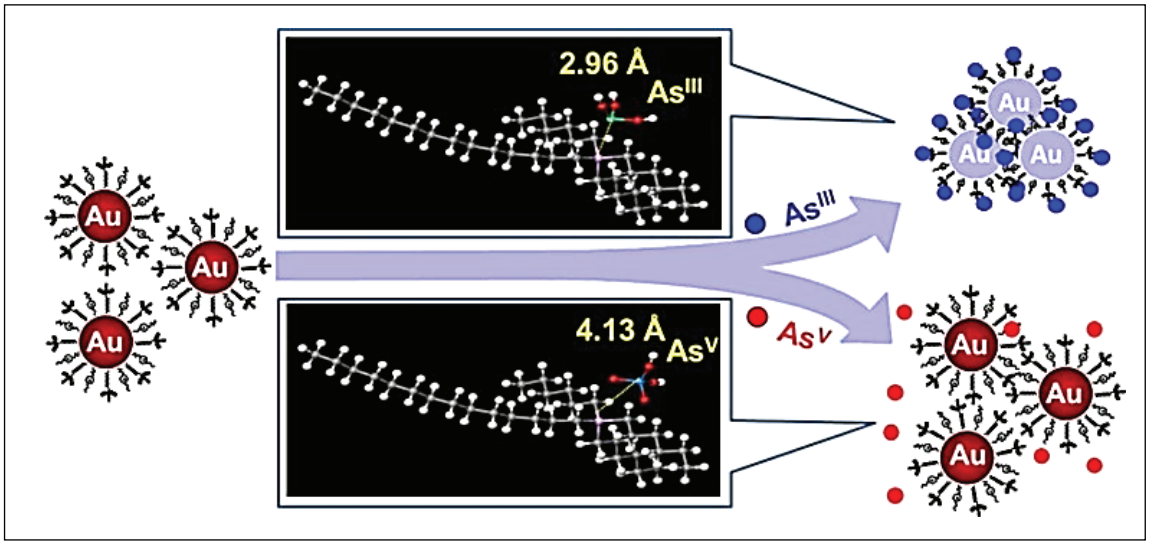

Fig. 7. Illustration of gold nanoparticle probe and its behavior with the presence of arsenic [61]

The unique properties of nanoparticles offer many advantages including simple, low cost, less time-consuming, nontoxic, and ease of data interpretation. Modifications of nanomaterials increase selectivity and sensitivity. Moreover, some sensors can regenerate and are reusable. However, there are some disadvantages such as complicated preparation processes, and long reaction times. Also, the external environment can be affected by nanoparticles' stability, and continuous temperature maintenance is essential [55-61].

2.1.2.3. Detection based on unmodified gold nanoparticles

Gold nanoparticle-based colorimetric assays consist of ligand modifications that can be synthesized through expensive processes. Therefore, scientists were encouraged to develop unmodified metal nanoparticles conveniently and cost-effectively [62,63]. For example, a simpler and more economical assay that relied on different adsorption properties on AuNPs between random coil G-/T-rich ssDNA and folded DNA bound to arsenite was synthesized. While arsenite can easily attach to the G-/T-rich ssDNA via hydrogen bonds, G-/T-rich ssDNA can efficiently adsorb onto AuNPs that prevent the salt-induced aggregation by enhancing the electrostatic repulsion between ssDNA-adsorbed AuNPs and maintain the stability of AuNPs. Therefore, adding enough salt leads to the collection, and the color of unmodified AuNPs changes from red to blue resulting in ssDNA becoming compact and folded DNA. Figure 8 represents the colorimetric strategy of arsenite detection. Visual inspection can be used for semi-quantitative detection of arsenite, while UV/Vis absorbance spectroscopy technique can be used for quantitative detection [63].

Peptide ligands are promising materials for desired target analytes, including metals, biomolecules, and drugs [64,65]. Yang et al. [65] have specifically As (III)-binding heptapeptide sequences of T-Q-S-Y-K-H-G through phage display peptide library techniques using a biopanning process. The sensing system contains a unique peptide sequence for target recognition and unmodified AuNPs as the sensing probe. Due to slow aggregation and the prerequisite of high concentration of heptapeptide, cysteine residue (C terminal) is conjugated to the end of the heptapeptide sequence resulting in an octapeptide sequence of T-Q-S-Y-K-H-G-C which induce the aggregation of AuNPs more effectively. In the absence of As (III), the octapeptide can bridge with AuNPs, and the color of unmodified AuNPs changes from wine red to blue. Nitrogen-containing functional groups (-NH, -N=), –OH groups, and sulfur-containing groups (-SH), which are present in the peptide sequence, can bind

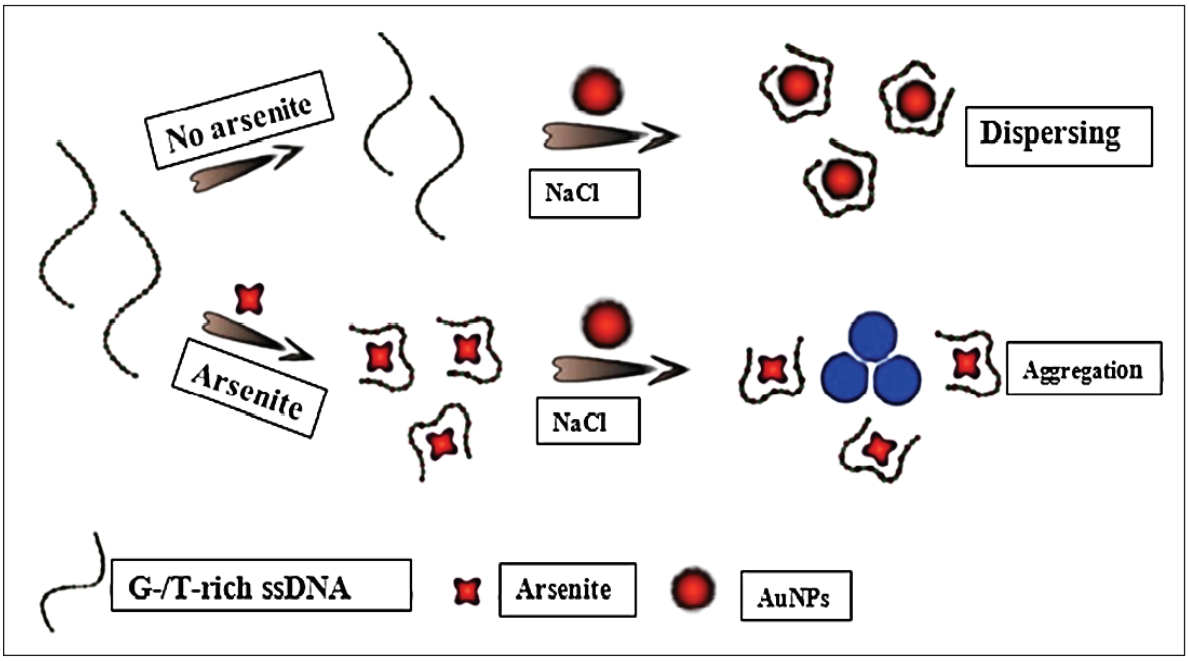

Fig. 8. AuNPs-based colorimetric strategy for arsenite detection [63]

with As (III) via strong hydrogen bonds. With As (III) presence, octapeptide binds to As (III) and prevents the peptide binding with AuNPs; the color remains red. UV/Vis spectroscopic technique can determine As (III) concentration. As (V) and other metal ions do not have significant affection on As (III) detection. Therefore, this method is unique for the determination of arsenite. Operation is easier and more convenient than other complicated methods based on modified AuNPs, aptamers, and aggregation inducers. Unmodified nanoparticles can be used for naked-eye detection without complicated instrumentation and much knowledge. They do not require chemical modifications. Therefore, they are more economical, convenient, simple, sensitive, selective, reliable, and cost-effective. Other competitive ions do not interfere or slightly interfere with the detection [62-65]

2.1.2.4. Detection based on arsenate adsorption on nanozymes

Some nanomaterials, such as metal oxide nanoparticles, noble metal nanoparticles, carbon-based nanomaterials, and two-dimensional nanomaterials, have a natural enzyme-mimicking activity called nanozymes. Among them, two-dimensional nanomaterials show excellent enzyme-mimicking activity. Therefore, researchers are interested in using nanozymes due to their ease of mass production with low cost, robustness, high stability, etc. For example, cobalt oxyhydroxide (CoOOH) nanoflakes, a promising material used in catalysis material for dual-mode assay of arsenate detection, rely on its peroxidase-like activity. CoOOH nanoflakes are synthesized by a one-pot ultrasonic process used for "signal off" colorimetric detection of arsenate. This excellent peroxidase-like activity of CoOOH nanoflakes can effectively catalyze chromogenic substrate (ABTS) into its green color oxidized product ($ABTS_{OX}$). The presence of arsenate, As (V), adsorbs onto the CoOOH surface, and interaction occurs between nanoflakes and As (V). It occurs through electrostatic and covalent interaction (As-O) to attenuate the peroxidase-like activity of CoOOH. As a result, catalytic activity decreased, and the green color solution changed to very pale green or close to colorless. Sensitivity can increase significantly by modifying the electrode surface. The assay is highly selective for arsenate and can detect total inorganic arsenic. The advantages are that it can be used for handy, onsite, sensitive,

selective, and signal-off assay for As (V). Also, CoOOH nanoflakes can be further developed to detect trace As (V) with obviously improved sensitivity and detection limit. Figure 9 shows the dual-mode assay for arsenate detection based on the peroxidase-like activity of CoOOH nanoflakes [66].

2.1.2.5. Detection of dual heavy metal ions together, including arsenite

Researchers developed simple chemical sensors to detect toxic heavy metals, including arsenic, cyanide, and mercury, due to their adverse effects on humans and the environment [67-69]. A simple Schiff's base colorimetric chemosensors have been designed for the naked eye detection of Hg^{2+} and As^{3+} using a simple step reaction. They used Isatin with 3,3-dihydroxybenzidine to obtain binding sites in the chemosensors that bind mercuric ions and arsenite. Three chemosensors, CS1, CS2, and CS3 were synthesized for different color changes. The color change of CS1 and CS3 changes from orange to colorless in the presence of Hg^{2+} and from orange to aqua-blue for As^{3+}. CS1 shows specific selectivity for Hg^{2+} and As^{3+}. However, it does not show significant color change with adding other cations. CS2 changes its color from yellow to pink with the addition of Hg^{2+}. Figure 10 shows the binding mechanism of CS1, CS2, and CS3 with Hg^{2+} and AsO_2^-. These sensors can monitor the mercury and arsenic level in the environment [68]. Neety Yadav and colleagues [69] developed a single chemical sensor capable of detecting both arsenite and cyanide ions, with detection limits in the micro- and nano-range. The probe was synthesized by the reaction of thiosemicarbazide dissolved in ethanol with 2-hydroxy-1-naphthaldehyde (Fig. 11). This probe has two acidic protons that are deprotonated through the interaction of arsenite and cyanide ions, which are indicated by the color change that occurs in this sensor. In the presence of arsenite and cyanide ions, the color of the probe changes from light yellow to dark yellow due to deprotonation and strong hydrogen bonding between the probe

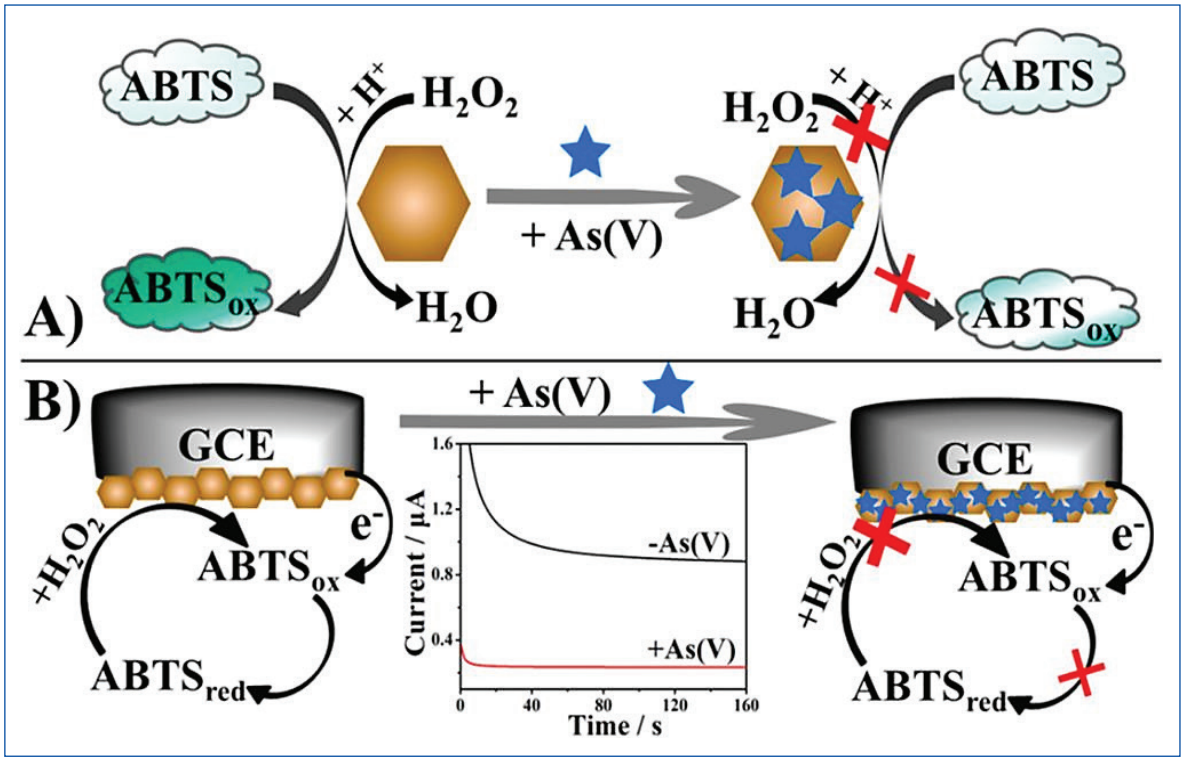

Fig. 9. Schematic illustration of the colorimetric probe of CoOOH nanoflakes for arsenate detection (A) and illustration of electrochemical assay of CoOOH nanoflakes modified electrode for arsenate detection (B) [66]

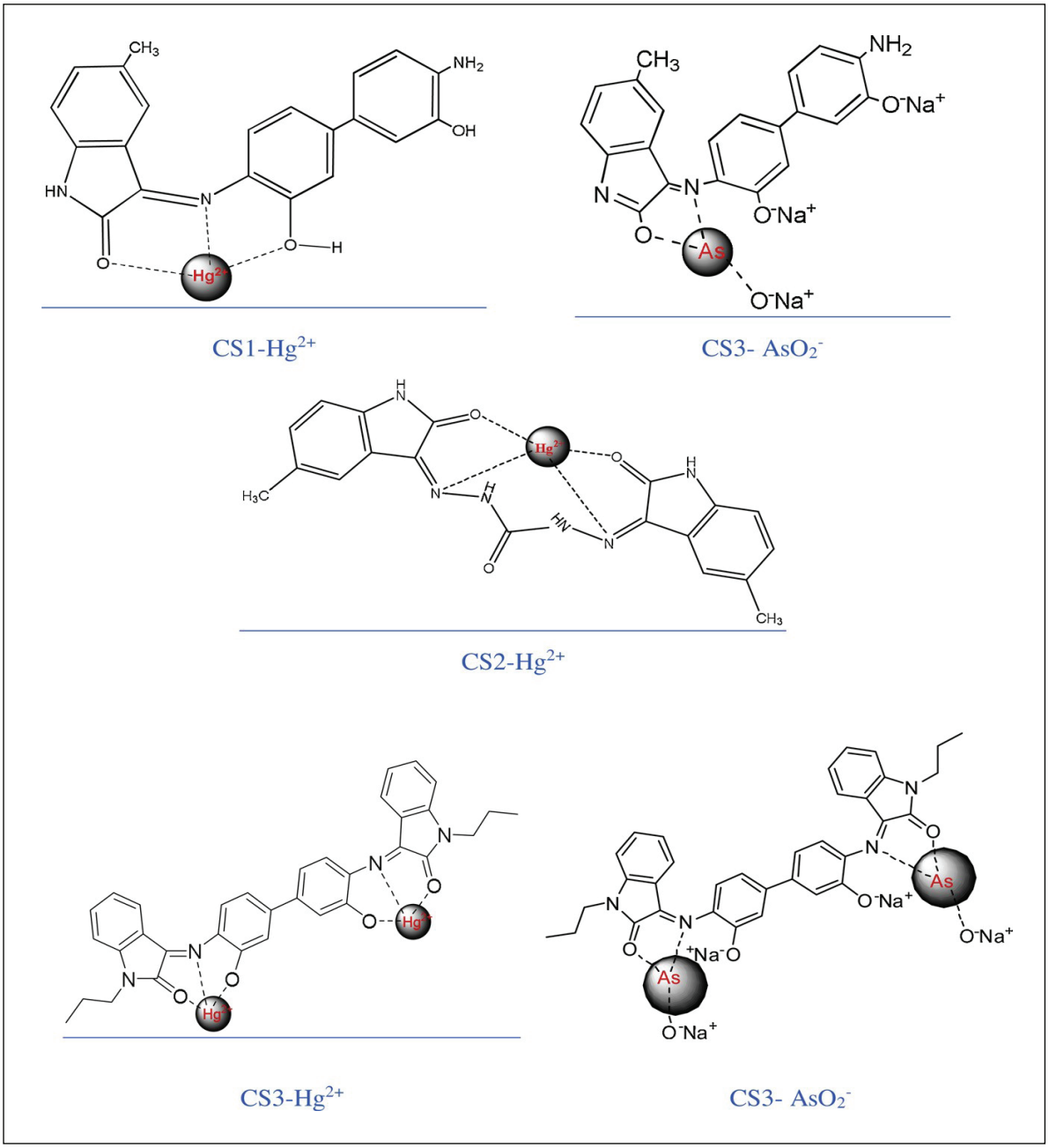

Fig. 10. Schematic representation of the binding mechanism of CS1, CS2 and CS3 with Hg^{2+} and AsO_2^- [68]

and anions. The fluorometric analysis is conducted using the same probe, utilizing the increase in fluorescence emission due to deprotonation and hydrogen bonding. The probe has the advantage of detecting the high toxicity of two anions, simply and cost-effectively.

When considering the above methods, most are shown low detection limits. Also, sensitivity and selectivity towards arsenate, arsenite or both forms are very high. It is especially high in nanomaterials compared to traditional methods. Table 1 shows the overview of above mentioned colorimetric methods, which offer low detection limits below the permissible limit of WHO. Many ways discussed in the text are used for the detection of As (III) due to the excellent oxidation property of As (III) which oxidizes into As (V). Therefore, total inorganic arsenic concentration can be detected using these methods.

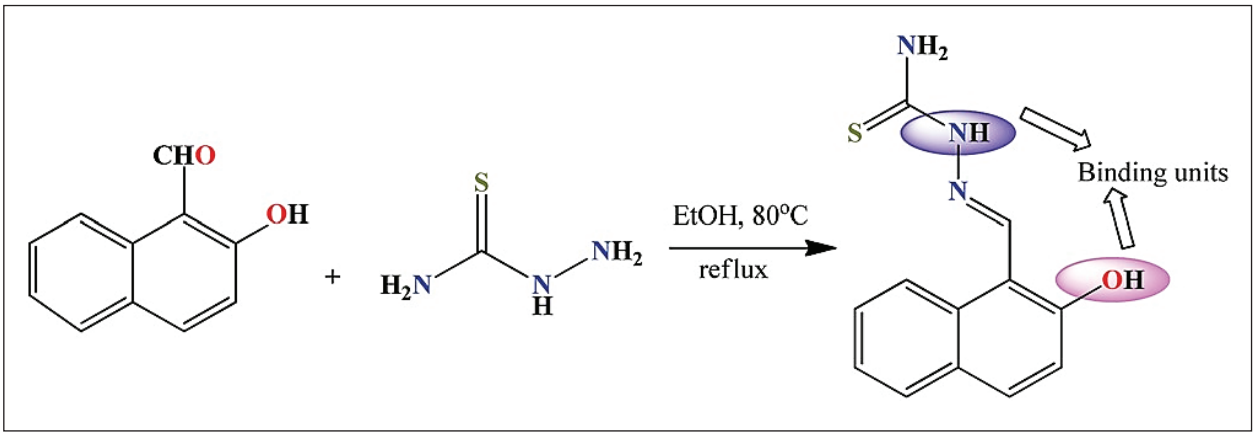

Fig. 11. Diagram of the synthesis of the probe for the detect arsenite and cyanide ions [69]

Table 1. Comparison of colorimetric methods discussed in this review based on structural modifications of molecules and usage of metal nanoparticles.

Materials	Arsenic	LR (µg L^{-1})	LOD (µg L^{-1})	References
Aptamer/ Hemin-H_2O_2 system	As (III)	-	6.00	[33]
GSH/DTT/Asn- AgNPs	As (III)	0.4-20	0.36	[52]
AgNPls/SiO_2-Fh	As (III) & As (V)	500-30000	0.50	[54]
GNR-PEG-DMSA	As (III) & As (V)	0.001-10	1.00	[55]
GNP-MMT@Eu	As (III) & As (V)	1-1000	1.00	[56]
AuNPs/ACP/AMP	As (V)	7.5-7520	7.50	[57]
AuNPs/G-T- rich DNA	As (III)	5-2000	2.00	[63]
Heptapeptide/ AuNPs	As (III)	-	4.00	[65]
CoOOH nanoflakes	As (V)	4-500	3.72	[66]

LOD: Detection limit
LR: Linear range

2.2. Fluorometric determination of arsenite

Fluorometric methods have tremendous attention for detecting arsenic due to their simplicity, less expensiveness, ease of operation, non-destructive, and fast response with low detection limits. Therefore, it is a promising technique for the detection of arsenic and it is very useful for environmental analysis [70-73].

2.2.1.Detection based on arsenite interacts with thiolated nanostructures.

Recently, quantum dots (QDs) have been used as one of the promising materials to detect arsenic due to their low toxicity and unique optical properties. QDs properties include high quantum yield, size-tunable spectral properties, long fluorescence lifetime, and narrow symmetrical emission peaks. Also, the preparation of QDs is very simple, straightforward, and does not require toxic precursors and organic solvents [73-77]. For example, environmentally friendly dithiothreitol (DTT) functionalized water-soluble carbon quantum dots (CQDs) were synthesized by microwave pyrolysis of citric acid and cysteamine to produce a fluorophore for

turn-on detection of arsenite. DTT exhibits on the surface of CQDs using S-S bonds to impart –SH functionalities on their surface formed DTT-CQDs complex. In the presence of As (III), arsenite binds with the sulfur group of CQDs through the –SH group of DDT ligand to form a stable As (III)-DDT-CQDs complex, and as a result, CQDs exhibit blue fluorescence. Figure 12 shows the synthesis of functionalized CQDs and arsenite binding processes on CQDs. Compared with metal-based semiconductor QDs such as CdS-QDs, ZnS-QDs, and CdTe-QDs, the mentioned approach is useful for real-world applications, including environmental analysis. Because metal-based semiconductor QDs influence the environment and human health due to their elemental composition and toxicity [77]

When considering a single colorful fluorescent probe, they only exhibit the change of fluorescence brightness with limited quantitative capability. Instead of the brightness changes, the detection of color variation is the most important factor for accurate quantification of the analyte. Therefore, pH and fluorescent test papers are widely used with fluorescent materials printed onto the paper. These analyses are low-cost, easy to operate, and portable. For example, a color multiplexing-based fluorescent test paper was developed for dosage-sensitive detection of As (III) with clear color visualization using fluorescent red and cyan probes, which can achieve a wide color variation from red to cyan. They have synthesized cyan CDs and red CdTe QDs-based cyan and red probes by hydrothermal and classical methods, respectively. Also, CdTe QDs are modified by GSH and DTT ligands, enhancing the aqueous solubility and strong binding affinity for As (III). As a result of the modification, many free–SH groups are on the surface of QDs. As-S bonds are formed byAs (III) addition and trigger the aggregation of GSH/DTT-QDs resulting in the fluorescence color change from red to cyan. A wide range of color variations

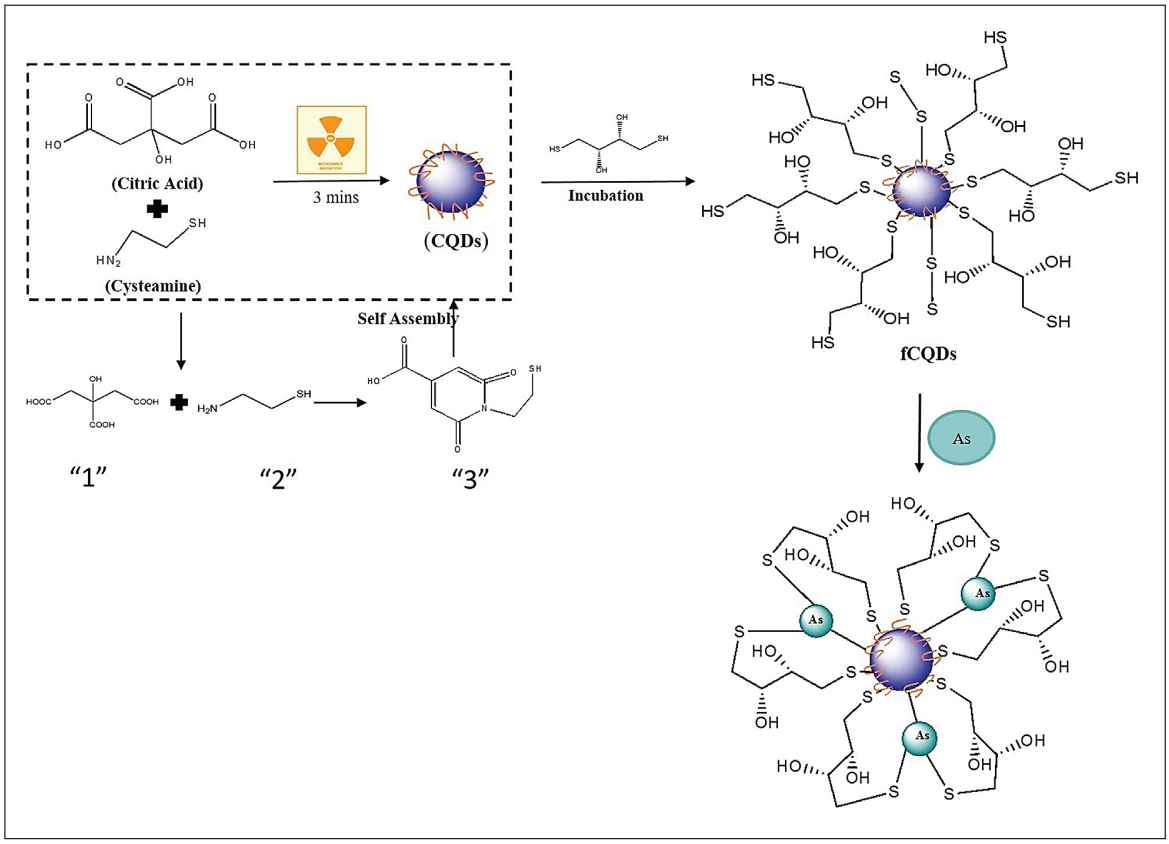

Fig. 12. Schematic representation of the synthesized DTT functionalized CQDs for detection of arsenite and binding mechanism of arsenite [77]

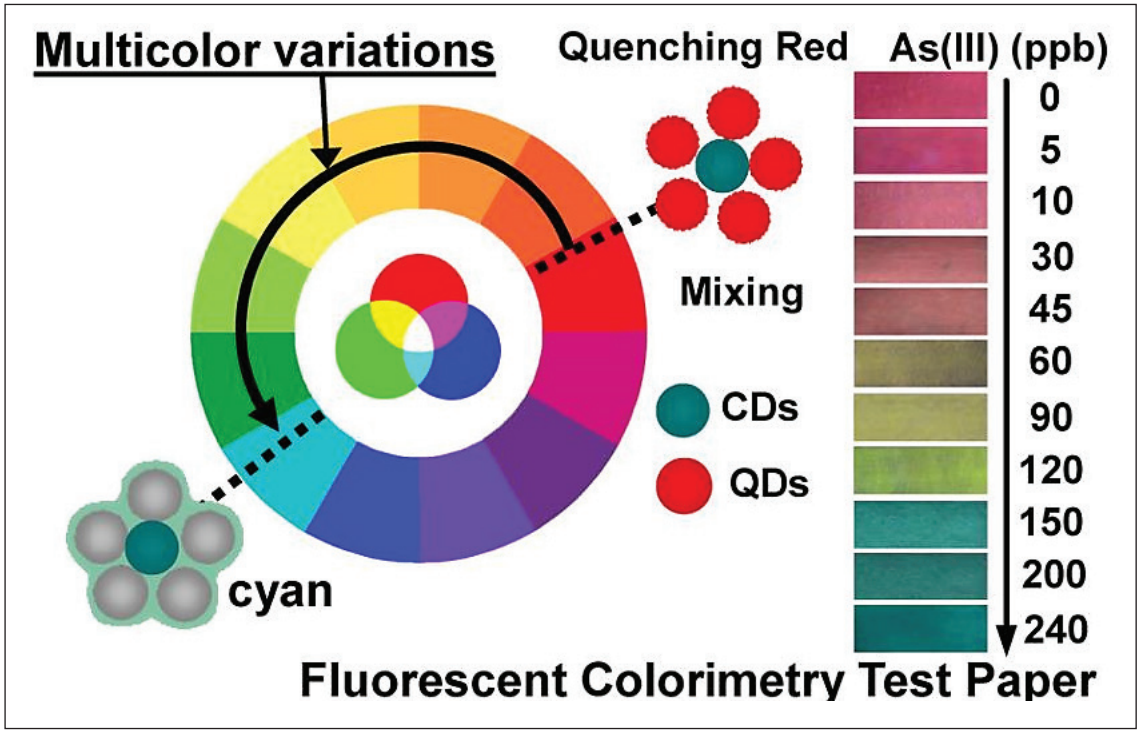

Fig. 13. Fluorescent colorimetry test paper for obtaining various color variations from red to cyan using CDs and QDs dual probe [78].

can be observed with As (III) concentration. They realized dosage-sensitive visualization of arsenite detection by the ink of sensory solution printed on the test paper. Figure 13 represents the fabricated fluorescent colorimetry test paper's various color variations from red to cyan for arsenite detection [78].

Nanoclusters containing fewer atoms show a high quantum yield and can be used to sense toxic metal ions. Gold nanoclusters and silver nanoclusters are commonly used to develop fluorometric sensing approaches. Quantum yield can be increased by adding capping ligands such as thiol-based and dipeptide ligands. Compared with other capping materials such as glutathione, dipeptide ligand-capped gold clusters show significantly high fluorescence yield. As an example, dipeptide (L-cysteinyl-Lcsteine) capped water-soluble fluorescent few-atom gold nanoclusters were synthesized using a core etching pathway through a "Top-down" mechanism for the detection of arsenite (Fig. 14). Synthesized dicysteine capped fluorescent gold cluster sensor is highly efficient, selective and extremely sensitive for arsenite without any extra modifications. With the addition of arsenite, fluorescence intensity enhances gradually. The reason may be due to the positive charge of As (III) interacting with the negative charge thiolated gold cluster and due to the electrons in the gold cluster that flow toward electron poor As (III) ions. Meanwhile, in the presence of arsenite, the radiative decay rate of the gold cluster is increased, and the fluorescence decay time is decreased. These fluorescent sensors can detect As (III) at low concentrations with high specific responses. Also, fluorescent sensors can be reused by adding succinic acid to chelates As (III) through complexation [79].

Selectively sensitive silver-doped hollow CdS/ZnS bi-layer nanoparticles (Ag-h-CdS/ZnS) are synthesized using the sacrificial core method to detect arsenite. AgBr nanoparticles were used as the core to synthesize Ag-h-CdS/ZnS nanoparticles. Also, L-cysteine is used to functionalize the nanoparticles. In the presence of arsenite, cysteine interacts with arenite, resulting in fluorescence

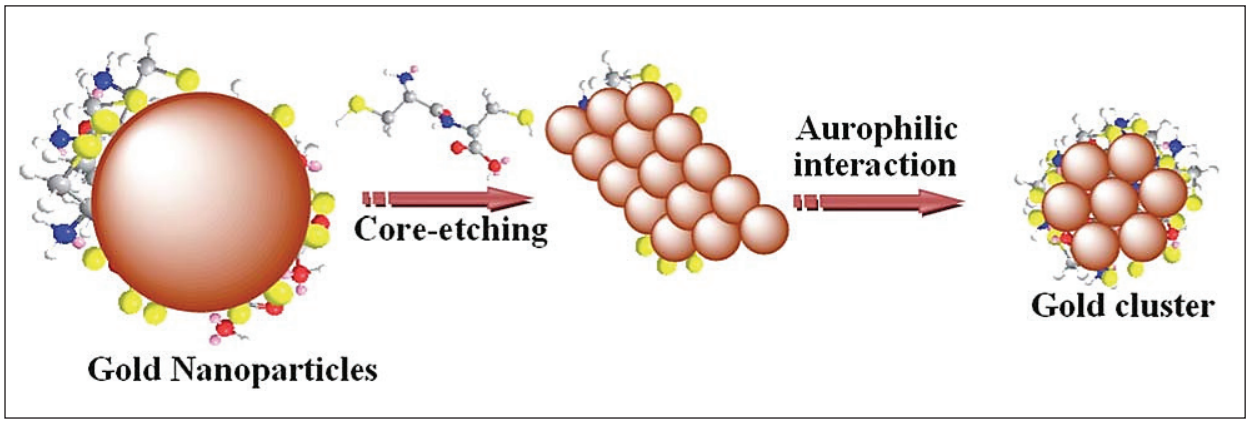

Fig. 14. Illustration of synthetic route for the formation of gold clusters through a top-down mechanism [79]

quenching of the nanoparticles due to changes in the electronic structure and accelerating the non-radioactive nature of excitons. This sensor has many advantages, including ease of use, selectivity, sensitivity, and cost-effectiveness [80]. A cysteine-functionalized tetraphenyl ethane (TPE)-based "Turn-on" fluorescent probe was developed for the highly selective detection of arsenite with a low detection limit. Free-SH groups in cysteine can bind with arsenite through As-S bonds, forming As $(CystPE)_3$ structure. TPE present in this complex promotes the formation of π-π aggregation, which results in turn-on fluorescence depending on the nature of the induced emission feature (AIE), thus creating a tendency to increase the fluorescence of the TPE complex. Figure 15 depicts the formation of As $(CystPE)_3$ complex and fluorescence activation [81].

There are many biological and chemical sensors developed for arsenite detection due to their redox properties and strong thiophilicity. The usage of thiol ligands can obtain many advantages, including high sensitivity and selectivity due to the presence of a vast number of sulphur that utilizes As-S bonds with arsenic in aqueous solutions. Also, CQDs show many advantages, including superior chemical stability, high aqueous solubility, tuneable surface functionalities, and resistance to photobleaching. However, complicated thiolated modifications lack visual analysis and limit their applications [75-81].

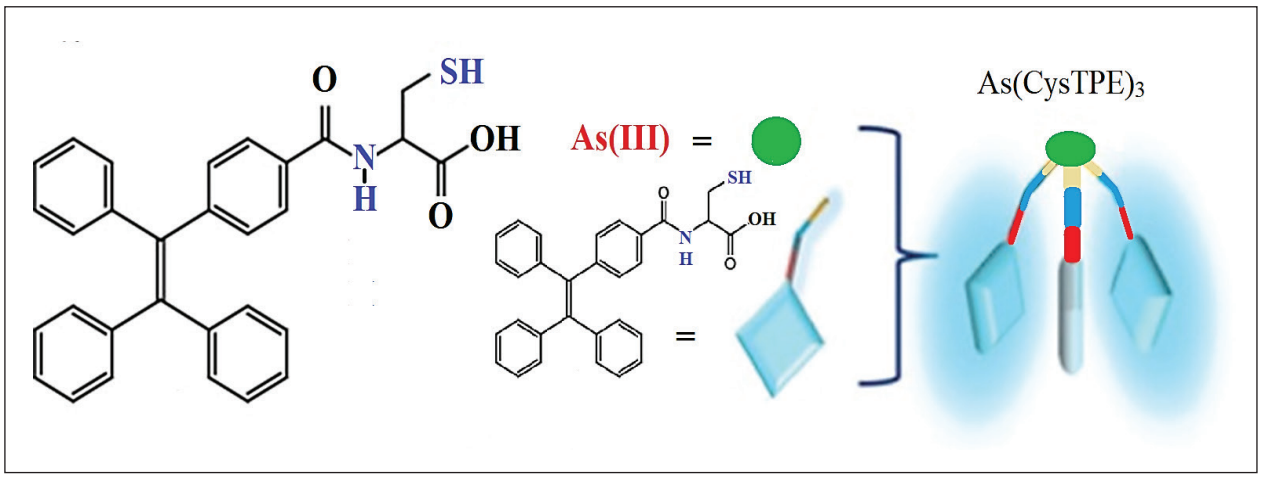

Fig. 15. Illustration of Asv$(CystPE)_3$ complex and florescent formation [81]

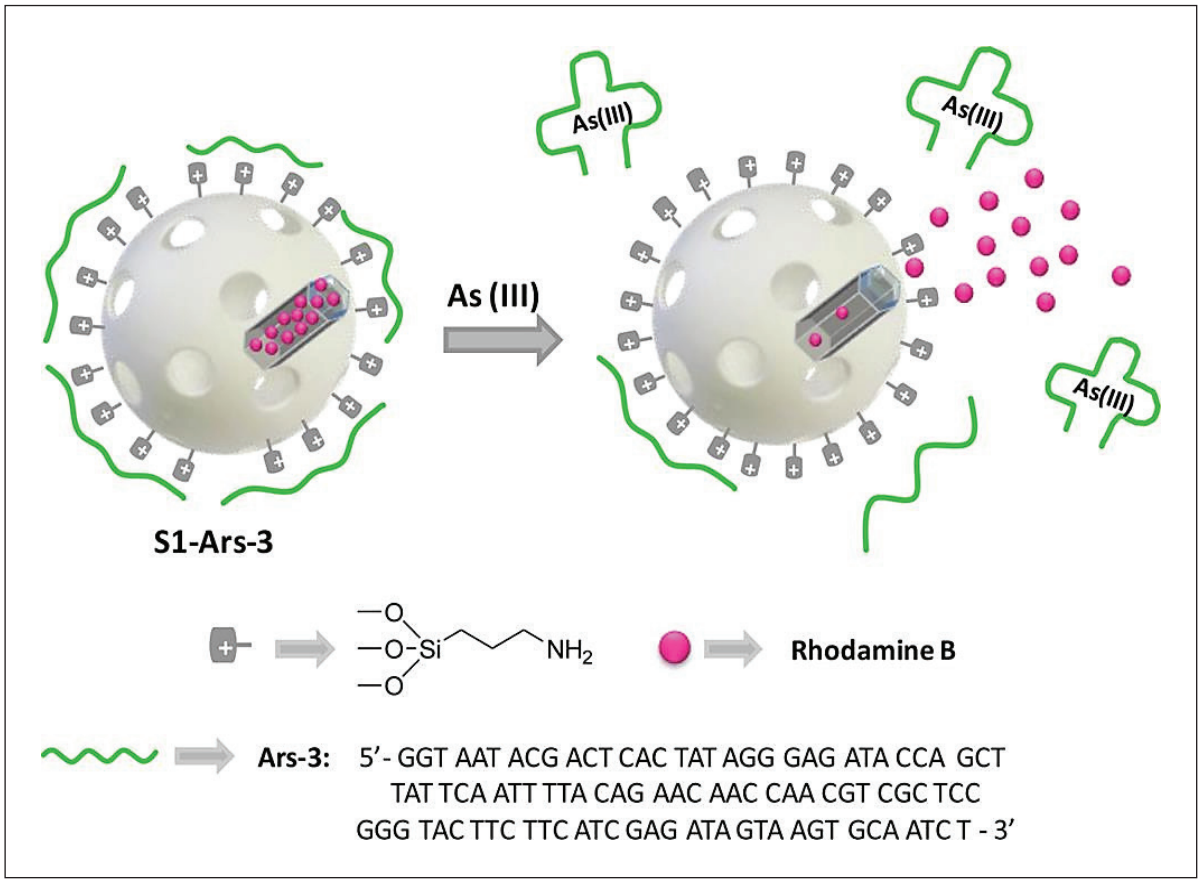

Fig. 16. Schematic representation of proposed modified Ars-3 aptamer and the sensing process of arsenite detection [86]

2.2.2.Detection based on arsenite interacts with biologically functionalized nanomaterials.

Nanostructure-based sensors provide many advantages including rapid and sensitive responses to detecting arsenic in cell living. For example, Mesoporous Silica Nanoparticles (MSNs) are considered a promising material for arsenic detection due to their high inner surface area and flexible surface modification capacity [82-86]. Therefore, MSNs can be functionalized by capping materials which enhance the detection capability. Aptamers are DNA sequences and act as capping material. Aptamer-based fluorescent sensors show high affinity, selectivity, and long-term stability for determining arsenite [83]. Oroval *et al.* [86] fabricated an arsenite sensing system using aptamer-capped MSNs. They used MCM-41 mesoporous silica nanoparticles and pores of MCM-41 inorganic support were loaded with rhodamine B. Rhodomine B was capped by Arsenite aptamer (Ars-3) in MSNs pores. As (III) has a high potential to bind with aptamer and then displace it from the MSN surface. Resulted of the fluorescence difference can be used for quantitative detection of As (III). This fluorescence system can be used for environmental analysis due to its simplicity. Figure 16 shows the functionalized Ars-3 aptamer in the sensory system for arsenite detection.

The dye-labeled G/T rich single-strand DNA-wrapped single-wall carbon nanotubes (SWCNT)-based fluorescent probe was designed to analyze arsenite quantitatively at the femtogram level. Here, 5-hexachloro-fluorescein phosphoramidite (HEX) was used to label the ssDNA, and that structure is the wrapping material of SWCNT. Arsenite can bind with the G/T bases of ssDNA in living cells, reducing the π-π interaction between ssDNA and SWCNTs. As a result, ssDNA can be dissociated

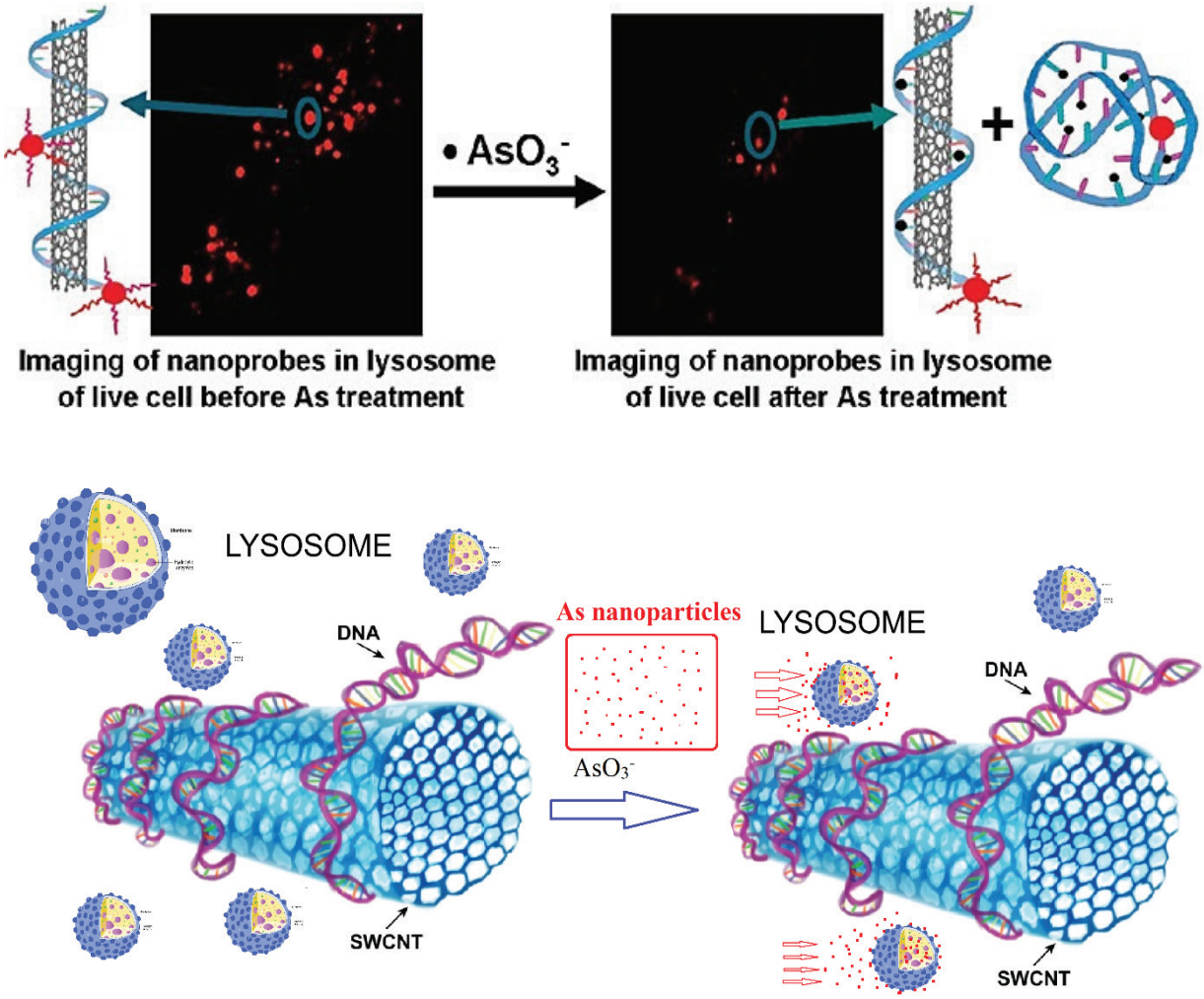

Fig. 17. Illustration of nanoprobe interaction with arsenite in living cells [87]

from the surface of SWCNTs and condensed in the live cells. The condensed structure of ssDNA facilitates the HEX to interact with G/T bases bound arsenite ions, resulting in significant fluorescent quenching of HEX dye. Figure 17 illustrates the nanoprobe interaction with arsenite in the lysosome of a living cell [87].

2.2.3.Detection based on arsenite interacts with chemosensor.

A simple Schiff base fluorescence probe (HL) was fabricated for "turn on" detection of arsenite through the intermolecular hydrogen bonding induced chelation-enhanced fluorescence (CHEF) process. Arsenite selective HL probe is synthesized by condensation of 2,6-diformyl-p-cresol with 4-aminoantipyrine. The absence of arsenite ions can obtain fluorescence with weak intensity. And the presence of arsenite, fluorescence intensity is higher than in the absence of arsenite. Fluorescence differences can be used for the quantitative detection of arsenite. When arsenite ions are present in the sample, intermolecular hydrogen bonds are formed between arsenite and the probe to form HL-As (III) complex and a resulting fluorescent signal. Its intensity increases with the increment of As (III) concentration. Arsenite ions interact with phenolic O-H to form strong hydrogen bonds, which can affect the photo-induced electron transfer (PET) process and enhance the fluorescence intensity through the chelation-enhanced fluorescence (CHEF) process. This probe can be used to imagine

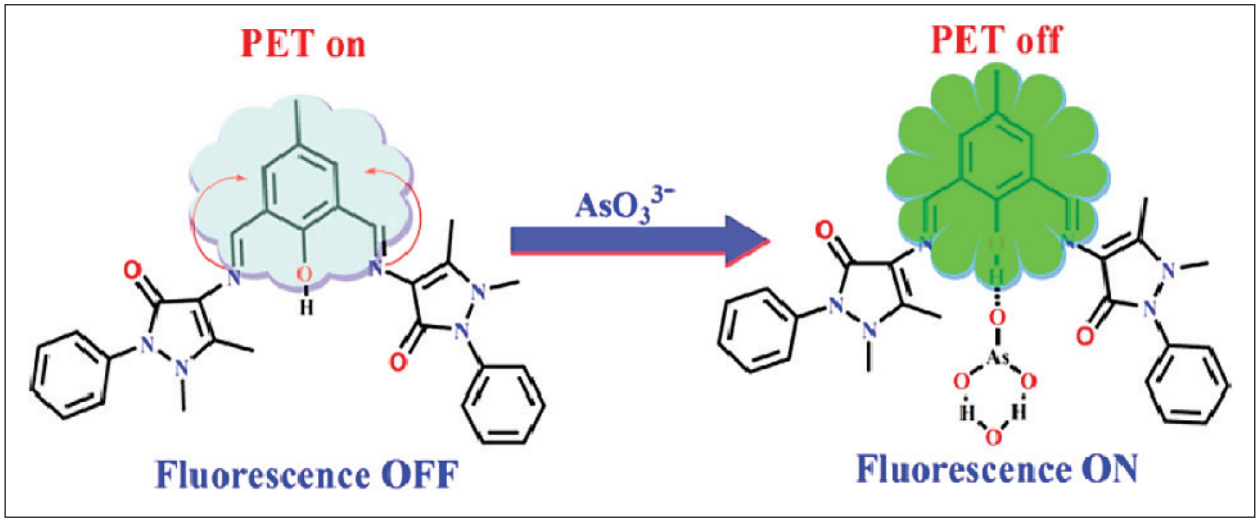

Fig. 18. Illustration of the fluorescence enhancement of HL probe in the presence of arsenite [88]

arsenite contributions in living cells, such as cancer cells, and is applicable for detecting trace-level arsenite in different water samples. Other competitive ions do not affect the fluorescence enhancement. Figure 18 depicts the fluorescence formation of HL in the presence of arsenite [88].

2.3. Fluorometric determination of arsenate

2.3.1. Detection based on the interaction of arsenate with iron-modified materials.

Nowadays, various types of solid nanomaterials are used as an adsorbent for arsenic removal processes. But most are toxic, difficult to separate after adsorption, and ineffective in impurities. Therefore, iron oxide and its modifications overcome these limitations [89-93]. Liu and co-workers [93] proposed an arsenate detection method that relies on the strong interaction between As (V) and the surface of metal oxides. They synthesized fluorescent DNA-loaded ferric oxide nanoparticles by incubating carboxyfluorescein (FAM)-labeled DNA with nanoparticles. DNA adsorbs on ferric oxide nanoparticles through phosphate in its backbone. This configuration covered the fluorescence signal of FAM-labelled DNA. The presence of arsenate competes with adsorbed DNA for binding sites and displaces adsorbed DNA by removing adsorbed DNA from the surface of nanoparticles. As a result, fluorescence is recovered. The sensitivity can be improved by increasing DNA adsorption affinity using shorter DNA due to adsorbing properties with high density and ease of desorption. In addition, they enhanced their scope for increasing adsorption capacity by using different nanoparticles. They used and compared three types of nanomaterials; CeO_2, $CePO_4$, and Fe_3O_4, which contain hard Lewis acids and a bonding preference for phosphate in DNA. Among them, CeO_2 nanoparticles perform better than the other two, achieving a ten times lower detection limit compared to Fe_3O_4 nanoparticles. The advantages of this method included the requirement for small sample volumes for the analysis and being highly sensitive to shorter DNA. They can be used to compare and identify nanomaterials' DNA adsorption affinity and sensitivity. Figure 19 shows the fluorescence recovery procedure with the induction of arsenate into the sensory system. The same group proposed a study based on fluorescent-labeled DNA-functionalized iron oxide nanoparticles for arsenate detection in environmental analysis. Polyphosphate present in DNA has a specific ability to adsorb on the surface of iron oxide. As the nature of DNA and Fe_3O_4 nanoparticles, salt induces the system for absorbance of DNA with high adsorption efficiency. Figure 20 shows the schematic of sensing arsenate by DNA-functionalized iron oxide nanoparticles. The configuration of fluorescent-labeled DNA binds to nanoparticles that quench the fluorescent

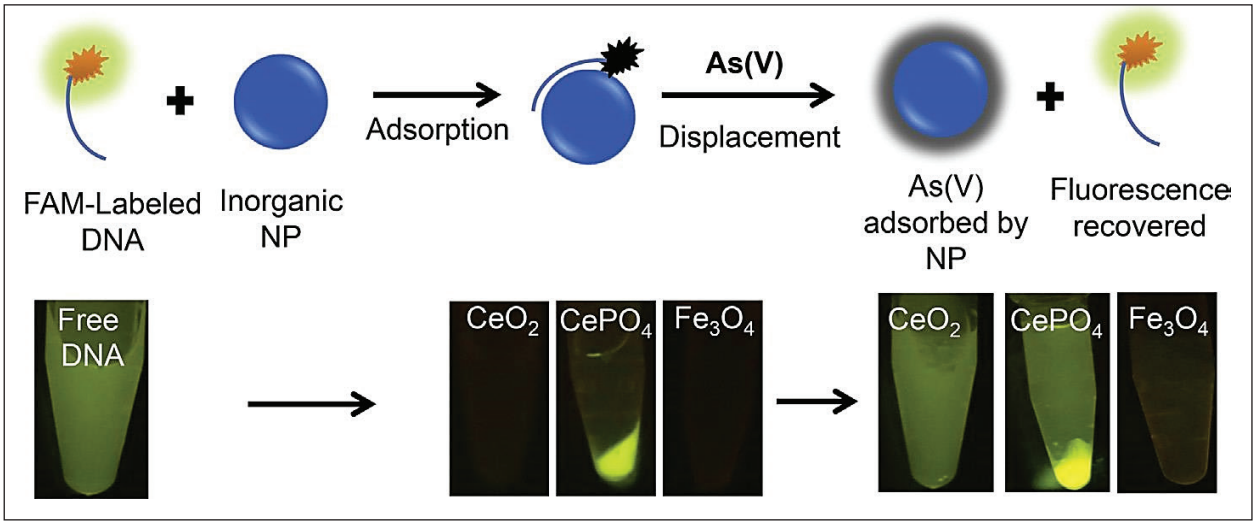

Fig. 19. Schematic representation of fluorescence recovery process with the presence of arsenate [93]

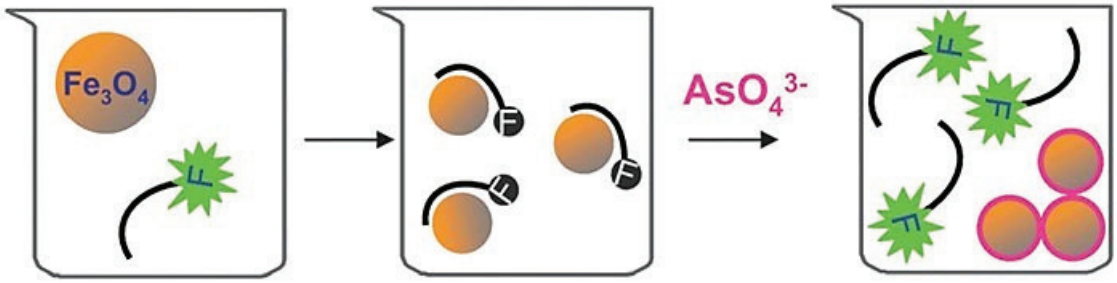

Fig. 20. Illustration of sensing arsenate by DNA functionalized iron oxide nanoparticles [94]

yield. In contrast, in the presence of arsenate, arsenate competes for the binding sites of DNA and replaces them. As a result, the fluorescent signal recovered in the system. The intensity of the fluorescent recovery is arsenate concentration-dependent [94].

In addition, Metal-Organic Framework (MOF) materials are considered sensing materials, facilitating many advantages in analyzing target materials. Because it has attractive characteristics such as the presence of organic binding ligands or metal centers and a large surface area that allow effective trapping and removal of target ions [95,96]. For example, amino-functionalized iron-containing MOFs were synthesized with powerful fluorescence emission capacity for detecting and removing arsenate. They fabricated NH_2-MIL-88(Fe) nano octahedra by solvothermal treatment of $FeCl_3$.6H2O and NH_2-BDC in DMF. Unsaturated iron sites in the sensory system have a highly selective affinity for arsenate by formatting As-O-Fe bonds. Synthesized MOFs show weak fluorescence due to the electron transfer from the NH_2-BDC organic linker to Fe_3-$_3$-oxo clusters. However, fluorescence recovery increases with the introduction of arsenate into the system. Moreover, fluorescence intensity increases with the increment of arsenate concentration. In the presence of arsenate, it can rapidly diffuse into the MOFs, and then aggregation occurs between iron-oxo-clusters and arsenate. This method has great potential for sensing arsenate compared to other methods, such as fluorescent DNA-loaded iron oxide NPs, CeO_2, and FAM-labelled DNA. Other MOFs' advantages include cost-effectiveness, readily available ease of fabrication, rapid response, high sensitivity

nature, and anti-interference ability. And applicable for polluted environmental analysis due to the fluorescence stability of MOFs [96].

2.3.2. Detection based on the interaction of arsenate with enzyme activity

Enzymes are biological molecules that speed up the reaction rate by binding to the reactant/substrate. Some arsenic detection processes involve enzymes' catalytic or inhibitory activity [97-99]. For example, a highly selective enzymatic catalysis system was synthesized using inexpensive glyceraldehyde 3-phosphate dehydrogenase (GAPDH) to detect a low arsenate concentration with a low detection limit. GAPDH catalytic system contains an enzyme (GAPDH), a coenzyme (NAD^+), and a substrate (G3P). In the reaction, cysteine in the holoenzyme interacts with the substrate to form an acyl-enzyme intermediate through hydride transfer from intermediate hemithioacetal to NAD^+. As a result, NADH is released, and another NAD^+ has an affinity to the enzyme-bound substrate to produce NAD^+-acyl-enzyme. Arsenate can act as an acyl acceptor, and present arsenate interacts with NAD^+-acyl-enzyme to form stable 1-arseno-3-phosphoglycerate (APG). The better performance of arsenate as a nucleophile leads to hydrolysis of arsenoglycerate, and the resulting holoenzyme re-enters the catalytic cycle. The result is that a fluorescent yield of NADH is amplified in the system. In addition, APG hydrolyzed rapidly to regenerate arsenate, which leads the catalytic cycle by continuously generating NADH with excess NAD^+. Fluorescence yield increases with the amount of arsenate are increased in the sample. Furthermore, the catalytic system is inexpensive, rapid response, highly sensitive, and useful for arsenate in environmental samples and safety applications. Figure 21 illustrates the enzyme catalytic system for sensing arsenate and APG hydrolysis reaction [97].

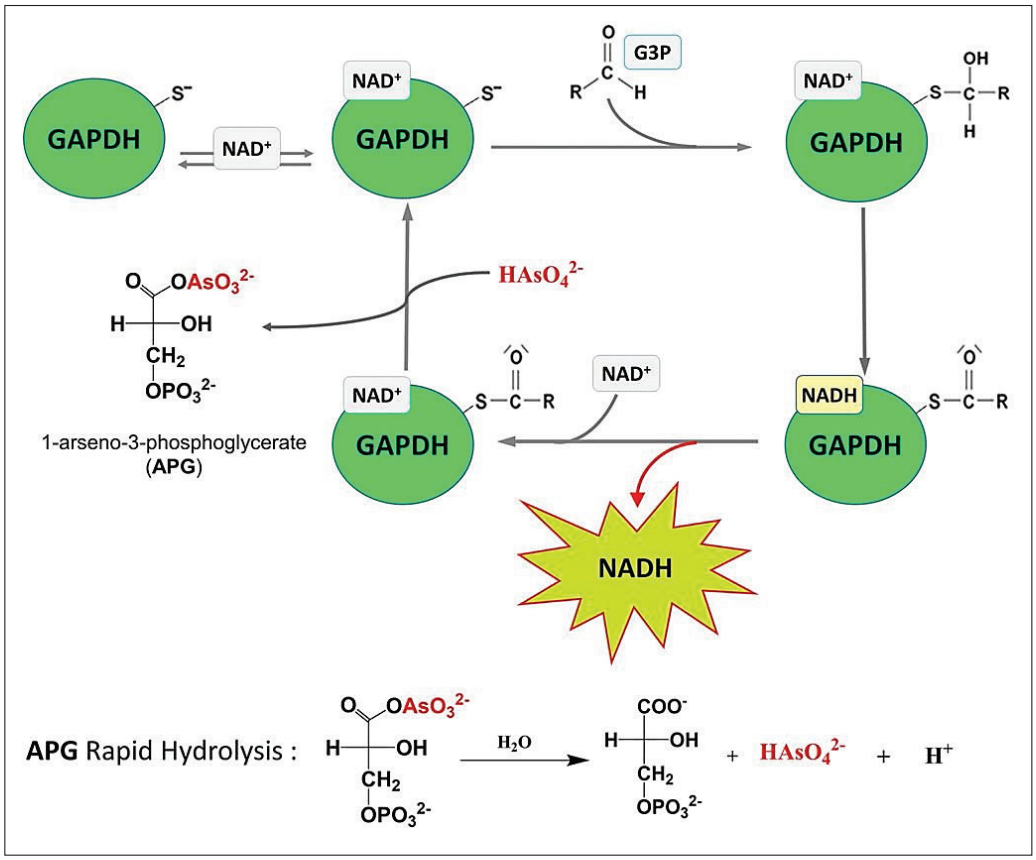

Fig. 21. Schematic illustration of catalytic enzyme mechanism for sensing of arsenate and APG hydrolysis reaction [97]

The involvement of arsenate inhibitory activity on phosphatase enzymes shows remarkable pathways to arsenate detection. As an example, Jian-Ding Qie and co-authors [98] synthesized a fluorescent nanoprobe containing CdSe/ZnS quantum dots (QDs) coated with the terbium (III) complex of guanosine monophosphate (Tb-GMP) using one-pot adaptive self-assembly process. Fabricated QD/TB-GMP composite which exhibited dual fluorescence emission and single wavelength excitation properties are used for ratiometric determination of arsenate. The presence of acid phosphatase enzyme (ACP) can catalyze the hydrolysis of GMP and as resulting phosphate ions and guanosine particles. The fluorescent intensity of Tb-GMP shows a signal off with ACP. But in the presence of arsenate, As (V) inhibits the catalytic activity of ACP. Therefore, hydrolysis of GMP does not take place effectively. So Tb-GMP complex recovered its fluorescence intensity and its intensity increased with the increment of arsenate concentration. This visual analysis method can be used to quantitatively determine arsenate with a 0.39 μg L^{-1} detection limit and high selectivity toward As (V). High solubility, facile preparation process, excellent single excitation, and dual emission fluorescence properties, visual analysis are advantages of nanoprobe. And it is a feasible method for environmental analysis. Figure 22 shows the synthesis of QD/Tb-GMP and fluorescent signal with As (V) and the absence of As (V).

2.3.3. Detection of arsenate that present in the living cell using chemosensors

Arsenate detection is essential in living cells due to its high toxicity. That might have a poisonous effect on cells. As an example, destroy the conversion of ATP into ADP permanently. Arsenate selective fluorescence sensors (APSAL) were designed by condensing salicylaldehyde with 4-amino-antipyrine. In the presence of arsenate, strong hydrogen bonds are created between APSAL and As (V) to form APSAL-As (V) complex. The molecular level interaction between As (V) and APSAL can be described using density functional theory (DFT). The presence of arsenate fluorescence intensity increases significantly without significant interference from other common ions. APSAL is highly selective for arsenate and obtains micromolar range detection limits. Optimal pH maintenance is essential for the efficiency of the sensor. This system applies to detect intracellular arsenate in living cells [99].

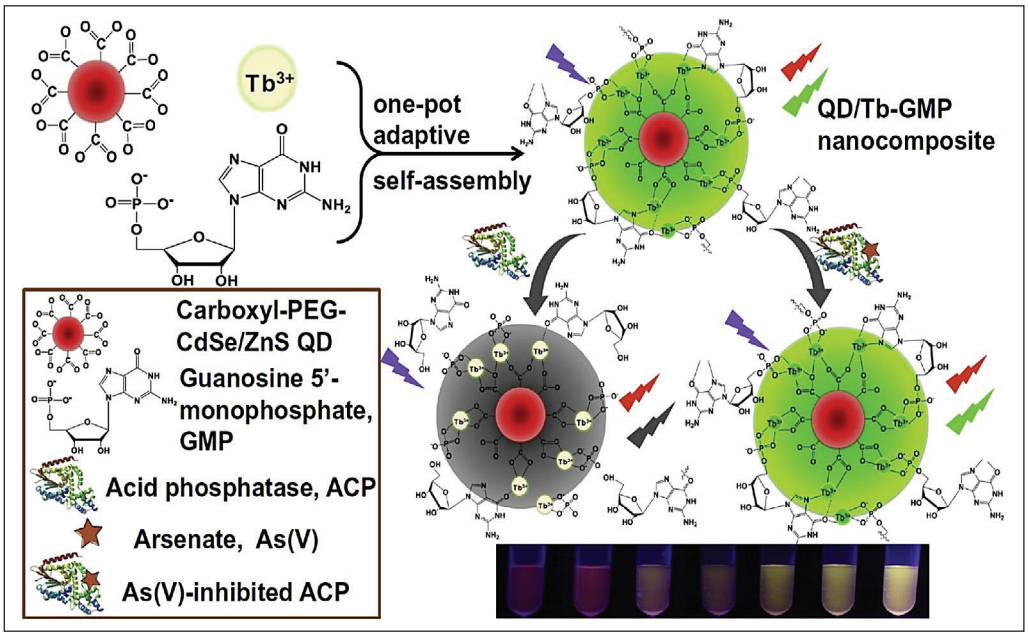

Fig. 22. Schematic representation of the formation of QD/Tb-GMP and fluorescent signal with the presence of As (V) and without As (V) [98].

Abu *et al.* proposed an oxime-based fluorescent probe to detect arsenate and arsenite in living cell-imaging applications [100]. Detection relies on formatting nano/microstructures by H-bonding interactions in the presence or absence of arsenate and arsenite. Arsenic (arsenate and arsenite) interacts with 2,6 diformyl-*p*-cresol-dioxime (DFC-DO) ligand, which has a remarkable sensing capacity for arsenite and arsenate detection and forms DFC-DO-$H_2AsO_4^-$ and DFC-DO-AsO_2^- respectively through intermolecular hydrogen bonding. As a result, the quantum yield of the free ligands increases. Above proposed methods exhibit low detection limits below the WHO permissible limit of 10 µg L^{-1} with high selectivity towards either arsenate or arsenite. Table 2 shows an overview of fluorometric methods mentioned in this review for determining arsenate and arsenite. Among them, MOF materials showed the lowest detection limit.

3. Conclusion

This review has covered colorimetric and fluorometric methods for detecting arsenate and arsenite. Discussed colorimetric methods highlighted the evolution of colorimetric methods, detections based on structurally modified molecules, and usage of nanoparticles with/without modifications. Among them, nanomaterials showed better performance compared to traditional methods. Discussed all methods are reliable, easy in usage, can be used for field analysis, relatively cost-effective compared to instrumental methods, modifications are enhanced sensitivity and selectivity and further indicated lower detection limits (below the WHO recommendations). Thiol-functionalized AgNPs showed the lowest detection limit (0.36 µg L^{-1}). However, modifications are complicated, and unmodified nanomaterials showed much cost-effectiveness. Therefore, the usage of unmodified nanomaterials is economically important. Proposed fluorometric methods were mostly based on nanostructural probes and facilitated high sensitivity and selectivity. Those are reliable, simple, non-destructive, and cost-effective. Also, they can use for field analysis with low detection limits. Among them, MOF materials showed the lowest detection limit (0.056 µg L^{-1}). Modifications in nanomaterials are enhanced sensitivity and accuracy of the fluorometric sensor. Especially thiolated modifications are very sensitive to arsenic.

4. Acknowledgement

We thank Dr. Arjuna Wijekoon for his kind guidance throughout the process. We acknowledge the Wallumattagal clan of the Dharug nation as the traditional custodians of the Macquarie University land. We strongly support equity, diversity, and inclusion in science [101]. The authors come from different countries (Sri Lanka and Australia) and

Table 2. Comparing Fluorometric methods for the detection of As (III) and As (V)

Materials	Arsenic	DR (µg L^{-1})	LOD (µg L^{-1})	References
DTT/CQDs	As (III)	5-100	0.086	[77]
GSH/DTT-QDs/CDs	As (III)	5-100	1.7	[78]
Dipeptide-AuCs	As (III)	-	~4.04	[79]
Aptamer/ MSNs	As (III)	-	0.9	[86]
HL probe	As (III)	-	4.1	[88]
DNA/CeO2 NPs	As (V)	0-150	2.2	[96]
NH2-Fe-MOF	As (V)	0.1-50	0.056	[95]
Enzyme catalytic activity	As (V)	0-200	10	[97]
QD/Tb-GMP	As (V)	0.5-200	0.39	[98]
APSAL probe	As (V)	-	5	[99]

LOD: Limit of Detection
DR: Detection Range

represent different career stages (Master's student, Ph.D. student, and ECR). The authors have no conflicts of interest to declare.

5. References

[1] M. M. Bradly, L. M. Siperko, M. D. Porter, Colorimetric-solid phase extraction method for trace level determination of arsenite in water, Talanta, 86 (2011) 64-70. https://dx.doi.org/10.1016/j.talanta.2011.08.004

[2] X. Tian, L. Chen, Y. Li, C. Yang, Y. Nie, C. Zohou, Y. Wang, Design and synthesis of a molecule with aggregation-induced emission effects and its application in the detection of arsenite in groundwater, J. Mater. Chem. C, 5 (2017) 3669-3672. https://doi.org/10.1039/C7TC00363C

[3] P. K. Sasgupta, H. Huang, G. Zhang, G. P. Cobb, Photometric measurement of trace As(III) and As(V) in drinking water, Talanta, 58 (2002) 153-164. https://doi.org/10.1016/S0039-9140(02)00264-3

[4] L. R. Lado, G. Sun, M. Berg, Q. Zhan, H. Xue, Q. Zheng, A. Johmson, Ground water arsenic contamination throughout China, Sci., 341 (2013) 866-868, https://dx.doi.org/10.1126/science.1237484

[5] T. Agusa, P. T. K. Trang, V. M. Lan, D. H. Anb, S. Tanabe, P. H. Viet, M. Berg, Human exposure to arsenic from drinking water in Vietnam, Sci. Total Environ., 48 (2013) 15348-15356, https://dx.doi.org/10. 1016/j.scitotenv.2013.10.039

[6] P. N. Williams, A. Roab, J. Feldmann, A. A. Mehary, Market basket survey shows elevated levels of As in south central U.S. processed rice compared to California: Consequences for human dietary exposure, Environ. Sci. Technol., (2007) 2178–2183. https://dx.doi.org/10. 1016/j.taap.2006.04.004

[7] Q. Zhang, H. Minami, S. Inoue, I. Atsuyn, Differential determination of trace amounts of arsenic(III) and arsenic(V) in seawater by solid sampling atomic absorption spectrometry after preconcentration by coprecipitation with a nickel–pyrrolidine dithiocarbamate complex, Anal. Chim. Acta, 15 (2004) 99-105. https://doi.org/10.1016/j.aca.2003.11.053

[8] Y. Cai, Speciation and analysis of mercury, arsenic, and selenium by atomic fluorescence spectrometry, TrAC Trends Anal. Chem., 19 (2000) 62-66. https://doi.org/10.1016/S0165-9936(99)00180-6

[9] K. Jitmanee, M. Oshima, S. Motomizu, Speciation of arsenic(III) and arsenic(V) by inductively coupled plasma-atomic emission spectrometry coupled with preconcentration system, Talanta, 66 (2005) 529-533. https://doi.org/10.1016/j.talanta.2004.09.024

[10] A. P. Packer, V. S. T. Ciminelli, A simplified flow system for inorganic arsenic speciation by preconcentration of As(V) and separation of As(III) in natural waters by ICP-MS, Atomic Spectroscopy, PerkinElmer Life and Analytical Sciences, 26 (2005) 131–136. https://www.chemeurope.com/en/companies/14457/perkinelmer-life-and-analytical-sciences-inc.html

[11] D. Gohosh, M. N. Luwang, Arsenic detection in water: YPO4:Eu3+ nanoparticles, J. Solid state Chem., 232 (2015) 83-90. https://dx.doi.org/10.1016/j.jssc2015.09.009

[12] G. Tang, J. Wang, Y. Li, X. Su, Determination of arsenic(III) based on the fluorescence resonance energy transfer between CdTe QDs and Rhodamine 6G, RSC Adv., 5 (2015) 17519-17525. https://dx.doi.org/10.1039/c4ra16789a

[13] E. Majid, S. Hrapovic, Y. Liu, K. B. Male, J. H. T. Luons, Electrochemical determination of arsenite using a gold nanoparticle modified glassy carbon electrode and flow analysis, Anal. Chem., 3 (2006) 762-769. https://doi.org/10.1021/ac0513562

[14] S. Sirawatcharin, A. Saithongdee, A. Chaicham, B. Tomapatanaget, A. Imyim, N. Praphairaksit, Naked-eye and colorimetric detection of arsenic (III) using difluroboron-curcumin in aqueous and resin bead support

system, Anal. Sci., 30 (2014) 1129-1134. https://doi.org/10.2116/analsci.30.1129

[15] L. Zhang, X-R. Chen, S-H. Wen, R-P. Lianh, J-D. Qiu, Optical sensors for inorganic arsenic detection, Trends Anal. Chem., 118 (2019) 869-879. https://doi.org/10.1016.j.trac.2019.07.013

[16] A. Lopez, Y. Zhang, J. Liu, Tuning DNA adsorption affinity and density on metal oxide and phosphate for improved arsenate detection, J. Colloid Interface Sci., 493 (2017) 249-256. https://doi.org/10.1016/j.jcis.2017.01.037

[17] K. Chauham, P. Singh, B. Kumari, R. K. Singhal, Synthesis of new benzothiazole Schiff base as selective and sensitive colorimetric sensor for arsenic on-site detection at ppb level, Anal. Methods, 9 (11) (2017) 1779-1785. https://doi.org/10.1039/c6AY03302D

[18] K. J. Parker, S. Kumar, D. A. Pearce, A. J. Sutherland, Design, synthesis and evaluation of a fluorescent peptidyl sensor for the selective recognition of arsenite, Tetrahedron Lett., 46 (2005) 7043-7045. https://doi.org/10.1016/j.tetlet.2005.08.058

[19] M. S. Hosseini, F. Belador, A novel spectrofluorometric method for the determination of arsenic in human hair using Dy2O3-doped CeO2 nanoparticles, Analyst, 139 (2014) 5007-5013. https://doi.org/10.1039/C4AN00746H

[20] J. R. Kalluri, T. Arbneshi, S. A. Khan, A. Neely, P. Candice, B. Varisli, M. Washington, S. McAfee, B. Robinson, S. Banerjee, A. K. Singh, D. Senapati, C. Ray, Use of gold nanoparticles in a sample colorimetric and ultrasensitive dynamic light scattering assay: selective detection of arsenic in groundwater, Chem. Int. Ed., 48 (2009) 9668-9671. https://doi.org/10.1002/anie.200903958.

[21] M. A. Karimi, A. Mohadesi, A. Hatefi-Mehrjardi, S. Z. Mphammadi, J. Yarahmadi,A. Khayrhah, Separation/preconcnetration and speciation analysis of trace amount of arsenate and arsenite in water samples using modified magnetite nanoparticles and molybdenum blue method, J. Chem., 2014 (2014) 1-9. https://doi.org/10.1155/2014/248065

[22] V. Lenoble, V. Deluchat, B. Serpaud, J-C. Bollinger, Arsenite oxidation and arseate determination by molybdenem blue method, Talanta, 61 (2003) 267-276. https:// doi.org/10.1016/S0039-9140(03)00274-1

[23] P. L. Smedley, D. G. Kinniburgh, A review of the source, behaviour and distribution of arsenic in natural waters, Appl. Geochem., 17(5) (2002) 517-568. https://doi.org/10.1016/S0883-2927(02)00018-5

[24] S. Hu, J. Lu, C. Jing, A novel colorimetric method for field arsenic speciation analysis, J. Environ. Sci., 24 (2012) 1341-1346. https://doi.org/10.1016/s1001-0742(11)60922-4

[25] S. Wang, C. N. Mulligan, Effect of natural organic matter on arsenic release from soils and sediments into groundwater, Environ. Geochem. Health, 28 (2006) 197-214. https://doi.org/10.1007/s/0653-005-9032-y

[26] T. J. Sorg, A. S. C. Chen, L. Wang, Arsenic species in drinking water wells in the USA with high arsenic concentrations, Water Res., 48 (2014) 156-169. https://doi.org/10.1016/j.watres.2013.09.016

[27] S. Bhattacharya, S. Sarkar, R. Shunmugam, Unique norbornene polymer based “in-field” sensor for As(III), J. Mater. Chem., 1 (2013) 8398–8405. https://doi.org/10.1039/c3ta11587a

[28] Y. Wu, S. Zhan, F. Wang, L. He, W. Zhi, P. Zhou, Cationic polymers and aptamers mediated aggregation of gold nanoparticles for the colorimetric detection of arsenic(III) in aqueous solution, Chem. Commun., 48 (2012) 4459-4461. https://doi.org/10.1039/c2cc30384a

[29] S. Zhan, M. Yu, J. Lu, L. Wang, P. Zhou, Colorimetric detection of trace arsenic(III) in aqueous solution using arsenic aptamer and gold nanoparticles, Aust. J. Chem., 67

(2014) 813-818. https://doi.org/10.1071/CH13512

[30] Y. Wu, S. Zhan, H. Xing, L. He, L. Xu, P. Zhou, Nanoparticles assembled by aptamers and crystal violet for arsenic(III) detection in aqueous solution based on a resonance Rayleigh scattering spectral assay, Nanoscale, 4 (2012) 6841-6849. https://doi.org/10.1039/c2nr31418e

[31] M. Tang, G. Wen, A. Liang, Z. Jiang, A simple and sensitive resonance Rayleigh scattering method for determination of As(III) using aptamer-modified nanogold as a probe, J. Biol. Chem. Lumin., 29 (2014) 603-608. https://doi.org/10.1002/bio.2589

[32] V. C. Ozaip, D. Cam, F. J. Hernandez, L. I. Hernandez, T. Schafer, H. A. Oktem, Small molecule detection by lateral flow strips via aptamer-gated silica nanoprobes, Analyst, 141 (2016) 2595-2599. https://doi.org/10.1039/C6AN00273K

[33] A. Krishna TG, V. Tekuri, M. Mohan, D. R. Trivedi, Selective colorimetric chemosensor for the detection of Hg2+ and arsenite ions using Isatin based Schiff's bases; DFT studies and Applications in test strips, Sens. Actuators B Chem., 284 (2018) 271-280. https:// doi.org/10.1016/j.snb.2018.12.003

[34] Y. Wu, F. Wang, S. Zhan, L. Liu, Y. Luo, P. Zhou, Regulation of hemin peroxidase catalytic activity by arsenic-binding aptamers for the colorimetric detection of arsenic(III), RSC Adv., 3 (2013) 25614–25619. https://doi.org/10.1039/c3ra44346a

[35] K. Shrivas, R. Shankar, K. Dewangan, Gold nanoparticles as a localized surface plasmon resonance based chemical sensor for on-site colorimetric detection of arsenic in water samples, Sens. Actuators B Chem., 220 (2015) 1376-1383. https://doi.org/10.1016/j.snb.2015.07.058

[36] D. Vilela, M. C. Gonzalez, A. Escarpa, Sensing colorimetric approaches based on gold and silver nanoparticles aggregation: Chemical creativity behind the assay, A review, Anal. Chim. Acta, 751 (2012) 24-43. https://doi.org/10.1016/j.acs.2012.08.043

[37] N. Oksuz, S. Sacmaci, M. Sacmaci, A. Ulgen, A new fluorescence reagent: Synthesis, characterization abd application for speciation of arsenic (III)/(VI) in tea samples, Food Chem., 270 (2019) 579-584. https://doi.org/10.1016/j.foodchem.2018.07.076

[38] S. S. Boxi, S. Paris, Fluorometric sensing of ultralow AS(III) concentrations using Ag doped hollow CdS/ZnS bi-layer nanoparticles, Dalton Trans., 44 (2015) 20464-20474. https:// doi.org/10.1039/c5dt03958d

[39] G. Hodake, V. S. Vassilliadis, J-H. Choi, J. Jang, D. S. Lee, Facile synthesis of gold nanoparticles by amino acid asparagine: selective sensing of arsenic, J. Nanosci. Nanotechnol., 15 (2015) 7235-7239. https://doi.org/10.1166/jnn.2015.10561

[40] B. S. Boruah, R. Biswas, Selective detection of arsenic (III) based on colorimetric approach in aqueous medium using functionalized gold nanoparticles unit, Mater. Res. Express, 5 (2018) 015059. https://doi.org/10.1088/2053-1591 /aaa661

[41] R. Qian, L. Ding, H. Ju, Switchable fluorescent imaging of intracellular telomerase activity using telomerase-responsive mesoporous silica nanoparticle, J. Am. Chem. Soc., 135 (2013) 13282-13285. https://doi.org/10.1021/ja406532e

[42] Y. Liu, C. V. Huang, Real-time dark-field scattering microscopic monitoring of the in situ growth of single Ag@Hg nanoalloys, ACS Nano, 7 (2013) 11026-11034. https://doi.org/10.1021/nn4040694e

[43] S. D. Rchardson, T. A. Ternes, Water analysis: emerging contaminants and current issues, Anal. Chem., 90 (2018) 398-428. https://doi.org/10.1021/acs.analchem.7b00661

[44] E. I. Brima, P. Haria, R. O. Jenking, D. A. Polya, A. G. Gault, C. F. Harrington, Understanding arsenic metabolism through

a comparative study of arsenic levels in the urine, hair and fingernails of healthy volunteers from three unexposed ethnic groups in the United Kingdom, Toxicol. Appl. Pharmacol., 216 (2016) 122-130. https://doi.org/10.1021/acs.analchem.7b04577

[45] K.-M. Wai, S. Wu, X. Li, D. A. Jaffe, K. D. Perry, Global atmospheric transport and source-receptor relationships for arsenic, Environ. Sci. Technol., 50 (7) (2016) 3714-3720. https://doi.org/10.1021/acs.est.5b05549

[46] V. C. Ezeh, T. C. Harrop, A sensitive and selective fluorescence sensor for the detection of arsenic(III) in organic media, Inorg. Chem, 51 (2012) 1213-1215. https://doi.org/10.1021/ic2023715

[47] L. P. Wu, Y. F. Li, C. Z. Huang, Q. Zhang, Visual detection of sudan dyes based on the plasmon resonance light scattering signals of silver nanoparticles, Anal. Chem., 78 (2006) 5570-5577. https://doi.org/10.1021/ac0603577

[48] J. Ling,Y. F. Li, C. Z. Huang, Visual sandwich immunoassay system on the basis of plasmon resonance scattering signals of silver nanoparticles, Anal. Chem., 4 (2009) 1707-1714. https://doi.org/10.1021/ac802152b

[49] B. Dey, R. Saha, P. Mukherjee, A luminescent-water soluble inorganic co-crystal for a selective pico-molar range arsenic(iii) sensor in water medium, Chem. Commun., 49 (2013) 7064-7066. https://doi.org/10.1039/c3cc43574A

[50] W. Siangproh, O. Chailapakul, K. Songsrirote, Simple and fast colorimetric detection of inorganic arsenic selectively adsorbed onto ferrihydrite-coated silica gel using silver nanoplates, Talanta, 153 (2016) 197–202. http:// doi.org/10.1016/j.talanta.2016.03.028

[51] R. Kanjanawarut, X. Su, Colorimetric detection of DNA using unmodified metallic Nanoparticles and peptide nucleic acid probes, Anal. Chem, 81 (2009) 6122-6129. https://doi.org/10.1021/ac900525k

[52] S.-H. Wen, R.-P. Liang, L. Zhang, J.-D. Qiu, Multimodal assay of arsenite contamination in environmental samples with improved sensitivity through stimuli-response of multiligands modified silver nanoparticles, ACS Sustain. Chem. Eng., 6 (2018) 6223−6232. https://doi.org/10.1021/acssuschemeng.7b04934

[53] R. Wilson, The use of gold nanoparticles in diagnostics and detection, Chem. Soc. Rev., 37 (2008) 2028-2045. https://doi.org/10.1039/B712179M

[54] L. E. S. Figueroa, M. E. Morague, E. Climent, A. Agostini, R. M. Manez, F. Sancenon, Chromogenic and fluorogenic chemosensors and reagents for anions. A comprehensive review of the year 2010-2011, Chem. Soc. Rev., 42 (2013) 3485-3613. https://doi.org/10.1039/c3cs35429f

[55] N. Priyadarshni, P. Nath, Nagahanumaiah, N. Chanda, DMSA-functionalized gold nanorod on paper for colorimetric detection and estimation of arsenic (III and V) contamination in groundwater, ACS Sustain. Chem. Eng., 6 (2018) 6264−6272. https://doi.org/10.1021/acssuschemeng.8b00068

[56] P. Nath, N. Priyadarshni, N. Chanda, Europium-coordinated gold nanoparticles on paper for the colorimetric detection of arsenic(III, V) in aqueous solution, ACS Appl. Nano Mater., 1 (2018) 73−81. https://doi.org/10.1021/acsanm.7b00038

[57] J. Zhang, C.-L. Zhang, S.-H. Yu, Tuning gold nanoparticle aggregation through the inhibition of acid phosphatase bioactivity: A plasmonic sensor for light-up visual detection of arsenate (AsV), Chem. Plus Chem., 81 (2016) 1147- 1151. http:// doi.org/10.1002/cplu.201600355J

[58] W. He, C. Z. Huang, Y. Fang, J. Ping, R. G. Yang, P. F. Zohou, J. Wang, One-step label-free optical genosensing system for sequence-specific DNA related to the

human immunodeficiency virus based on the measurements of light scattering signals of gold nanorods, Anal. Chem., 22 (2008) 8424-8430. https://doi.org/10.1021/ac801005d

[59] S. S. Mendez, O. D. Renedo, M. J. A. Martines, Development of acid phosphatase based amperometric biosensors for the inhibitive determination of As(V), Talanta, 9 (2012) 301-306. https://doi.org/10.1016/j.talanta.2012.02.037

[60] P. Nath, R. K. Arun, N. Chanda, A paper based microfluidic device for the detection of arsenic using a gold nanosensor, RSC Adv., 4 (2014) 59558-59561. https:// doi.org/10.1039/c4ra12946f

[61] Z.-Q. Tan, J-F. Liu, Y-G. Yin, Q-T. Shi, C-Y. Jing, G-B. Jiang, Colorimetric Au nanoparticle probe for speciation test of arsenite and arsenate inspired by selective interaction between phosphonium ionic liquid and arsenite, ACS Appl. Mater. Interfaces, 6 (2016) 19833-19839. https://doi.org/10.1021/am5052069

[62] N. Xia, Y. Shi, R. Zhang, F. Zhao, F. Liu, L. Liu, Simple, rapid and label-free colorimetric assay for arsenic based on unmodified gold nanoparticles and a phytochelatin-like peptide, Anal. Methods, 4 (2012) 3937-3941. https:// doi.org/10.1039/c2ay25803j

[63] R.-P. Liang, Z.-X. Wang, L. Zhang, J.-D. Qiu, Label-free colorimetric detection of arsenite utilizing G-/T-rich oligonucleotides and unmodified Au nanoparticles, Chem. Eur. J., 19 (2013) 5029-5033. http:// doi.org/10.1002/chem.201203402

[64] N. Yogaraja, S. S. H. Tsai, Detection of trace arsenic in drinking water: challenges and opportunities for microfluidics, Environ. Sci.: Water Res. Technol., 1 (2015) 426-441. https://doi.org/10.1039/C5EW00099H

[65] T. Yang, X.-X. Zhang, J.-Y. Yang, Y.-T. Wang, M.-L. Chen, Screening arsenic (III)-binding peptide for colorimetric detection of arsenic (III) based on the peptide induced aggregation of gold nanoparticles, Talanta, 177 (2017) 212-216. http:// doi.org/10.1016/j.talanta.2017.07.005

[66] S.-H. Wen, X.-L. Zhong, Y.-D. Wu, R.-P. Liang, L. Zhang, J.-D. Qiu, Colorimetric assay conversion to highly sensitive electrochemical assay for bimodal detection of arsenate based on cobalt oxyhydroxide nanozyme via arsenate absorption, Anal. Chem., 91 (2019) 6487-6497. https://doi.org/10.1021/acs.analchem.8b05121

[67] M. Li, H. Gou, I. Al-Ogaidi, N. Wu, Nanostructured sensors for detection of heavy metals: A review, ACS Sustain. Chem. Eng., 7 (2013) 713-723. https://doi.org/10.1021/SC4000199

[68] C. A, De Villiers, M. C. Lapsley, E. A. H. Hall, A step towards mobile arsenic measurement for surface water, Analyst, 140 (2015) 2644-2655. https:// doi.org/10.1039/c4an02368d

[69] N. Yadav, A. K. Singh, Dual anion colorimetric and fluorometric sensing of arsenite and cyanide ions, RSC Adv., 6 (2016) 100136–100144. https:// doi.org/10.1039/c6ra19781g

[70] D. Pooja, S. Saini, A. Thakur, B. Kumar, S. Tyagi, M. K. Nayak, A turn-on thiol functionalized fluorescent carbon quantum dotbased chemosensory system for arsenite detection, J. Hazard. Mater., 328 (2017) 117–126. http:// doi.org/10.1016/j.jhazmat.2017.01.015

[71] G. K. Das, C. S. Bonofacio, J. De Rojas, K. Liu, K. Benthem, Ultra-long magnetic nanochains for highly efficient arsenic removal from water, J. Mater. Chem. A, 2 (2014) 12974-12981. https://doi.org/10.1039.C4TA02614D

[72] L. Zhang, X-Z. Cheng, L. Kuangn, A-Z. Xu, R. P. Liang, J-D. Qui, Simple and highly selective detection of arsenite based on the assembly-induced fluorescence enhancement of DNA quantum dots, Biosens. Bioelectron., 94 (2017) 701-706. https://doi.org/10.1016/j.bios.2017.03.057

[73] Z. Liu, G. Li, T. Xia, X. Su, Ultrasensitive fluorescent nanosensor for arsenate assay and removal using oligonucleotide-functionalized CuInS2 quantum dot@ magnetic Fe_3O_4 nanoparticles composite, Sens. Actuators B Chem., 220 (2015) 1205-1211. https://doi.org/10.1016/j.snb.2015.06.111

[74] A. A. Ensafi, N. Kazemifard, B. Rezaei, A simple and sensitive fluorimetric aptasensor for the ultrasensitive detection of arsenic(III) based on cysteamine stabilized CdTe/ZnS quantum dots aggregation, Biosens. Bioelectron., 77 (2016) 499-504. https://doi.org/10.1016/j.bios.2015.10.011

[75] S. K. Pal, N. Akhtar, S. K. Ghosh, Determination of arsenic in water using fluorescent ZnO quantum dots, Anal. Methods, 8 (2016) 445-452. https://doi.org/10.1039/C5AY02472B

[76] S. Cosnier, C. Mousty, X. Cui, X. Yang, Specific determination of As(V) by an acid phosphatase−polyphenol oxidase biosensor, Anal. Chem., 78 (2006) 4985-4989. https://doi.org/10.1021/ac060064d

[77] X. Ge, Y. Ma, X. Song, G. Wang, H. Zhang, Y. Zhang, H. Zhao, β-FeOOH nanorods/carbon foam-based hierarchically porous monolith for highly effective arsenic removal, ACS Appl. Mater. Interfaces, 9 (2017) 13480-13490. https://doi.org/10.1021/ascami.7b01275

[78] Y. Zhou, X. Huang, C. Liu, R. Zhang, X. Gu, G. Guan, C. Jiang, L. Zhang, S. Du, B. Liu, M.-Y. Han, Z. Zhang, Color-multiplexing-based fluorescent test paper: dosage-sensitive visualization of arsenic(III) with discernable scale as low as 5 ppb, Anal. Chem., 88 (2016) 6105−6109. https://doi.org/10.1021/acs.analchem.6b01248

[79] S. Roy, G. Palui, A. Banerjee, The as-prepared gold cluster-based fluorescent sensor for the selectivedetection of As(III) ions in aqueous solution, Nanoscale, 4 (2012) 2734-2740. https://doi.org/10.1039/c2nr11786j

[80] M. Shah, D. Fawcett, S. Sharma, S. K. Tripathy, G. E. D. Poineru, Green synthesis of metalic nanoparticles via biological entities, Materials, 8 (2015) 7278-7308. https://doi.org/10.3390/ma811577

[81] M. Bagan, S. Atilgan, Selective and sensitive turn-on fluorescent sensing of arsenite based on cysteine fused tetraphenylethene with AIE characteristics in aqueous media, Chem. Commun., 49 (2013) 495325-5327. https://doi.org/10.1039/c3cc42238k

[82] F. Sancenon, L. Pascual, M. Oroval, E. Pznrr, R. M. Manez, Gated silica mesoporous materials in sensing applications, Chem. open, 4 (2015) 418-437. https://doi.org/10.1002/open.201500053

[83] X. He, Y. Zhao, D. He, K. Wang, F. Xu, J. Tang, ATP-responsive controlled release system using aptamer-functionalized mesoporous silica nanoparticles, Langmuir, 28 (2012) 12909-12915. https://doi.org/10.1021/19302767b

[84] M. Oraval, E. Climent, C. Coll, R. Eritja, A. Avino, M. Dolores, F. Saneenon, R. M. Manez, P. Amoros, An aptamer-gated silica mesoporous material for thrombin detection, Chem. Commun., 49 (2013) 5480-5482. https://doi.org/10.1039/C3CC42157k

[85] C. Argyo, V. Weiss, C. Brauchle, T. Bein, Multifunctional mesoporous silica nanoparticles as a universal platform for drug delivery, Chem. Mater., 26 (2014) 435-451. https://doi.org/10.1021/cm402592t

[86] M. Oroval, C. Coll, A. Bernardos, M. D. Marcos, R. M. Manez, D. G. Shchukin, F. Sancenon, Selective fluorogenic sensing of As(III) using aptamer-capped nanomaterials, ACS Appl. Mater. Interfaces, 9 (2017) 11332−11336. https://doi.org/10.1021/acsami.6b15164

[87] R. Liu, Z. Chen, Y. Wang, Y. Cui, H. Zhu, P. Huang, W. Li, Y. Zhao, Y. Tao, X. Gao, Nanoprobes: quantitatively detecting the Femtogram level of arsenite ions in live cells, ACS Nano, 5 (2011) 5560-5565.

https://dx.doi.org/10.1021/nn200994r

[88] S. Lohar, S. Pal, B. Sen, M. Mukherjee, S. Banerjee, P. Chattopadhyay, Selective and sensitive turn-on chemosensor for arsenite ion at the ppb level in aqueous media applicable in cell staining, Anal. Chem., 86 (2014) 11357-11361. https://doi.org/10.1021/ac503255f

[89] M. Tuzen, K. O. Saygi, I. Karaman, M. Soylak, Selective speciation and determination of inorganic arsenic in water, food and biological samples, Food Chem. Toxicol., 48 (2010) 41-46. https://doi.org/10.1016/j.fct.2009.09.012

[90] R. Lv, J. Zhang, H. Li, L. Yang, S. Liao, W. Gu, X. Liu, An amino-decorated dual fucntionalized metal-organic framework for highly selective sensing of Cr(III) and Cr (VI) ions and detection of nitroaromatic explosive, J. Master. Chem. A, 4 (2016) 15494-15500. https://doi.org/10.1039/C6TA05965A

[91] Y-L. Shi, W-Q. Chen, S-L. Wu, Y-G. Zhu, Anthropogenic cycles of arsenic in mainland china: 1990–2010, Environ. Sci. Technol., 51(13) (2017) 1670-1678. https://doi.org/10.1021/acs.est.6b01669

[92] D. S. Tawflk, R. E. Viola, Arsenate replacing phosphate: alternative life chemistries and ion promiscuity, Biochem., 50 (2011) 1128-1134. https://doi.org/10.1021/b12004529

[93] Y. Liu, C. Yu, Z. Cao, D. Shvarts, W. Trogler, A highly sensitive enzymatic catalysis system for trace detection of arsenic in water, Chem. Eur. J., 23 (2017) 10289-10292. https://doi.org/10.1002/chem.201702769

[94] B. Liu, J. Liu, DNA adsorption by magnetic iron oxide nanoparticles and its application for arsenate detection, Chem. Commun., 50 (2014) 8568-8570. https://dx.doi.org/10.1039/c4cc03264k

[95] M. Elias, A. Wellner, K. G. Azulay, E. Chabriere, J. A Vorholt, T. J. Erb, D. S. Tawflk, The molecular basis of phosphate discrimination in arsenate-rich environments, Nature, 491 (2012) 134-137. https://doi.org/10.1021/ac0661455

[96] D. Xie, Y. Ma, Y. Gu, H. Zhou, H. Zhang, G. Wang, Y. Zhang, H. Zhoa, Bifunctional NH_2-MIL-88(Fe) metal–organic framework nanooctahedra for highly sensitive detection and efficient removal of arsenate in aqueous media, J. Mater. Chem. A, 5 (2017) 23794–23804. https://doi.org/10.1039/c7ta07934f

[97] T. Wang, R. D. Milton, S. Abdellaoui, D. P. Hickey, S. D. Minteer, Laccase inhibition by arsenite/arsenate: determination of inhibition mechanism and preliminary application to a self-powered biosensor, Anal. Chem., 88 (2016) 3243-3248. https://doi.org/10.1021/acs.analchem.5b04651

[98] S.-H. Wen, R.-P. Liang, H.-H. Zeng, L. Zhang, J.-D. Qiu, CdSe/ZnS quantum dots coated with carboxy-PEG and modified with the terbium(III) complex of guanosine 5′-monophosphate as a fluorescent nanoprobe for ratiometric determination of arsenate via its inhibition of acid phosphatase activity, Microchim. Acta, (2019) 1-10. https://doi.org/10.1007/s00604-018-3125-7

[99] S. Lohar, A. Sahana, A. Banerjee, A. Banik, S. K. Mukhopadhyay, J. S. Matalobos, D. Das, Antipyrine based arsenate selective fluorescent probe for living cell imaging, Anal. Chem., 85 (2013) 1778-1783. https://dx.doi.org/10.1021/ac3031338

[100] A. S. M. Islam, R. Alam, A. Katarkar, K. Chaudhuri, M. Ali, Di-oxime based selective fluorescent probe for arsenate and arsenite ions in a purely aqueousmedium with living cell imaging applications andH-bonding induced microstructure formation, Analyst, 140 (2015) 2979-2983. https://dx.doi.org/10.1039/c5an00236b

[101] D. C. RoBler, S. Lotters, L. Fernando, M. D. Fonte, Author declaration: have you considered equity, diversity and inclusions, Nature, 584 (2020) 525-525. https://doi.org/10.1038/d41586-020-02429-8

Anal. Methods Environ. Chem. J. 6 (1) (2023) 58-68

AMECJ

Research Article, Issue 1
Analytical Methods in Environmental Chemistry Journal
Journal home page: www.amecj.com/ir

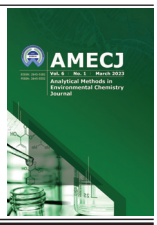

Study of the behavior and determination of phenol Based on modified carbon paste electrode with nickel oxide-nitrogen carbon quantum dots using cyclic voltammetry

Khalil Ibrahim Alabid [a,*] **and Hajar Naser Nasser** [a]
[a]*Analytical Chemistry - Department of Chemistry - Faculty of Science - Tishreen University – Syria.*

ARTICLE INFO:
Received 2 Dec 2022
Revised form 7 Feb 2023
Accepted 29 Feb 2023
Available online 29 Mar 2023

Keywords:
Phenol,
Cyclic voltammetry,
Modified carbon paste electrode,
Nickel oxide nanoparticles,
Nitrogen carbon quantum dots,
Kinetic

ABSTRACT
The behavior of phenol was studied and determined using the modified carbon paste electrode (*MCPE*) with nickel oxide nanoparticles doped by nitrogen carbon quantum dots as nanoadsorbent (NiO-NCQD) and cyclic voltammetry (CV). The MCP electrode was manufactured in a laboratory. The modified carbon paste consisted of 12% (NiO-NCQD), 44% of graphite powder and 44% of paraffin oil to get a modified carbonate paste. Cyclic voltammetry can provide behavior information; as such: diffusion coefficient (D), charge transfer coefficient ($\alpha.n\alpha$), the mass transport (m_{trans}) found that diffusion coefficient, the reducing of mass transport (m_{trans}) by increasing the phenol concentration in the solution, and increasing of constant K^0 when the concentration of phenol increased in the solution. Also, the highest occupied molecular orbital (HOMO), lowest unoccupied molecular orbital (LUMO), and Gibbs free energy (ΔG) are studied and calculated. In this study, E_{HOMO}=4.92eV, E_{LUMO}=0.32eV, and ΔG=-4.17 were considered. The drinking water samples from Latakia city were analyzed based on NiO-NCQD adsorbent using the *MCPE* method (NiO-NCQD/MCPE). The phenol concentration in the drinking water sample in Latakia was achieved less than the quantitative detection limit (LOQ), and the proposed procedure was validated by spiking samples.

1. Introduction

Phenol is described as an aromatic organic compound C_6H_5OH. Phenol and its derivatives are the main pollutants in water sources [1]. It is highly toxic [2-4] and enters the human body through ingestion, inhalation, or contact with the skin; exposure to phenol for long periods causes severe damage. Among these damages: Damage to the lungs, liver, kidneys, urinary and reproductive tracts, cardiovascular disease, shortness of breath, neurological problems, as well as severe abdominal pain, gastrointestinal irritation, nausea, vomiting, diarrhea, sweating, coma, and death. Ingestion of 1g of phenol is a lethal dose [5-9]; phenol increases oxidative stress in biological materials, disrupting endocrine metabolism and promoting cancer [10]; the maximum permissible level of phenol according to the world health organization (WHO) that its concentration does not exceed one µg L^{-1} in drinking water [11]. Phenol and total phenol can be estimated spectrophotometrically in the visible (VIS) [12-19], in the ultraviolet (UV) [20], and High-Performance Liquid Chromatography (HPLC) [21-22]. Schema 1 showed the phenol oxidation (one-electron oxidation) and reaction process [23,24].

*Corresponding Author: Khalil Ibrahim Alabid
Email: khalilibrahimalabid@gmail.com
https://doi.org/10.24200/amecj.v6.i01.227

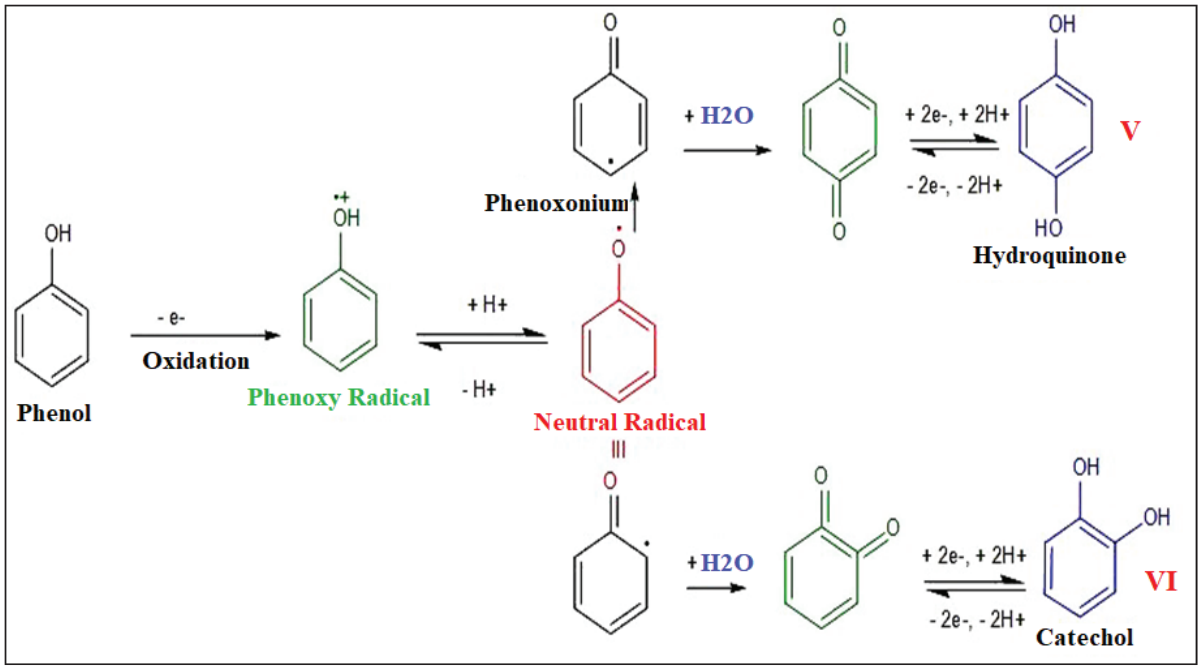

Schema 1. The oxidation and reaction of phenol

Cyclic voltammetry is one of the most important electrochemical techniques that help provide information about the kinetics, mechanics, and behavior of the studied material [25]; it is also possible from cyclic voltammetry to know if the reaction is subject to oxidation, reduction, or both. It has three cases: reversible, quasi-reversible, or irreversible [26]. Cyclic voltammetry can provide kinetic and mechanistic information; as such: Diffusion coefficient (D) [27-30], mass transport (m_{trans}) [31-33], Charge Transfer Coefficient ($\alpha . n_{\alpha}$), [34], and constant K^0 [35], the highest occupied molecular orbital (HOMO), lowest unoccupied molecular orbital (LUMO) [36, 37], Gibbs free energy (ΔG) [38] and interface trap density (Dit) [39].

The diffusion coefficient is calculated from Randles-Sevcik irreversible Equation 1 [27-30]. The mass transport is given by Equation 2 [31-33]. Also, the charge transfer coefficient (CTC) is given by Equation 3 [34]. Constant (k^0) is defined by the standard rate constant (k^0) ratio to mass transfer. It is given by Equation 4 [35]. The HOMO-LUMO values are given by Equations 5 and 6 [36-37]. Gibbs free energy ΔG is given by Equation 7 [38].

The interface trap density (Dit) can be obtained by Equation 8[39].

$$i_p = \mp 0.4961 \sqrt{\alpha . n_{\alpha}}\, nFA_{real} C \left(\frac{nFvD}{RT}\right)^{\frac{1}{2}} \quad \text{(Eq.1)}$$

Where, i_p: Peak current (A), n: Number of electrons, F: faraday's constant (C. mol^{-1}), A: electrode area (cm^2), α: transfer coefficient of the redox reaction, C: concentration (mol. cm^{-3}), R: gas constant (J. mol^{-1} K^{-1}), T: Temperature (K), D: diffusion coefficient ($cm^2 s^{-1}$), v: Scan rate (V s^{-1}).

$$m_{trans} = \left(\frac{\pi n F D v}{RT}\right)^{\frac{1}{2}} \quad \text{(Eq.2)}$$

$$\alpha . n_{\alpha} = \frac{15.1RT}{\Delta E_p F} \quad \text{(Eq.3)}$$

Where α: is the charge transfer coefficient and represents a measure of the symmetry barrier in a non-reversible electrode process, nα: is the number of electrons involved in the rate-determining step.

$$k^0 = \frac{i_0}{F} \quad \text{(Eq.4)}$$

Where: i_o: exchange current density (A m^{-2}), in the case where the oxidation is irreversible it must be: $k^0 \ll m_{trans}$, as for according to Nicholson, must be $k^0 < 3.5 \times 10^{-4} \times v^{1/2}$.

$$E_{HOMO}\ eV = [E_{ox} - E_{1/2} + 4.8] \quad \text{(Eq.5)}$$

$$E_{LUMO} = (E_{HOMO} - E_g) \quad \text{(Eq.6)}$$

Where: E_{ox}: oxidation potential (From CV), $E_{1/2}$: half-oxidation potential for peak, E_g: Optical Bandgap (from absorption studies).

$$\Delta G = E_{ox} - E_{red} - E_g + C \quad \text{(Eq.7)}$$

Where: E_{ox}: Oxidation potential, E_{red}: Redaction potential, E_g: the excited singlet state energies, C: is the electrostatic interaction energy for the initially formed ion pair, generally considered negligible in polar solvents.

$$Dit = \frac{C_{OX} * \Delta V}{q\,A * E_g} \quad \text{(Eq.8)}$$

A, q, Cox, V, and Eg are the gate area, electron charge, accumulation capacitance, flat-band voltage shift, and bandgap.

Carbon/graphite paste electrodes (CPE) are important for being chemically inert, easy to fabricate, electrode surface renewability, low ohmic resistance, low cost, and environmentally friendly. However, its kinetics, stability, and selectivity are weak. To solve this problem, surface modification (CPE) is resorted to by modifiers [40]; therefore, in this study, modified carbon paste electrodes were relied upon, as they are more selective and sensitive to organic compounds. This research is one of the critical research studies on the behavior of phenol in the electrochemical cell and determines the concentration of phenol in a drinking water sample using a selective electrode for carbon paste with nanoparticles by cyclic voltammetry.

2. Experimental

2.1. Instruments

Voltammetry system for trace analysis and education. Complete accessories with VA Computrace software and all electrodes for a complete measurement system: Multi-Mode Electrode pro (MME pro), Ag/AgCl reference electrode, and Pt auxiliary electrode. In this study, a modern voltammetric was connected to a PC based on a USB port (Metrohm 797; volt-amperometric analyzer with analyzer cell). Sartorius pH meter type PB-11 was used from Data Weighing System Company (pH meter and mV meter; DWS Inc., USA)

2.2. Reagents and Materials

All chemicals with high purity were purchased from Sigma or Merck Company (Germany). Phenol C_6H_6O purchased from Acros Organics Company (AC221755000, molecular weight 94.11g mol^{-1}, specific density d=1.070 g cm^{-3}, high purity 99%). The monopotassium dihydrogen phosphate (KH_2PO_4) was prepared from Sigma, Germany (CAS No.: 7778-77-0). The boiled and cooled double distilled water (DDW, 18.2 MΩ.cm, 1.5 L, Sigma).

2.3. Synthesis of NiO-NCQD nanocomposite

Take 0.6 g of NiO Nanoparticles (20nm) are added with 30 mL of nitrogen quantum carbon dot after filtering it with a micro-filter (syringe with filter 0.45µm) and subjected to ultrasonic for 1.5h, then washed three times with distilled water and dried in an oven at 60 for 12h to get NiO-NCQD nanocomposite.

2.4. General procedure

2.4.1. Fabrication of selective electrode

The selective electrode is made (in the laboratory). It consists of a glass tube that is open at both ends and contains at its lower end modified carbon paste at the upper back; it is connected to the device. A copper wire conducting electric current is connected between the modified carbon paste and the device. The modified carbon paste using NiO-NCQD nanocomposite (12 %),

graphite (44%), and paraffin oil (44 %) for a total weight of the modified carbon paste of 0.5 g; the components are mixed in specific proportions and then packed in the electrode body is made of glass. Symbolizes the factory electrode (NiO-NCQD/MCPE) shown in Figure 1. Then the electrode is connected to the volt-amperometric cell (VA), which consists of a working electrode (WE) and a comparison electrode, and it is usually an Ag/AgCl electrode where its potential is 0.222v at 25°C and an Auxiliary Electrode (AE).

2.4.2.Preparation of stock solution and *monopotassium phosphate buffer*

To prepare a 0.1036 M phenol solution, take 0.974 g of phenol, then dissolve it into 100 ml distilled water using a volumetric flask. The buffer was prepared from KH_2PO_4 at a concentration of 0.1 M and a solution of KOH potassium hydroxide at 0.1 M by mixing different volumes of both of them to obtain a pH of 4 and 7.

3. Results and discussion

3.1. Effect of pH

The effect of pH is studied within the range of (3-8) on the current intensity I(µA) of a standard phenol solution shown in Figure 2.

From the previous drawing curve, Through the values of and U(V), it is noted that it two peaks

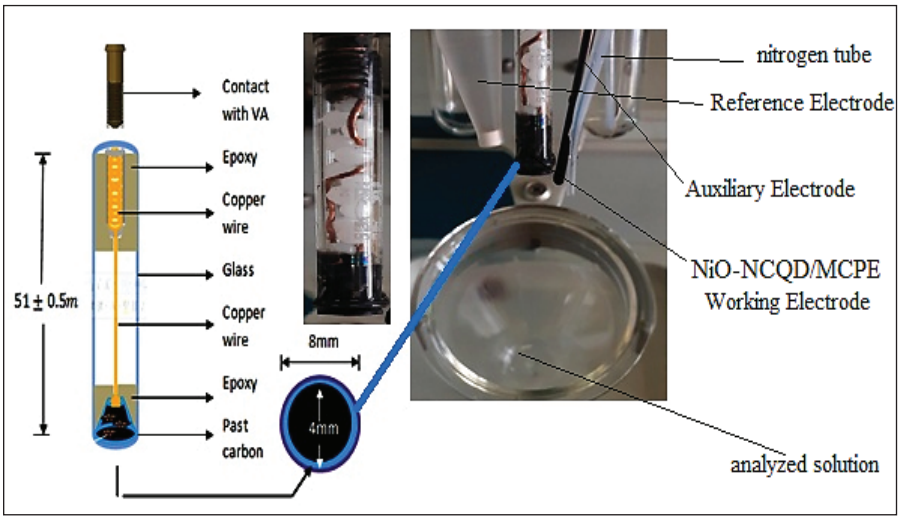

Fig. 1. Schematic of factory electrode components (NiO-NCQD/MCPE)

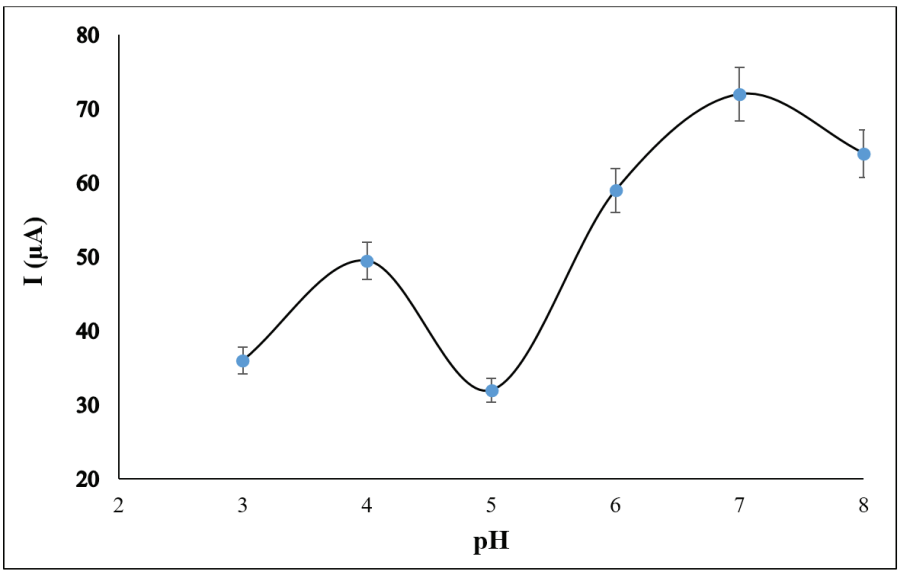

Fig. 2. Effect pH on ip and U(V) for 1 mM phenol on the electrode (NiO-NCQD/MCPE)

and achieves the highest value of peak current = 49.5µA, =72µA at pH =7 respectively, so these two values are adopted. In the case of phenol, when used CV method, it undergoes an oxidation process only without reduction, so the system is irreversible, phenol concentration is studied with ranges of phenol (10 - 250 - 500 – 750 – 1000) µM by (CV) method using a buffer solution of at pH (4,7), scan rate = 100mv.s^{-1} = 0.1v. s^{-1} both of pH (4,7), step voltage is 0.04166V and 0.05991V for both (pH =4,7), respectively, using the electrode (NiO-NCQD/MCPE).

Cyclic voltammetry can provide behavior information; as such: the diffusion coefficient (D), charge transfer coefficient (α. n_α), the mass transport (m_{trans}), and the values of each are calculated (Table 1).

3.2. Effect of phenol concentration

The curve of each diffusion coefficient, charge transfer coefficient, constant K^o, and mass transport and interface trap density (Dit) are studied for the phenol concentrations, as in Figures 3(A-D).

From previous curves, the mass transport and diffusion coefficients with the increase of phenol concentration, probably due to increasing phenol concentration, cause the blockage of the electrode surface. In the case where the oxidation is irreversible, it must be: $K^o < m_{trans}$, according to Nicholson, must be $k^0 < 3.5 \times 10^{-4} \times v^{(1/2)}$, from previous curves, In this research, $K^0 < m_{trans}$ and $K^0 < 3.5 \times 10^{-4} \times 0.1 = 3.5 \times 10^{-5}$, the HOMO-LUMO values are studied from cyclic voltammetry using modified carbon paste using NiO-NCQD nanocomposite, where E_{ox} = 0.43 V, and $E_{1/2}$ = 0.31 V, the gap from absorption studies at 270 nm=4.6 from (UV) so, E_{HOMO} = 4.92 ev, optical band, so

Table 1. Values of charge transfer coefficient, diffusion coefficient, and mass transport of phenol at pH=4 and pH=7 using (NiO-NCQD/MCPE)

pH	CµM	I (µA)	$D \times 10^9$ ($m^2 \cdot s^{-1}$)	n_α α.	m_{trans}	$K^o \times 10^7$	(Dit) eV^{-1} cm^{-2}
4	1000	90	0.036278	1.615581	2.20006E-05	1.485325000	2.95483E+13
	750	72	0.033772	1.974600	2.1227E-05	1.18826000	2.85093E+13
	500	64	0.060039	1.974600	2.83026E-05	1.056231000	3.80124E+13
	250	56	0.194084	1.870673	5.08868E-05	0.924202000	6.83445E+13
	١0	45	88.63469	1.653153	0.001087458	0.742663000	1.46053E+15
7	1000	104	0.048443	1.615581	2.54229E-05	1.716375904	3.41447E+13
	750	99	0.067397	1.870673	2.99869E-05	1.633857832	4.02745E+13
	500	92	0.151635	1.615581	4.4979E-05	1.518332531	6.04099E+13
	250	83	0.594651	1.341237	8.90721E-05	1.369800001	1.1963E+14
	١0	69	220.0211	1.565762	0.001713337	1.138749398	2.30113E+15

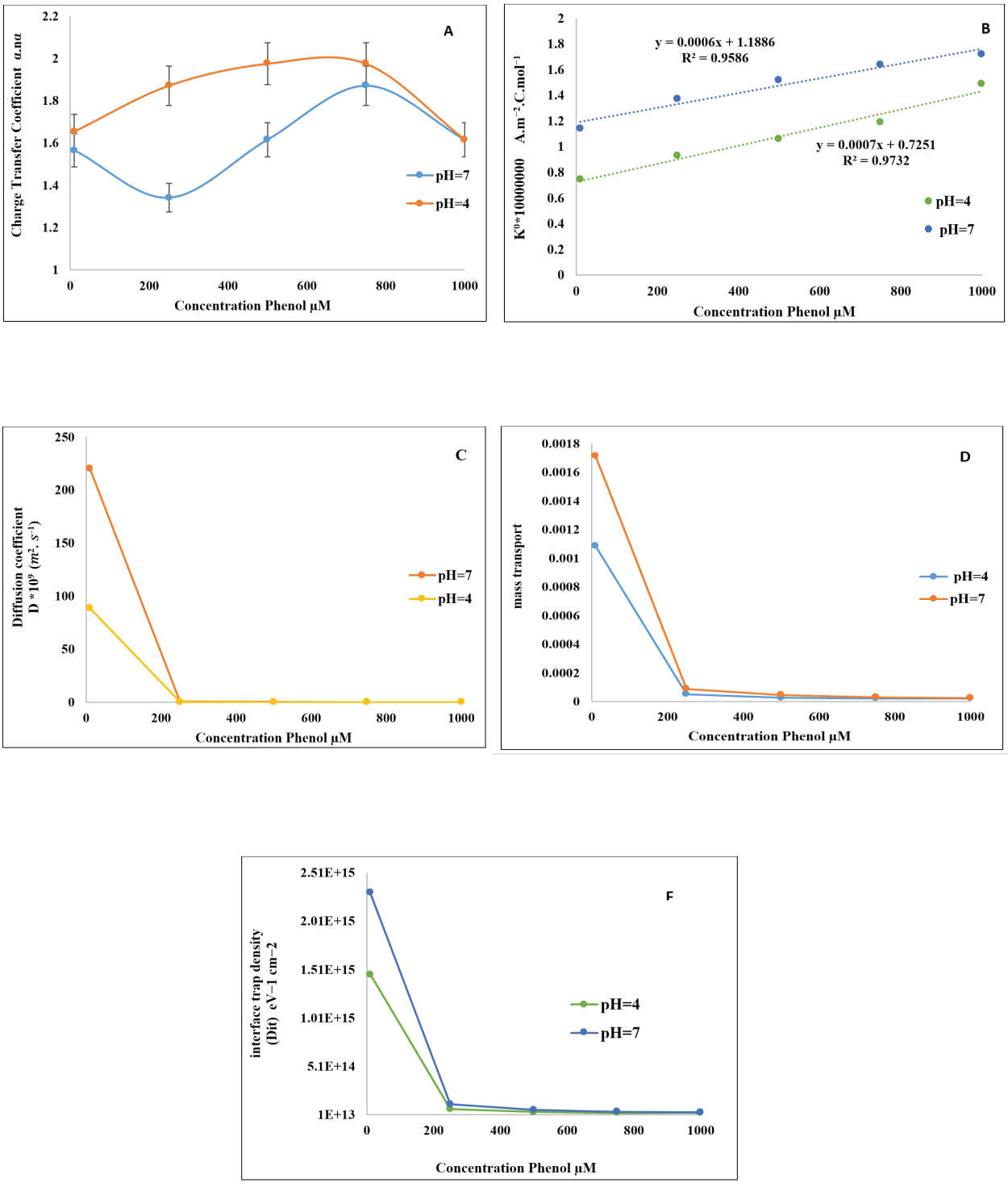

Fig. 3. Effect of phenol concentration on
A) charge transfer coefficient,
B) constant K0,
C) diffusion coefficient,
D) mass transport,
F) and interface trap density on the surface of the proposed electrode NiO-NCQD/MCPE

$E_{LUMO=}$ 0.32 ev, As for the value of Gibbs free energy ΔG was -4.17. In this case, ΔG, the reaction is spontaneous in the direction with electric current. The interface trap density (Dit) of the electrode has a value within ($2.95483\times10^{+13}$- $1.46053\times10^{+15}$) eV^{-1} cm^{-2} at pH=4 and ($3.41447\times10^{+13}$- $2.30113\times10^{+15}$) eV^{-1} cm^{-2} at pH=7. The large values indicate good corresponding and, as noted, interface trap density (Dit) decrease in value with increasing concentration. stirring the solution has a significant effect on the response, so the solution is stirred initially in the pre-measurement stage at a rate of 2000 rpm, where the motion of a chemical compound in solution inside the electrochemical cell are, principally three :(convection, migration, and diffusion), stirring the solution helps in homogenizing the solution in addition, stirring and adding the buffer solution both help to get rid of unwanted motion (migration and convection), it remains the diffusion. It is the most important that expresses the behavior of phenol within the electrochemical cell; during the stirring stage, nitrogen gas gurgles inside the electrochemical cell solution for 50 sec. The effect of temperature on behavior where the temperature of the solution was fixed during all stages of the study at 25±2°C.

3.3. Application on drinking water samples by the proposed electrode (NiO-NCQD/MCPE)

A drinking water sample from Latakia city was analyzed using the proposed method, and it was found that the sample was less than the detection limit (<LOD) of the method. The standard addition method found that the sample does not contain phenol, according to Table 2 and Figures 4-5. Due to previous curves, the results can be placed in Table 2.

It is noted from the above that the phenol concentration in the drinking water sample in Latakia is less than the quantitative detection limit (LOQ) of the method, less than 10µM (0.9411 mg L^{-1}).

4. Conclusion

This paper deals with fabricating a phenol-selective electrode using carbon paste modified with Nickel Oxide nanoparticles (NiO) doped with Nitrogen Carbon Quantum Dots (NCQD) using Cyclic voltammetry. The electrode was manufactured in a laboratory. Results best conditions are obtained at pH= 7.0 and 4.0 using KH_2PO_4 buffer, buffer, and the behavior of a phenol solution is studied in an electrochemical cell (Cyclic voltammetry) using NiO-NCQD/MCPE. The phenol concentration in

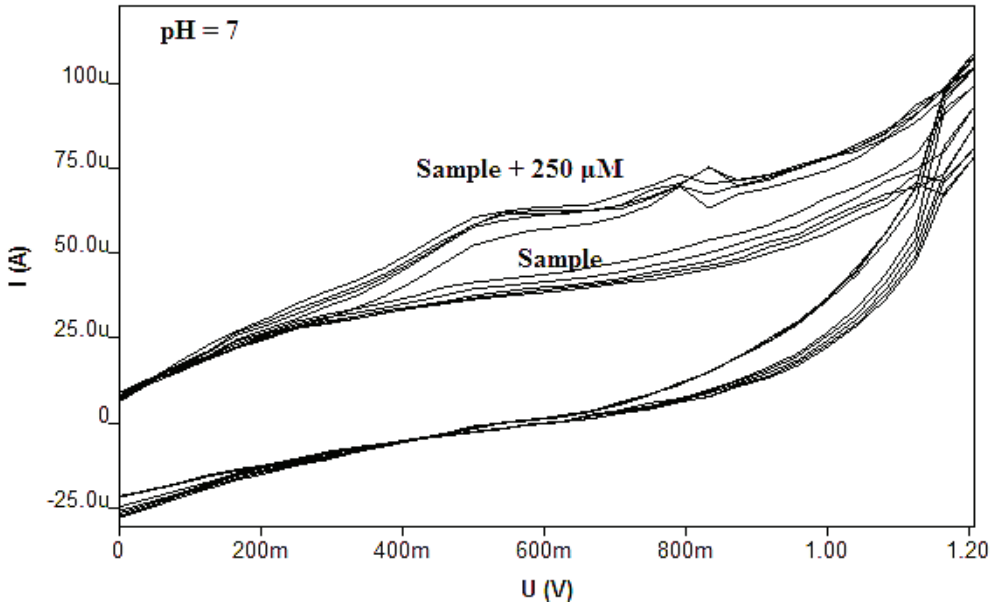

Fig. 4. Determination of phenol concentration in drinking water using the proposed electrode (NiO-NCQD/MCPE) at pH = 4

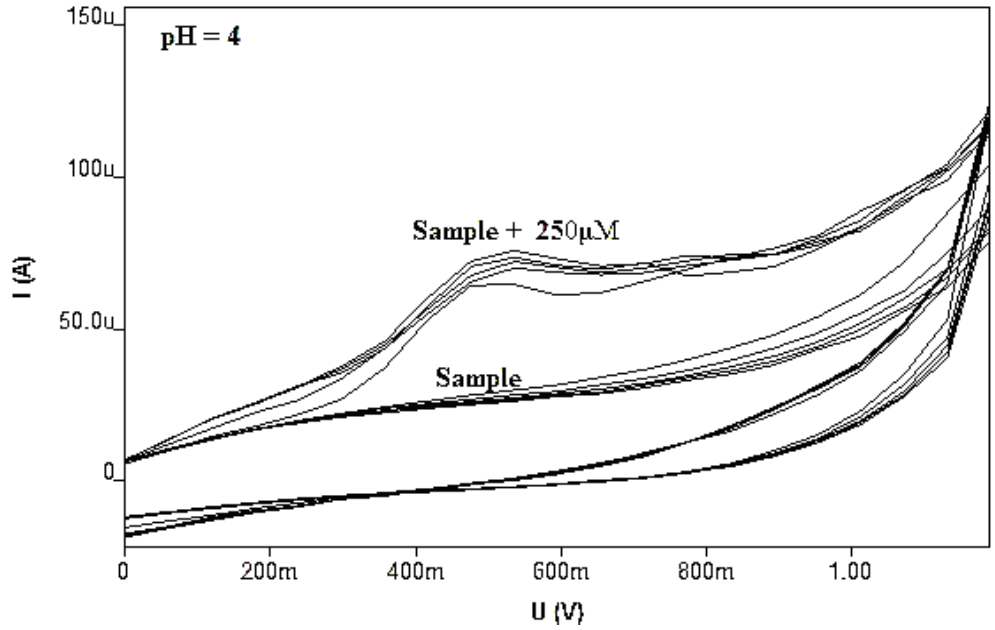

Fig. 5. Determination of phenol concentration in drinking water using the proposed electrode (NiO-NCQD/MCPE) at pH = 7

Table 2. Phenol analysis in water samples (n=5) at pH = 4 at pH = 7*

Sample	Added Phenol (µM)	Expected Phenol (µM)	Found phenol (µM)	RSD (%)	Recovery (%)
Drinking Water	--	--	LOQ	--	-
	250	250.0002	[240.2-259.8]	3.15672	100.0001
Drinking Water	--*	--*	LOQ *	--*	--*
	250*	232.8361*	[220.27-245.41] *	4.3488*	93.1344*

the drinking water sample in Latakia is less than the quantitative detection limit (LOQ) of the method, that is, less than 10µM (0.9411 mg L^{-1}).

5. Acknowledgments

The authors thank the Faculty of Science-Tishreen University- Syria and the Higher Institute for Environmental Research - Tishreen University-Syria for their help and support during this work.

6. References

[1] M. Alizadeh, P. Nasehi, M.S. Moghaddam, S. Agarwal, V.K. Gupta, Electrochemical sensing of phenol in different water sources by a titanium oxide nanotubes/single-wall carbon nanotubes nanocomposite-ionic liquid amplified sensor, Int. J. Electrochem. Sci., 16 (2021) 210774. https://doi.org/10.20964/2021.06.6

[2] A. Abd Gami, M.Y. Shukor, K.A. Khalil, F.A. Dahalan, A. Khalid, S.A. Ahmad, Phenol and its toxicity, J. Environ. Microbiol. Toxicol., 2 (2014) 11-23. https://doi.org/10.54987/jemat.v2i1.89

[3] M. Chand Meena, R. Band, G. Sharma, Phenol and its toxicity: A case report, Iran. J. Toxicol., 8 (27) (2015) 1222-1224. http://ijt.arakmu.ac.ir/article-1-383-en.html

[4] A. Tyagi, S. Tyagi, N. Malik, H. Chawla, Suicidal phenol ingestion: A case report, Int. J. Forensic Med. Toxicol. Sci., 2(1) (2021) 22-23. https://www.academia.edu/download/54620082/IJFMTS_21_22-23.pdf

[5] W.W. Anku, M.A. Mamo, P.P. Govender, Phenolic compounds in water: sources, reactivity, toxicity and treatment methods, Chapter 17, (2017) 419-443. http://dx.doi.org/10.5772/166927

[6] A.O. Adeola, Fate and toxicity of chlorinated phenols of environmental implications: a review, Med. Anal. Chem. Int. j., 2 (4) (2018) 000126. http://doi.org/10.23880/macij-16000126

[7] R.M. Bruce, J. Santodonato, M.W. Neal, Summary review of the health effects associated with phenol, Toxicol. Ind. Health, 3 (4) (1987) 535-568. https://doi.org/10.1177/074823378700300407

[8] J. Michałowicz, W. Duda, Phenols-sources and toxicity, Polish J. Environ. stud., 16 (3) (2007) 347–362. http://www.pjoes.com/Phenols-Sources-and-Toxicity,87995,0,2.html

[9] D. Ferraz, D.V. Thomaz, R.S. Antunes, F.M. Lopes, Development of a low-cost colorimetric paper-based spot test for the environmental monitoring of phenolic pollutants, Environ. Challenges, 4 (2021) 100128. https://doi.org/10.1016/j.envc.2021.100128

[10] A. Mulyasuryani, A.M. Mustaghfiroh, Development of potentiometric phenol sensors by Nata de coco membrane on screen-printed carbon electrode, J. Anal. Methods Chem., 2019 (2019) 4608135. https://doi.org/10.1155/2019/4608135

[11] N.G. Simões, V.V. Cardoso, E. Ferreira, M. J. Benoliel, C.M. Almeida, Experimental and statistical validation of SPME-GC–MS analysis of phenol and chlorophenols in raw and treated water, Chemosphere, 68 (2007) 501-510. https://doi.org/10.1016/j.chemosphere.2006.12.057

[12] O. Folin, V. Ciocalteu, On tyrosine and tryptophane determinations in proteins. J. Biol. Chem, 73 (1927) 627-650. https://doi.org/10.1016/S0021-9258(18)84277-6

[13] A. Blainski, G.C. Lopes, J.C.P. De Mello, Application and analysis of the folin ciocalteu method for the determination of the total phenolic content from Limonium brasiliense L, Molecules, 18 (2013) 6852-6865. https://doi.org/10.3390/molecules18066852

[14] C. Priyanthi, R. Sivakanesan, The total antioxidant capacity and the total phenolic content of rice using water as a solvent, Int. J. Food Sci., 2021 (2021) 1-6. https://doi.org/10.1155/2021/5268584

[15] D. Bajčan, L. Harangozo, D. Hrabovská, D. Bončíková, Optimizing conditions for spectrophotometric determination of total polyphenols in wines using Folin-Ciocalteu reagent, J. Microbiol. Biotechnol. Food Sci., 2 (2013)1699-1708. https://www.jmbfs.org/

[16] N. Siddiqui, A. Rauf, A. Latif, Z. Mahmood, Spectrophotometric determination of the total phenolic content, spectral and fluorescence study of the herbal Unani drug Gul-e-Zoofa (Nepeta bracteata Benth), J. Taibah Uni. Med. Sci., 12 (2017) 360-363. https://doi.org/10.1016/j.jtumed.2016.11.006

[17] M. González, B. Guzman, R. Rudyk, E. Romano, M.A. Molina, Spectrophotometric determination of phenolic compounds in propolis, Acta Farmaceutica Bonaerense, 22 (2003) 243-248. http://portalrev.enfermagem.bvs.br/index.php?issn=0326-2383&lang=en

[18] V.L. Singleton, R. Orthofer, R.M. Lamuela-Raventós, Analysis of total phenols and other oxidation substrates and antioxidants by means of folin-ciocalteu reagent, Meth. Enzymol., 299 (1999) 152-178. https://doi.org/10.1016/S0076-6879(99)99017-1

[19] K.C. Guimarães, D.L. Salgado, E.E.N. Carvalho, Evaluation of different methodologies for the determination of phenolic compounds in tropical fruits, Brazil.

J. Food Technol., 23 (2020) 01519. https://doi.org/10.1590/1981-6723.01519

[20] X. Chen, Y. Liang, X. Zhou, Y. Zhang, Phenol removal by a novel non-photo-dependent semiconductor catalyst in a pilot-scaled study: effects of initial phenol concentration, light, and catalyst loading, J. Nanomater., 2014 (2014) 1-8. https://doi.org/10.1155/2014/457485

[21] K. Nakashima, S. Kinoshita, M. Wada, N. Kuroda, W.R. Baeyens, HPLC with fluorescence detection of urinary phenol, cresols and xylenols using 4-(4, 5-diphenyl-1 H-imidazol-2-yl) benzoyl chloride as a fluorescence labeling reagent, Analyst, 123 (1998) 2281-2284. https://doi.org/10.1039/A804582H

[22] M.D.P. Fernández-Poyatos, A. Ruiz-Medina, C. Salazar-Mendías, E.J. Llorent-Martínez, Spectrophotometric determination of the antixidant properties and characterization of the phenolic content by high-performance liquid chromatography–diode array detection–tandem mass spectrometry (HPLC–DAD–MS/MS) of Berberis hispanica Boiss. & Reut. Leaves, Anal. Lett., 54(4) (2021) 646-657. https://doi.org/10.1080/00032719.2020.1775628

[23] A.S. Adekunle, O.A. Arotiba, B.O. Agboola, N.W. Maxakato, B.B. Mamba, Voltammetric and impedance studies of phenols and its derivatives at carbon nanotubes/prussian blue films platinum modified electrode, Int. J. Electrochem. Sci., 7 (2012) 8035-8051. https://core.ac.uk/download/pdf/54194818

[24] T.A. Enache, A.M. Oliveira-Brett, Phenol and para-substituted phenols electrochemical oxidation pathways, J. Electroanal. Chem., 655 (2011) 9-16. https://doi.org/10.1016/j.jelechem.2011.02.022

[25] K.J. Lee, B.D. McCarthy, J.L. Dempsey, On decomposition, degradation, and voltammetric deviation: the electrochemist's field guide to identifying precatalyst transformation, Chem. Soc. Rev., 48 (11) (2019) 2927-2945. https://doi.org/10.1039/C8CS00851E

[26] A. Habekost, Simulation and fitting of cyclic voltammetry and chronoamperometry curves of electrochemical reactions with different mechanisms—A didactic perspective, World J. Chem. Educ., 7 (2019) 53-64. https://doi.org/10.12691/wjce-7-2-4

[27] M.C. Henstridge, E. Laborda, E.J. Dickinson, R.G. Compton, Redox systems obeying Marcus–Hush–Chidsey electrode kinetics do not obey the Randles–Ševčík equation for linear sweep voltammetry, J. Electroanal. Chem., 664 (2012) 73-79. https://doi.org/10.1016/j.jelechem.2011.10.015

[28] J.E. Randles, A cathode ray polarograph. Part II, the current-voltage curves, Trans. Faraday Soc., 44 (1948) 327-338. https://doi.org/10.1039/TF9484400327

[29] A. García-Miranda Ferrari, C.W. Foster, P.J. Kelly, D.A. Brownson, C.E. Banks, Determination of the electrochemical area of screen-printed electrochemical sensing platforms, Biosens., 8 (2018) 53. https://doi.org/10.3390/bios8020053

[30] Y. Uchida, E. Kätelhön, R.G. Compton, Cyclic voltammetry with non-triangular waveforms: Electrochemically irreversible and quasi-reversible systems, J. Electroanal. Chem., 810 (2018) 135-144. https://doi.org/10.1016/j.jelechem.2017.12.053

[31] N. Aristov, A. Habekost, Cyclic voltammetry-A versatile electrochemical method investigating electron transfer processes, World J. Chem. Edu., 3 (2015) 115-119. https://doi.org/10.12691/wjce-3-5-2

[32] A. Oleinick, I. Svir, C. Amatore, Transient cyclic voltammetry: new theoretical challenges to bring up to date a famous electrochemical lady, J. Solid State Electrochem., 24 (2020) 2023-2025. https://link.springer.com/article/10.1007/s10008-020-04553-x

[33] M. Favaro, stochastic analysis of electron transfer and mass transport in confined solid/

liquid interfaces, Surf., 3 (2020) 392-407. https://doi.org/10.3390/surfaces3030029

[34] S.M. Sayyah, M. Shaban, A.B. Khaliel, M. Rabia, Electropolymerization of m-cresol on platinum electrode from aqueous acidic solution, Int. J. Chem., 35 (2014) 2051-2732. https://www.ccsenet.org/journal/index.php/ijc

[35] J. J.Y. Wong, Electrochemical focal hypoxia for cell models, Ph.D. thesis, Department of Chemical Engineering and Biotechnology, University of Cambridge, 2021. https://doi.org/10.17863/CAM.75017

[36] R. Pakkath, E.K. Reddy, S. Kuriakose, C. Saritha, A.M. Sajith, R.P. Karuvalam, K.R. Haridas, Synthesis, characterization and determination of HOMO-LUMO of the substituted 1, 3, 5-triazine molecule for the applications of organic electronics, J. Korean Chem. Soc., 63 (2019) 352-359. https://doi.org/10.5012/jkcs.2019.63.5.352

[37] J. Ebrahimian, M. Khayatkashani, N. Soltani, Q.A. Yousif, M. Salavati-Niasari, Catechin mediated green synthesis of Au nanoparticles: Experimental and theoretical approaches to the determination HOMO-LUMO energy gap and reactivity indexes for the (+)-epicatechin (2S, 3S), Arab. J. Chem., 15 (2022) 103758. https://doi.org/10.1016/j.arabjc.2022.103758

[38] Y.C. Chen, Y.T. Kuo, T.H. Ho, Photo-polymerization properties of type-II photoinitiator systems based on 2-chlorohexaaryl biimidazole (o-Cl-HABI) and various N-phenylglycine (NPG) derivatives, Photochem. Photobiol. Sci., 18 (2019) 190-197. https://link.springer.com/article/10.1039/c8pp00300a.

[39] H. Zhang, L. Yuan, X. Tang, J. Hu, J. Sun, Y. Zhang, R. Jia, Influence of metal gate electrodes on electrical properties of atomic-layer-deposited Al-rich HfAlO/Ga_2O_3 MOSCAPs. IEEE Trans. Electron Devices, 67 (2020) 1730-1736. https://doi.org/ 10.1109/TED.2020.2974794

[40] G.K. Jayaprakash, B.K. Swamy, S. Rajendrachari, S.C. Sharma, R. Flores-Moreno, Dual descriptor analysis of cetylpyridinium modified carbon paste electrodes for ascorbic acid sensing applications. J. Mol. Liq., 334 (2021) 116348. https://doi.org/10.1016/j.molliq.2021.116348

Anal. Methods Environ. Chem. J. 6 (1) (2023) 69-78

AMECJ

Research Article, Issue 1
Analytical Methods in Environmental Chemistry Journal
Journal home page: www.amecj.com/ir

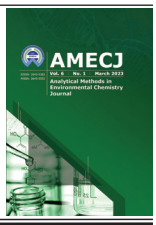

Chemical analysis of essential oils of Thymus Carmanicus Jalas by gas chromatography-mass spectrometry and toxicity activity against the major Iranian malaria vector, Anopheles Stephensi

Nazanin Sadat Mousavi [a], Alireza Sanei-Dehkordi [b],, Ismaeil Alizadeh [c,d], Ali Faghihi Zarandi [e], Mohsen Mehdipour Rabori [a], Nasrollah Saberi [f] and Mohammad Amin Gorouhi [d] *

[a] *Department of Environmental Health Engineering, Faculty of Public Health, Kerman University of Medical Sciences, Kerman, Iran*
[b] *Department of Biology and Control of Disease Vectors, Faculty of Health, Hormozgan University of Medical Sciences, Bandar Abbas, Iran*
[c] *Research Center of Tropical and Infectious Diseases, Kerman University of Medical Sciences, Kerman, Iran*
[d] *Department of Vector Biology and Control, Faculty of Public Health, Kerman University of Medical Sciences, Kerman, Iran*
[e] *Department of Occupational Health Engineering and Safety at Work, Faculty of Public Health, Kerman University of Medical Sciences, Kerman, Iran*
[f] *Bam University of Medical Sciences, Bam, Iran*

ARTICLE INFO:

Received 13 Nov 2022
Revised form 22 Jan 2023
Accepted 10 Feb 2023
Available online 28 Mar 2023

Keywords:
Chemical analysis,
Gas chromatography-mass spectrometry,
Thymus Carmanicus Jalas,
Essential oil,
Malaria

ABSTRACT

In the last few years, using chemical insecticides to control the malaria vector has caused environmental pollution and resistance to chemical insecticides. This study aimed to investigate the chemical analysis of essential oils of *Thymus carmanicus* Jalas by gas chromatography and mass spectrometry (GC-MS) and toxicity activity against the major Iranian malaria vector, *Anopheles stephensi*. The essential oil of Thymus carmanicus Jalas was prepared from dried leaves using the hydro-distillation method. Gas chromatography mass spectrometer (GC-MS) was used to analyze and identify thyme essential oil compounds. Bioassay was performed using World Health Organization (WHO) standard test. The *T. Carmanicus* Jalas essential oil consisted of 15 compounds, with Carvacrol (61%), Thymol (6%), and β-caryophyllene (5%) being the major components by volume. The LC_{50} and LC_{90} of thyme oil were 20.37 and 41.38 mg L^{-1} at 24h after application, respectively. At 24h after application, significant differences were observed between the toxicity of 5%, 20%, 25%, 40%, 50%, and 80% concentrations of Thyme essential oil ($P<0.05$). The 80% concentration of Thyme essential oil exhibited 100% toxicity against *A.stephensi* larvae at 24h after application. *T. Carmanicus* has a rich source of bioactive compounds for use as a mosquito larvicide.

1. Introduction

Malaria is among the most important parasitic diseases transmitted to humans by Anopheles mosquitoes. This disease has been reported in 91 countries worldwide [1]. Five Plasmodium species are transmitted by the bite of Anopheles mosquitoes [2]. More than 90% of malaria cases were reported in three southeastern provinces of Iran, including Sistan and Baluchistan, Kerman, and Hormozgan [3]. Out of the 476 Anopheles

*Corresponding Author: Mohammad Amin Gorouhi
Email: amingruhi@gmail.com
https://doi.org/10.24200/amecj.v6.i01.225

species identified in the world, 70 species are capable of transmitting malaria, and 40 species are known as the main vectors. In addition to malaria transmission, Anopheles could transmit filariasis and some arboviruses. In Iran, 7 Anopheles species are disease carriers, the most important of which is Anopheles stephensi, found in the southern regions [4]. Insecticide resistance has become a threat to the effectiveness of chemical vector control methods. This issue is of particular importance considering the malaria elimination program in Iran [5]. Therefore, special attention has been paid to plants as natural reservoirs with fewer side effects to fight against disease vectors. Currently, controlling mosquito larvae using larvicides is a major part of controlling mosquito-borne diseases. The most common larvicides contain organophosphorus compounds such as temephos, fenthion, and chlorpyrifos. However, their toxicity for aquatic organisms and the environment as well as the phenomenon of insecticide resistance and acute and chronic toxicity for humans are increasingly reported. Therefore, it seems necessary to find new larvicides from alternative sources such as plants [6, 7]. Herbal insecticides have been recently used to control vectors due to their relatively high efficiency, degradability, and lack of adverse effects on the environment. Several plant products have been reported as insecticides for mosquito control. Various vegetable oils have shown a wide range of insecticidal activity against pests. Also, these oils have anti-nutritional and repellent properties, reduce oviposition and disrupt the natural growth process of pests [7]. Thyme is among the important genera of the Lamiaceae family and has been widely used in food industry, pharmaceutical and cosmetic due to its various biological activities [8]. According to recent studies, Lamiaceae family consists of 4,000 plant species with 220 genera. Thyme, with 300-400 species, is among the most important species of this family. This genus includes 18 perennial and aromatic species that grow in different regions of the country. *Thymus caramanicus* is among the species of this genus [9]. Thyme branches contain essential oil, tannin, basic bitter substances, saponin and herbal disinfectants. The plant essential oil contains variable amounts of phenolic compounds such as thymol and carvacrol [10]. Various constituents of the oil of *T. carmanicus* were reported in previous studies. Although carvacrol is the most abundant constituent in the oils obtained from all the mentioned studies, percentage of the compound varied, based on the origins of the plant. While it has been reported as 47.55-96.2.7% from *T. carmanicus* cultivated in Kerman, 42.1-93.4 % in Isfahan, 42% in Shahroud, and 19.8-81.1% Semnan [11-15]. Generally, there are two devices including Soxhlet and Clevenger to essential oil extraction [16]. To analysis the composition of an essential oil sample, use Gas chromatography columns with different polarities [17]. The previous studies used several methods to essential oil analysis, such as Gas Chromatography and Mass Spectrometry (GC/MS) and capillary gas chromatography (GC) [18]. Netopilova et al. in 2021 used the GC– flame ionization detector (FID)/MS for analysis the *Origanum vulgare* and *Thymus vulgaris* [19]. In the present study, we aimed to investigate the chemical analysis of essential oils of *Thymus carmanicus* Jalas by GC-MS and also the toxicity activity of this essential oil was evaluated against the major Iranian malaria vector, *Anopheles stephensi* as an environmentally friendly method.

2. Materials and methods

2.1. Plant collection

The fresh leaves of the *Thymus carmanicus* Jalas plant were collected from the Hezar mountain (Kūh-e Hazār) located at 29° 30′ 42″ N and 57° 16′ 18″ E at 120 km from Kerman city in southeast of Iran (Fig. 1). Collected Thyme specimens were identified by the Department of Pharmacognosy in Kerman University of Medical Sciences.

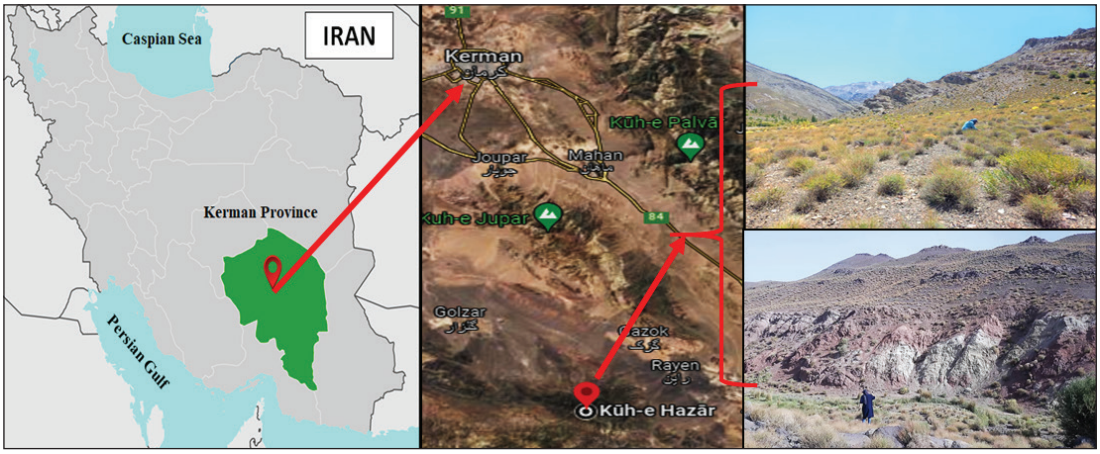

Fig 1. Map of the location of collected Thyme specimens in Kerman province (southeast of Iran)

2.2. Extraction of eessential oil

To extract essential oils, 100 g of dried leaves of *Thymus caramanicus* was poured into a 1L flask [10]. Then, 600 cc of deionized water was added to the flask and then were subjected to hydrodistillation in a clevenger-type apparatus for 3.5 to 4 h. The essential oil was extracted approximately 3.5 to 4 h at 60 °C [20] (Fig. 2). Then, the extracts were exsiccated by anhydrous sodium sulphate and stored in a dark glass vial at 4 °C in a refrigerator for further experiment [11, 12].

2.3. Gas chromatographic-mass spectral analysis

Gas chromatography-mass spectrometer (GC-MS) was used for the analysis and identification of thyme essential oil compounds (Hewlett-Packard 6890, Agilent Technology, Santa Clara, California, USA) (Fig. 2). It is equipped with HP–5MS column (30 m× 0.25 mm× 0.25 µm). The initial temperature was 40 °C for 1 min and later was raised to 220 °C at a rate of 3 °C per min and finally raised to 270 °C for 5 min at a rate of 20 °C per minute. Other parameters of the GC-MC machine included carrier gas Helium (99/999%), injector temperature (260 °C), detector temperature (FID, 270 °C), split-less mode, the ionization potential of 70eV, scan rate of 1 scan per sec, the scan range of m/z 40–48 was used for all analysis. The essential oil constituents were identified by comparing their retention indices, and mass spectra fragmentation with those in a stored Wiley 7n.1 mass computer library and those of National Institute of standards and Technology (NIst) [21-23].

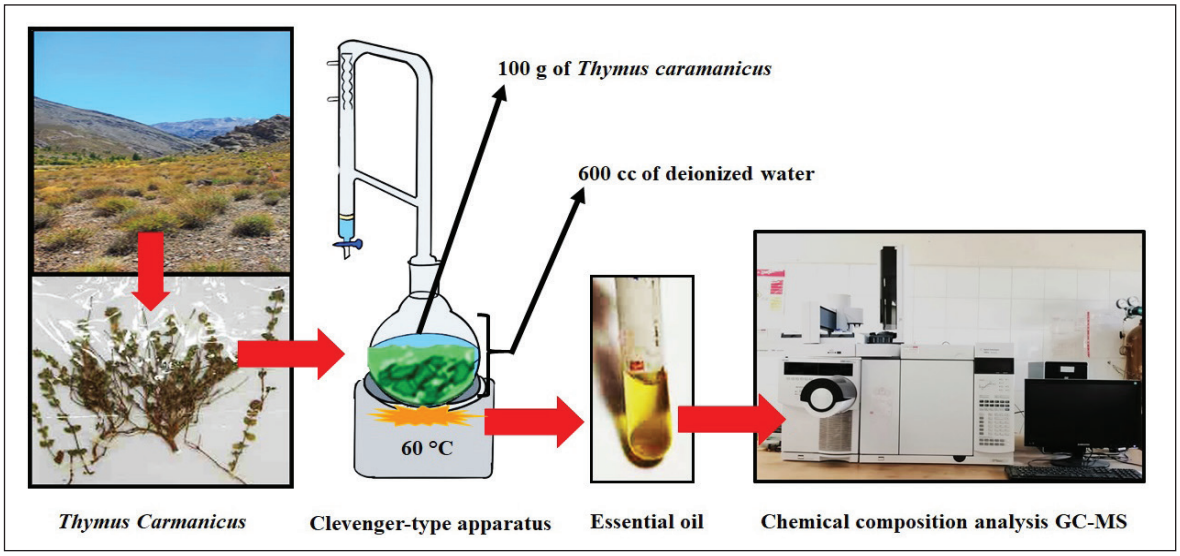

Fig. 2. The procedure of collecting plants, extracting and GC-MS analysis of essential oils.

2.4. Larvae collection and Toxicity assay

Anopheles stephensi larvae were collected from the Paykam area, Bam, south of Kerman Province. Bioassay was performed using World Health Organization (WHO) standard test [24]. Different concentrations (20, 40, 80, 160, and 320 mg L^{-1}) of the essential oils obtained from the studied plant were prepared using ethanol as the solvent. Thus, twenty-five of the 3rd or 4rd instar larvae of *Anopheles stephensi* were exposed to these concentrations in each 400 mL beaker. The experiments were replicated four times for any concentrations of thyme essential oil and ethanol.

2.5. statistical Analysis

Probit analysis was used to calculate the LC_{50} and LC_{90}. Toxicity indices were compared using analysis of (ANOVA) followed by the Dunnett test to distinguish between the treatments. All statistical analyses were performed using the SPSS version. 16. A p-value of less than 0.05 was considered statistically significant.

3. Results and Discussion

Thyme essential oil was found to contain 15 compounds using GC-MS analyses. Carvacrol, thymol, and beta-caryophyllene had the highest frequency with 61.92%, 6.13%, and 5.55%, respectively. The most common compounds are shown in Table 1. In addition, the chemical analysis of the essential oil of *Thymus carmanicus* Jalas is shown in Figure 3.

Table 1. Constituents of *Thymus carmanicus* Jalas essential oil by GC-MS analyses.

Thyme essential oil components	Retention time	Major Constituents (%)
γ-cadinene	10.029	0.58
β-caryophylene	11.099	5.55
Copaene	11.187	1.1
Limonene	12.274	0.99
Isoledene	14.224	2.63
β-burbunene	14.634	1.26
terpinene	15.251	1.92
Sabinene	16.609	0.41
β-pinane	17.932	1.95
Carvacrol	18.541	61.92
β-elemene	24.681	0.87
P-cymene	41.959	1.26
β-phelanderene	45.059	0.32
Thymol	48.209	6.13
Naphthalene	54.345	3.34
Other compounds	-	9.77

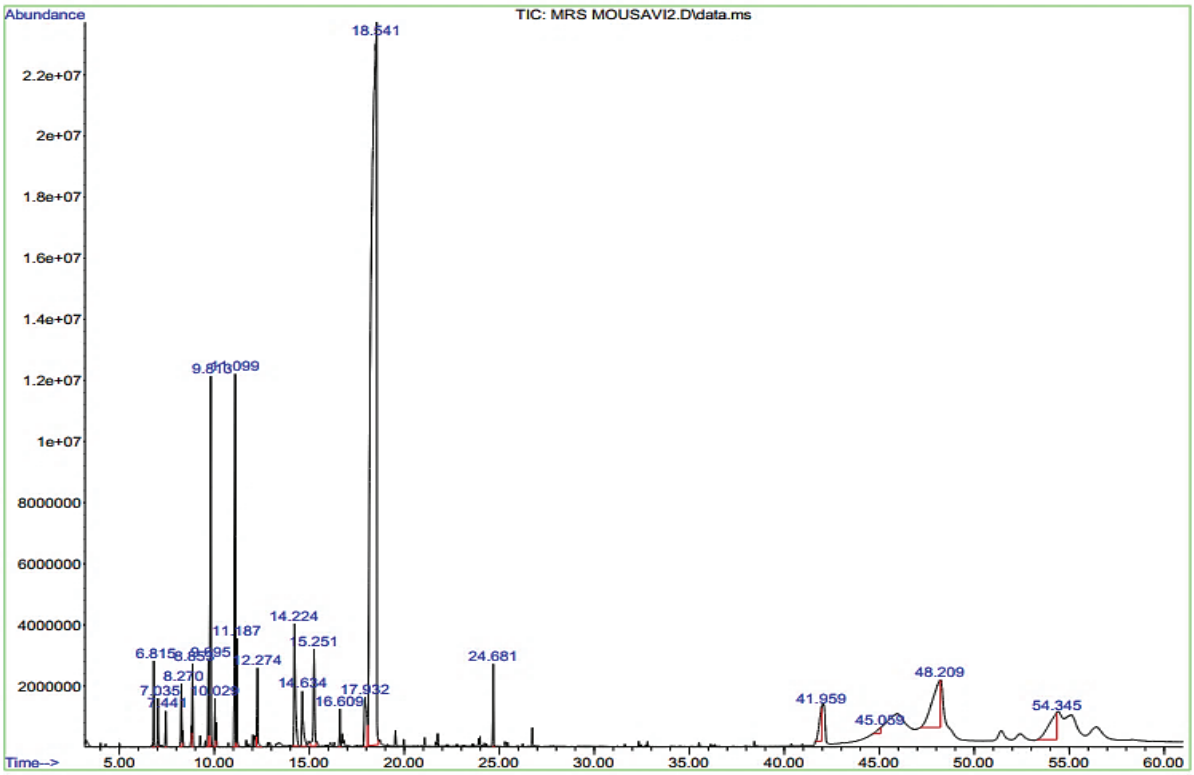

Fig. 3. A typical GC-MS chromatogram showing the chemical analysis of essential oil from *Thymus carmanicus* Jalas.

The results of the dose-response test are shown with the calculation of toxicity lethal concentration as ppm (mg L^{-1}) essential oil (LC_{50} and LC_{99}) in Table 2. They were 20.37 and 41.38 mg L^{-1} for LC_{50} and LC_{90} at 24h after application, respectively. The calculated dose-response curve for Thyme essential oil after 24h is shown in Figure 4.

The Dunnett test showed no significant difference in toxicity between 5%, 20%, and 25% of Thyme essential oil (P>0.05). As well as, there was no significant difference in toxicity between 40%, 50%, and 80% of Thyme essential oil (P>0.05). At 24h after application, significant differences were observed between the toxicity of 5%, 20%, 25%, and 40%,

Table 2. Lethal doses of thyme essential oil against *Anopheles stephensi* larvae.

Time	LC_{50} (CL*) mg L^{-1}	LC_{90} (CL*) mg L^{-1}	Slope (±SE)**	Chi-Square*** (*df*)	*P*
After 24 h	20.37 (18.02-22.52)	41.38 (38.26-45.41)	40.6 (0.005)	1.16 (4)	0.001>

$LC_{50\ and}$ $LC_{90:}$ Lethal dose necessary to kill 50% and 90% of larvae, respectively.
*Confidence limits.
**standard error.
***Chi-square (degree of freedom).
P: significance level of Probit model.

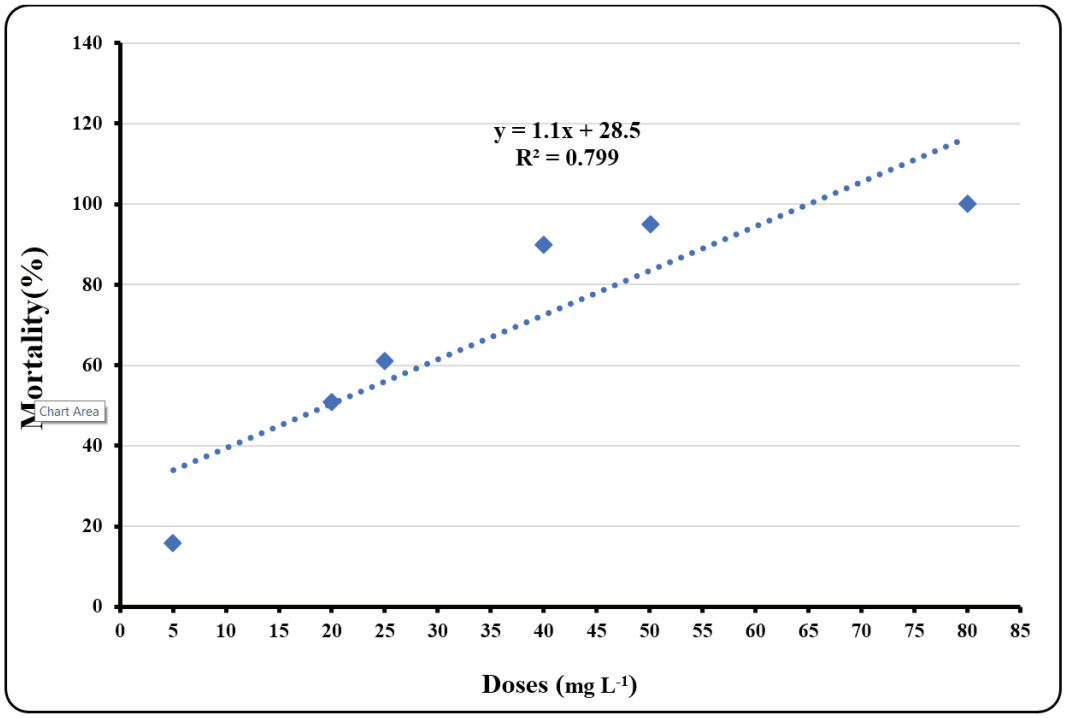

Fig. 4. Dose-response curve for *Thymus carmanicus* Jalas essential oil after 24h

50%, and 80% concentrations of Thyme essential oil ($P<0.05$). The 80% concentration of Thyme essential oil exhibited 100% toxicity against *Anopheles stephensi* larvae at 24h after application (Fig. 5).

3.1. Discussion

Tropical regions are more vulnerable to parasitic diseases and risk contracting diseases due to climate change and increased globalization. Mosquitoes

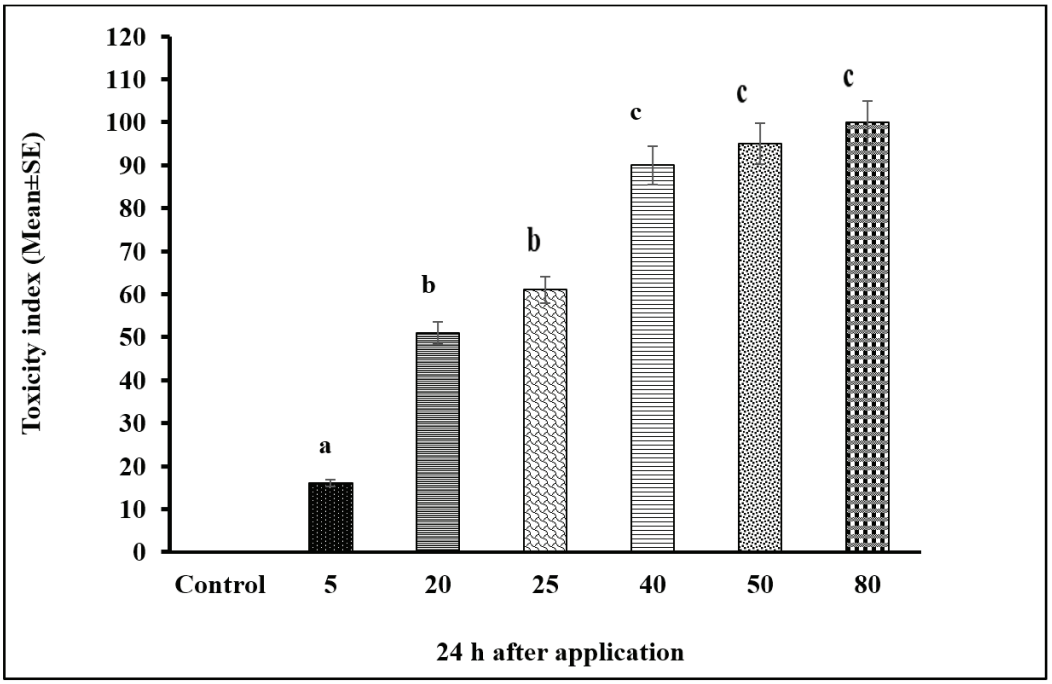

Fig. 5. Toxicity of ethanol, different concentrations of *Thymus carmanicus* Jalas essential oil against *An. stephensi* larvae. Different letters above the bars indicate significant differences at $\alpha = 0.05$

are the most important public health insects in tropical and subtropical regions because they carry important parasites and pathogens worldwide that cause death, poverty, and social impairment [25]. Makizadeh Tafti et al. (2010) stated that carvacrol constituted the largest part of the essential oil in all thyme ecotypes in Kerman Province, followed by thymol, para cymene, and gamma-terpinene. It is worth noting that the content of each element underwent changes in this research that could be due to geographical differences and reproduction or even in-vitro conditions [10]. Ebrahimi et al. (2009) observed the same compounds with different contents in GC-MS device investigations [26]. The contents observed in the study by Makizadeh Tafti showed that carvacrol constituted about 80% of the composition. However, Ebrahimi's analysis reduced this amount to 60%. Eftekhar et al. (2010) found 68% carvacrol in *Thymus caramanicus*. This study showed that the superiority of carvacrol content compared to other constituents was around 62% [27]. In the research by Mazandarani and Rezaei (2005) on *Thymus caramanicus* grown in Mazandaran Province, it was observed that pulegone (26%) was the most frequent element in the essential oil due to climate change, and carvacrol content decreased to 8% [28]. It was observed that *Thymus caramanicus* desirably affected malaria larvae and significantly increased larval mortality. The lethal property of *Thymus caramanicus* essential oil was extremely high, so lethality reached 50% and 90% at concentrations of 20 and 41, respectively. Damtie and Mekonnen (2021) found that several genera of thyme could effectively prevent Anopheles larvae proliferation and growth at concentrations of 20-50 and showed desirable resistance to adult insects at lower concentrations. This resistance was significantly observed in groups with different doses ($P<0.05$), which was consistent with observations [29]. Dargahi et al. (2014) found that Thymus transcaspicus essential oil exhibited strong insecticidal activity against An. stephensi, which could be due to its constituent compounds, especially carvacrol and thymol phenols [30]. These compounds were present in abundance in *Thymus caramanicus*. *Thymus transcaspicus* could significantly eliminate 50% and 90% of larvae at 154 and 248 µg L^{-1}, respectively ($P<0.05$). There was a significant difference between these two plants in terms of concentration, which could be attributed to the high concentration of carvacrol and thymol in *Thymus caramanicus* compared to *Thymus transcaspicus.*

Gupta et al. (2022) stated that the phenolic compounds present in the thyme could significantly increase the larval population of various disease-carrying mosquitoes ($P<0.05$). The results showed LC_{50} and LC_{90} values of this plant for *An.stephensi*, *Ae. aegypti* and *tritaeniorhynchus* larvae were equal to 56 and 124 µg L^{-1}, 58 and 270 µg L^{-1}, and 22.58 and 193 µg L^{-1} [31]. In the current study, LC_{50} and LC_{90} values were decreased due to changes in the phenolic compounds present in *Thymus caramanicus*, which could be attributed to the greater toxicity of these compounds. Kelidari et al. (2021) investigated the effect of solid-lipid nanoparticles containing *Zataria multiflora* essential oil and found that these particles could significantly prevent the proliferation of *Anopheles stephensi* larvae [32]. Firooziyan et al. (2022) investigated the effect of *Myrtus* nanoemulsion and found that this plant could eliminate 50% and 90% of *An. stephensi* larvae at concentrations of 26 and 46 µg L^{-1} [33]. Zarenzhad et al. (2021) confirmed the promising larvicidal effects of chitosan nanoparticles containing *Laurus nobilis* and *Trachyspermum ammi* essential oils against *An. stephensi* and stated that the essential oil of these plants was a significantly lethal effect [34]. Similarly, in the present study, the Thyme essential oil provided a significant toxic against *An. stephensi* larvae.

4. Conclusion

This study indicated that *T. Carmanicus* has a rich source of eco-friendly bioactive compounds for use as a mosquito larvicide. Its considerable capability might be the high percentage of Carvacrol, which can be used as a larvicidal agent for mosquito control programs. In that way, our findings provide

a possible way for further studies to determine the active molecule. Carvacrol with 61.92% was the highest compound of Thyme essential oil. LC_{90} of Thyme essential oil at 24h after the application was 41.38 mg L^{-1}. A concentration of 80% of this essential oil killed 100% of larvae at 24 hours. However, further investigations must be conducted to describe the mode of action of each constituent s independently and also its effects on non-target organisms.

5. Acknowledgements

The authors wish to thank Dr. Fariba sharififar, Zahra Mahdavi and Miss Pakravanan for helping in the essential oil preparation and interpretation of GC-MS results. This article is part of Nazanin Sadat Mousavi MSPH thesis, and it was financially supported by and conducted at Kerman University of Medical Sciences (Project Number 400001144). This study was approved by the Ethics Committee of Kerman University of Medical Sciences (IR. KMU.REC1401.059).

6. References

1] M. Thellier, F. Simard, L. Musset, M. Cot, G. Velut, E. Kendjo, Changes in malaria epidemiology in France and worldwide, 2000–2015, Med. Mal. Infect., 50 (2020) 99-112. https://doi.org/10.1016/j.medmal.2019.06.002

[2] G. Benelli, J. Beier, Current vector control challenges in the fight against malaria, Acta Trop., 174 (2017) 91-96. https://doi.org/10.1016/j.actatropica.2017.06.028.

[3] S. Azari-Hamidian, B. Norouzi, R. Harbach, A detailed review of the mosquitoes (Diptera: Culicidae) of Iran and their medical and veterinary importance, Acta Trop., 1 (2019) 106-122. https://doi.org/10.1016/j.actatropica.2019.03.019.

[4] M. Ahmad, V. Hassan, O. Ali, AM. Reza, Anopheline mosquitoes and their role for malaria transmission in an endemic area, southern Iran, Asian Pac. J. Trop. Dis., 1 (2011) 209-211. https://doi.org/10.1016/S2222-1808(11)60030-3

[5] B. Fazeli-Nasab, M. Solouki, A. Sobhanizadeh, Green synthesis of silver nanoparticles using an ephedra sinica Herb extract with antibacterial properties, J. Med. Bacteriol., 10 (2021) 30-47. https://jmb.tums.ac.ir/index.php/jmb/article/view/434

[6] M. Khanavi, H. Vatandoost, N. Dehaghi, A. Dehkordi, M. Sedaghat, A. Hadjiakhoondi, Larvicidal activities of some Iranian native plants against the main malaria vector, Anopheles stephensi, Acta Med. Iran, 15 (2013) 141-147. https://acta.tums.ac.ir/index.php/acta/article/view/4474

[7] M. Soleimani-Ahmadi, M. Gorouhi, A. Mohammadi, Y. SalimAbadi, A. Paksa, G. Rashid, Larvicidial Effects of essential oil and methanol extract of Achilleawilhelmsii C. Koch (Asteraceae) against Anopheles stephensi Liston (Diptera: Culicidae), a malaria vector, J. Kerman Uni. Med. Sci., 24 (2017) 58-67. https://jkmu.kmu.ac.ir/article_42498_76c1b6a54dac8f6 df8c3288168c19e7d.pdf

[8] S. Fan, J. Chang, Y. Zong, G. Hu, J. Jia, GC-MS analysis of the composition of the essential oil from Dendranthema indicum Var. Aromaticum using three extraction methods and two columns, Molecules, 23 (2018) 1-11. https://doi.org/10.3390/molecules23030576.

[9] S. Safai L, H. Zeinali, M. Mirza, study on essential oil content and composition of Thymus caramanicus Jalas in different harvesting stages, Iran. J. Med. Aromat. Plants Res., 29 (2013) 313-324. https://doi.org/10.22092/IJMAPR.2013.2858

[10] M. MakizadehTafti, H. Naghdibadi, S. Rezazadeh, Y. Ajani, Z. Kadkhoda, Evaluation of botanical characteristics and yield and essential components of Thymus carmanicusJalasin Iran, J. Med. Plants., 9 (2010) 57-65. https://doi.org/20.1001.1.2717204.2010.9.36.6.8.

[11] B. Bahreininejad, J. Razmjoo, M. Mirza, Effect of water stress on productivity and

essential oil content and composition of Thymus carmanicus, J. Essent. Oil-Bear. Plants., 17(2014) 717-725. https://doi.org/10.1080/0972060X.2014.901605

[12] M. Tafti, H. Badi, S. Rezazadeh, Y. Ajani, Z. Kadkhoda, Evaluation of botanical traits and oil content/chemical composition in Iranian Thymus carmanicus Jalas ecotypes, J. Med. Plant. Res., 9 (2010) 57-212. http://jmp.ir/article-1-246-en.html

[13] M. Bigdeloo, J. Hadian, V. Nazeri, Composition of essential oil compounds from different populations of Thymus caramanicus Jalas, J. Appl. Res. Med. Aromat. Plants, 7 (2017) 95-98. https://doi.org/10.1016/j.jarmap.2017.06.005_

[14] J. Hadian, M. Bigdeloo, V. Nazeri, A. Khadivi-Khub, Assessment of genetic and chemical variability in Thymus caramanicus, Mol. Biol. Rep., 41 (2014) 3201-3210. https://doi.org/10.1007/s11033-014-3180-z

[15] P. Ghasemi, M. Barani, B. Hamedi, K. Ataei, A. Karimi, Environment effect on diversity in quality and quantity of essential oil of different wild populations of Kerman thyme, Genetika,45 (2013) 441-450. https://doi.org/10.2298/GENSR1302441P

[16] M. Akhgar, M. Moradalizadeh, A. Faghihi -Zarandi, P. Rajaei, Chemical composition of the essential oils of Ferula oopoda (Boiss. & Buhse) Boiss. and Ferula badghysi (Korovin.) from Iran, J. Essent. Oil-Bear. Plants., 14 (2011) 297-301. https://doi.org/10.1080/0972060X.2011.10643937

[17] T. He, X. Li, X. Wang, X. Xu, X. Yan, X. Li, X. Liu, Chemical composition and anti-oxidant potential on essential oils of Thymus quinquecostatus Celak. from Loess Plateau in China, regulating Nrf2/Keap1 signaling pathway in zebrafish, Sci. Rep., 10 (2020) 1-18. https://doi.org/10.1038/s41598-020-68188-8

[18] M. Hudaib, E. Speroni, A. Di Pietra, V. Cavrini, GC/MS evaluation of thyme (Thymus vulgaris L.) oil composition and variations during the vegetative cycle, J. Pharm. Biomed. Anal., 29 (2002) 691-700. https://doi.org/10.1016/S0731-7085(02)00119-X

[19] M. Netopilova, M. Houdkova, K. Urbanova, J. Rondevaldova, L. Kokoska, Validation of qualitative broth volatilization checkerboard method for testing of essential oils: Dual-column GC–FID/MS analysis and in vitro combinatory antimicrobial effect of Origanum vulgare and Thymus vulgaris against staphylococcus aureus in liquid and vapor phases, Plants, 10 (2021) 393. https://doi.org/10.3390/plants10020393

[20] C. Zhang, X. Hu, H. Wang, F. Yan, GC–MS Analysis of essential oil extracted from Acori tatarinowii Rhizoma: An experiment in Natural product analysis, J. Chem. Educ., 98 (2021) 3004-3010. https://doi.org/10.1021/acs.jchemed.1c00451

[21] M. Sharififard, I. Alizadeh, E. Jahanifard, C. Wang, M. Azemi, Chemical composition and repellency of Origanum vulgare essential oil against Cimex lectularius under laboratory conditions, J. Arthropod. Borne Dis., 12 (2018) 387. https://jad.tums.ac.ir/index.php/jad

[22] M. Sharififard, M. Kouchak, I. Alizadeh, E. Jahanifard, Oregano (Origanum vulgar subsp. viride) essential oil: extraction, preparation, characterization, and encapsulation by Chitosan-Carbomer Nanoparticles for biomedical application, Jundishapur J. Nat. Pharm., 16 (2021) 1-9. https://doi.org/10.5812/jjnpp.101013

[23] M. Moradalizadeh, M. Akhgar, P. Rajaei, A. Faghihi-Zarandi, Chemical composition of the essential oils of Levisticum officinale growing wild in Iran, Chem. Nat. Compd., 47 (2012) 1007-1009. https://doi.org/10.1007/s10600-012-0130-7

[24] WHO, Instructions for determining the susceptibility or resistance of mosquito larvae to insecticides: World Health Organization, division of vector biology and control, 1981. https://apps.who.int/iris/handle/10665/69615

[25] D. Swale, D. Engers, S. Bollinger, A. Gross, E. Inocente, E. Days, An insecticide resistance-breaking mosquitocide targeting inward rectifier potassium channels in vectors of Zika virus and malaria, Sci. Rep., 6 (2016) 1-11. https://doi.org/10.1038/srep36954

[26] S. Ebrahimi, J. Hadian, M. Mirjalili, A. Sonboli, M. Yousefzadi, Essential oil composition and antibacterial activity of Thymus caramanicus at different phenological stages, Food Chem., 110 (2008) 927-931. https://doi.org/10.1016/j.foodchem.2008.02.083

[27] F. Eftekhar, F. Nariman, M. Yousefzadi, J. Hadian, S. Ebrahimi, Anti-Helicobacter pylori activity and essential oil composition of Thymus caramanicus from Iran, Nat. Prod. Commun., 4 (2009) 1139-1144. https://pubmed.ncbi.nlm.nih.gov/19769000/

[28] M. Mazandarany, M. Rezaee, Chemical constituents of essential oil from Thymus carmanmicus JALAS, scov. Nov, Iran. J. Med. Aromat. Plants Res., 18 (2003) 111-122. https://ijmapr.areeo.ac.ir/article_115521.html?lang=en

[29] D. Damtie, Y. Mekonnen, Toxicity and oviposition deterrent activities of thyme essential oils against Anopheles arabiensis, J. Entomol., 2021 (2021) 1-7. https://doi.org/10.1155/2021/6684156

[30] L. Dargahi, K. Razavi-Azarkhiavi, M. Ramezani, M. Abaee, J. Behravan, Insecticidal activity of the essential oil of Thymus transcaspicus against Anopheles stephensi, Asian Pac. J. Trop. Biomed., 4 (2014) 89-91. https://doi.org/10.12980/APJTB.4.2014APJTB-2014-0077

[31] P. Gupta, S. Preet, N. Singh, Preparation of Thymus vulgaris (L.) essential oil nanoemulsion and its chitosan encapsulation for controlling mosquito vectors, Sci. Rep., 12 (2022) 1-14. https://doi.org/10.1038/s41598-022-07676-5

[32] H. Kelidari, M. Moemenbellah-Fard, K. Morteza-Semnani, F. Amoozegar, M. Shahriari-Namadi, M. Saeedi, Solid-lipid nanoparticles (SLN) s containing Zataria multiflora essential oil with no-cytotoxicity and potent repellent activity against Anopheles stephensi, J. Parasit. Dis., 45 (2021) 101-108. https://doi.org/10.1007/s12639-020-01281-x

[33] S. Firooziyan, M. Osanloo, H. Basseri, S. Moosa-Kazemi, H. Hajipirloo, A. Amani, Nanoemulsion of Myrtus communis essential oil and evaluation of its larvicidal activity against Anopheles stephensi, Arab. J. Chem., 15 (2022) 104064. https://doi.org/10.1016/j.arabjc.2022.104064

[34] E. Zarenezhad, N. Ranjbar, S. Firooziyan, M. Ghoorkhanian, M. Osanloo, Promising larvicidal effects of chitosan nanoparticles containing Laurus nobilis and Trachyspermum ammi essential oils against Anopheles stephensi, Int. J. Trop. Insect Sci., 42 (2022) 895-904. https://doi.org/10.1007/s42690-021-00615-3

Anal. Methods Environ. Chem. J. 6 (1) (2023) 79-99

AMECJ

Research Article, Issue 1
Analytical Methods in Environmental Chemistry Journal
Journal home page: www.amecj.com/ir

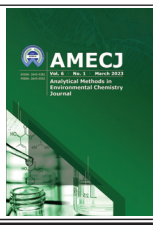

Artificial neural network and response surface design for modeling the competitive biosorption of pentachlorophenol and 2,4,6-trichlorophenol to Canna indica L and analyzed by UV-Vis spectrometry in Aquaponia

Christian Ebere Enyoh [a,c,*], Prosper Eguono Ovuoraye[b], Beniah Obinna Isiuku[c], and Chinenye Adaobi Igwegbe[d]

[a]*Graduate School of Science and Engineering, Saitama University, Saitama, Japan*
[b]*Department of Chemical Engineering, Federal University of Petroleum Resource, P.M.B 1221 Effurun, Nigeria*
[c]*Department of Chemistry, Faculty of Physical Sciences, Imo State University, Imo State, Nigeria*
[d]*Department of Chemical Engineering Nnamdi Azikiwe University, P. M. B. 5025, Awka, Nigeria*

ARTICLE INFO:

Received 11 Nov 2022
Revised form 21 Jan 2023
Accepted 16 Feb 2023
Available online 30 Mar 2023

Keywords:
Phytoremediation,
UV-Vis spectrometry,
Chlorophenol biosorption,
Canna Indica L plant,
ANN modeling,
RSM optimization

ABSTRACT

The continuous exposure of the environment to carcinogenic wastes and toxic chlorophenols such as pentachlorophenol (PCP) and 2,4,6-trichlorophenol (TCP) resulting from industrial production activities has become a great concern to research scientists and environmental policymakers. The search for a cost-efficient and eco-friendly approach to the phytoremediation of water will guarantee sustainability. The present research concerns the cost-benefit evaluation and the optimization modeling of the competitive biosorption of PCP and TCP from aqueous solution to Cana indica. L (CiL-plant) using response surface methodology (RSM) , artificial neural network (ANN) model, and UV-Vis Spectrometry. The predictive performances of the ANN model and the RSM were compared based on their statistical metrics. The antagonistic and synergetic effects of significant biosorption variables (pH, initial concentration, and exposure time) on biosorption were studied at p-values ≤0.005. The findings from the phytoremediation process confirmed that PCP and TCP removal rate reached equilibrium at the optimum conditions corresponding to predominantly acidic pH (4), required initial concentration of 50 mg L^{-1}, and exposure time of 25 days in aquaponia. The optimized output transcends to PCP and TCP removal rates of 90% and 87.99% efficiencies at predicted r-squared ≤0.9999 and a 95% confidence interval. The cost-benefit evaluation established that at the optimum conditions, the cost of operating the removal of TCP from the aqueous solution would save $ 7.72 compared to PCP. The optimization model's reliability based on the experiment's (DoE) design was more sustainable than the one-factor-at-a-time (OFAT) methodologies reported in previous research.

1. Introduction

Chlorinated phenols, such as Pentachlorophenol (PCP) and 2,4,6-Trichlorophenol (TCP), have been used since the 1930s in a variety of industries including wood preservation, pest control, and herbicide production [1,2]. As a result, wastewater from these industries can contain high levels of

*Corresponding Author: Christian Ebere Enyoh
Email: cenyoh@gmail.com
https://doi.org/10.24200/amecj.v6.i01.228

these chemicals, leading to the pollution of water resources and potential harm to ecosystems [3]. The use of pesticides on farms is a significant contributor to the contamination of water resources with chlorinated compounds. studies have shown the presence of significant amounts of organochlorines in water and fish samples [4,5,6]. TCP and PCP are classified as Group B2 probable human carcinogens and 1B highly hazardous; due to their high toxicity, carcinogenic potential, and environmental persistence [1,2]. These chemicals can cause serious health issues such as respiratory problems, cardiovascular disease, gastrointestinal issues, and cancer in humans and have been linked to an increased risk of lymphomas, leukemia, and liver cancer in animal studies [1,2]. Removing these chemicals from water resources or wastewater before they are released into the environment is essential to prevent potential harm to humans and ecosystems. Various methods are available for removing PCP and TCP from water, including biological and physicochemical approaches such as photochemistry, air stripping, incineration, and adsorption technologies using activated clay and plant-based carbons [7]. While some of these methods are effective, they can be challenging to implement. Using aquatic plants for wastewater treatment is a newer method for removing pollutants, and studies have shown that it can be effective when using constructed wetlands, pilot-scale systems, or hydroponic setups [7]. The efficiency of plant-based treatment systems can vary depending on the specific plant species and their productivity. In Nigeria and other tropical countries, various plants effectively remove pollutants from water. Canna lilies, a type of flowering plant, are a commonly used species for this purpose in Nigeria due to their wide distribution and dominance in aquatic environments. Additionally, canna lilies can effectively remove inorganic and organic pollutants such as PCP and TCP through phytoremediation [8-11] and can survive in polluted areas [12]. Central composite design and response surface methodology are statistical approaches used in pollutant removal studies to design experiments and optimize treatment conditions [13]. They allow selecting the most effective experimental conditions through statistical software, reducing the number of costly experiments and trials needed [14]. These methods have been applied to various processes, including coagulation to remove dyes from wastewater [15,16]. They can be helpful in predicting the behavior and outcomes of treatment systems and analyzing existing processes. Artificial neural networks (ANN), which utilize learning algorithms to evaluate the relationships between input and output variables, can also be used to model and predict the behavior of water management processes [17, 18]. While artificial neural networks require many data points to be effective, they are fast, adaptable, and can produce real-time predictions [18]. Both response surface methodology and artificial neural networks have been compared in their predictive capabilities for various processes [17]. This study examined the effectiveness of using *C. indica* L (CiL-plant), an aquatic plant, to remove PCP and TCP from water using response surface methodology and artificial neural networks. The use of aquatic plants for wastewater treatment, specifically for removing organic pollutants such as chlorophenols, is a relatively new method known as aquatic phytoremediation. This study aims to optimize the ability of C. indica to remove PCP and TCP from water using a hydroponic system, and to the best of our knowledge, is the first study of its kind. Furthermore, the removal behavior of C. indica for PCP and TCP has been predicted for the first time by a highly efficient developed ANN model. A techno-economic and cost-benefit evaluation of the phytoremediation process was also examined beyond removal efficiency to ascertain the suitability of the CiL-plant for Aquaponia.

2. Materials and methods

2.1. Preparation of plant material and pesticides solutions

We discussed how the plant material and pesticide solutions were manufactured in our earlier papers [8-10]. In a flood basin in Amakohia, Owerri, Imo state, Nigeria, Canna indica L. seeds and soil for

growing the plant were collected. The plant was raised in nurseries with natural environmental conditions. To conduct the study, properly harvested seedlings with an average height of (14±1 cm) were employed. Without additional refinement, the PCP and TCP (analytical grade, 99.5%) was used after being acquired from FinLab in Owerri. Distilled water and ethanol were used to make the solutions for this experiment. An ethanol-water solution (10% v/v ethanol/distilled water) was used to dissolve 1.0 g of PCP/TCP per liter of solution in a 1.0 liter-volumetric flask while stirring continuously. The stock had a 1000 mg L^{-1} equivalent. By dilutions with distilled water, working solutions of 50, 100, 150, 200, and 250 mg L^{-1} were produced from the stock solution and labeled accordingly. Working solutions were made, and absorbance was measured at 220 nm for PCP and 296 nm for TCP using a UV spectrophotometer. The calibration curve (concentration vs. absorbance) was created using the recorded absorbance, and it was then utilized to calculate the amounts of PCP and TCP. With coefficients of determination more than 0.9995, the absorbance for PCP and TCP starting concentrations rose as the initial concentration increased. This indicates strong linearity of the regression line with good correlation, consequently, and satisfaction of the instrument calibration.

2.2. Batch studies

Uptake of PCP and TCP by *C. indica L.* in pesticide-contaminated water was studied in batch culture experiment using hydroponic, cylindrical (pots) containers with dimensions 18 cm in length, 37 cm in diameter (external) and 19 cm depth [9, 10]. The containers were filled with 500 mL working solutions. Then the plant was introduced into the solution and allowed to stand. This was done for four other pots, representing different time durations (i.e., 10 days, 15 days, 20 days, and 25 days). In total, 5 pots were prepared and at each interval of 5 days a plant was removed and the residue was analyzed by UV-vis spectrophotometer at 220 nm for PCP and 296 nm for TCP [9, 10]. The effect of pH on the removal of PCP and TCP by *C. indica* was determined in 500 mL of test solutions containing 100 mg L^{-1} of PCP and TCP at different pH (4- 9). 1 M nitric acid (HNO_3) and 1 M sodium hydroxide (NaOH) were used for pH adjustments. The pH of each solution was measured with a digital pH meter (Model Jenway 3510). The initial and final concentrations of PCP and TCP solutions were determined on a UV–visible spectrophotometer (Spectrum Lab 23A) at its maximum absorbance wavelength of 220 nm and 296 nm, respectively. All set-ups were conducted in triplicate (total pots were 80 for batch studies, including control and 90 for pH effect), each for PCP and TCP, and were placed randomly with position shifted once a week. After one week, all set-ups were supplemented with N.P.K. fertilizers (1%, i.e., 5 ml: 500 ml). For each treatment method mentioned, there was a corresponding control group that only consisted of deionized water; no pesticide was added, and only the nutrient needed for plant growth in water was provided.

2.3. Response surface design of Experiment

The Central Composite Design (CCD) is an empirical model used for multi-objective optimization of the adsorption or bio-sorption of microplastics from an aqueous solution [19,20]. The CCD optimization is based on the Response Surface Methodology (RSM) [15]. It is used to access and fit experimental data into a linear, cubic, quadratic, cubic, or polynomial model [21]. The model coefficients developed via the RSM can establish an optimal model equation and describe the antagonistic or synergetic interactions and relationship of experimental variables and their significance level with the response within the range studied [13]. In this study, the CCD matrices consisted of 20 experimental runs. The modeling of the bio-sorption of PCP and TCP to CiL-plant (Canna indica L.) in terms of actual values is shown in Table 1. The final model equation following the prediction of the optimum conditions for bio-sorption (pH, initial concentration, and time) for the removal of PCP and TCP is described by Equation 1.

$$Y = \beta_0 + \sum_{i=1}^{k} \beta_i x_i + \sum_{i=1}^{k} \beta_{ii} x_i^{\,2} + \sum_{i=1}^{k} \sum_{j=1}^{k} \beta_{ij} x_i x_j + \varepsilon$$

(Eq.1)

Where x_{ij} experimental variable and β are ranked model coefficients, the summation symbols signify the interactive effect of the dependent and independent variables (pH, time, and concentration), ε is the model intercept, and Y is the response (PCP and TCP removal rate). The optimization modeling of the biosorption of TCP and PCP to the CIL plant was executed using Design Expert software v12.0. The experimental variables contact time (A) (days), initial concentration (B) (mg L^{-1}), and pH (C) shown in Table 1 were varied to 3-Levels with 5 replications. The toxicity was modeled following the CCD matrix. The initial concentration of the biosorbent and the contact time was varied to 5-Levels at an experimentally determined pH of 4.

2.4. Artificial Neural Network

Aside from RSM modeling, data modeling via artificial intelligence tools such as the artificial neural network (ANN) was implemented in this study to create a better understanding of the model validation of the bioremediation process. The neural network tool in MatLab 2018a was used to model the CiL-plant biosorption process. As input data, the experimental data set obtained from the experimental design supplied by CCD space (Table 2) via the RSM was employed. The network was trained using the Multi-Layer Perceptron (MLP) Levenberg-Marquardt (LM) method (*trainlm*) to fit the inputs and targets. The network was made up of the input layer (which included the five process parameters: time, concentration, and pH), neurons (the hidden layer), and the output layer (which contained the PCP or TCP removal efficiency, expressed in %) (Fig. 1). The input data with 20 samples were divided randomly (*dividrand*) into a training set (75%-14 points), validation (15%-3 points) and testing sets (15%-3 points). Based on R^2 and mean square error values, the ideal number of hidden layer neurons was determined by trial and error. More data for training decreases processing time and improves the model; testing provides an impartial evaluation of the network's performance. The training was stopped when the network generalization was improved indicated by the increase in MSE error of the validation samples. To eliminate network error, the input and output variables were normalized between 0 and 1 [17].

2.5. Cost estimation theory for the biosorption process

The techno-economic evaluation of the CiL-plant-driven bioremediation of the comparative removal of PCP and TCP from an aqueous solution was determined following the established cost-benefit analysis model [15]. The cost benefit and alternative cost models were used to describe the feasibility of CiL-plant biosorption of PCP and TCP beyond removal efficiency following the model equation described in Equations 2-5. The total cost for the biosorption of PCP, and TCP from 1.0 L of the aqueous solution to CiL-plant at optimum operating conditions was evaluated using

Table 1. Showing experimental factors in terms of coded values

Factor	Name	Units	Minimum	Maximum	Coded Low	Coded High	Mean	Std. Dev.
A	Time	Days	5.00	25.00	-1 ↔ 5.00	+1 ↔ 25.00	14.50	8.87
B	Conc	mgL^{-1}	50.00	250.00	-1 ↔ 50.00	+1 ↔ 250.00	122.50	67.81
C	pH		4.00	9.00	-1 ↔ 4.00	+1 ↔ 9.00	5.85	2.06

Table 2. Design matrix in terms of actual and predicted values for the RSM and ANN optimization process

		Factors			Response 1: %PCP Removal Efficiency			Response 1: %TCP Removal Efficiency		
Std	Run	A: Time (Days)	B: Concentration (mg L^{-1})	C: pH	Actual	RSM predicted values	ANN predicted values	Actual	RSM predicted values	ANN predicted values
11	1	25	250	4	78.31	77.91	78.04	78.74	78.70	78.76
14	2	15	100	6	52.70	54.81	52.64	66.19	64.97	61.62
18	3	5	100	9	7.56	12.20	7.56	4.81	8.34	5.78
8	4	5	100	6	50.37	33.52	50.32	32.33	21.30	31.17
16	5	25	100	4	82.00	77.11	81.96	85.71	81.89	85.75
13	6	15	100	9	36.33	27.88	36.33	52.29	33.60	48.70
1	7	5	50	4	34.64	35.65	34.6	9.04	9.15	9.07
17	8	25	100	9	49.26	48..85	49.19	53.00	53.81	52.85
10	9	15	100	6	52.70	54.81	52.64	66.19	64.97	61.62
12	10	25	100	6	73.00	81.40	76.81	81.05	83.45	80.53
3	11	15	100	6	52.70	54.81	52.64	52.70	64.97	61.62
15	12	5	250	4	13.24	13.58	12.71	3.85	3.89	3.81
2	13	25	50	4	90.00	87.99	85.37	82.09	81.87	82.18
7	14	5	100	9	7.56	12.20	7.56	4.81	8.31	5.78
9	15	5	100	4	16.86	21.75	27.52	5.00	8.73	2.12
6	16	15	100	6	52.70	54.81	52.64	66.19	64.97	61.62
4	17	5	250	4	13.24	13.58	12.71	3.85	3.89	3.81
19	18	25	100	9	49.26	48..85	49.19	53.00	53.81	52.85
5	19	5	50	4	34.64	35.65	34.60	9.04	9.049.15	9.07
20	20	25	250	4	78.31	77.97	78.04	78.74	78.70	78.76

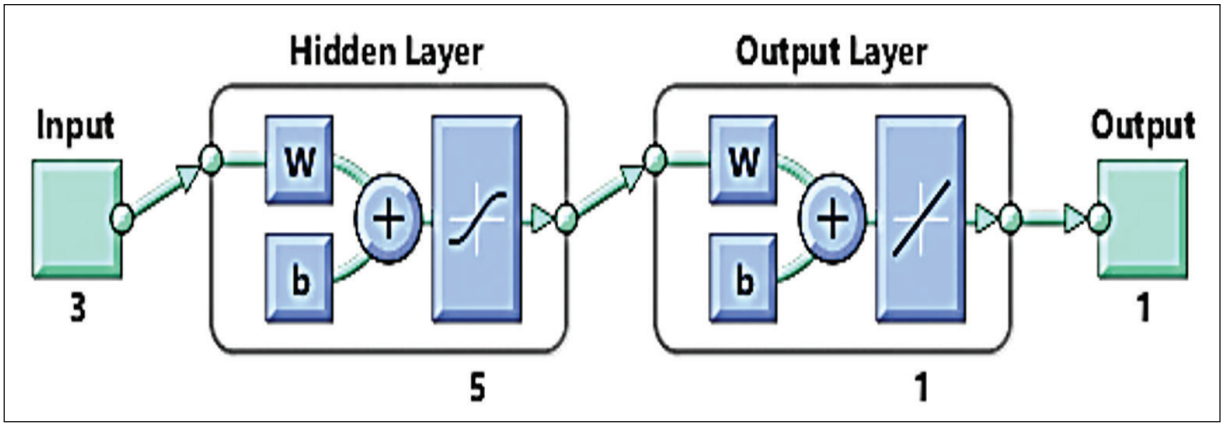

Fig. 1. ANN network of the PCP and TCP optimization sequence

the expression shown in Equation 3**.** The energy consumption (*EC*) was evaluated using Equation 2 [15, 23]. and given by:

$$E_C = P_C(f \times t \times C) \qquad \textbf{(Eq.2)}$$

Where P_C is the power consumption by the device (kW), f is the load factor. In a full mode, f =1, t is the time of usage of the device (hour), and C is the energy estimated cost ($) per (KWh) in Nigeria as of the month of April 9, 2021.

Total cost is a function of all costs, including

biosorbent production, labour, and energy. C_m is the costs incurred from transportation, and renting [24].

$$T_C = C_P + C_L + C_m \quad \textbf{(Eq.3)}$$

$$C_B = F_O - C_O \quad \textbf{(Eq.4)}$$

Where F_O is the return on the selected and forgone option (PCP versus TCP), in this case, it's the performance of CiL-plant for the bioremediation of aqueous medium and C_O is the return on chosen option from PCP versus TCP, and C_B is the opportunity cost based derived based on environmental impact and regulatory risk (Eq. 4). In this case, the return on chosen option which defines the return on investment as a function of direct and indirect cost [15]. The parameter F_0 was evaluated following modified model Equation 5, expressed as:

$$F_0 = T_C + E_C + M_c \quad \textbf{(Eq.5)}$$

3. Result and Discussion

In our previous studies [8-10], the results for the removal of PCP and TCP have been presented. This current study is a step further in which removal processes are optimized and predicted using RSM and ANN, respectively, to determine the optimum operating variable for modeling the performance CiL-plant-driven bioremediation process. Furthermore, the techno-economic and cost-benefit analysis for the method was evaluated in the current study to ascertain the feasibility of the CiL-driven bioremediation of PCP and TCP in aquaponia beyond removal efficiency.

3.1. Central composite design modeling of the CiL-driven biosorption process

The findings from the CCD optimization modeling following the biosorption of PCP and TCP to CIL-plant from an aqueous solution follow a second-order quadratic model shown in the ANOVA (Tables 3 and 4). Tables 3 and 4 showed that the selected quadratic model recorded consistent outputs from the CCD that adequately describes the CiL-plant-driven biosorption of PCP and TCP from an aqueous solution. It was observed that model f-values PCP (30.55) and TCP (62.75) obtained a lack-of-fit value >3 recorded at a p-value less than 0.05. This statistical output indicates that there is only a 0.01% chance that f-values this large could occur in the optimization modeling of the phytoremediation process variables due to noise [19, 24]. A p-value ≤ 0.0500 obtained with the CCD space suggests that the quadratic model terms and subsequent assumptions on the phytoremediation process are significant at a 95% confidence level. The statistical output also suggests that the quadratic model results significantly describe the CiL-plant-driven biosorption of PCP and TCP from an aqueous medium [21]. The model fit statistics that describe the removal of PCP from the aqueous medium established that the predicted R^2 (0.8322), adjusted R^2 (0.9256), is in reasonable agreement with the correlation coefficient R^2 (0.9256) recorded from the central composite design space. Similarly, the model predicted R^2 (0.9329) was also in reasonable agreement with the adjusted R^2 (0.9630) reported for the CiL-plant biosorption of TCP from an aqueous solution. These r-squared values are close to unity (1), and their differences are less than 0.2, indicating that the selected quadratic model description of the CiL-plant-driven phytoremediation process is significant at a 95% confidence level [19, 21, 22]. However, where the adequacy of precision output >4 is desirable [15], the selected quadratic model recorded adequacy of precision (16.11) value measures the signal-to-noise ratio (16.11), and the model f-value (5.36) can be used to navigate design space for modeling the PCP removal rate [24]. The adequacy of precision (19.41), and signal ratio (19.41) recorded for the TCP biosorption modeling were > 4, confirming that the quadratic model following the design space adequately describes the modeling of the biosorption of PCP and TCP to CiL-plant. Few insignificant model terms are reported with the central composite design space, not counting those required to support hierarchy. Regarding PCP removal rate, the first-order

phytoremediation variables such as; contact time, pH, and initial concentration, and the second-order degree of pH $(C)^2$ are significant model terms. This outcome indicated that contact time (A), initial concentration of CiL-plant (B), and pH (C) all have a significant antagonistic influence on CiL-plant biosorption of PCP from aqueous solution. The pH also has a second-order degree of significant impact on removing PCP from aqueous solution compliance to CiL-plant at p-values <0.100 [15]. The statistical outcome suggests model reduction was negligible, and the interactive effect of model factors A*B, and A*C which transcends to contact time*concentration (A*B), and contact time*pH (A*C) both have synergetic effects on the biosorption of PCP to Canna indica. L (CiL-plant) in the combined system. Comparatively, the quadratic model statistics and assumptions describing the CiL-plant-driven TCP removal rate established that contact time (A) and pH (C) of solution significantly affect on the phytoremediation process. However, the interactive effect of contact time*pH of solution (A*C) had a synergetic effect on the TCP removal from the aqueous solution. Also, the model assumption established that a higher order degree of contact time (A^2) and pH (C^2) are significant model terms for TCP biosorption to Canna indica L. (CiL-plant). This translates to both model terms having an antagonistic first and second-order impact on TCP biosorption to CiL-plant. The contact time-initial concentration (A*B) has a synergetic effect on the biosorption of TCP and PCP to *Canna indica* L. Consequently, the selected model assumption proved that sufficient contact time and optimized initial concentration of samples are consequential to the overall performance of CiL-plant in Aquaponia. The results from model fit statistics following the established design space also showed that the coefficient of estimate representing the expected change in TCP and PCP removal efficiency per unit change in the values of significant phytoremediation variables when non-significant factors are held constant [21] confirmed the range of variance inflation factors (VIFs) values (-2.91≤ VIFs ≤ 8.27) were recorded for the CiL-plant driven biosorption of PCP from aqueous solution. This range of VIFs output (1.22 ≤ VIFs ≤ 3.27) is consistent with the removal rate of TCP from an aqueous solution. The model-established VIFs outputs fell within the range 1≥ VIFs <10, suggesting that the intercept in an orthogonal design [17], while model coefficients are adjustments around that average based on the significant factors describing the efficacy of CiL-plant. The factors are orthogonal when the VIFs are equal to a unit (1); there is a situation of multi-collinearity at VIFs outputs >1 [17]. The moderate VIFs recorded with the CCD indicate a negligible level of severity of the correlation of factors [21]. Consequently, the VIFs <10 recorded for PCP and TCP are tolerable. The summary based on the VIFs obtained via the established quadratic model, the subsequent model hierarchy based on the level significance of the experimental factors following the biosorption of PCP, and TCP to Canna indica L. (CiL-plant) from an aqueous solution follows the Table order.

The established quadratic model equations describing the biosorption of PCP, and TCP to Canna indica L were obtained from the CCD optimization outputs. The outcome showed that the final model equation for the PCP removal rate is given by Equation 6, and the TCP removal rate is described by Equation 7.

PCP ↔↔ *Contact time > Initial Concentration > pH > Time*pH > Time*Initial Concentration*

TCP ↔↔ *Contact time > Initial Concentration > pH > Time*pH > Time*Initial Concentration*

$$Y_{PCP} = 47 + 25Time - 8Conc - 10pH + 3Time * Conc - 5Time * pH - 16pH^2 \quad \text{(Eq. 6)}$$

$$Y_{TCP} = 63 + 30Time - 7pH - 7Time * pH - 13Time^2 - 13pH^2 \quad \text{(Eq. 7)}$$

Table 3. ANOVA for the Quadratic modeling of PCP biosorption to CiL-plant

Source	Sum of Squares	df	Mean Square	F-value	p-value	
Model	12028.39	8	1503.55	30.55	< 0.0001	**Significant**
A-Time	6707.47	1	6707.47	136.28	< 0.0001	
B-Concentration	421.62	1	421.62	8.57	0.0138	
C-pH	497.35	1	497.35	10.11	0.0088	
AB	66.62	1	66.62	1.35	0.2693	
AC	215.55	1	215.55	4.38	0.0604	
A^2	14.93	1	14.93	0.3034	0.5928	
B^2	97.68	1	97.68	1.98	0.1865	
C^2	450.18	1	450.18	9.15	0.0116	
Residual	541.40	11	49.22			
Lack of Fit	541.40	3	180.47			**Not significant**
Pure Error	0.0000	8	0.0000			
Cor Total	12569.79	19				

Pred R^2 = 0.832; Adj R^2 = 0.9256; R^2 =0.9565; stdv = 7.02; Adeq of Precision =16.105 and Mean value =46.27

Table 4. Showing ANOVA for Quadratic modeling of the TCP biosorption to CiL-plant

Source	Sum of Squares	df	Mean Square	F-value	p-value	
Model	18743.53	8	2342.94	62.75	< 0.0001	**Significant**
A-Time	10015.46	1	10015.46	268.24	< 0.0001	
B-Concentration	29.10	1	29.10	0.7794	0.3962	
C-pH	284.22	1	284.22	7.61	0.0186	
AB	2.02	1	2.02	0.0540	0.8205	
AC	473.96	1	473.96	12.69	0.0045	
A^2	338.64	1	338.64	9.07	0.0118	
B^2	1.12	1	1.12	0.0301	0.8654	
C^2	300.46	1	300.46	8.05	0.0162	
Residual	410.71	11	37.34			
Lack of Fit	274.23	3	91.41	5.36	0.0257	**Not significant**
Pure Error	136.49	8	17.06			
Cor Total	19154.25	19				

Pred R^2 = 0.9329; Adj R^2 = 0.9630; R^2 =0.9786; stdv = 7.02; Adeq of Precision =19.41 and Mean value =44.43

3.2 Optimization outputs following the CiL-plant-driven biosorption process

The interpretation of the CiL-plant-driven biosorption of PCP, and TCP from an aqueous solution follows from the established model Equations 6-7. The results based on the interpretation of the optimization ramp (Fig. 2) confirmed that the optimum comparative conditions describing the best performance of the CiL-plant-driven biosorption of PCP and TCP from an aqueous solution correspond to pH (4), initial concentration (50 mg L^{-1}), and contact time (25 days). The predicted optimum based on the quadratic model output is confirmed from the optimization ramp shown in Figure 2. The predicted optimum outputs translate to a removal efficiency of 87.88 %, and 81.87 % for the biosorption of PCP, and TCP to CiL-plant as indicated in the optimization ramp in Figure 2. The optimum points transcend to a standard deviation of PCP (7.01), and TCP (6.80) from the actual observations practicable. The outcome is represented by the flag points shown on the 3-D plots in Figure 3 (a-b). The flag points confirmed that the predicted optimum points are located within the CCD design space [17, 24], and maintained within the range of the experimental values under investigation.

The predicted optimum indicates that the best biosorption of PCP, and TCP occurred via an active

initial concentration of 50 mg L^{-1} of Canna indica L. plant. The phytoremediation progressed in a predominantly acidic medium (pH 4), and requires sufficient contact time (25 days) to drive the biosorption of PCP, and TCP to lower residual that guarantees sustainability. The optimization results established that under similar optimum operating conditions, the comparative biosorption rate of PCP to CiL-plant was most favorable compared to TCP with a significant difference of ≥6%.

3.3 Artificial neural network performance validation of the CiL-driven biosorption process

The validation performance in Figures 4 (a-b) shows how the number of epochs varied with the MSE for the optimal neural network. The best validation performance was 4.8753 and 2.8482 at epoch 3 for PCP and TCP biosorption. The scatter plots depicting the linearity of the output values of the network with the target values for the training, testing, validation, and overall data (as generated

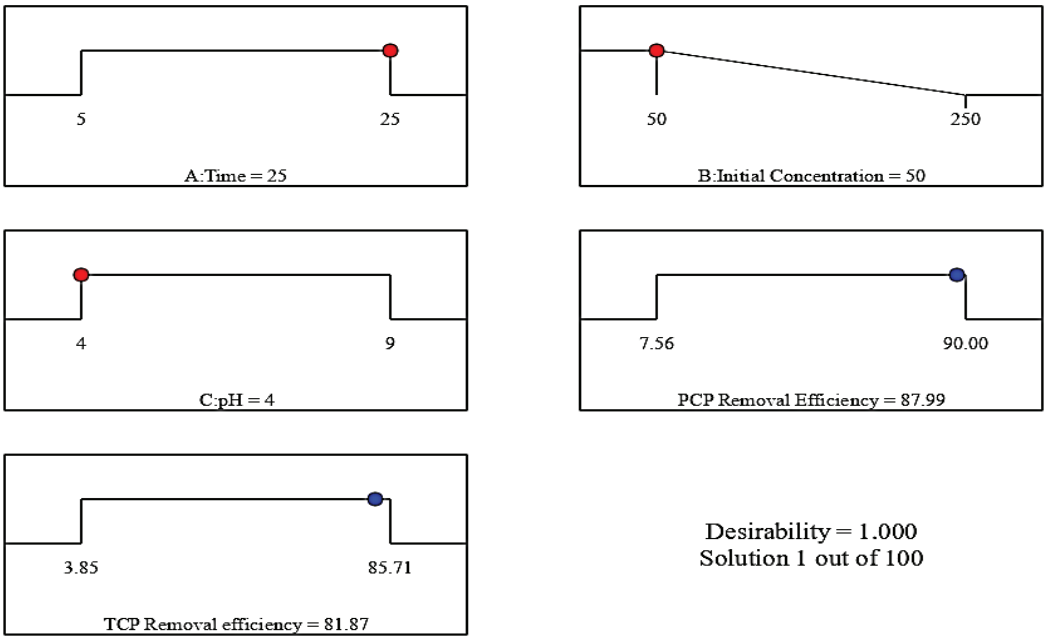

Fig 2. Optimization ramp for CiL-plant driven biosorption of PCP and TCP

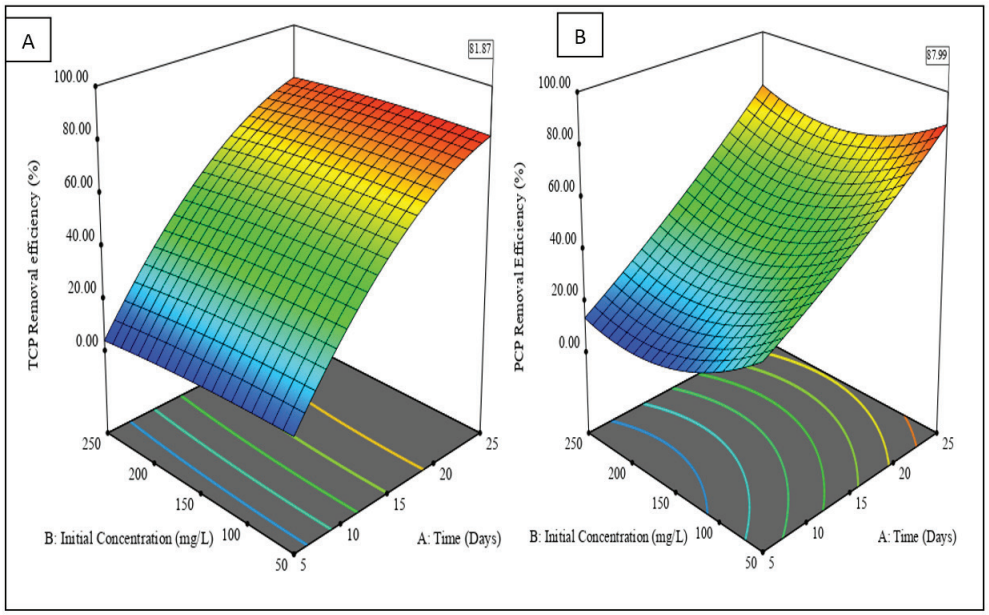

Fig. 3. 3D surfaces for the removal efficiency at different times and concentrations for (a) TCP and (b) PCP

by the MLP platform) are illustrated in Figures 5 (a, b). The predicted R^2 values were used to indicate the linearity – with the training network having the highest value of 0.9999 and 0.9945 for the optimal neural network for PCP and TCP biosorption, respectively. The outputs design matrix in Table 2 (presented in section 2.4 above) displayed the anticipated responses at various experimental setups. It can be concluded from the outline of Figure 4 that the summary of the statistical and evaluation metrics from the ANN indicates an increase in model errors as the number of epochs increased. This outcome reasonably agrees with the optimization modeling procedure reported in the literature [16, 27]. The train and validation curves' curvature indicates that overfitting has been greatly minimized [27].

The performance of each model (ANN and RSM) was validated by evaluating their prediction accuracy using statistical tools (MSE, RSME, X^2 and SSE) [27, 28]. The mathematical equations representing the statistical tools are summarized in Table 5. A better predictive model has a high R^2 value (almost 1) and low statistical errors (close to 0) [11, 12]. The high R^2 values and statistical errors proved a good correlation with the actual observations practicable than the RSM. When compared to the RSM, the ANN outputs yielded significant statistics performance with minimal error (R^2 ≤0.9945, RMSE≤0.06, and X^2 ≤0.0001). The low statistical error indicates reliable adequacy of precession [25, 26], suggesting minimal error due to noise [27]. However, the statistical outcome from both optimization tools is in reasonable agreement with the actual values obtained from the experimentation with the RSM output indicating a ±0.005 deviation from the ANN output. The RSM performance evaluation has the benefit of providing a prediction equation, and demonstrating the influence of operational parameters and their interactions on the response [18]. The statistical model assumptions of the RSM have been ascertained for reliability, and the design space (CCD) has been tested based on the design of experiments (DoE). As a result, the predicted optimum reported for the RSM was employed to further optimize the CiL-plant driven biosorption process.

Table 5. Summary of the optimization fit statistics and errors factor

Error factor	Equation	RSM	ANN
MSE	$\mathrm{MSE} = \frac{1}{\mathrm{N}}\sum_{i=1}^{N}(y_i - y_i^*)^2$	0.0080	0.0036
RMSE	$RMSE = \sqrt{\frac{1}{\mathrm{N}}\sum_{i=1}^{N}(y_i - y_i^*)^2}$	0.0894	0.0604
X^2	$X^2 = \sum_{i=1}^{N}\frac{(y_i - y_i^*)^2}{y_i^*}$	2.8478	0.0001
SSE	$SSE = \sum_{i=1}^{N}(y_i - y_i^*)^2$	0.1600	0.0729
Predicted R^2		0.9329	0.9954

Where yi, yi*, and y_m stand for the experimental, predicted, and mean value of the actual responses, *N* represents the number of experimental outcomes; MSE: mean squared error, RMSE: root mean square error, X^2: Chi-square and SSE: sum of squares errors

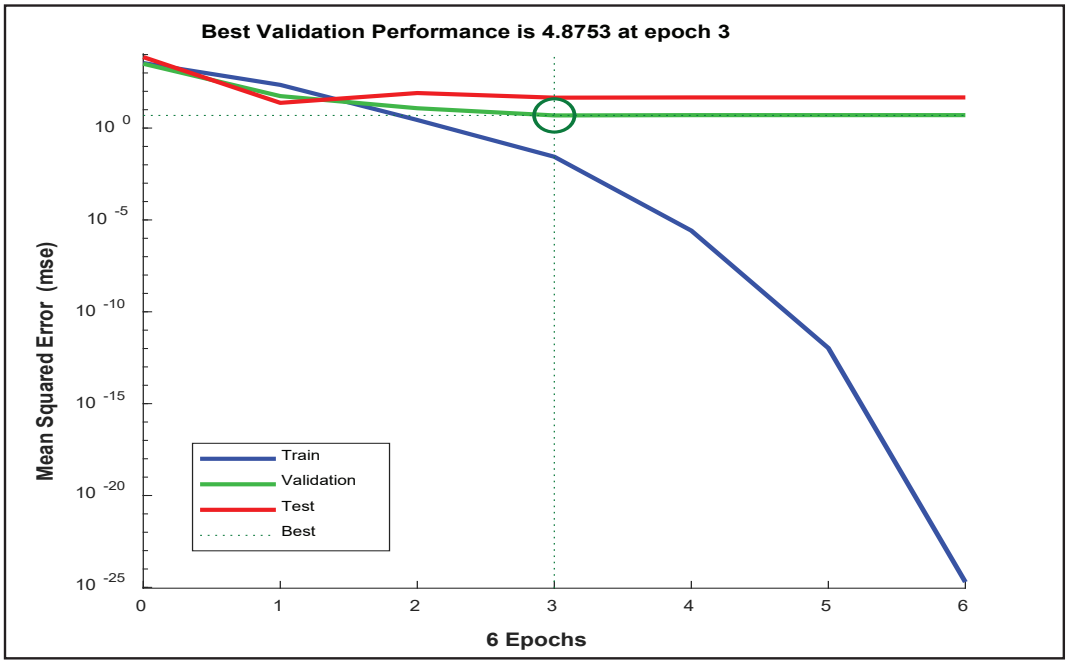

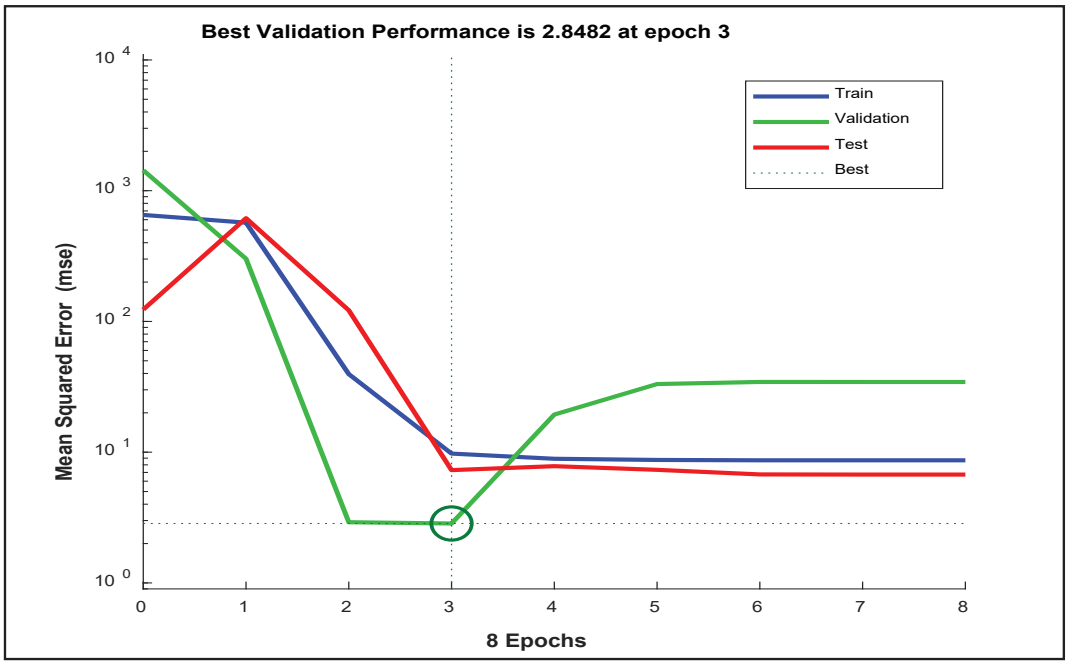

Fig. 4. Optimal neural network's validation performance graph for the **(a)** PCP, and **(b)** TCP biosorption processes

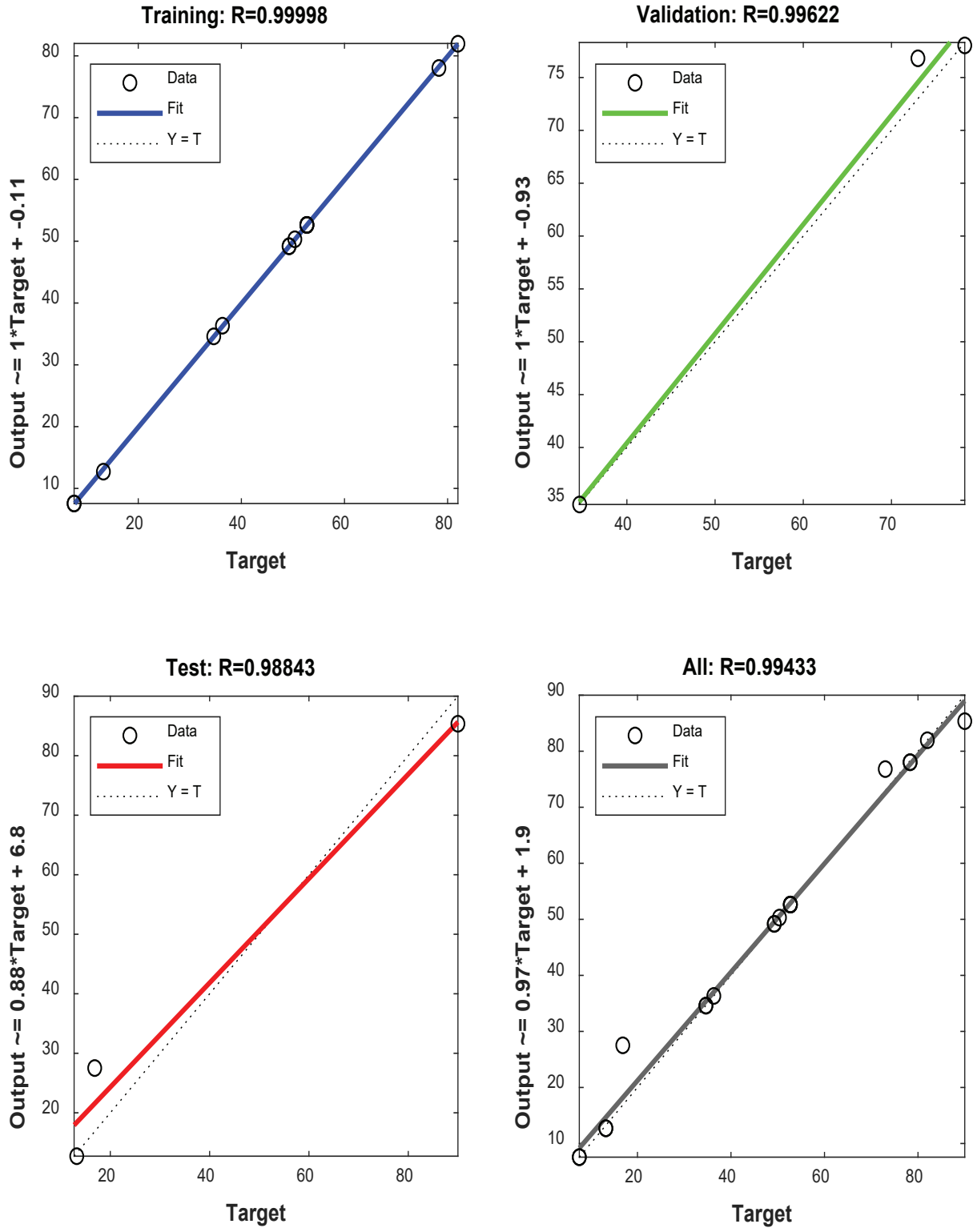

Fig. 5(a). The output/target values for the PCP biosorption processes' training, testing, validation, and overall data

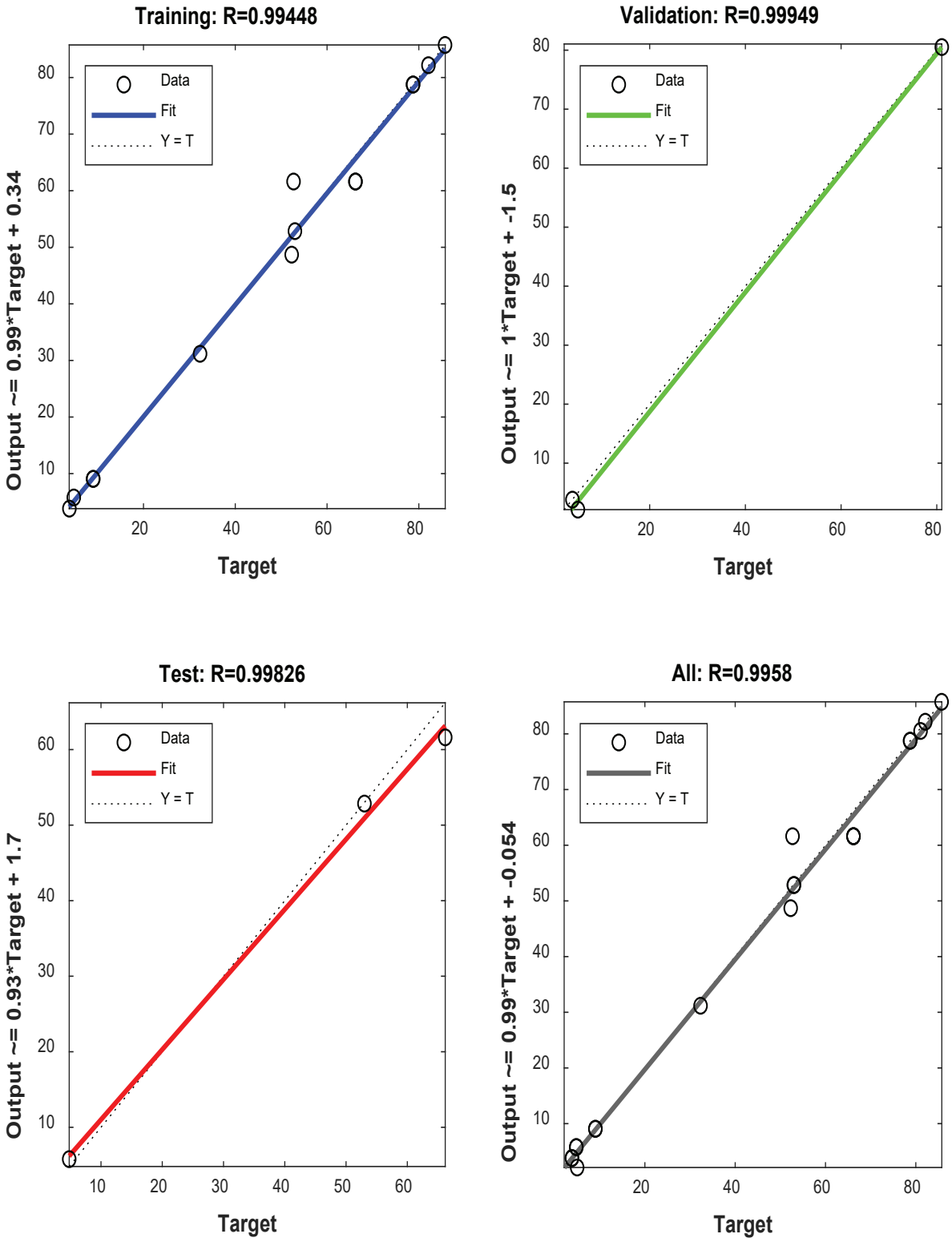

Fig. 5(b). The output/target values for the TCP biosorption processes' training, testing, validation, and overall data

3.4 Effects of experimental variables on the overall performance of the CiL-plant

The effects of the phytoremediation variables on the CiL-plant driven biosorption of PCP, and TCP from an aqueous solution were based on the CCD statistics (VIFs), and model hierarchy model parameters shown in section 3.1. The relative impact of significant model factors pH (C), and contact time (A) on the biosorption of PCP, and TCP aqueous solution compliance to CiL-plant in the single and interactive system when the significant variable is kept constant are presented in Figures 6 and 7.

3.4.1 Antagonistic effect of contact time on the Phytoremediation process

Figure 6 confirmed the antagonistic effect of contact time on the biosorption of PCP, and TCP to CiL-plant at the optimum concentration (50 mg L^{-1}). The graph showed that the CiL-plant-driven biosorption of PCP, and TCP from an aqueous solution increased significantly as the contact time increased in days. The overall performance under the influence of contact time corresponds to the maximum PCP removal rate (90%) recorded in 25 days and was consistent with the maximum removal rate recorded for TCP (87.99%). At contact time < 5 days removal efficiency was less than 10%; the outcome suggests biosorption of the chemical species (TCP) was slow on the CiL-plant surface or had not yet occurred for PCP. Comparatively, the antagonistic effect of contact time significantly favored the removal of PCP removal from the aqueous solution compared with the performance of CiL-plant biosorbent on the removal of TCP at maximum contact for 25 days. Sufficient time >20 days allowed for the biosorption of the contaminants (TCP and PCP) on CiL-plant from the solution to reach equilibrium [29]. The outline of the red and blue bars indicated that biosorption of TCP reached equilibrium faster than PCP. The finding suggests a relatively higher level of tolerance of the CiL-plant index to PCP-contaminated medium [8]. Overall performance was very satisfactory, confirming the potential of the CiL-plant as an active biosorbent for the sustainable removal of PCP and TCP to guarantee a tolerable residual contaminant level. The outcomes confirmed the influence of the optimum contact time on the removal of PCP and TCP from an aqueous solution recorded at a p-value of 0.0001 at a 95% confidence interval.

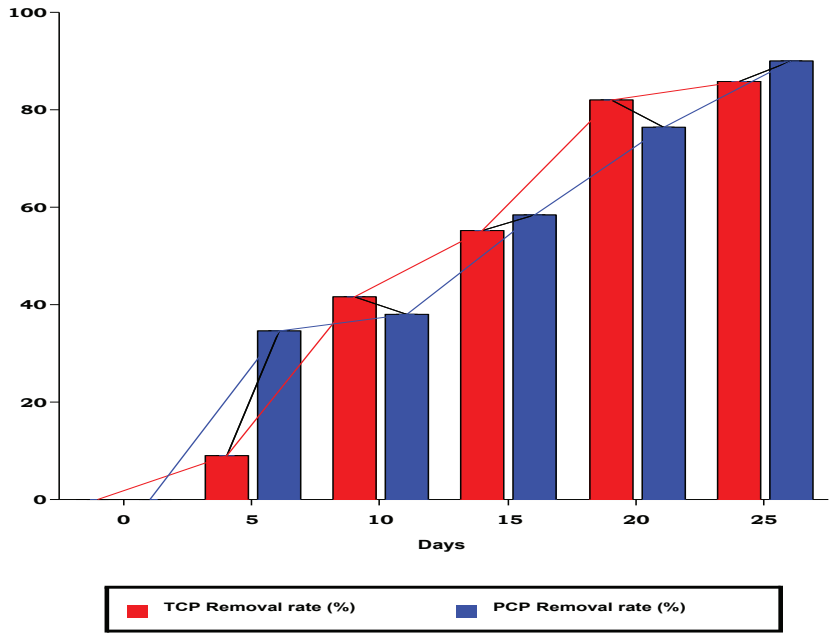

Fig 6. Effects of time on the removal of PCP and TCP to Canna indica L. at an optimum initial concentration (50 mg L^{-1}) and pH 4

3.4.2 Antagonistic impact of pH on the Phytoremediation process

The influence of pH on the CiL-plant drove biosorption of TCP from an aqueous solution at an initial concentration of 100 mg L^{-1} at pH 4 is shown in Figure 7. The graph showed that the biosorption of PCP and TCP to CiL-plant at varying pH decreased rapidly in an alkaline solution. The performance of the CiL-plant translates to a removal rate of 49.3% for PCP, and 53.2% for TCP at pH 9 and an optimum of 25 days, respectively. The removal rate increased significantly in a predominantly acidic medium transcending to 82% for PCP, and 85.7% for TCP at pH 4. The protonated chlorophenols were more absorbable [30], which accounted for the higher removal efficiency recorded for PCP and TCP at the lower pH value. The analysis of the significant impact of pH 4 on the treatment process confirmed that, irrespective of the pH window, the CiL-driven biosorption process favored TCP removal from an aqueous medium in an acidic medium compared to PCP at a p-value value of 0.0006 at 95% confidence interval. This outcome was consistent with the optimum pH 2 reported for the removal of PCP and TCP reported in the work of Radhika and Palanivelu et al. [29]. The outline of the figure also indicates that CiL-plant has a higher affinity for TCP at the optimum conditions than PCP [8], suggesting a superior solubility of 2,4,6-TCP in water than PCP at optimum pH 4 in aquaponia. Comparative evaluation of the maximum efficacy of CiL-plant under the effect of contact time of 25 days (90, 87.99%), and effect of pH (4) of solution corresponding (82, 85.7%) established that contact time had a significant main effect on the overall performance of CiL-plant-driven phytoremediation for sustainability.

3.4.3. Synergetic impact of Time-pH and concentration-pH on the Biosorption process

The significance of the synergetic effect of pH*Time and Time*initial concentration on the response PCP and TCP removal rate was confirmed based on the hierarchy from the VIFs at a p-value less than 0.005 and 95% CI. The 3-D surface plots in Figure 8 (a-d) were obtained from the response surface design space to understand better how the biosorption process works under the interactive influence of significant parameters [5, 8]. The red color gradient corresponds to higher removal efficiency of >87%. In comparison, the yellow contour gradient corresponds to moderate

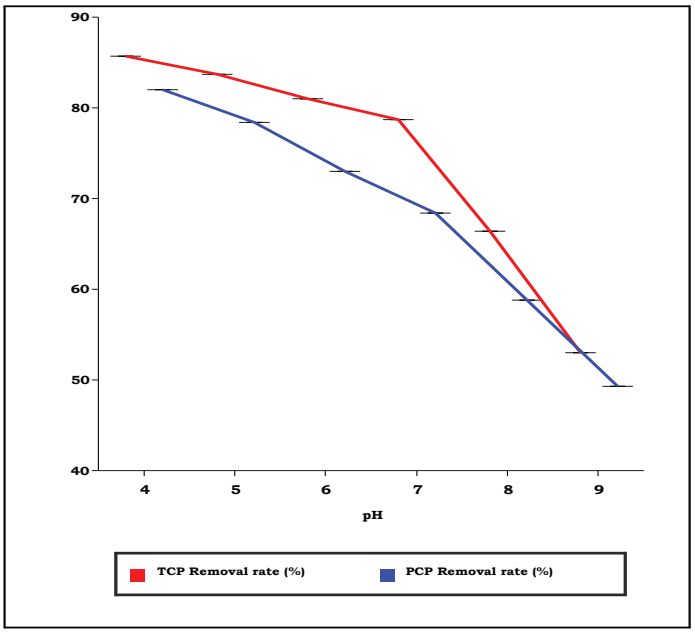

Fig 7. Effect of pH on the removal of PCP and TCP to Canna indica L. at optimum Time (25days) and initial concentration of 100 mg L^{-1} at pH 4

removal efficiency of less than 70%, and the dominant greenish-blue contour orientation translates to lower removal efficiency of less than 50%. The decrease in removal efficiency can be traced to possible charge reversal from surplus ions arising from the binary solution of PCP and TCP under changing pH in the medium. These excess negative charges contributed to the building up of the concentrations of the PCP and TCP molecules in an aqueous solution causing efficiency to drop significantly. The curvature of the red hue gradient on the base of the surfaces Figures 8 (a-b) show that the efficiency of removal of PCP and TCP increased significantly as the pH of the solution decreased from 9 to predominantly pH 4, as the exposure time of CiL-plant increased from 20 to 25 days. The phytoremediation performance of the biosorbent in aquaponia transcends to increase in PCP biosorption rate from 70 to 90%, while the TCP removal rate increased from 70 to 87.99%, as illustrated by the flag-point in the respective contour plots in Figure 8 (a,b). The pH depression from 7 to 4 yielded better performances that can be attributed to the synergetic influence of pH depression towards the acidic window and the prolonged exposure time of 25 days. This outcome is indicated by the curvatures of the dominant red contour deviation from the yellowish-green contour lines shown in Figure 8 (a,b). The basic tendency of CiL-plant-driven biosorption of PCP and TCP can be expressed from the plant's capability to drive the removal rate towards a dominantly acidic medium (pH 4) with no change in phase. The influence of the superior pH on the overall biosorption of PCP and TCP in aquaponia was attributed to the dissociation of most chlorophenol in the form of a salt which loses its negative charge easily when pH is increased [30], thus making it difficult to be adsorbed. The variation in the removal efficiency established that CiL-plant is tolerant in a solution of PCP, compared to TCP. This observation agrees with previous research works reported in the literature [8, 30] and confirms the optimization report in section 3.1. The synergetic effect of initial concentration*contact time is illustrated in the outline the contour plot in Figure 8 (c,d). The overall performance of the CiL-plant in the phytoremediation remediation of aquaponia is illustrated by the deviation of the green color contour from the dominant blue gradient on the base of the surfaces in Figure 8c and Figure 8d, respectively. The curvature of the light green from the dominant blue color orientation is attributed to areas of good performance of the biosorbent morphology and adaptation of Canna indica L for the removal of PCP and TCP. The data points and orientation of the dominant blue contour lines transcend to areas of poor performance of the biosorbent on PCP and TCP in solution. The intensity of the blue contour gradients in Figure 8 (c,d) confirmed that the best performance of the CiL-plant is adapted to an initial concentration of less than 100 mg L^{-1}. The PCP and TCP removal efficiency of the biosorbent decreased as the initial concentration was increased beyond 100 to 250 mg L^{-1}. The output reduces efficiency from 75% to 63% for PCP and <65% for TCP, as indicated by the curvature of the blue contour gradient in Figure 8 (c,d) and corresponding 3D surfaces in Figure 3. This outcome indicates that the initial concentration has a ceiling effect on the driving force of CiL-plant biosorption of PCP and TCP [30, 31]. In contrast, the contact time or exposure had a significant main effect on the phytoremediation process. The findings are consistent with the reports on TCP biosorption [29]. The authors reasoned that if the concentration was to be increased slightly beyond 100 mg L^{-1}, and a reduction in equilibrium exposure time below 25 days would decrease mass transfer to the surface of the biosorbent, would influence a reduction in PCP, and TCP removal efficiency significantly from 90% to 40%. This outcome established the significant impact of the interactive effect of initial concentration and exposure time on the overall performance of the CiL-plant-driven phytoremediation process in Aquaponia.

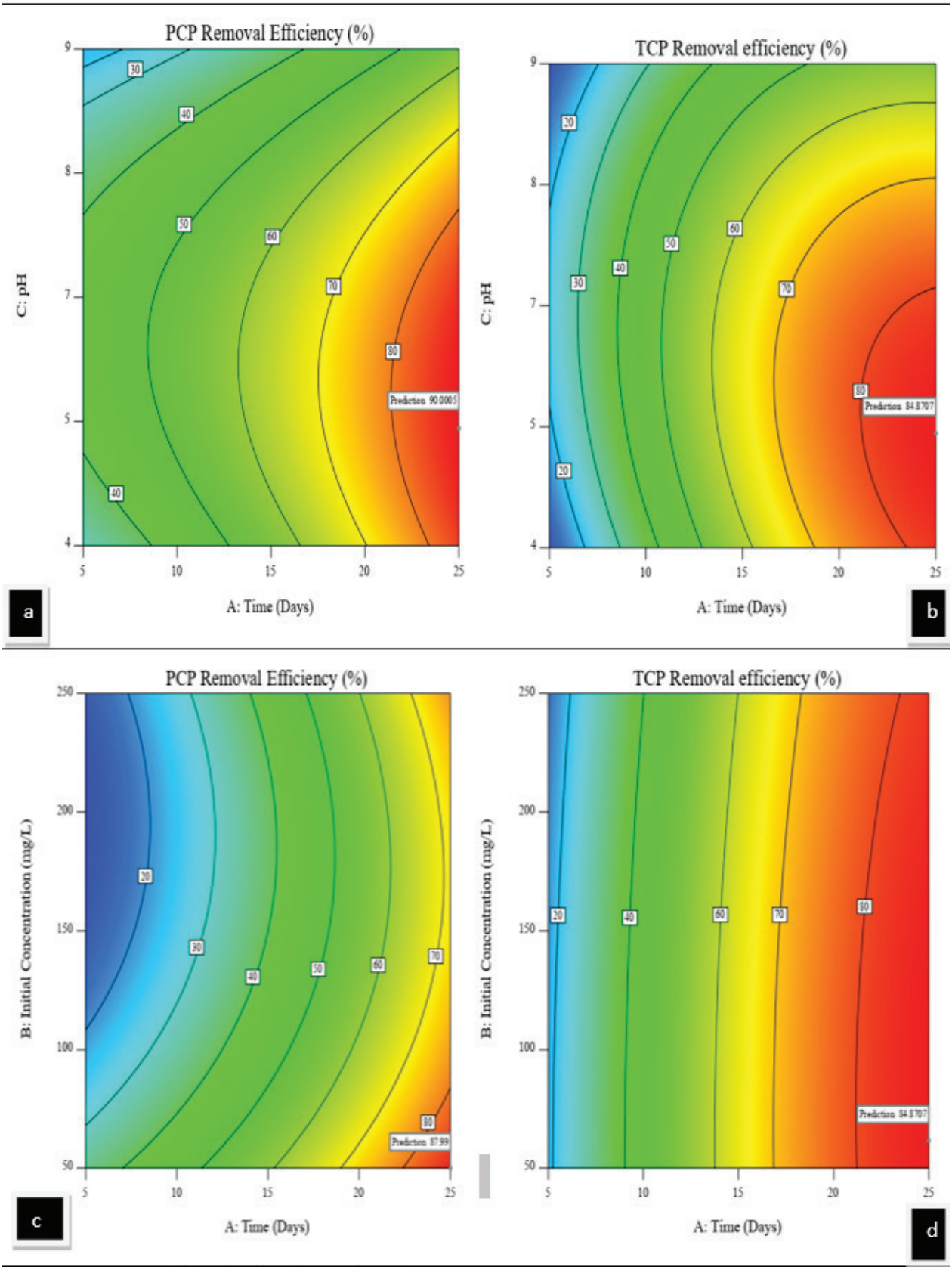

Fig. 8. Synergetic effect of process variables on Phytoremediation of Aquaponia **(a)** pH and Time on PCP, **(b)** pH-Time on TCP, **(c)** Conc-Time on PCP, **(d)** Conc-Time on TCP

3.5. Cost analysis of the treatment process

The authors explored the cost-benefit evaluation of the biosorption process as a decision-making tool to test the feasibility of the active CiL-plant as a biosorbent for removing PCP and TCP from an aqueous solution. The cost of the phytoremediation operation is based on the performance of the active CiL-plant, energy consumption, transportation to the remediation site, labor and technology used to remove contaminants [4, 8], and environmental and regulatory risk. The techno-economic feasibility of the biosorption process and phytotoxicity handling necessitates using low-cost materials (Canna indica L.) with negligible environmental impact and regulatory risk. The operating cost of treating 1.0 L of the aqueous solution was calculated by considering the cost of preparing the 100 mg L^{-1} initial concentration of the aqueous solution for CiL-plant as biosorbent. The labor cost was determined as a function of the number of working personnel on board for the treatment operation. The power consumption rate per unit of equipment utilized at full scale (f=1), and the time spent following the model report from previous research [15], were evaluated following equations 2-5 presented in section 2.5.

Analysis of Figure 9 confirmed that the operating cost of energy consumption corresponds to $ 27.80 for PCP, and $ 21.28 for TCP, respectively. It can be observed from Figure 9 that, the cost of operating the phytoremediation process for PCP removal was slightly higher than the cost of TCP removal in terms of energy consumption by $ 6.52. The preparation of 100 mg L^{-1} initial concentration of CiL-plant for removal of PCP from the aqueous solution cost $ 177.4 against $ 176.2 for removal of TCP from the aqueous solution under similar operating conditions. The labor cost was projected to be $ 100.2 per annum, while the cost of transportation of materials and personnel on board to the remediation site was $12.00, irrespective of operating with PCP or TCP. It can be concluded from the analysis of Figure 9 showed that the overall cost for using the biosorption of PCP from aqueous solution to CiL-plant at optimum conditions was computed as $ 321.20 and $ 313.48 for TCP, respectively. The analysis of the phytoremediation process proved that, at the established optimum condition, the opportunity cost of operating the biosorption of TCP from aqueous solution to CiL-plant would save $ 7.72 compared with PCP for sustainability. The authors reasoned that the outcome is largely due to higher solubility and rapid biosorption of TCP to the surface of the CiL-plant in aquaponia, irrespective of the longer exposure time required for the CiL-plant driven biosorption of PCP and TCP to reach equilibrium.

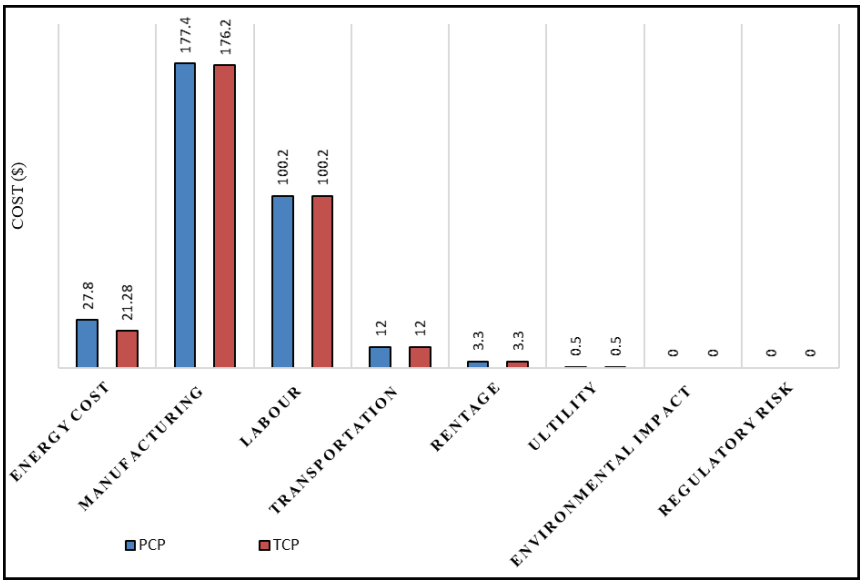

Fig. 9. Cost evaluation summary of the CiL-plant-driven biosorption treatment

Table 6. Comparative analysis of the optimization report

Methodology	DoE		OFAT	
	This study		Reference	
Parameter	(PCP)	(TCP)	(PCP)	(TCP)
pH		4		---
Initial Conc. (mg L^{-1})		50		100
Contact time (days)		25		25
optimum Efficiency %	90	81.87	87	80

OFAT: Reference [8]

3.6. Comparison of CiL-plant for the remediation of PCP and TCP from solution

The performance comparison of the biosorption of PCP, and TCP from aquaponia was analyzed and the report is summarized in Table 6 below. The previous research reports on the CiL-plant phytoremediation analysis applied the one-factor-at-a-time (OFAT) approach for determining the optimum PCP and TCP removal rate. The current study applied the design of experiment (DoE) approach via the RSM for the optimization modeling of the uptake of PCP and TCP to CiL-plant in aquaponia. The findings from the comparison of the results showed that with the RSM, the removal efficiency was higher than the optimum reported via the OFAT approach. The difference corresponds to ± 1.87 and ±3 for TCP and PCP, respectively.

4. Conclusion

The techno-economic evaluation and optimization modeling of the competitive biosorption of PCP and TCP from aqueous solution to the Cana indica plant have been investigated. The aqueous solution of fertilizer contaminated with PCP and TCP was prepared. The CiL-plant-driven phytoremediation of the aqueous medium was studied at varying pH, initial concentration, and constant time based on the design of experiments. The optimization modeling tools for ANN and RSM have yielded good statistical evaluation metrics for modeling the CiL-plant-driven phytoremediation process. The results confirmed that a statistical difference of ±0.005 was obtainable and adjusted R^2 ≤1.00. The adopted RSM optimization outputs have to test their reliability based on DoE. The predicted optimum corresponds to pH, concentration, and exposure time of 4, 50 mg L^{-1}, and 25 days guaranteed PCP and TCP biosorption to CiL-plant ≤90%. The established optimum condition required $7.75 more for sustainable PCP removal than TCP.

5. Acknowledgement

We acknowledge the help of the technical staff at Chemistry Laboratory, Imo state University, for their support during the experimental set-up and analysis

6. Conflict of interest

There are no conflicts of interest to declare

7. References

[1] USEPA, 2,4,6 Trichlorophenol. United states EnvironmentalProtectionAgency,2000.https://www.epa.gov/sites/default/files/2016-09/documents/2-4-6-trichlorophenol.pdf

[2] WHO, The World Health Organization recommended classification of pesticides by hazard and guidelines to classification 2004, International Programme on Chemical Safety, pp.19-39, 2005. https://apps.who.int/iris/rest/bitstreams/1278712/retrieve

[3] ATSDR, Pentachlorophenol, Agency for Toxic Substances and Disease Registry, 2021. https://wwwn.cdc.gov/TSP/substances/ToxSubstance.aspx?toxid=70

[4] A.I. Olayinka, F.A. Ademola, I.A. Emmanuel, Assessment of Organochlorine and Organophosphorus pesticides residue in water and sediments from Ero River in South-Western Nigeria, J. Chem. Biol. Phys. Sci. D,

5 (2015) 4679–4690. https://www.jcbsc.org_

[5] A.W. Verla, J. E. Ejiako, E.N. Verla, I. G. Ndubuisi, C. E. Enyoh, Potential health risk index of polyaromatic hydrocarbons (PAHs), polychlorinated biphenyls (PCBs) and organochlorine pesticides (OCPs) in fish species from Oguta Lake, Nigeria, Int. J. Environ. Anal. Chem., (2021) 1946687. https://doi.org/10.1080/03067319.2021.1946687

[6] B. M. Obidike, A. W. Verla, C. E. Enyoh, E. N. Verla, O. N. Onyekachi, Fate and distribution of pesticides residues in water sources in Nigeria: A review, Int. J. Agrochem., 6 (2020) 29–48. https://chemical.journalspub.info/index.php?journal=IJCPD&page=article&op=view&path%5B%5D=1015

[7] B.O. Isiuku, C.E. Enyoh, Water pollution by heavy metal and organic pollutants: Brief review ofsources, effects and progress on remediation with aquatic plants, Anal. Methods Environ. Chem. J., 2 (3) (2019) 5-38. https://doi.org/10.24200/amecj.v2.i03.66

[8] C. E. Enyoh, B. O. Isiuku, Competitive biosorption and phytotoxicity of chlorophenols in aqueous solution to Canna indica L, Curr. Res. Green Sustain. Chem., 4 (2021) 100094. https://10.1016/j.crgsc.2021.100094

[9] C.E. Enyoh, B. O. Isiuku, Removal of pentachlorophenol (PCP) from aqueous solution using Canna indica L.: kinetics, isotherm and thermodynamic studies, Arab. J. Chem., 8(2) (2021) 193-213. http://www.mocedes.org/ajcer/volume8/AJCER-13-Enyoh-2021.pdf

[10] C.E. Enyoh, B.O. Isiuku, 2,4,6-Trichlorophenol (TCP) removal from aqueous solution using Canna iindica L.: kinetic, isotherm and Thermodynamic studies, Chem. Ecol., 37 (2020) 64-82. https://doi.org/10.1080/02757540.2020.1821673

[11] D.H. Tran, T.M.H. Vi, T.T.H. Dang, R. Narbaitz, Pollutant removal by Canna Generalis in tropicalconstructed wetlands for domestic wastewater treatment, Global J. Environ. Sci. Manage., 5 (3) (2019) 331-344. https://www.gjesm.net/article_35321_dc150b14811afe228b6bea1bcc85228f.pdf

[12] C.E. Enyoh, B.O. Isiuku, Determination and human health risk assessment of heavy metals in flood basin soils in Owerri, southeastern Nigeria, Chem. Africa, 3 (2020) 1059–1071. https://doi.org/10.1007/s42250-020-00171-2

[13] C.E. Enyoh, Q. Wang, P.E. Ovuoraye, Response surface methodology for modeling the adsorptive uptake of phenol from aqueous solution using adsorbent polyethylene terephthalate microplastics, Chem. Eng. J. Adv., 12 (2022) 100370. https://doi.org/10.1016/j.ceja.2022.100370

[14] S. Saini, J. Chawla, R. Kumar, Response surface methodology (RSM) for optimization of cadmium ions adsorption using C16-6-16 incorporated mesoporous MCM-41, SN Appl. Sci., 1 (2019) 894. https://doi.org/10.1007/s42452-019-0922-5

[15] P. E. Ovuoraye, V.I. Ugonabo, G.F. Nwokocha, Optimization studies on turbidity removal from cosmetics wastewater using Aluminum Sulfate and blends of fishbone, SN Appl. Sci., 3 (2021) 488. https://dio.org/10.1007/s42452-021-04458-y

[16] C. A. Igwegbe, L. Mohammed, S. Ahmadi, A. Rahdar, Modeling of adsorption of methylene blue dye on Ho-CaWO4 nanoparticles using response surface methodology and artificial neural network (ANN) techniques, Methods X, 6 (2019) 1779-1797. https://doi.org/10.1016/j.mex2019.07.016

[17] C.A. Igwegbe, O.D. Onukwuli, J.O. Ighalo, M.C. Menkiti, Bio-coagulation-flocculation (BCF) of municipal solid waste leachate using picralima nitida extract: RSM and ANN modelling, Curr. Res. Green Sustain. Chem. 4 (2021) 100078. https://doi.org/10.1016/j.crgsc.2021.100078

[18] C.E. Enyoh, C. E. Duru, P. E. Ovuoraye, Q.

Wang, Evaluation of nanoplastics toxicity to the human placenta in systems, J. Hazard. Mater., 446 (2023) 130600. https://doi.org/10.1016/j.jhazmat.2022.130600

[19] R. Hasanzadeh, M. Mojaver, T. Azdast, C. B. Park, Polyethylene waste gasification syngas analysis and multi-objective optimization using central composite design for simultaneous minimization of required heat and maximization of exergy efficiency, Energy Convers. Manag., 247 (2021) 114713. https://doi.org/10.1016/j.enconman.2021.114713

[20] L. Lujian, S. Tang, X. Wang, X. Sun, A. Yu, Adsorption of malachite green from aqueous solution by nylon microplastics: Reaction mechanism and the optimum conditions by response surface methodology, Process Saf. Environ. Prot., 140 (2020) 339-347. https://doi.org/10.1016/j.psep.2020.05.019

[21] C. E. Enyoh, Q. Wang, P. E. Ovuoraye, T. O. Maduka, Toxicity evaluation of microplastics to aquatic organisms through molecular simulations and fractional factorial designs, Chemosphere, 308 (2022) 136342. https://doi.org/10.1016/j.chemosphere.2022.136342

[22] C.E. Duru, C.E. Enyoh, I.A. Duru, M. Enedoh, Degradation of PET nanoplastic oligomers at the novel PHL7 target: insights from molecular docking and machine learning, J. Niger. Soc. Phys. Sci., 5 (2023) 1154. https://doi.org/10.46481/jnsps.2022.1154

[23] G. Aicha, I. Soumaya, E. Noureddine, A. T. Mohamed, G. Djamel, H. Ahmed, M. Abdelhakim, A. Badreddine, K. Lioua, Comparative study of chemical coagulation and electrocoagulation for the treatment of real textile wastewater: optimization and operating cost estimation, ACS Omega, 7(26) (2022) 22456–22476. https://doi.org/10.1021/acsomega.2c01652

[24] P.E. Ovuoraye, L.C. Okpala, V.I. Ugonabo, Clarification efficacy of eggshell and aluminum base coagulant for the removal of total suspended solids (TSS) from cosmetics wastewater by coag-flocculation, Chem. Pap., 75 (2021) 4759–4777. https://doi.org/10.1007/s11696-021-01703-x

[25] D. Wang, S. Thunell, L. Ulrika, A machine learning framework to improve effluent quality control in wastewater treatment plants, Sci. Total Environ., 784 (2021) 147138. https://doi.org/10.1016/j.scitotenv.2021.147138

[26] Y. Zhang, Y. Wu, Introducing machine learning models to response surface methodologies. Publisher: Intechopen, 270 pages, 2021. https://doi.org/10.5772/intechopen.9819

[27] P. E. Ovuoraye, V. I. Ugonabo, M. A. Tahir, P. A. Balogun, Kinetics-driven coagulation treatment of petroleum refinery effluent using land snail shells: An empirical approach to environmental sustainability, Clean. Chem. Eng., 4 (2022) 100084. https://doi.org/10.1016/j.clce.2022.100084

[28] H. Guo, Prediction of effluent concentration in a wastewater treatment plant using machine learning models, J. Environ. Sci., 32 (2015) 90-101. https://doi.org/10.1016/j.jes.2015.01.007.

[29] M. Radhika, K. Palanivelu, Adsorptive removal of chlorophenols from aqueous solution by low-cost adsorbent—Kinetics and isotherm analysis, J. Hazard. Mater., 138(1) (2006) 116-124. https://doi.org/10.1016/j.jhazmat.2006.05.045

[30] S.K. Nadavala, M. Asif, A. M. Poulos, M. Suguna, M. I. Al-Hazza, Equilibrium and kinetic studies of biosorptive removal of 2,4,6-trichlorophenol from aqueous solutions using untreated agro-waste pine cone biomass, Processes, 7 (2019) 757. http://doi:10.3390/pr7100757

[31] R. Bhutiani, N. Rai, P. K. Sharma, K. Rausa, F. Ahamad, Phytoremediation efficiency of water hyacinth (E. crassipes), canna (C. indica) and duckweed (L. minor) plants in treatment of sewage water, Environ. Conserv. J., 20 (2019) 143-156. https://doi.org/10.36953/ECJ.2019.1008.1221

Anal. Methods Environ. Chem. J. 6 (1) (2023) 100-114

AMECJ

Research Article, Issue 1
Analytical Methods in Environmental Chemistry Journal
Journal home page: www.amecj.com/ir

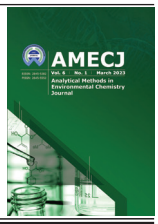

Determination and analysis of pesticide residues in field-grown and greenhouse-grown tomatoes using liquid chromatography-mass spectrometry

Fatemeh Norouzi [a,b], Maryam Faraji [a,b,*], Ramezan Sadeghi [c], Ali Faghihi-Zarandi [d], and Farshid Shabani Boroujeni [e]

[a] *Environmental Health Engineering Research Center, Kerman University of Medical Sciences, Kerman, Iran*
[b] *Department of Environmental Health Engineering, Faculty of Public Health, Kerman University of Medical Sciences, Kerman, Iran*
[c] *Department of Environmental Health of Engineering, Faculty of Health, Shahrekord University of Medical Sciences, Shahrekord, Iran*
[d] *Department of Occupational Health Engineering and Safety at Work, Faculty of Public Health, Kerman University of Medical Sciences, Kerman, Iran*
[e] *Department of Plant Protection, Faculty of Agriculture, University of Tabriz, Tabriz, Iran*

ARTICLE INFO:

Received 14 Nov 2022
Revised form 20 Jan 2023
Accepted 12 Feb 2023
Available online 29 Mar 2023

Keywords:
Liquid chromatography-mass spectrometry,
Analysis,
QuEChERS method,
Pesticide residues,
Field and Greenhouse-grown tomatoes

ABSTRACT

The present study aimed to extract pesticide residues in the field and greenhouse-grown tomatoes and homemade paste based on the quick, easy, cheap, effective, rugged, and safe sample preparation method (QuEChERS) before determined by the liquid chromatography-mass spectrometry (LC-MS). The mean difference in percentage reduction of deltamethrin (DLM) and acetamiprid (ACT) in raw tomatoes of greenhouse-grown was obtained at 91.42 and 90.00%, respectively, which was insignificantly more than filed condition (84.91% and 86.34%). Maximum reduction percentages of the DLM in paste under greenhouse and field tomato conditions were achieved by more than 95.86% and 93.11%, respectively. The residual concentration of both DLM (91.42%) and ACT (90.00%) in the greenhouse decreased more than the field (84.91% and 86.34%), respectively. Abamectin(ABA) reached below the MRL in a shorter time after spraying (2 days). Considering the pre-harvest interval (PHI) period of deltamethrin and abamectin can reach their residual concentration to the MRL in both conditions, which were determined by LC-MS. According to the results of the current study, 7 and 5 days can be suggested as the PHI period of the acetamiprid for field and greenhouse-grown tomatoes, respectively. Therefore, using pesticides in the proper dosage, considering appropriate PHI, and harvesting can reduce their residues in agricultural products.

1. Introduction

Tomato, scientifically known as *Solanum Lycopersicum*, is one of the world's most widely used and popular vegetables. It's used as raw and processed due to having high antioxidants such as ascorbic acid, vitamins E and A, carotenoids, flavonoids, and phenolic acid that can reduce the risk of cardiovascular diseases and prevent diabetes and cancer [1, 2]. Several pesticides are used to maintain agricultural products. Improper consumption of pesticides in farm products and non-compliance with the pre-harvest interval (PHI) period can

*Corresponding Author: Maryam Faraji
Email: m.faraji@kmu.ac.ir and m_faraji28@yahoo.com
https://doi.org/10.24200/amecj.v6.i01.234

cause adverse effects due to the presence of residual pesticides in the crops [3]. Therefore, the European Union (EU) has set a maximum pesticide residue limit (MRL). The MRLs for studied pesticides in the present study included acetamiprid, deltamethrin, and abamectin in tomatoes are defined as 500, 70, and 90, respectively, regardless of the growth conditions [4, 5]. Ratnamma et al.'s study on the residual acetamiprid in okra showed that using 10 g and 20 g of 20% acetamiprid per hectare led to the residual of 2.034 and 4.044 mg kg^{-1}, respectively [6]. The results of Yazdan Pak et al.'s study on the residual pesticides in the greenhouse tomatoes during 2, 5, 7, 10, 14, 17, and 21 days after spraying showed that the residual of acetamiprid, diazinon, imidacloprid, and pirimicarb declined after the PHI period approached [7]. Mohamed et al. reported that imidacloprid decomposed faster than acetamiprid in tomatoes grown under greenhouse conditions [8]. Iran ranks seventh globally, accounting for 4.7% of the total world production of tomatoes, with an annual production of 5.8 million tons and an average yield of 38 tons per hectare [9]. According to the high production and consumption of raw and processed tomatoes in Iran and the use of high levels of pesticides in their cultivation, this study aimed to determine deltamethrin, abamectin, and acetamiprid residues in cultivated tomatoes in the field and greenhouse as raw and home processed using QuEChERS (quick, easy, cheap, effective, rugged, and safe) method and analysis of residual pesticides by liquid chromatography-mass spectrometry (LC-MS) method.

In this study, the residual concentrations of pesticides, including acetamiprid, deltamethrin, and abamectin, were extracted and determined by the QuEChERS procedure coupled to LC-MS. The residual concentration of three high-consumption pesticides of Iran in raw and processed tomatoes was determined and compared. Also, the residual concentration of the three mentioned pesticides in outdoor-grown (field-grown) and greenhouse tomatoes were studied and compared together. The current study was innovative in comparing the residual pesticides.

2. Material and Methods

This study was done in several stages included planting and spraying of tomatoes in field and greenhouse and harvesting, preparation of the samples through the QuEChERS method and their analysis of samples via LC-MS and statistical analysis of the data. Study stages are illustrated in Schema 1.

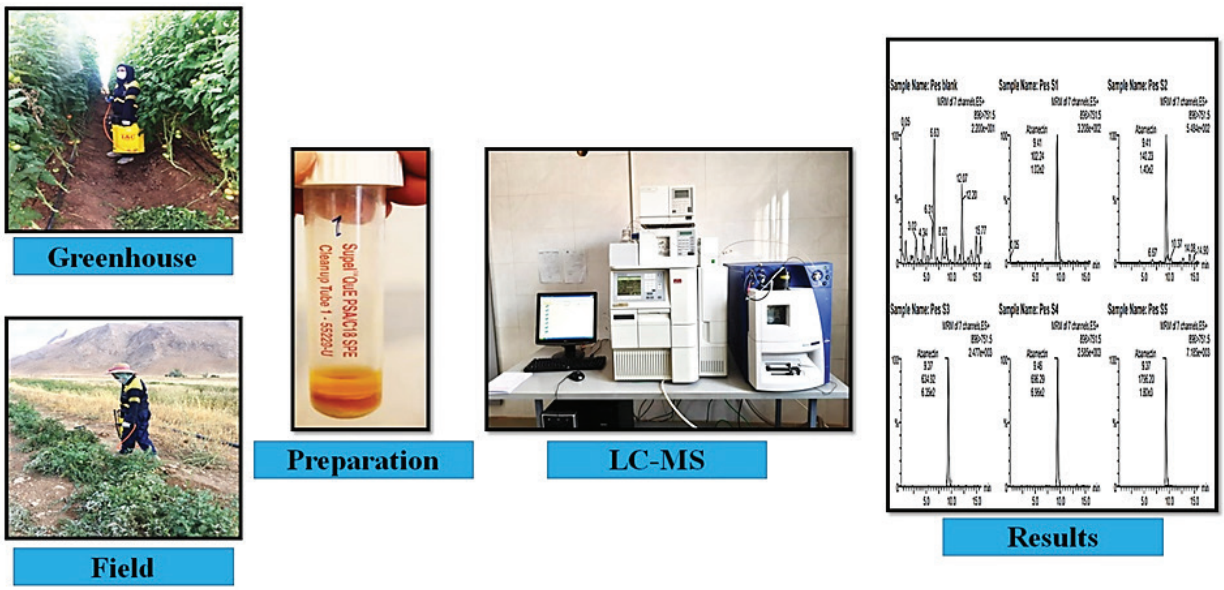

Schema 1. Study stages of sampling, the QuEChERS preparation method and determination by LC-MS

2.1. Instrumental

LC-MS is an accurate and precise method to separate, identification and analysis of compounds. It can be successfully and efficiently adopted for quality control analysis of compounds. It can also be used in combination with other analytical methods to further elucidate the components of mixtures [17]. LC-MS (model: Waters Alliance 2695 (UK)) using a matrix-matched method was used to analyze samples in the present study. The type of detector was Micromass Quattro Micro API Triple Quadruple Mass Spectrometer (UK). Column specifications were Waters Sunfire C18 Column 100 Å, 150 mm × 2.1 mm × 1.5 µm. The samples of 20 µL were injected into the device. Chromatograms of the standard samples to provide calibration curve have been illustrated in Schema 2.

2.2. Chemicals and reagents

Standards of Acetamiprid (99.9%), abamectin (95%), deltamethrin (98.5%), deltamethrin (2.5%EC), acetamiprid (20%SP), abamectin (1.8%EC) and other chemicals and reagents included acetonitrile, anhydrous magnesium sulfate, the internal standard of triphenyl phosphate, sodium chloride, trisodium citrate dihydrate, disodium hydrogen citrate, primary, secondary amine (PSA), and carbon adsorbent (C18) were purchased from Sigma Aldrich, Germany. Dilutions of 50, 100, 250, 500, and 1000 ng g^{-1} were used to plot the calibration curve of the pesticides using a matrix-matched method. The limit of detection (LOD), the limit of quantification (LOQ), the regression equation of calibration, and the MRL for the studied pesticides are mentioned in Table 1.

2.3. Planting and spraying of tomatoes in the field and greenhouse

A field and a greenhouse were respectively considered for planting tomatoes outdoors and in a greenhouse in the summer of 2020. The average temperature in the study period, namely the summer and fall of 2020, in the greenhouse and field was 20±3 and 8.9 °C. Four terraces were allocated for each treatment in the greenhouse and the field. The distance between tomato plants was considered to be 40 cm. Distances of 120 and 100 cm were defined between terraces in the greenhouse and field, respectively. An empty terrace was spaced between the terraces to eliminate the effects of overlap and possibly dispersion of pesticides through the wind. The control samples were grown on the unsprayed terrace. Randomized spraying was performed with a 20 L calibrated rechargeable back sprayer (model: IAC CODE: E2) according to the doses recommended by the Iran Plant Protection Organization, including 0.6 liters per hectare for abamectin, 300 cc per hectare for deltamethrin, and

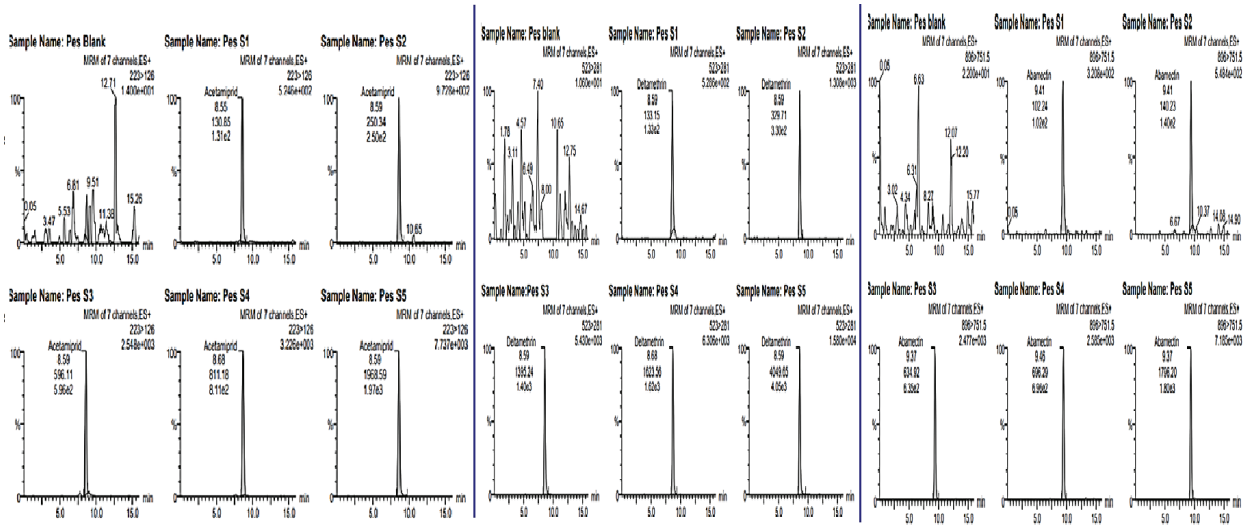

Schema 2. Chromatograms of the five standard pesticides, including acetamiprid, deltamethrin, and abamectin for calibration curve

Table 1. Limit of detection (LOD), the limit of quantification (LOQ), the regression equation, and the maximum residue limit (MRL) for the studied pesticides

Pesticide		Abamectin	Deltamethrin	Acetamiprid
Chemical structure		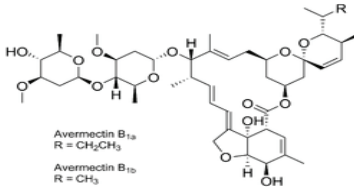	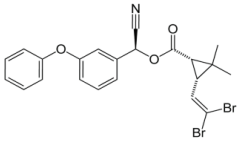	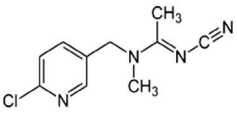
Chemical formula		$C_{95}H_{142}O_{28}$	$C_{22}H_{19}Br_2NO_3$	$C_{10}H_{11}C_lN_4$
MW (g mol^{-1})		1732.1	505.21	222.68
Water solubility		1.21 mg L^{-1} at 25 ºC	<0.002 mg L^{-1} at 25 ºC	4.25 g L^{-1} at 25 ºC
Octanol/water coefficient	partition	4.4	6.10	0.8
Chemical Family		Insecticide, a natural fermentation product of soil-dwelling actinomycete, Streptomyces avermitilis	Pyrethroid insecticide	Neonicotinoid insecticide

0.5 kg per 1000 liters of water for acetamiprid. The physical and chemical characteristics of the studied pesticides [10-12] are reported in Table 2.

2.4. Sample harvesting

According to the manufacturer's instrument, the PHI period for deltamethrin and abamectin was defined as three days. Therefore, sample harvesting in the case of deltamethrin and abamectin was done in the suggested PHI period and before and after that, 1, 2, 3, 4, and 5 days after spraying. The manufacturer did not define the PHI period for acetamiprid. Thus, sample harvesting in the case of acetamiprid was done according to similar studies [13, 14], and the farmers' performance was 3, 5, 7, 9, and 11 days after spraying. After time elapsed, 2 kg samples harvested from different terraces were mixed and, after coding, placed in a black bag and maintained at 4 °C. Then, part of the samples was homogenized after washing to measure the residual pesticide in the raw sample, and the other part was used to prepare homemade tomato paste. To make tomato paste, the washed tomatoes were chopped, salted, and stored at room temperature for 24 hours. Then, the tomato juice was strained and heated at 96 °C for one hour. After cooling, the samples were packaged and coded separately.

Also, one sample of each treatment was taken one hour after spraying to compare the amount of pesticide residues in washed and unwashed tomatoes. Then, the samples were divided into two equal parts; one part was washed with tap water, and another part was reserved unwashed. Finally, the samples were maintained at -21 °C until experiments.

Table 2. Physical and chemical characteristics of the studied pesticides

Pesticide	LOD (mg kg^{-1})	LOQ (mg kg^{-1})	Regression equation of calibration	R^2	*MRL
Abamectin	13.2	40	y=3.37761x +0.313794	0.9848	0.09
Deltamethrin	13.2	40	y=7.78742x-7.7343	0.9931	0.07
Acetamiprid	13.2	40	y=11.8763x-8.70884	0.9946	0.50

***MRL**: maximum residue limit of the European Union

2.5. Preparation and analysis of samples

The QuEChERS method, with its high sensitivity, is used to extract the residual pesticides in the products in many reference laboratories [15]. To extract pesticides in the current study by the QuEChERS method, each sample was homogenized in a blender, and 10 g of samples were transferred to the centrifuge tube. Then, 10 mL of acetonitrile and 100 µL of the internal standard of triphenyl phosphate were added to each centrifuge tube at the concentration of 10 ppm. Next, 4g anhydrous magnesium sulfate, 1.0 g sodium chloride, 1.0 g Trisodium citrate dehydrate, and 0.5 g disodium hydrogen citrate were added to each centrifuge tube after a vigorous shake for one minute. Again, the mixture was vortexed for one minute at 5000 rpm for 5 minutes at -10 °C. Then, 3 mL of the transparent top layer was transferred into the tube containing 75 mg PSA, 450 mg anhydrous magnesium sulfate, and 75 mg C18 adsorbent. Samples were finally moved into a vial after vortex for one minute and re-centrifuged [16]. Residual concentrations of pesticides in the samples were measured by the method of LC-MS. LC is an accurate and precise method to separate, identify and analyze compounds. It can be successfully and efficiently adopted for quality control analysis of compounds. It can also be combined with other analytical methods to further elucidate the components of mixtures [17].

2.6. Statistical analysis

Statistical analysis was performed using R software version 3.4.1. Results were reported as the mean ± standard deviation. The mean concentration of pesticides in different samples was compared via ANOVA. P-value < 0.05 was considered as the significance level.

3. Results and discussion

3.1. Deltamethrin

The EU has determined the deltamethrin MRL in tomatoes as 70 µg kg^{-1}. The residual concentration of deltamethrin was reached less than MRL in the field and greenhouse on the fifth and fourth days after spraying, respectively (Fig. 1a). Therefore, considering the PHI period for deltamethrin, which has defined to be three days according to the manufacturer's instrument, its residual concentration met the MRL in both conditions. Residual concentration and reduction percentage of deltamethrin in raw tomato and paste of field- and greenhouse-grown are shown in Table 3. Comparison between the mean residual concentration of deltamethrin at different harvest times from 1 to 5 days with the MRL showed a non-significant difference in the field ($p = 0.14$) and greenhouse ($p = 0.43$). The mean difference of percentage reduction in raw tomato between the field (84.91%) and greenhouse (91.42%) conditions was not significant ($p=0.18$). The residual concentration of deltamethrin in tomato paste made from both field-grown and greenhouse-grown products showed a decreasing trend (Fig.1b). The concentration of deltamethrin in the paste from field products was decreased up to 95% on the fifth day after spraying. While its removal was more than 95% in the greenhouse products (Table 3).

3.2. Abamectin

The comparison of the residual concentration of abamectin in the field and greenhouse-grown tomatoes with the MRL of 90 µg kg^{-1} was shown in Figure 2a. The residual concentration of abamectin was less than MRL on the second day after spraying in both growing conditions (58 µg kg^{-1} and 77 µg kg^{-1}, respectively). The PHI period for abamectin has been defined to be three days based on the manufacturer's instrument. Thus, considering the PHI period for abamectin can reach its residual concentration below the MRL in tomatoes grown in the field and greenhouse. The decreasing trend was observed in the residual concentration of abamectin in the tomato paste made from field-grown and greenhouse-grown products (Fig. 2b). The concentration of abamectin was reduced to more than 89% in the paste made from crops in both conditions after five days (Table 3). The residual concentration of abamectin in the paste can reach below 40 µg kg^{-1} in the field and 46 µg kg^{-1} in the greenhouse, considering the PHI period in tomato (three days).

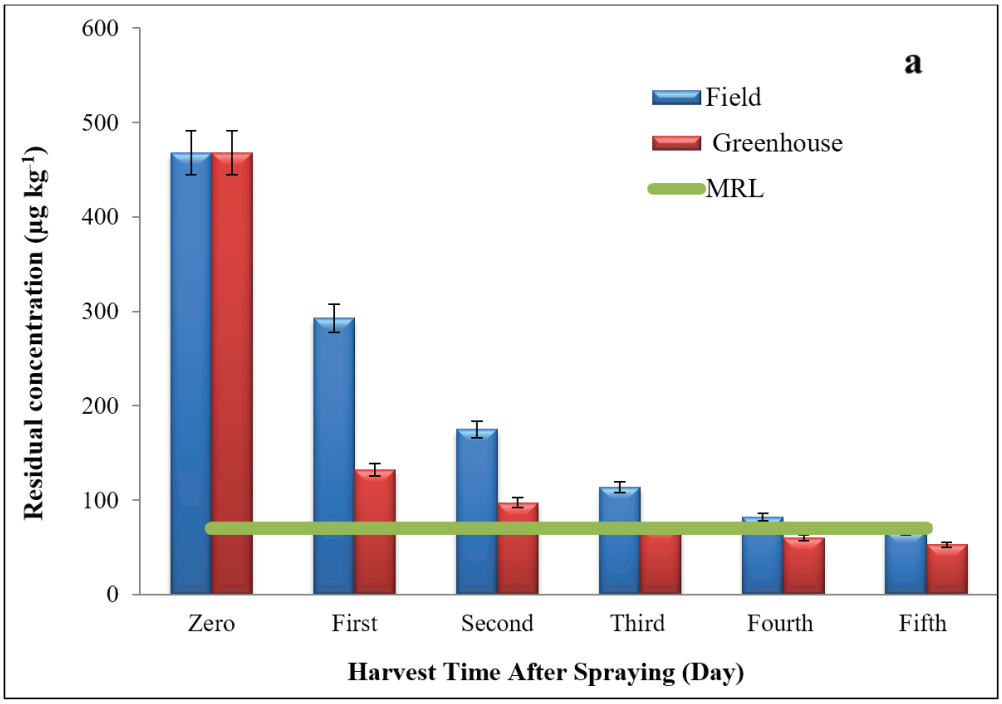

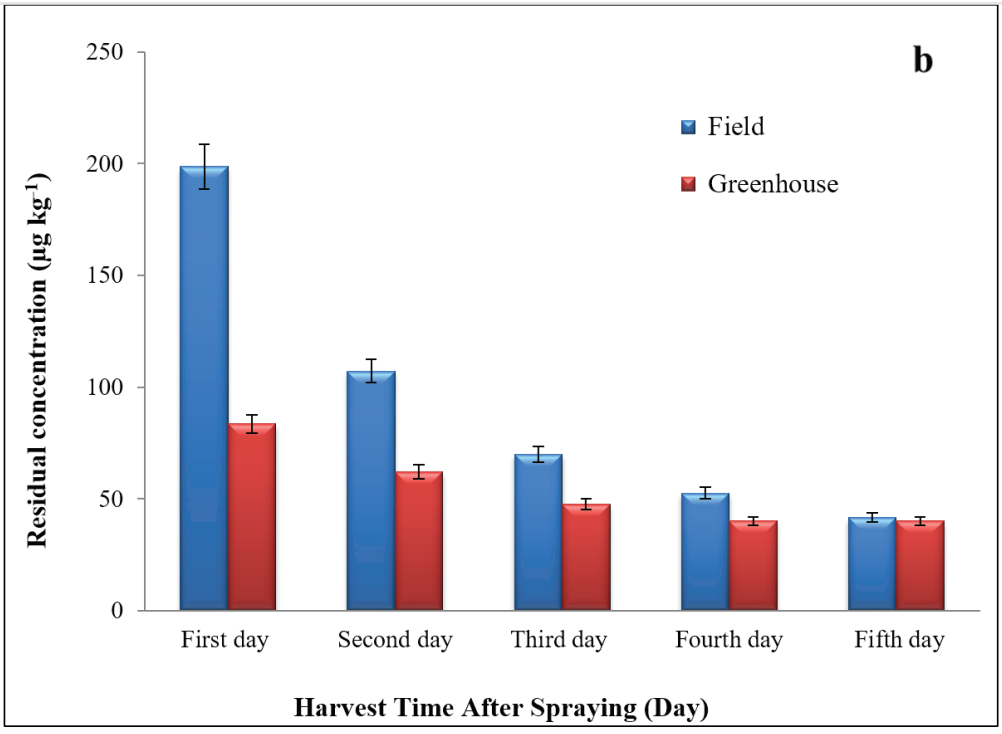

Fig. 1. The comparison of the mean residual concentrations of deltamethrin in field-grown and greenhouse-grown tomatoes (a) and paste (b)

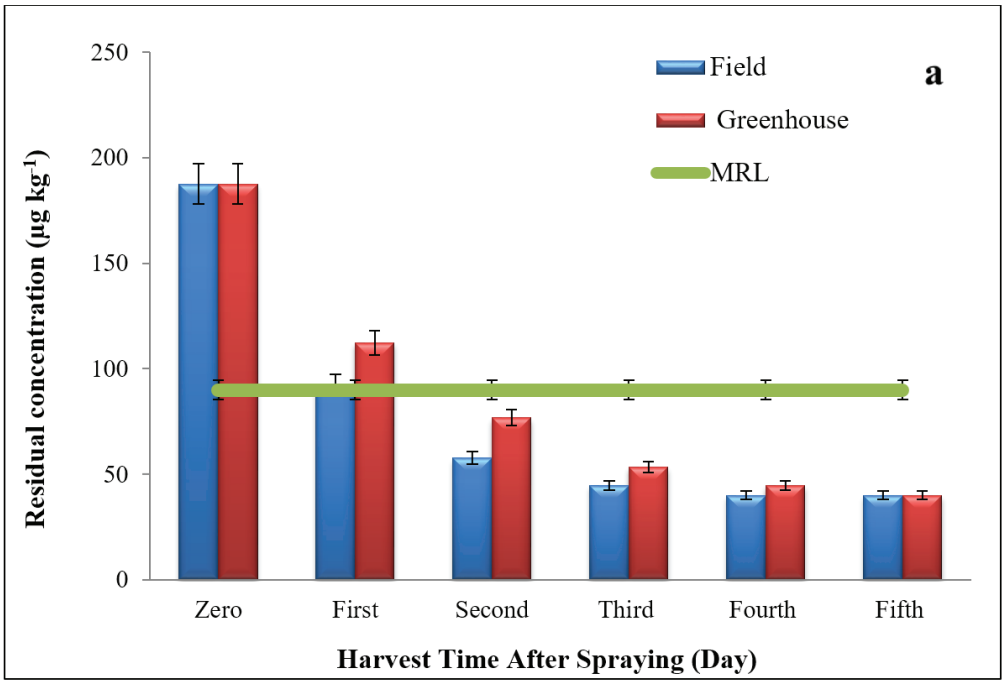

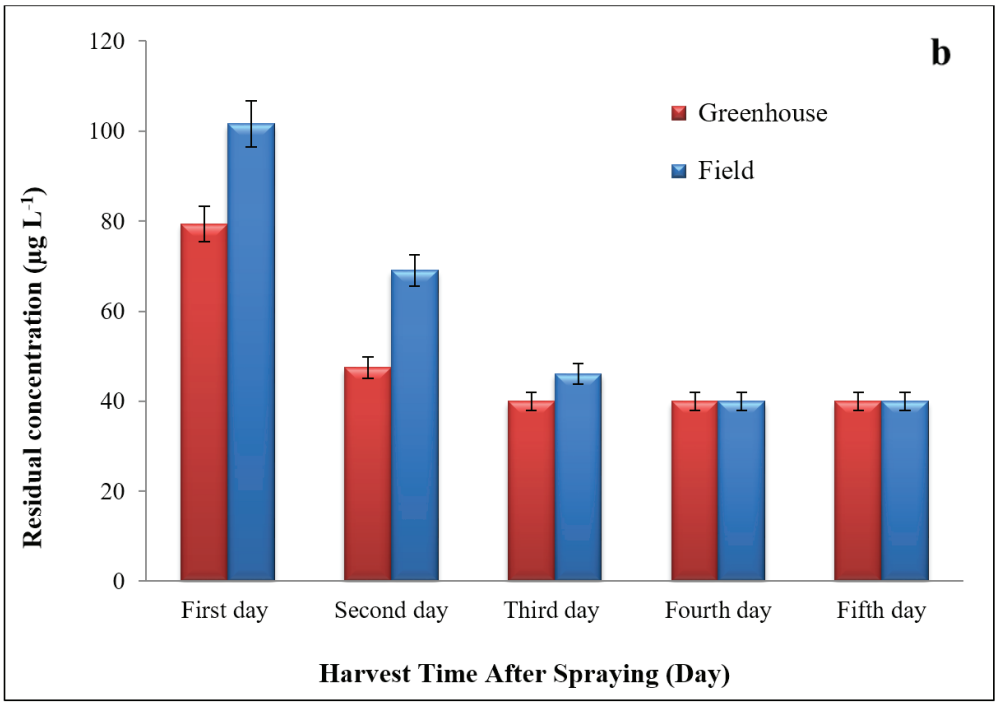

Fig. 2. The comparison of the mean residual concentrations of abamectin in field-grown and greenhouse-grown tomatoes (a) and paste (b) and the EU maximum residue limits

Table 3. Residual concentration and reduction percentage of deltamethrin, abamectin, and acetamiprid in raw tomato and paste of field-grown and greenhouse-grown

Pesticide		Raw tomatoes				Tomato paste			
		Field		Greenhouse		Field		Greenhouse	
	Day	RC (µg kg^{-1})	PR (%)	RC (µg kg^{-1})	PR (%)	RC (µg kg^{-1})	PR (%)	RC (µg kg^{-1})	PR (%)
Deltamethrin	1	292.62	69.74	131.91	86.36	198.70	79.45	83.50	91.36
	2	174.80	81.92	97.30	89.93	107.20	88.91	62.10	93.57
	3	113.40	88.27	71.61	92.51	69.91	92.77	47.90	95.08
	4	81.91	91.53	59.82	93.80	52.50	94.57	<40	>95.86
	5	66.60	93.11	52.52	94.50	41.60	95.69	<40	>95.86
Mean		145.87	84.91	82.63	91.42	93.98	90.28	-	-
MRL		70	-	70	-	-	-	-	-
p-value		0.14*	0.18**	0.43*	-	-	-	-	-
Abamectin	1	92.60	75.58	112.34	70.38	79.40	79.06	101.60	73.21
	2	57.80	84.75	76.80	79.74	47.50	87.47	69.11	81.77
	3	44.81	88.18	53.50	85.89	<40	>89.45	46.12	87.84
	4	<40	>89.45	44.70	88.21	<40	>89.45	<40	>89.45
	5	<40	>89.45	<40	>89.45	<40	>89.45	<40	>89.45
Mean		-	-	-	-	-	-	-	-
MRL		90	-	-	-	-	-	-	-
p-value		-	-	-	-	-	-	-	-
Acetamipride	3	835.61	77.76	538.41	85.67	476.33	87.32	328.11	91.27
	5	577.622	84.63	418.91	88.85	340.71	90.93	242.91	93.53
	7	462.33	87.69	359.71	90.42	277.40	92.61	215.81	94.25
	9	371.61	90.11	301.62	91.97	234.11	93.77	193.21	94.85
	11	319.52	91.49	259.81	93.08	210.61	94.39	172.51	95.41
Mean		513.34	86.34	375.69	90.00	307.83	91.80	230.51	93.86
MRL		500	-	500	-	-	-	-	-
p-value		0.89*	0.22**	0.06*	-	-	0.19**	-	-

*Comparison between mean concentration and maximum residue limit (MRL),
**Comparison between percentage reduction in field and greenhouse
RC: Residual concentration
PR: Percentage reduction

3.3. Acetamiprid

The EU defined the concentration of 500 µg kg^{-1} as the MRL level for acetamiprid. The mean residual concentration of acetamiprid in the field, greenhouse, and MRL level is compared in Figure 3a. The results showed that the residual concentration of acetamiprid in raw tomato in the field from the seventh day (462 µg kg^{-1}) and in the greenhouse from the fifth day (419 µg kg^{-1}) reached below the MRL by LC-MS. The manufacturer has not defined the PHI period for acetamiprid. Therefore, the acetamiprid PHI period of 7 days for the field-grown and 5 days for the greenhouse-grown tomato can be suggested based on the results of the current study. The difference in the mean reduction percentage of acetamiprid in the field-grown (86.34%) and greenhouse-grown (90.00%) samples were not significant (p=0.22). Comparing the mean residual concentration of acetamiprid in raw tomato and the MRL (500 µg kg^{-1}) showed a non-significant difference in the field (p=0.89) and greenhouse (p=0.06). The residual concentration of the acetamiprid in the tomato paste after spraying field-grown and greenhouse-grown products followed a decreasing trend (Fig. 3b). The concentration of acetamiprid was approximately reduced to 95% in the paste made from crops in both conditions after 11 days (Table 3). The mean percentage reduction of acetamiprid in the paste from greenhouse crops (93.86%) was insignificantly (p = 0.19) more than field crops (91.80%).

Elbashir et al. measured the residual concentrations of fenpropathrin, λ-cyhalothrin, and deltamethrin in field-grown tomatoes for 30 days. The results showed that the pesticide residues of fenpropathrin after 27 days, λ-cyhalothrin after 18 days, and deltamethrin after three days immediately after washing reached below the MRL defined by the Codex and the EU [18]. In Salghi's study on evaluating residual pesticides' organochlorine, pyrothyroid, and dicarboximide in greenhouse-grown tomatoes, the residual concentration of deltamethrin was reported in the range of 1-0.01 mg kg^{-1}. The residual concentration of pesticides in the two studied samples was higher than the MRL [19]. Due to the Rafiei's study, the results of deltamethrin in greenhouse-grown cucumber showed that the residual concentration of pesticide reached the allowable limit (0.2 mg kg^{-1}) on the fifth day after spraying and was not measurable on the seventh day after it [20]. In Abdelfatah's study on the residual concentrations of abamectin, acetamiprid, spinosad, diniconazole, penconazole, and fipronil in the field-grown tomatoes, residual concentrations of abamectin and acetamiprid were reported one hour after spraying as 5.80 and 1.10 mg kg^{-1}, respectively. The results of this study showed that ten days after spraying with abamectin and one day after spraying with acetamiprid, the residual pesticides reached below the EU MRL [21]. The study of Fujita et al on the residual amount of acetamiprid, azoxystrobin, permethrin, and dinotefuran in field-grown and greenhouse-grown lettuce showed that the residual concentrations of pesticides in the greenhouse crop were approximately the same as in the field, but for dinotefuran, the residual pesticides in the greenhouse crop were higher than that in the field [22]. According to Badawy et al.'s study, the residual concentrations of acetamiprid and imidacloprid in greenhouse-grown tomatoes reached below the Europe MRL within three days and five days after spraying, respectively [8]. The results of Chen et al.'s study on the residual concentration of propamocarb in greenhouse-grown and field-grown vegetables showed that the residual of propamocarb in the greenhouse crop was higher than the field crop [23].

3.4. Comparison of different condition

In comparison between mean reduction percentages of pesticides in tomato grown in different condition in the present study, it can be stated that residual concentration of both deltametrin (91.42%) and acetamiprid (90.00%) in the greenhouse was decreased more than field (84.91 and 86.34%, respectively) by LC-MS. Abamectin reached below the MRL in a shorter time after spraying (2 days) compared to other pesticides. The extent of pesticide residues in the agricultural products depends on several factors such as the properties of pesticide, its formulation and applied concentration, light, temperature, plant morphology and plant growth factors [24].

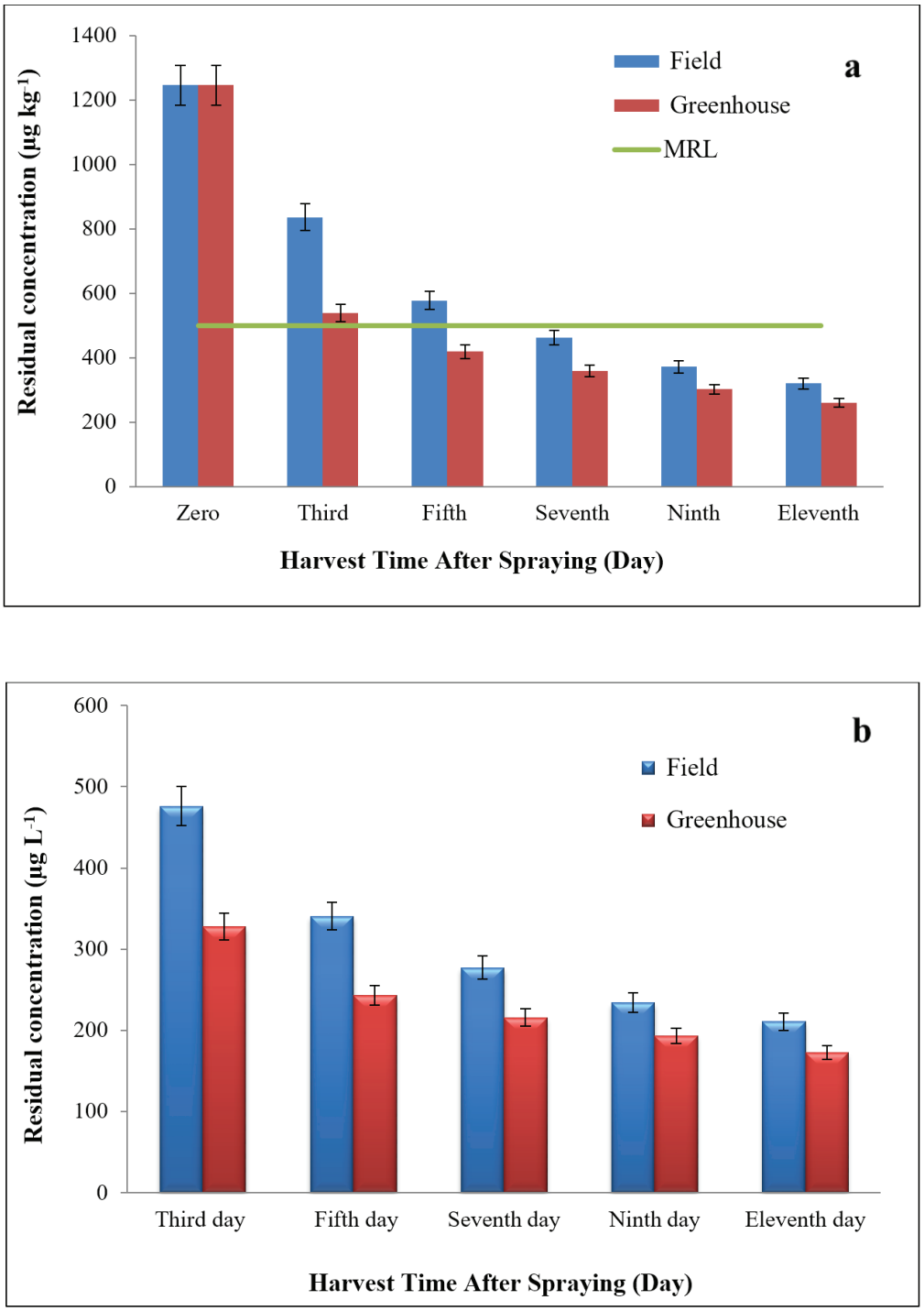

Fig. 3. The comparison of the mean residual concentrations of acetamiprid in field-grown and greenhouse-grown tomatoes (a) and paste (b)

In comparison between raw tomato and tomato paste in both grow condition, it was found that processing of the raw tomato through cooking could decrease the concentration of pesticides in all experiments by LC-MS. Difference of residual concentration of pesticides in the raw and processed products was found to be in the range of 0-10%, and a significant reduction was not observed with the processing product. In Medina et al.'s study evaluating the effect of cooking on the residual pesticides deltamethrin, penconazole, cresoxime methyl, cyproconazole, epoxiconazole, and azoxystrobin in rice, the results reported the reduction of pesticides as 20.73% to 57.72% for home cooking, 32.74% to 70.39% for washing with excess water, and 68.87% to 87.50% for soaking rice before cooking, respectively [25]. The results of Romeh's study examining the processing process on the residual acetamiprid in field-grown eggplant showed that washing 24.73%, boiling 56%, grilling 99%, and frying 46.24% affected the reduction of its residual one day after spraying with the recommended dose [26]. In 2016, Hanafi et al. examined the reduction of non-systemic and low-systemic (indoxacarb, chlorfenapyr, and fenarimol) and systemic (acetamiprid) pesticides in okra after the cooking process. The residual acetamiprid was reduced up to 90% using cooking methods, indicating that the tissues of the okra disintegrated during cooking, so the internal remnants of acetamiprid were exposed to water dissolution and thermal decomposition [27]. The reduction percentage of pesticides in washed and unwashed tomato samples was compared. The significant effect of reducing the residual pesticides of abamectin, deltamethrin, and acetamiprid was observed after washing with tap water. Rinsing with tap water reduced the residual concentrations of acetamiprid, abamectin, and deltamethrin in the crops harvested during one hour after spraying up to 66.85%, 51.62%, and 50.52%, respectively (Table 4). Acetamiprid, as a systemic pesticide, with the highest solubility in water (4250 mg L^{-1}), had the highest reduction percentage after washing compared to the other pesticides. Washing is the first step in the food preparation process and processing methods. Many residual pesticides can be removed by washing them with tap water. Various factors affect the residual pesticides after washing, including the location of the pesticide in the crop (on the surface or in the tissue), washing method, soaking time, physicochemical properties of the plant and pesticide, and the type of pesticide. Pesticides with high water solubility can be more easily eliminated, probably due to their reduced tendency to enter the inner layers [24, 28, 29]. Ajeep et al.'s study on the effect of washing with tap water and washing with an acetic acid solution on the residual amount of five insecticides (dimethoate, carbaryl, chlorpyrifos, cypermethrin, and fenvalerate) and one herbicide (2, 4-dichloro phenoxy acetic acid) in tomato showed that both washing methods reduced the concentration of pesticides by a maximum of 63.08% [30]. In Shalaby's study, it was reported that washing with tap water and acetic acid (1%) could decrease the residual concentrations of abamectin and buprofezin in eggplant and pepper plants two hours after spraying up to 21.86% for washing with water and 41.68% with acetic acid [31]. In Hanafi et al.'s study on okra, the initial residual concentration for chlorfenapyr and acetamiprid was reported to be 7.5 mg kg^{-1} and 0.8 mg kg^{-1}, respectively, which after washing the okra with water, the residual reduction percentage was reported to be 90% for chlorfenapyr and 48% for acetamiprid. This finding is contrary to the water solubility of two studied pesticides [27]. In Elbashir et al.'s study, the residual concentrations of fenpropathrin, λ-Si haloterine, and deltamethrin in outdoor-grown tomatoes were measured over 30 days. The results showed that the residual pesticides fenpropathrin after 27 days, λ-Si haloterine, after 18 days, and deltamethrin after three days in unwashed samples reached below the MRL set by the Codex and the EU. This amount immediately after washing reached below the MRL in the washed samples [18]. Moreover, some methods such as ultrasound-assisted dispersive micro solid-phase extraction, micro-column solid-phase extraction, adsorption (silver nanoparticles, Sulfide Nanoparticles) were used for extraction process [33-38]. The results of similar studies were compared with proposed methods in Table 5.

Table 4. Comparison of reduction percentage of deltamethrin, abamectin, and acetamiprid in unwashed and washed tomato

Pesticide	Unwashed	Washed	Reduction (%)
Acetamiprid	3758.40	1245.80	66.85
Abamectin	967.10	467.80	51.62
Deltamethrin	379.20	187.60	50.52

Table 5. Comparison of proposed method based on LC-MS technique with the published similar studies

Pesticide	Instrument	Product	Condition	Pesticide Residues	Ref.
Acetamiprid	HPLC	Tomato	Greenhouse	Acetamiprid residues were below the already established European maximum residue limits (EU MRLs) (0.5 mg/kg) 3 days after application.	[8]
Abamectin	HPLC	Tomato	Field	The maximum residues level (MRL) values set by EU for abamectin are 0.02 mg/kg (EU, 2005). Based on these MRL values, PHIs were 7 d.	[21]
Acetamiprid	HPLC	Tomato	Greenhouse	The residual amount of acetamiprid pesticides in tomatoes is decreasing as the PHI approaches.	[32]
Acetamiprid	LC-MS/MS	Lettuce	Field and Greenhouse	No clear difference between the two growing conditions was observed.	[22]
Acetamiprid	LC-MS	Tomato	Field and Greenhouse	The reduction rate of acetamiprid residue in tomato was faster in greenhouse conditions than in the field.	This Work
Deltamethrin				The reduction rate of delthamethrin residue in tomato was faster in greenhouse conditions than in the field.	
Abamectin				The reduction rate of abamectin residue in tomato was faster in the field than in the greenhouse.	

4. Conclusion

The present study aimed to investigate the residual concentrations of pesticides deltamethrin, abamectin and acetamiprid in field-grown and greenhouse-grown tomatoes as raw and processed in the form of homemade tomato paste by LC-MS. The rank of reduction percentage of pesticides at the end of the harvest period in the raw and paste products under both conditions followed as deltamethrin, acetamipride and abamectin. Considering the PHI period for deltamethrin and abamectin (3 days) can reach their residual concentration to the MRL in both conditions. According to results of the current study, the times of 7 days and 5 days can be suggested as PHI period of the acetamiprid for field-grown and greenhouse-grown tomato, respectively. According to the data obtained from the current study and the reduction percentage of the residual amount of

pesticide from raw product to processed product under field and greenhouse conditions, it was found that the difference was in the range of 0-10% and significant reduction was not observed with the processing product. The general conclusion that can be inferred from this study was that the highest and most remarkable reduction in the residual amounts of pesticide was related to the washing step, which can reduce the residual pesticide up to 66% which analyzed by LC-MS. It can be suggested to study the initial residues in unwashed, washed, and processed samples, and the residual concentration of pesticides in the soil during the harvest period, and environmental effects in future studies.

5. Acknowledgment

The authors would like to acknowledge the Vice-Chancellor for Research and Technology of Kerman University of Medical Sciences for financial supports. The datasets analyzed during the current study are available from the corresponding author on reasonable request. FN performed executive part of the study; RS performed the instrumental analysis; FSB analyzed data, and MF designed and managed the study.

6. Funding

This work was extracted from the Master of Science thesis supported by the Vice-Chancellor for Research and Technology of Kerman University of Medical Sciences under grant number 99000482.

7. Conflicts of interest

The authors declare that they have no known competing financial interests or personal relationships that could have appeared to influence the work reported in this paper. This work was supported by the Vice-Chancellor for Research and Technology of Kerman University of Medical Sciences under the code of research ethics certificate IR.KMU.REC.1399.600.

8. References

[1] J. Mahugija, F. Ngabala, F. Ngassapa, Effectiveness of common household washing of tomatoes on the removal of pesticide residues, Tanzan. J. Sci, 47 (2021) 390-404. https://dx.doi.org/10.4314/tjs.v47i1.33.

[2] K. Waheed, Medicinal Plants of South Asia, Elsevier, 2020. https://www.elsevier.com/books/medicinal-plants-of-south-asia/hanif/978-0-08-102659-5

[3] A. Fghihi-Zarandi, F. Dabaghzadeh, A. Vaziri, S. Karami-Mohajeri, B. Ghorbaninejad, A. Zamani, K. Rahimi-Sadegh, Occupational risk assessment of organophosphates with an emphasis on psychological and oxidative stress factors, Toxicol. Ind. Health, 38 (2022) 342-350. https://doi.org/10.1177/07482337221096315.

[4] L. Carrasco Cabrera, P. Medina Pastor, The 2020 European Union report on pesticide residues infood, Eu. Food Safety Authority J., 20 (2022) 7215. https://doi.org/10.2903/j.efsa.2022.7215

[5] I. Ferrer, Multi-residue pesticide analysis in fruits and vegetables by liquid chromatography–time-of-flight mass spectrometry, J. Chromatogr. A, 1082 (2005) 81-90. https://doi.org/10.1016/j.chroma.2005.03.040.

[6] H.N.R. Ratnamma, Determination and dissipation of acetamiprid using LC-MS/MS in okra, J. Entomol. Zool. Stud., 9 (2021) 110-116. https://www.entomoljournal.com/archives/2021/vol9issue1/PartB/8-6-198-106.pdf

[7] A.Yazdanpak, Effects of washing, peeling and storage on residue contents of four pesticides in cucumbers grown in greenhouses (Cucumis sativus var:vista), J. anim. Environ., 12 (2020) 427-434. https://doi.org/10.22034/AEJ.2020.105708

[8] M.E. Badawy, A.M. Ismail, A.I. Ibrahim, Quantitative analysis of acetamiprid and imidacloprid residues in tomato fruits under greenhouse conditions, J. Environ. Sci. Health B, 54 (2019) 898-905. https://doi.org/10.1080/03601234.2019.1641389.

[9] A. Shekhi Gorjanet, Toxicity of some new generation insecticides against tomato leafminer moth, Tuta absoluta (Meyrick) under

laboratory and greenhouse conditions, J. Appl. Res. Plant Prot., 7 (2018) 99-108. https://arpp.tabrizu.ac.ir/article_7498_en.html

[10] J. Wang, H. Hirai, H. Kawagishi, Biotransformation of acetamiprid by the white-rot fungus Phanerochaete sordida YK-624, Appl. Microbiol. Biotechnol., 93 (2012) 831-835. https://doi. 10.1007/s00253-011-3435-8.

[11] N.A. Ghalwa, M. Nasser, N. Farhat, Removal of abamectin pesticide by electrocoagulation process using stainless steel and iron electrodes, J. Environ. Anal. Chem., 2 (2015) 134. https://doi.org/10.4172/2380-2391.1000134

[12] R.A. Nugroho, C. van Gestel, The acute single and mixture toxicity of paraquat dichloride and deltamethrin to Guppy (Poecillia reticulata), j. Biosci., 2 (2021) 47-53. https://doi.org/10.4308/hjb.29.1.47-53

[13] A. Yazdanpak, H. Ostovan, Assessment of four pesticide residues (diazinon, imidacloprid, primicarb and acetamiprid) in cucumber under greenhouse condition of Iran (Fars province), J. Entomol. Res., 10 (2018) 139-148. https://jer.arak.iau.ir/article_665015_en.html

[14] A.S. El Din, Persistence of acetamiprid and dinotefuran in cucumber and tomato fruits, J. Toxicol. Sci., 4 (2012) 103-107. https://doi.10.5829/idosi.aejts.2012.4.2.1101.

[15] S.K. Sahoo, Analysis of fluopicolide and propamocarb residues on tomato and soil using QuEChERS sample preparation method in combination with GLC and GCMS, Food Anal. Methods, 7 (2014) 1032-1042. https://doi. 10.1007/s12161-013-9709-2.

[16] P. Komitet Normalizacyjny, Foods of plant origin Determination of pesticide residues using GC-MS and/or LC-MS/MS following acetonitrile extraction/partitioning and cleanup by dispersive SPE- QuEChERS-method, EN 15662, British Standard, 2008. http://www.chromnet.net/Taiwan/QuEChERS_Dispersive_SPE/ChERS_%E6%AD%90%E7%9B%9F%E6%96%B9%E6%B3%95_EN156622008_E.pdf

[17] M.R. Rezaei Kahkha, A. Zarandi, N. Shafighi, S. Kosari, B. Rezaei Kahkha, Magnetic bentonite nanocomposite for removal of amoxicillin from wastewater samples using response surface methodology before determination by high performance liquid chromatography, Anal. Methods Environ. Chem. J., 3 (2020) 25-31. https://doi.org/10.24200/amecj.v3.i03.108.

[18] A.A. Elbashir, A. Albadri, H.E. Ahmed, Effect of post-harvest and washing treatments on pesticide residues of fenpropathrin, λ-cyhalothrin, and deltamethrin applied on tomatoes grown in an open field in Sudan, Food Sci. Technol. Res., 2 (2013) 103-109. https://www.karger.com/Journal/Home/227093

[19] R. Salghi, G. Luis, C. Rubio, A. Hormatallah, L. Bazzi, A. J. Gutiérrez, A. Hardisson, Pesticide residues in tomatoes from greenhouses in Souss Massa Valley, Morocco, Bull. Environ. Contam. Toxicol., 88 (2012) 358-361. https://doi.org/10.1007/s00128-011-0503-9.

[20] B. Rafiei, S. Imani S. Bastan, Determination of residue of deltamethrin on greenhouse cucumber, J. Entomol. Res., 7 (2016) 307-316. https://jer.arak.iau.ir/article_522525.html?lang=en

[21] R.M. Abdelfatahet, Dissipation of some pesticide residues in tomato (Lucopersicon esculentum L.) fruits using QuECHERS methodology under the Egyptian field conditions, J. Plant Prot. Pathol., 11 (2020) 327-332. https://doi.org/10.21608/jppp.2020.108835.

[22] M.Fujita, Comparison of pesticide residue levels in headed lettuce growing in open fields and greenhouses, J. Pestic. Sci., 39 (2014) 69-75. https://doi.org/10.1584/jpestics.D13-064.

[23] X. Chen, W. Wang , F. Liu, Y. Bian, Improved analysis of propamocarb and cymoxanil for the investigation of residue behavior in two vegetables with different cultivation conditions, J. Sci. Food Agric., 100 (2020) 3157-3163. https://doi.org/10.1002/%28ISSN%291097-0010.

[24] N. Yigit, Y.S. Velioglu, Effects of processing and storage on pesticide residues in foods, Crit. Rev. Food Sci. Nutr., 60 (2020) 3622-3641. https://doi.org/10.1080/10408398.2019.1702501.

[25] M.B. Medina, M.S. Munitz, S.L. Resnik, Effect of household rice cooking on pesticide residues, Food Chem., 342 (2021) 128311. https://doi.org/10.1016/j.foodchem.2020.128311.

[26] A.A. Romehsup, M.Y. Hendawisup, Effect of processing on acetamiprid residues in eggplant fruits, Solanum melongena L, Afr. J. Agric. Res., 8 (2013) 2033-2037. https://doi.org/10.5897/AJAR2013.7240.

[27] A. Hanafi, H.E. Elsheshetawy, S.F. Faied, Reduction of pesticides residues on okra fruits by different processing treatments, J. Verbrauch. Lebensm., 11 (2016) 337-343. https://doi.org/ 10.1007/s00003-016-1054-0

[28] T.T. Nguyen, Fate of residual pesticides in fruit and vegetable waste (FVW) processing, Foods, 9 (2020) 1468. https://doi.org/10.3390/foods9101468.

[29] M. Amirahmadi, Effect of Iranian traditional cooking on fate of pesticides in white rice, Toxin. Rev., 36 (2017) 177-186. https://doi.org/10.1080/15569543.2017.1301956.

[30] L.Ajeep, Z. Alnaser, M.K. Tahla, Effect of household processing on removal of multi-classes of pesticides from tomatoes, J. Microbiol. Biotechnol. Food Sci., 10 (2021) 2015-2015. https://doi.org/10.15414/jmbfs.2015.

[31] A. Shalaby, Health risk assessment of abamectin and buprofezin residues in eggplant and pepper plants, J. Plant Prot. Pathol., 11 (2020) 693-699. https://doi.org/10.21608/jppp.2020.166218.

[32] A. Yazdanpak, Determination of residue levels of pesticides (acetamipride, diazinon, imidacloprid, primicarb) in greenhouse tomato (Solanum lycopersicum) var. Izmir in Fars, J. Anim. Environ, 11 (2019) 289-296. http://www.aejournal.ir/article_103902.html?lang=en

[33] M. Osanloo, Validation of a new and cost-effective method for mercury vapor removal based on silver nanoparticles coating on micro glassy balls, Atm. Pollut. Res., 8 (2017) 359-365. https://doi.org/10.1016/j.apr.2016.10.004

[34] M. Ghazaghi, H.Z. Mousavi, A. Rashidi, Ultrasound assisted dispersive micro solid-phase extraction of four tyrosine kinase inhibitors from serum and cerebrospinal fluid by using magnetic nanoparticles coated with nickel-doped silica as an adsorbent, Microchim. Acta, 183 (2016) 2779-2789. https://doi.org/10.1007/s00604-016-1927-z

[35] A.A.M. Beigi, M.M. Eskandari, B. Kalantari, Dispersive liquid-liquid microextraction based on task-specific ionic liquids for determination and speciation of chromium in human blood, J. Anal. Chem., 70 (2015) 1448-1455. https://doi.org/10.1134/S1061934815120072

[36] S. Golkhah, H. Zavvar Mousavi, Removal of Pb (II) and Cu (II) Ions from aqueous solutions by cadmium sulfide nanoparticles, Int. J. Nanosci. Nanotechnol., 13 (2017) 105-117. http://www.ijnnonline.net/5609_8848b0eec7cbc60717bff650d460f600.pdf

[37] H.Z. Mousavi, Chromium speciation in human blood samples based on acetyl cysteine by dispersive liquid–liquid biomicroextraction and in-vitro evaluation of acetyl cysteine/cysteine for decreasing of hexavalent chromium concentration, J. Pharm. Biomed. Anal., 118 (2016) 1-8. https://doi.org/10.1016/j.jpba.2015.10.018

[38] A. Khaligh, H.Z. Mousavi, A. Rashidi, Graphene oxide-packed micro-column solid-phase extraction combined with flame atomic absorption spectrometry for determination of lead (II) and nickel (II) in water samples, Int. J. Environ. Anal. Chem., 95 (2015) 16-32. https://doi.org/10.1080/03067319.2014.983437